UNIVERSIDAD COMPLUTENSE DE MADRID
FACULTAD DE CIENCIAS QUÍMICAS
DEPARTAMENTO DE QUÍMICA ORGÁNICA I

TESIS DOCTORAL

Covalent and supramolecular wires in the search for electrical and thermoelectrical properties

Cables covalentes y supremoleculares en la búsqueda de propiedades eléctricas y termoeléctricas

MEMORIA PARA OPTAR AL GRADO DE DOCTORA

PRESENTADA POR

Valentina Sacchetti

DIRECTORES

Beatriz María illescas Martínez
Nazario Martín León

Madrid, 2019

UNIVERSIDAD COMPLUTENSE DE MADRID

FACULTAD DE CIENCIAS QUÍMICAS

Departamento de Química Orgánica I

COVALENT AND SUPRAMOLECULAR WIRES IN THE SEARCH FOR ELECTRICAL AND THERMOELECTRICAL PROPERTIES

CABLES COVALENTES Y SUPRAMOLECULARES EN LA BÚSQUEDA DE PROPIEDADES ELÉCTRICAS Y TERMOELÉCTRICAS

TESIS DOCTORAL

Valentina Sacchetti

Madrid, 2018

COVALENT AND SUPRAMOLECULAR WIRES IN THE SEARCH FOR ELECTRICAL AND THERMOELECTRICAL PROPERTIES

CABLES COVALENTES Y SUPRAMOLECULARES EN LA BÚSQUEDA DE PROPIEDADES ELÉCTRICAS Y TERMOELÉCTRICAS

Directores:

Dra. Beatriz M. Illescas Martínez

Dr. Nazario Martín León

Memoria que para optar al grado de

DOCTOR EN CIENCIAS QUÍMICAS

presenta

Valentina Sacchetti

Madrid, 2018

Valentina Sacchetti benefited from a Marie Curie fellowship as ESR in the EU Marie Curie Initial Training Network (ITN) MOLECULAR-SCALE ELECTRONICS: "MOLESCO" (project Number 606728, from January 1, 2014 until December 31, 2017).

She attended special courses and conferences on topics of general European interests presented by international experts:

Media Training Workshop, St John's College, Durham, UK (13-15 July 2016)

- Introduction to the Mass Media world

- Media materials and their use;

- Production planning;

- Basics of storytelling structuring a film and storyboarding;

- Basic skills to shoot your own short film (tips on how to capture pictures and sound);

- Personal short science film shooting.

Complementary Skills Training Course, IBM Research – Zürich, Rüschlikon, Switzerland (18-22 April 2016).

- Introduction into Intellectual Property;

- Eyes on research in firms;

- Start-ups and Spin-offs introduction;

- Improving communication skills such as, interpersonal relationships, giving talks, writing papers.

Training School on Quantum Transport Simulation Techniques,, University of Oviedo, Spain (18-22 May 2015)

- Introduction to Tight-Binding scattering Theory:

- Hands on: First tight-binding examples;

- Cursory introduction to Gollum;

- Hands on: Advanced tight-binding examples;

- Cursory introduction to DFT, SIESTA for Gollum;

- Hands on: First DFT-Gollum examples, Advanced DFT-Gollum examples, Advanced DFT-Gollum examples.

Transferable Skills Training Course, University of Durham (16-21 November 2014)

- Focus on communication, impact, personal effectiveness, collaborative working, time management and project management skills.

Workshop on Molecular Scale Electronics, Muggendorf, Germany. (24-27 September 2017)

Topic: Workshop on Single Molecule Electronics and Nanoscale Systems Graphene based

Talk: Electronic Properties of Supramolecular Systems and Carbon Nanoforms

www.dur.ac.uk/chemistry/molesco/meetings/muggendorf/

MOLESCO meeting, Lancaster, United Kingdom (15-19 May 2017)

Topic: Workshop on Molecular Electronics

Talk: Wires based on Amidinium-Carboxylate salt-bridgeinteraction: single molecule-junction approach

3rd Annual Meeting and Workshop, Granada, Spain (17-21 January 2017)

Topic: Electron Transport at Molecular Level

Talk: Graphene Based Nanostructures for Novel Heterojunctions

www.dur.ac.uk/chemistry/molesco/meetings/granada17/

Joint MOLESCO-iSwitch Workshop, Freiburg, Germany (13-17 September 2016)

Summer School on the topics:

- Chemistry at the single-molecule scale - Electron Transfer versus Electron Transport

- Molecular switches and machines

Poster: Supramolecular Wires for Molecular Charge Transport

www.dur.ac.uk/chemistry/molesco/meetings/iswitch/

"A Journey through Carbon Nanostructures: from Fullerenes to Graphene", Toledo, Spain (27-28 June 2016)

Symposium in Honor of Nazario Martín and Maurizio Prato

Poster: Molecular Charge Transport Properties Affected by Medium Features

http://www.journeynanostructures.com/

MOLESCO Workshop , IBM Research , Zürich, Rüschlikon, Switzerland (18-22 April 2016)

Topic: Single Molecule Conductance.

Talk: Amidinium-Carboxylate based Supramolecular Wires

www.dur.ac.uk/chemistry/molesco/meetings/workshop2016/

2nd Annual Meeting, Workshop, and mid-term Review (MTR), Delft, Netherlands (11 - 15 January 2016).

Topic: Electric components built from single molecules and mid-term review of the Marie Curie project MOLESCO.

Talk and Poster Presentation

www.dur.ac.uk/chemistry/molesco/meetings/mtr/

Joint MOLESCO-DFG Network Workshop on Single-Molecule Electronics, Regensburg, Germany, (15-18 September 2015).

Topic: Single-Molecule Electronics

Talk: Chemically Bound Fullerene-Graphene Carbon Hybrids

Poster: Chemically Bound Fullerene-Graphene Carbon Hybrids

www.physik.uni-regensburg.de/forschung/gk_carbonano/ws_home_Sep15.phtml

ISNA16-16th International Symposium on novel aromatic compounds , Madrid, Spain (6-10 July 2015)

Topic: Novel Aromatic Compounds Theory, Synthesis, and Experiments

Poster: Solvent Effects on Molecular Charge Transport Properties

http://isna2015.com

Workshop and Training Course, Oviedo, Spain (18-22 May 2015)

Topic: Molecular Electronics and its applications

http://www.cinn.es/molesco-workshop-training-course/

1st Annual Meeting and Joint MOLESCO-SYMONE Workshop, Engelberg, Switzerland, (8-11 February 2015)

Topic: Molecular Electronics

Poster: Graphene Covalent Functionalization by Fullerene Derivatives

www.dur.ac.uk/resources/chemistry/SYMOLESCOAbstractbooklet.pdf

International Workshop and MOLESCO Meeting, Konstanz, Germany (Sept 29th - Oct 3rd 2014)

Topic: Controlled Charge and Heat Transport at the Molecular Scale

Poster: Covalent Chemical Modification of Graphene

www.dur.ac.uk/chemistry/molesco/meetings/konstanz/

Kick-Off Meeting and Workshop, Madrid, Spain (March 31st - April 2nd, 2014)

Topic: Molecular-Scale Electronics and Business Meeting-Procedures; Recruitment of ESRs in the Marie Curie Project

Talk: Gating Charge Recombination Rates through Dynamic Bridges in Tetrathiafulvalene–Fullerene Architectures

www.dur.ac.uk/chemistry/molesco/meetings/kick-off-meeting/

"Quimica respuestas para un mundo mejor" , Madrid, Spain (8-9 October 2014)

Topic: International Symposium

In the Seventh Framework Programme (FP7-PEOPLE) of the "MOLESCO" project, Valentina Sacchetti spent a secondments period, consisting of a stage and formation experience of overall 360 hours. These secondments period was realized under the supervision of Dr. Peter Nirmalraj from the 25th of November to the 18th of December 2015 and the supervion of Dr. Bernd Gotsmann from the 5th to the 30th of September 2016, at IBM Research Laboratories, Rüschlikon, Zurich, Switzerland. The main target of the undertaken secondments was the learning of the basic operating principle and of the STM and AFM use for the physical characterizations and conductance studies of some of the molecules reported in the present memory.

Acknowledgements

Andrés, Jorge, Alicia, gracias por todos los buenos ratos que hemos compartimos, echo mucho de menos los intentos de ir al cine acabados en cerve...

Sin duda, luego, no puedo olvidarme de las muchas maravillosas compañeras de piso con las cuales compartí mis espacios a lo largo de esto camino de cuatros años. En primer lugar, gracias a Laura (imprescidible compañera de fiestas, viajes y miles de aventuras) que junta con Elisella y Simoncella han sido y siguen siendo super buenas amigas. Luego, gracias también a Elly, Yu y Myriam (y Yago también, compañero de piso "part-time"!) por compartir momentos buenisimos y culturas diferentes.

Fabri, amigo mio, sin ti Madrid hubiese sido seguramente menos divertida, grazie per avermi fatto conoscere questa meravigliosa città in tutti i suoi bares y garitos vari, i pranzi della domenica e tutto il resto ovviamente!

Un grazie speciale, poi, va a la mia famiglia (nonni sicuramente inclusi), mamma, papà, Diego, Mara e Fabio, siete stati e sarete sempre un attracco sicuro.

Infine, grazie a chi ha reso possibile il più bel capolavoro della mia vita, Ivan.

Abbreviations and Acronyms

In addition to the standard abbreviations and acronyms in organic chemistry (as defined in the *Journal of Organic Chemistry* author guidelines,http://pubs.acs.org/paragonplus/submission/joceah/joceah_authguide.pdf) the following terms have been used in this manuscript:

Å	Angstrom(s)
anhyd	Anhydrous
atm	Atmosphere
AFM	Atomic force microscopy
BH	Bulk heterojunction
BJ	Break junction
BPDN	Bipyridyl-dinitrooligophenylene–ethynylene dithiol
COSY	Correlation spectroscopy
CT	Charge transfer
CVD	Chemical vapor deposition
CV	Cyclic voltammetry
δ	Chemical shift in parts per million downfield from tetramethylsilane
D-A	Donor-Acceptor
DAE	Diarylethene
DBA	Donor-bridge-acceptor
DCM	Dichloromethane
dd	Double dobled
DEPT	Distortionless enhancement by polarization transfer
DFT	Density functional theory
DMF	*N,N*-Dimethylformamide
DMSO	Dimethyl sulfoxide
DNA	Deoxyribonucleic acid

E_F	Fermi energy
ESI	Electrospray ionization
EI	Electron impact
ET	Electron transport
ex-TTF	Extended tetrathiafulvalene
FLG	Few layer graphene
FMO	Frontier molecular orbital
F_4TCNQ	Tetrafluorotetracyano-p-quinodimethane
FTIR	Fourier transformed infrared spectroscopy
GO	Graphene oxide
GOS	Graphene on surface
GQDs	Graphene quantum dots
h	Hour(s)
Hex	Hexane
HMQC	Heteronuclear multiple quantum correlation
HOMO	Highest occupied molecular orbital
HOPG	Highly oriented pyrolytic graphite
HOPG	Horseradish peroxidase
Hz	Hertz
IPR	Isolated pentagon rule
J	Coupling constant (in NMR spectroscopy)
K	Kelvin
K_a	Association constant
LUMO	Lowest unoccupied molecular orbital
μ	Micro
m	Multiplet (spectral); meter(s); milli
M	Molar (moles per liter)

MALDI	Matrix-assisted laser desorption ionization
MBE	Molecule based electronics
MCBJ	Mechanically controlled breack junction
MS	Mass spectroscopy
NEGF	Non-equilibrium Green's function
NLO	Nonlinear optical properties
nm	Nanometer
NMR	Nuclear magnetic resonance
o-DCB	*ortho*-dichlorobenzene
OFETs	Organic field effect transistors
OPE	Oligo(*p*-phenylene ethynylene)
P	Porphyrin
Pc	Phthalocyanine
$PC_{61}BM$	(6,6)phenyl C_{61} butyric acid methyl ester
$PC_{71}BM$	(6,6)phenyl C_{71} butyric acid methyl ester
PCE	Power conversion efficiency
PET	Photo-induced electron transfer
PMα-CD	Permethylated α-cyclodextrin
PCTE	Polycarbonate track etched
PPA	Polyphosphoric acid
PPP	Poly(*p*-phenylene)
PTB_7-Th	Poly[4,8-bis(5-(2-ethylhexyl)thiophen-2-yl)benzo[1,2-b:4,5-b′] dithiophene-*c*o-3-fluorothieno[3,4-b]thiophene-2-carboxylate]
PTFE	Polytetrafluoroethylene
PV	Photovoltaic
Py	Pyridine
QD	Quantum dot

rf-cCVD	Radiofrequency catalytic chemical vapour deposition
RT	Room temperature
s	Singlet
SLG	Single layer graphene
SPM	Scanning probe microscopy
STHM	Scanning tunneling hydrogen microscopy
STM	Scanning tunneling microscopy
STMBJ	Scanning tunneling microscopy break junction
t	Triplet
TCNQ	7,7',8,8'-tetracyano-p-quinodimethane
TEM	Transmission electron microscopy
TTF	Tetrathiafulvalene
TGA	Thermogravimetric analysis
THF	Tetrahydrofuran
TLC	Thin-layer chromatography
TPPO	Triphenylphosphine oxide
Tol	Toluene
UME	Unimolecular electronics
UPy	Ureido pyrimidinedione
UV	Ultraviolet
V	Volts
vs.	*Versus* ("against")
XPS	X-ray photoelectron spectroscopy

Table of Contents

4. Conclusions   93

5. Experimental Part   977

6. Appendix   1311

Chapter 2.

7. Background   139

A Beatrice

Introduction

Introduction

I.   Nanoscience and Nanotechnology

Scientists have investigated nanoscale materials for at least 150 years, ever since the sizes of atoms were first determined.[1] Specifically, the study of the unique size-dependent properties of solid-state materials and the discovery of the rules that govern these properties define the field of *nanoscience*. Conversely, *nanotechnology* can be considered, strictly speaking, as technology using single nanoscale building blocks, and Feynman's lectures[2] or Norio Taniguchi's original use of the term[3] are often mentioned as the starting points for the concept. Its basic essence relies on the ability of manipulating matter atom-by-atom or molecule-by-molecule, but, in more informal words, nanotechnology can be thought as the exploitation of the findings of nanoscience. In this respect, nanotechnology became really possible only with the advent of single-molecule manipulation techniques, such as the scanning tunnelling microscope (STM)[4] and later the atomic force microscope (AFM).[5] The invention of these techniques allowed scientists the ability not just to see molecules, but to pick them up and to move them as single building blocks. Indeed, many products either enabled or improved by nanotechnology have already been on the market from 2005 (Table 1).[6]

---

[1] a) M. Faraday, *Philos. Trans. R. Soc. London* **1857**, *147*, 145; b) G. Mie, *Ann. Phys.* **1908**, *25*, 377.

[2] R. Feynmann, *Plenty of Room at the Bottom*, American Physical Society annual meeting, CalTech, **1959.**

[3] N. Taniguchi, *On the Basic Concept of Nano-Technology*, Proc. ICPE, Tokyo, Part II, Japan Society of Precision Engineering, **1974** ; "nano-technology mainly consists of the processing of separation, consolidation, and deformation of materials by one atom or one molecule".

[4] G. Binnig, H. Rohrer, C. Gerber, E. Weibel, *Appl. Phys. Lett.* **1982**, *40*, 178.

[5] G. Binnig, C. F. Quate, C. Gerber, *Phys. Rev. Lett.* **1986**, *56*, 930.

[6] Meridien Institute, *Nanotechnology and the Poor, Opportunities and Risks*, **2005**, http://www.merid.org.

Table 1: Existing and near-term applications of nanotechnology across 12 different sectors. Ref 6.

Automotive Industry	Chemical Industry	Construction	Cosmetics
-Lightweight construction -Painting -Catalysts -Tires (fillers) -Sensors -Coatings for windshields and auto bodies	-Fillers for paints -Composite materials -Impregnation of papers -Adhesives -Magnetic fluid	-Materials -Insulation -Flame retardants -Surface coatings for wood, floors, stone, tiles, roofing, etc. -Mortar	-Sunscreens -Lipsticks -Skin creams -Toothpaste
Electronics	**Energy**	**Engineering**	**Food&Drinks**
-Displays -Data memory -Laser diodes -Fiber optics -Optical switches -Filters -Conductive, antistatic coatings	-Fuel cells -Solar cells -Batteries -Capacitors	-Protective coatings for tools and machines -Lubricant-free bearings	-Packaging -Sensors for storage life -Additives -Clarifiers (for juices)
Household	**Medicine**	**Sports/Outdoors**	**Textile**
-Ceramic coatings for irons -Odour removers -Cleaners for glass, ceramics, metals, etc.	-Drug delivery systems -Contrast media -Rapid testing systems -Prostheses and implants -Antimicrobial agents -In-body diagnostic	-Ski wax -Tennis rackets, golf clubs -Tennis balls -Antifouling coatings for boats -Antifogging coatings systems for glasses/goggles	-Surface coatings -Smart textiles

What makes the nanometre scale intriguing is that material properties at this level differ from those in bulk and from those of molecules or their clusters of small size. Indeed, any matter in nano-sized form exhibits a change of properties which is considered attributable to the quantum-sized confinement effects and the increased surface-to-volume ratio compared to bulk materials. Therefore, the nanoscale is two-faced like the Roman god Janus and can be considered the doorway between the

bulk and the molecular states. Thus, being the nano-world bursting with promising discoveries of physical phenomena that are not accessible using traditional materials or approaches, it is comprehensible the optimism manifested by nanoscientists around the new horizons (in health care, materials, energy and so on) opened by the exploitation of these properties. However, apart from this enthusiastic point of view, the hype surrounding this new field has also naturally led to some cynicism among the non-nanoscientists, but more alarming is the rising of violent antinanotechnology activisms,[7] which fear environmental disaster and sci-fi apocalyptic scenarios. Obviously, because of the interdisciplinary nature of nanotechnology, it exists a higher probability of rising philosophical and ethical questions. Therefore, it is surely required providing nanoscientists with a multi-disciplinary scientific formation, which would also be implemented with an ethical education in the direction of the potential societal implications. On the other hand, though, it is fundamental a major scientific divulgation focused on the topic, to avoid that any scientifically ignorant activism can proliferate, and all the possible concerns about the future of nanotechnologies remain within the confines of a democratic debate about technology, science, and ethics.

II.   Molecular-Scale Electronics[8]

The integrated electronics field, with its specific market demand for further miniaturization of the electronic devices, perfectly fits the current trend of technology towards the reduction of the size, which is clearly stimulated by the exciting different properties displayed by nanoscaled structures. Over the past few decades, traditional transistors have shrunk dramatically reaching a dimension of less than 10 nm,[9] but, due to either technique limitations and lack of fundamental

---

[7] In 2011, for example, a group calling itself the "ELF Switzerland Earth Liberation Front" was caught in Switzerland trying to bomb an IBM nanotechnology facility while it was under construction. The same year, a group in Mexico, known as "Individualidades Tendiendo a lo Salvaje" sent letter bombs to nanotechnology researchers injuring several people.

[8] D. Xiang, X. Wang, C. Jia, T. Lee, X. Guo, *Chem. Rev.* **2016**, *116*, 4318.

[9] a) E. Lortscher, *Nat. Nanotechnol.* **2013**, *8*, 381; b) L. Wilson, *International Technology Roadmap for Semiconductors (ITRS)*; Semiconductor Industry Association, **2013**.

understanding of the transport mechanisms,[10] the further downscaling remains extremely challenging. In this context, the bottom-up approach to the creation of functional electrical circuits exploiting the intrinsic properties of individual molecules (or their ensembles) displays several advantages compared to traditional silicon-based electronic components. First, being molecules the smallest building blocks of matter, electrical components made only by them would enable heightened capacities reaching faster performance. Second, the flexibility of the chemical design allows the tailoring of the desired or required properties. Third, being chemically identical, molecules can be synthesized in bulk, thus lowering the cost of manufacturing. Therefore, the use of single molecules or nanoscale collections of single molecules as electronic components (concept which is at the base of the long history of the "molecular-scale electronics", Figure 1), besides showing the potential to partly replace traditional solid-state devices, provides also an ideal window to investigate the intrinsic properties of nano-reduced materials.
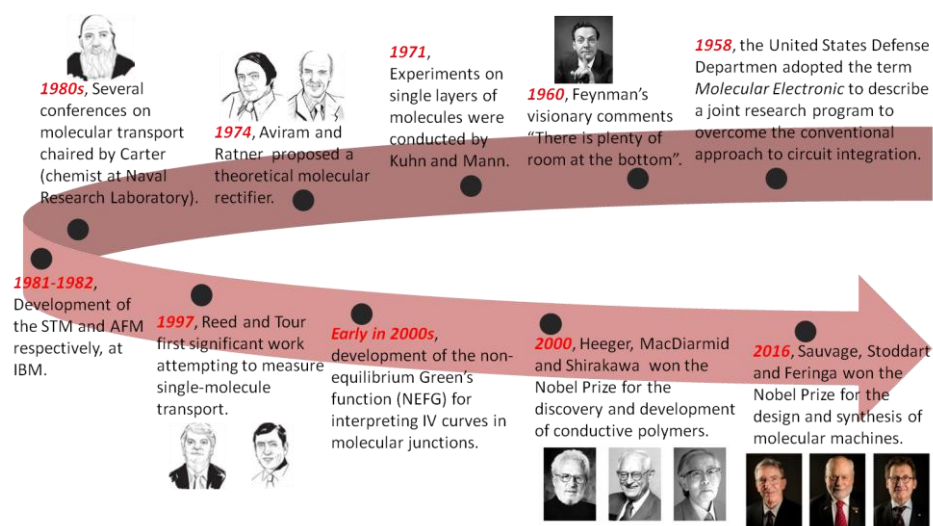
Figure 1: Summary chart of the long history of the molecular-scale electronics.

Nonetheless, the commercial outlet of molecular-scale electronic devices seems to be still far. In fact, from the exact determination of the

---

[10] A. T. Haedler, K. Kreger, A. Issac, B. Wittmann, M. Kivala, N. Hammer, J. Kohler, H. W. Schmidt, R. Hildner, *Nature* **2015**, *523*, 196.

structure-function relationship to the lack of a standardized process for the molecular fabrication and the too high costs for a bulk production, numerous challenges need to be addressed before devices based on single-molecules can be developed. Indeed, over the past decade, the comprehension of the working principles of conceptually simple molecular junctions was considerably enhanced through significant improvements in both experiments and theory.[11] However, there is still much to do in this respect and the field of molecular electronics remains a seductive playground for scientists to explore new fundamental concepts and new applications.

[11] a) J. M. Tour, W. A. Reinerth, L. Jones, T. P. Burgin, C. W. Zhou, C. J. Muller, M. R.; Deshpande, M. A. Reed, *Ann. N. Y. Acad. Sci.* **1998**, *852*, 197; b) A. H. Flood, J. F. Stoddart, D. W. Steuerman, J. R. Heath, *Science* **2004**, 306, 2055; c) R. L. McCreery, A. J. Bergren, Adv. Mater. **2009**, *21*, 4303; d) K. Moth-Poulsen, T. Bjornholm, *Nat. Nanotechnol*. **2009**, *4*, 551; e) Q. Shen, X. F. Guo, M. L. Steigerwald, C. Nuckolls, *Chem. Asian J.* **2010**, *5*, 1040; f) M. G. Schultz, *Phys. Rev. B* **2010**, *82*, 155408; g) J. C. Cuevas, E. Scheer, *Molecular Electronics: An Introduction to Theory and Experiment*; World Scientific: River Edge, NJ, **2010**; h) D. Natelson, Y. J. Li, J. B. Herzog, *Phys. Chem. Chem. Phys*. **2013**, *15*, 5262; i) L. Sun, Y. A. Diaz-Fernandez, T. A. Gschneidtner, F. Westerlund, S. Lara-Avila, K. Moth-Poulsen, *Chem. Soc. Rev.* **2014**, *43*, 7378; l) L. Sánchez, R. Otero, J. M. Gallego, R. Miranda, N. Martín, *Chem. Rev.*, **2009**, *109*, 2081; m) D. M. Guldi, B. M. Illescas, C. M. Atienza, M. Wielopolski, N. Martín, *Chem. Soc. Rev.*, **2009**, *38*, 1587.

Chapter 1.

1.   Background

1. Background

1.1. *Molecular Wires*

A molecular wire is the most elementary building block for molecular nanoscale devices. It is a structure which can serve as a transport for electrons, generally composed by a molecule-bridge connected to a source and drain of electrons that can be two molecules themselves, the donor and acceptor moieties respectively, or rather two metal electrodes.

Different definitions from literature have outlined the concept of molecular wire over time. It has been described as "a molecule connected between two reservoirs of electrons",[12] or whose behaviour is referred to "a molecule that conducts electrical current between two electrodes",[13] or, even more strictly, as a device that conducts in a regime "wherein the distance dependence of electron transfer may be very weak".[14]

Several studies have shown the influences of different structural parameters on the properties of molecular wires. Their structure–property relationships can be determined by probing the electron transfer (ET) process through such systems.

1.1.1. *Charge Transfer Mechanisms*

At macroscopic level, the charge transport in conductors obeys Ohm's law and their resistance is proportional to their length. However, these laws are no more valid at nanometric scale, where the conductance is quantized.

The charge transfer process in a molecular wire at long distance is an inherent non-adiabatic process[15] whose rate is distance dependent. The tunneling effect or "super-exchange electron transfer" is favorable if the molecular bridge's length is small, whilst if the molecular bridge's length is large, the hopping mechanism is preferred.

---

[12] E. G. Emberly, G. Kirczenow, *Phys. Rev. B* **1998**, *58*, 10911.

[13] A. Nitzan, M. A. Ratner, *Science* **2003**, *300*, 1384.

[14] W. B. Davis, W. A. Svec, M. A. Ratner, M. R. Wasielewski, *Nature* **1998**, *396*, 60.

[15] J. Jortner, *J. Chem. Phys.* **1976**, *64*, 4860.

Anyway, the quality of a molecular wire as a charge carrier can be obtained by the Equation 1, where the kinetic constant of the electron transfer process is given by:

$$k_{et} = k_0 \exp(-\beta r_{DA})$$

Equation 1. Equation for the kinetic constant of ET processes.

In which k_0 is the temperature-dependent prefactor, it is typical for the deactivation of charge transfer processes and depends on the donor-acceptor distance (r_{DA}). β, the so called "*attenuation factor*", is independent of the distance and it is employed to define the quality of the wire. The smaller the β value, the weaker is the distance dependence of the wire or, in other words, the longer is the distance that the charge can transfer without any penalty. This value of β can be considered as a parameter for the whole DBA system, where donor and acceptor are molecular units or metallic contacts and it is strictly not referred to the bridge itself. Therefore, for a fixed bridge, the attenuation factor is a result of the existing difference between the energetic levels of the subunits forming the bridge,[16] that means, in conclusion, that β value depends on the electronic coupling between the different components of the systems under study.

1.1.1.1.   *Super-exchange Mechanism*

During the tunneling effect (denominated for the first time by Kramers[17] and then by Anderson)[18] the electron transfer occurs from the donor to the acceptor through a tunnel in the energy barrier (Figure 2). During the electron transfer, the orbitals of the bridge are only used as a mean of coupling with no nuclear movement along the bridge (no charge resides on the bridge). This mechanism, no temperature dependent, occurs when the bridge orbitals (above all the LUMO) are not energetically accessible.

---

[16] M. P. Eng, B. Albinsson, *Angew. Chem. Int. Ed.* **2006**, *45*, 5626.

[17] H. A. Kramers, *Physica* **1934**, *1*, 182.

[18] a) P. W. Anderson, *Phys. Rev.* **1950**, *79*, 350; b) P. W. Anderson, *Phys. Rev.* **1959**, *115*, 2.
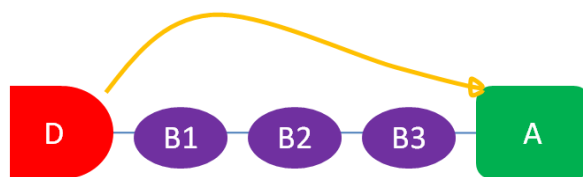
Figure 2: Coherent charge transport or super-exchange mechanism.

1.1.1.2.   *Hopping Mechanism*

In case that hopping mechanism is prevailing, there are real energetically affordable intermediate states that actively transport the electron or hole along the wire. Changes in the molecular geometry can take place due to the formation of a charged intermediate excited state which evolves to the more stabilized species where positive charge resides on the donor and negative charge on the acceptor. The bridge is thus acting as a pathway for the electron transport (Figure 3); the electronic coupling between the bridge and terminal moieties is now considerable and the orbitals of the bridge (especially LUMO) are energetically accessible to promote an electron transfer along the bridge itself. This phenomenon is temperature dependent, and is frequently named as thermally activated hopping mechanism.
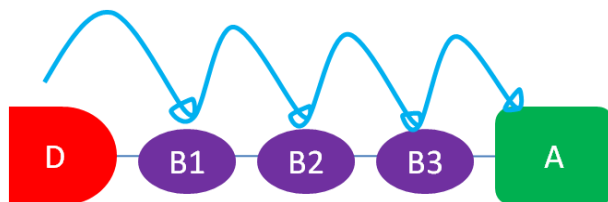
Figure 3: Incoherent charge transport or hopping mechanism.

In general, in systems in which there is a large energy gap between the initial and intermediate states, super-exchange will be the dominant mechanism. However, if this energy gap is comparable to the reorganization energy or electronic coupling, hopping mechanism can compete. In many real cases the transfer is expected to be governed by a mixture of the two mechanisms.

1.1.2. *Approaches*

To probe the ET process through a wire's structure three different approaches are typically employed:

- The *"donor-bridge-acceptor systems"* (DBA) method, where the photoinduced electron-transfer processes are studied by measuring the kinetics of electron transfer process by the photophysical study of the decay of the relevant transient species;

- The *"molecule based electronics"* (MBE) approach, which studies electrical processes in molecular assemblies of any scale, creating a molecular sandwich between two electrodes;[19]

- The *"unimolecular electronics"* (UME) approach, which studies the conductance properties at the single-molecule level by interfacing a molecule between two metal electrodes.[20]

Although the concept of molecular electronics was initially promising because of a visionary future where silicon-based technology would be replaced by the use of single molecules or nanoscale collections of single molecules as electronic components, real commercial implementation of molecular based devices appear to be a distant dream. Instead, something fundamentally different from the initial perspective seems to promise the UME strategy. Beyond the electronic transport that led the initial interest, researchers start now to focus on the rich physics of metal–molecule–metal junctions, in addition to explore new paradigms taking full advantage from the quantum properties of molecules, window into non-equilibrium processes, that have no analogues in conventional electronics.

Generally, at single-molecule level, the structure–property relationships of a junction can be discussed by deconstructing the junction into three distinct components: the electrode, the anchor group, and the molecular bridge (Figure 4).

---

[19] J. M. Tour, M. Kozaki, J. M. Seminario, *J. Am. Chem. Soc.* **1998**, *120*, 8486.

[20] R. M. Metzger, *NATO ASI Ser.* **1991**, B248, 659.
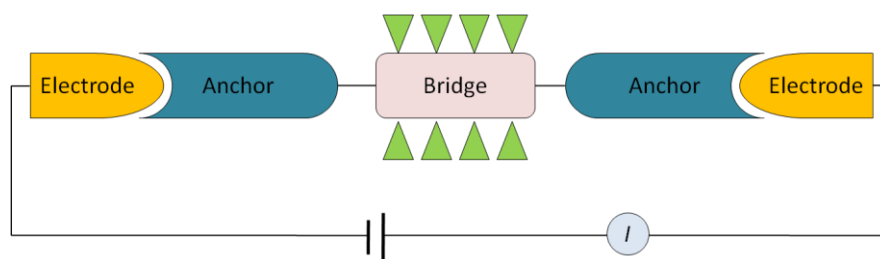
Figure 4: Scheme of a single-molecule junction. The bridge unit can be further deconstructed into backbone (light orange block) and substituent (green triangles) subunits. I, is the current.

Electron transport through molecules in nanoscale junctions is sensitive to very small changes in atomic configuration.[21] The specific anchoring group, whose role is fundamental to define the interface interaction of the molecule with the electrodes,[22] but also variations in the type of electrode material,[23] different molecular geometries[24] and conformations[25] deeply influence measurable properties of the metal–molecule-metal junction. Powerful techniques have been developed to characterize and manipulate the conductance properties of single molecules, including mechanical break junctions,[26] electrochemical deposition,[27] electromigration,[28] electron beam lithography,[29] shadow

[21] L. Sun, Y. A. Diaz-Fernandez, T. A. Gschneidtner, F. Westerlund, S. Lara-Avilab, K. Moth-Poulsen, *Chem. Soc. Rev.* **2014**, *43*, 7378.

[22] a) B. Xu and N. J. Tao, *Science* **2003**, *301*, 1221; b) L. A. Zotti, T. Kirchner, J. C. Cuevas, F. Pauly, T. Huhn, E. Scheer, A. Erbe, *Small* **2010**, *6*, 1529; c) C. Jia, X. Guo, *Chem. Soc. Rev.* **2013**, *42*, 5642; d) E. Leary, A. La Rosa, M. T. González, G. Rubio-Bollinger, N. Agraït, N. Martín, *Chem. Soc. Rev.* **2015**, *44*, 920.

[23] a) A. Danilov, S. Kubatkin, S. Kafanov, P. Hedegard, N. Stuhr-Hansen, K. Moth-Poulsen, T. Bjornholm, *Nano Lett.* **2008**, *8*, 1; b) Y. Cao, S. Dong, S. Liu, Z. Liu, X. Guo, *Angew. Chem. Int. Ed.* **2013**, *52*, 3906; c) X. Y. Zhou, Z. L. Peng, Y. Y. Sun, L. N. Wang, Z. J. Niu, X. S. Zhou, *Nanotechnology* **2013**, *24*, 465204.

[24] a) M. Kamenetska, S. Y. Quek, A. C. Whalley, M. L. Steigerwald, H. J. Choi, S. G. Louie, C. Nuckolls, M. S. Hybertsen, J. B. Neaton, L. Venkataraman, *J. Am. Chem. Soc.* **2010**, *132*, 6817; b) S. V. Aradhya, L. Venkataraman, *Nat. Nanotechnol.* **2013**, *8*, 399.

[25] L. Venkataraman, J. E. Klare, C. Nuckolls, M. S. Hybertsen, M. L. Steigerwald, *Nature*, **2006**, *442*, 904.

[26] M. A. Reed, C. Zhou, C. J. Muller, T. P. Burgin, J. M. Tour, *Science* **1997**, *278*, 252.

[27] A. F. Morpurgo, C. M. Marcus and D. B. Robinson, *Appl. Phys. Lett.* **1999**, *74*, 2084.

[28] H. Park, A. K. L. Lim, A. P. Alivisatos, J. Park and P. L. McEuen, *Appl. Phys. Lett.* **1999**, *75*, 301.

[29] A. Bezryadin, C. Dekker and G. Schmid, *Appl. Phys. Lett.* **1997**, *71*, 1273.

mask evaporation,[30] scanning probe techniques,[31] on-wire lithography[32] and molecular rulers.[33]

Specifically, the focus of the present memory is to investigate the electrical properties of different sets of novel compounds as molecular wires, on the basis of the UME approach, and probe the molecular conductance for the developed wire systems by methods based on scanning probe techniques.

1.1.3. *Scanning Probe Microscopy (SPM)*

The invention of the scanning tunneling microscope (STM) and the atomic force microscope (AFM) that gave birth to the SPM techniques, is regarded as a milestone in the history of molecular electronics, because its great contribution to the development of the field continues to promote advances still now.

The attractive features of STM and AFM is that they make interrogation of matter with atomic-scale resolution simple and affordable. Previous to the invention of those techniques, defining the structure of materials with atomic-scale precision was troublesome, expensive and difficult. In addition to the interrogation at the nanoscale, the SPM can be also used to manipulate and control various properties of matter in the nanoworld, together with the ability to operate in different environments The 2000 U.S. National Nanotechnology Initiative evidenced the importance of the development of these techniques by saying "STMs, AFMs, and near-field microscopes provide the eyes and fingers required for nanostructure manipulation and measurement".[34]

---

[30] S. Kubatkin, A. Danilov, M. Hjort, J. Cornil, J. L. Bredas, N. Stuhr-Hansen, P. Hedegard, T. Bjornholm, *Nature* **2003**, *425*, 698.

[31] X. D. Cui, A. Primak, X. Zarate, J. Tomfohr, O. F. Sankey, A. L. Moore, T. A. Moore, D. Gust, G. Harris, S. M. Lindsay, *Science* **2001**, *294*, 571.

[32] L. Qin, S. Park, L. Huang, C. A. Mirkin, *Science* **2005**, *309*, 113.

[33] T. Dadosh, Y. Gordin, R. Krahne, I. Khivrich, D. Mahalu, V. Frydman, J. Sperling, A. Yacoby, I. Bar-Joseph, *Nature* **2005**, *436*, 677.

[34] National Science and Technology Council, Committee on Technology, Subcommittee on Nanoscale Science, Engineering and Technology, "National nanotechnology initiative: The initiative and its implementation plan", July 2000. [Online]. Available: http://www.nano.gov/nni2.pdf

The common feature of SPM techniques is that they share the operating principles of the STM and AFM, which is the use of a probe and the ability to position the material under investigation in relation to the probe with atomic-scale precision.

1.1.3.1.   *STM and AFM techniques*

In 1981, Binnig and Rohrer conducted the first successful tunneling experiment[4] giving birth to the scanning tunneling microscopy (STM). Some years later, in 1986, Binnig, Quate, and Gerber[5] developed the atomic force microscopy (AFM), following the necessity of an instrument that displayed the same performance of the STM but going beyond its intrinsic limit of being applied only to conductor and semiconductor materials. They made possible imaging with atomic-scale resolution also of insulators.

A general SPM setup is based on the combination of two electrodes, the top electrode is a tip of different possible materials and the down electrode is a surface where the sample of molecules is deposited.

Different operating principles are at the base of functioning for the two equipments.

STM working principle uses the quantum-mechanical phenomenon of tunneling current which corresponds to a flow of electrons from the surface of one material to the surface of another, even when the surfaces are not in direct contact. The magnitude of this phenomenon is appreciable when the separation between the surfaces is of just few nanometers. A criterion of paramount importance is, for that, to maintain at really small distances the separation between the probe and the surface of the material investigated. The introduction of a feedback loop that allowed to control the gap between the surfaces of the probe and the sample was indeed the crucial step in the success of the tunneling experiment of the two IBM's scientists in 1981 (Figure 5).
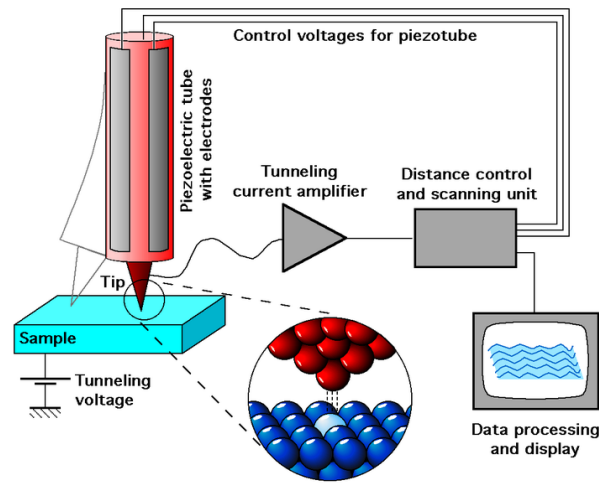
Figure 5: STM schematic representation.

On the other side, in AFM, force instead of current is used to control the tip-positioning. Its principle of operation consists in the ability to sense the small forces exerted on the tip by the atoms in the sample. The specific probe is composed by a microcantilever provided with a sharp tip. A fundamental requisite is that the cantilever probe must be insensitive to external interferences from the surrounding environment. A control system for the cantilever is given by a laser beam incident on it, which reflects onto a split photodiode which has the responsibility of measuring the deflection of the cantilever itself. The cantilever deflects, due to the experienced forces between the atoms on the surface of the sample and the atoms on the surface of the tip, changing, for that, the angle that the incident laser beam makes with its surface. In turn, the incidence position of the laser on the photodiode changes and this variation is registered as a change in the photodiode voltage (Figure 6).
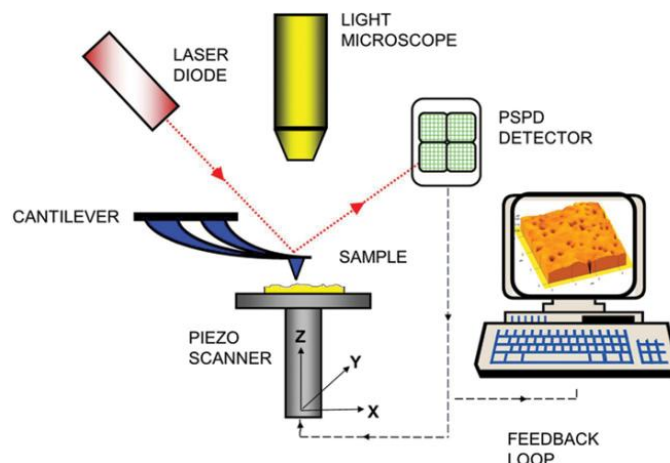
Figure 6: Atomic force microscope schematic representation.

Allowing for the direct observation of the system under investigation and permitting simultaneously the realization of other types of studies, such as electron transport, since their conception, SPM-based techniques have become the main experimental techniques in nanoscience to perform single-molecule electronic investigation by forming a metal–molecule–metal junction between the metallic tip and the substrate.

To form the aforementioned molecular junction, the tip or substrate can be either immersed in the target molecule solution during the experiments or decorated with molecules before measurements.

A unique role in the field of molecular electronics is covered by a specific STM technique called scanning tunneling microscopy break junctions (STMBJ) (Figure 7).
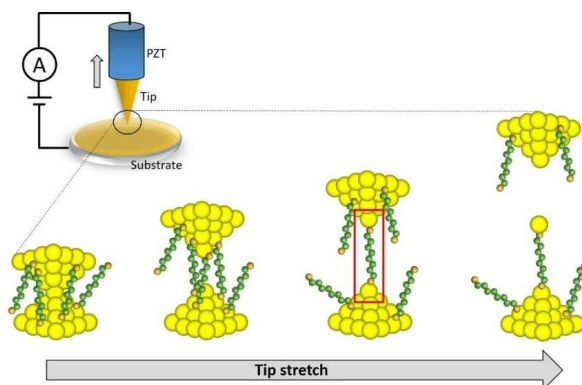
Figure 7: Working principle of STMBJ technique.

In the STMBJ technique, a voltage bias is applied between a sharp tip of an STM, typically made of gold, and a substrate, also made of gold, covered with a layer of molecules that are chemically bound to the substrate via anchoring groups that can be of different nature. The tip is brought in contact with the substrate while the electrical conductance between the tip and the sample is being monitored. The formation of Au–Au atomic contacts is established when an electrical conductance of ~5 G_0 or greater is observed. At this point the "crashed" tip is progressively withdrawn, until just a single atom of gold remains in the junction, just before the breakage. During this process, in addition to the formation of Au–Au contacts, also some deposited molecules can statistically bridge the electrodes. This means that in the withdrawal process of the tip, a single-molecule junction can be formed, instead of the single gold atom connection, before the rupture of the electrodes union. During this process the electrical conductance of the tip-molecule-substrate junctions is monitored by conductance-distance measurements. In Figure 8 is reported an example of the relative curves.[22a]
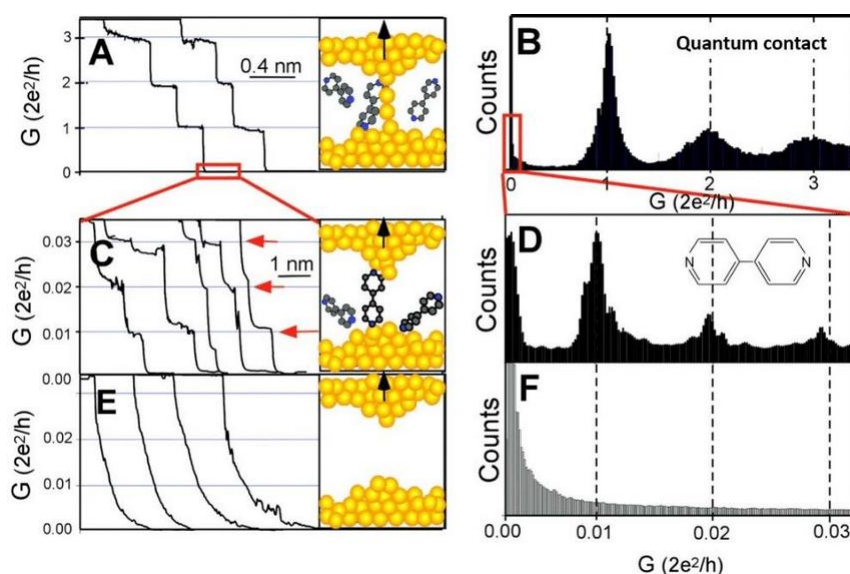
Figure 8: (A,C,E) Single-molecule conductance measurement. (B,D,F) Corresponding conductance histogram illustrate well-defined peaks near 1 G_0, 2 G_0, and 3 G_0 due to the conductance quantization. After the gold–gold contact is completely broken, a new series of conductance steps appear due to the formation of the molecular junctions. Ref 22a.

The presence of a plateau (as in the left side A) or a peak (as in the right side B) around G_0 corresponds to the formation of a single gold atom junction, which indicates atomically sharp electrodes. Typically, thousands of stretching traces are recorded and only curves with clear plateaus are selected for the subsequent statistical analysis based on the criterion of stretching distance.

Recent progress on SPM-based techniques were also achieved in the imaging of organic molecules. For the first time, the individual atoms within the molecules were resolved, indicating the potential of this technique not only in resolving molecular structure, but also bonding within and between molecules, molecular conformational changes and chemical reactions at the single-molecule level.[35] For both techniques the key step consists in the atomic functionalization of the probe. This fundamental step corresponds to place a well-defined atom or molecule at the tip of the scanning probe. In the case of AFM, the tip is modified by deliberately picking up one molecule of carbon monoxide (Figure

---

[35] L. Gross, *Nature Chemistry* **2011**, *3*, 273.

9),[36] whereas in the case of scanning tunneling hydrogen microscopy (STHM), the resolution was increased after filling the gap between the tip and the sample by the introduction of a single molecular hydrogen.[37]
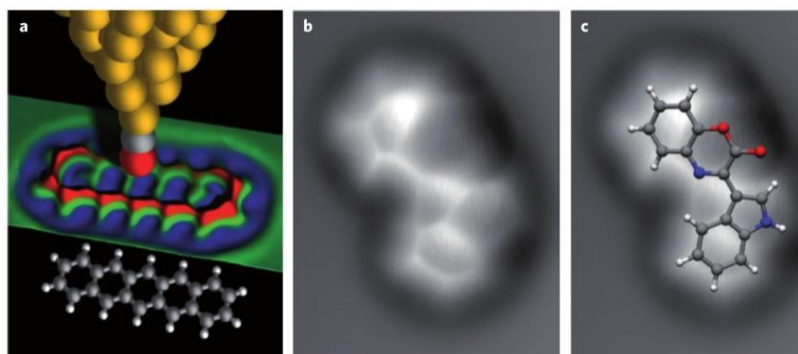
Figure 9: a) Schematic representation of the imaging process. b) Molecule imaged with atomic resolution using non contact AFM-CO-functionalized tips. c) Correspondence of the imaged molecule with the theoretical structure. Ref 36a.

1.1.4. *Molecular Wires: Origins and Development*

The concept of molecular wires has evolved starting from the design of linear species covalently bonded, whose constitutive structural core consists in bridge systems composed by identical repetitive molecular motifs of π-conjugated units. The choice of π-conjugated bridges resides in many convenient aspects, which go from their seeming rigidity, to their rod-like structure and more importantly their high degree of electron delocalization. The electronic communication between the individual bridge units has been gaining fundamental relevance in building efficient wire systems. Specifically, the electron delocalization ability is substantial to achieve a favorable mediation of charge/energy transfer over long distances. A systematic experiment to prove the ability of a bridge to sustain charge transport corresponds to the distance-dependence studies. ET reactions are traditionally triggered using light excitation by selectively exciting either the donor or the acceptor unit. These reactions are called photo-induced electron

---

[36] L. Gross, F. Mohn, N. Moll, G. Meyer, R. Ebel, W. M. Abdel-Mageed, M. Jaspars *Nature Chem.* **2010**, *2*, 821.
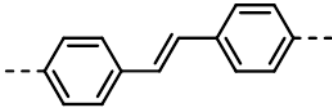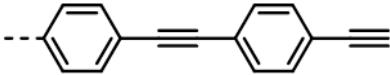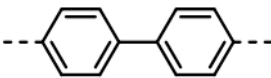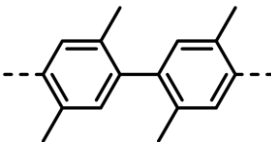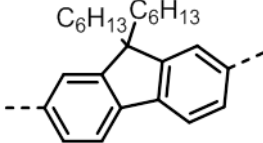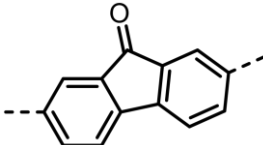
[37] J. I. Martínez, E. Abad, C. González, F. Flores, J. Ortega, *Phys. Rev. Lett.* **2012**, *108*, 246102.

transfer (PET) reactions and can be considered the ancestors of single molecule experiments. Indeed, valuable knowledge on wire-like properties has been acquired by experimentally studying excited state properties and their relative ET processes. The results of such investigation are, for convenience, often summarized in the already mentioned parameter called attenuation factor, β. Representative examples of different bridge structures drawn from literature are reported in Table 2.[38] A variety of β values for covalently bonded donor-acceptor systems of different nature are given (Table 2).

---

[38] a) F. Giacalone, J. L. Segura, N. Martín, D. M. Guldi, *J. Am. Chem. Soc.* **2004**, *126*, 5340; b) G. de la Torre, F. Giacalone, J. L. Segura, N. Martín, D. M. Guldi, *Chem. Eur. J.* **2005**, *11*, 1267; c) K. Pettersson, J. Wiberg, T. Ljungdahl, J. Mårtensson, B. Albinsson, *J. Phys. Chem. A* **2005**, *110*, 319; d) C. Atienza, N. Martín, M. Wielopolski, N. Haworth, T. Clark, D. M. Guldi, *Chem. Commun.* **2006**, *0*, 3202; e) E. A. Weiss, M. J. Ahrens, L. E. Sinks, A. V. Gusev, M. A. Ratner, M. R. Wasielewski, *J. Am. Chem. Soc.* **2004**, *126*, 5577; f) C. Schubert, M. Wielopolski, L. H. Mewes, G. de Miguel Rojas, C. van der Pol, K. C. Moss, M. R. Bryce, J. E. Moser, T. Clark, D. M. Guldi, *Chem. Eur. J.* **2013**, *19*, 7575; g) C. Atienza, M. Wielopolski, D. M. Guldi, C. van der Pol, M. R. Bryce, S. Filippone, N. Martín, *Chem. Commun.* **2007**, *0*, *5164*; h) A. B. Ricks, K. E. Brown, M. Wenninger, S. D. Karlen, Y. A. Berlin, D. T. Co, M. R. Wasielewski, *J. Am. Chem. Soc.* **2012**, *134*, 4581.

Table 2: List of structures and relative β values for different DBA systems.

Bridge	D	A	β_{cs}/A^{-1}	Ref.
OPV	exTTF[a]	C_{60}	0.01	Guldi-Martín (37a)
OPE	Zn^{II}TPP[b]	C_{60}	0.03	Guldi-Martín (37b)
	Zn^{II}P	Au^{III}P	0.31	Albisson (37c)
	exTTF[a]	C_{60}	0.2	Guldi (37d)
Ph$_n$ (or PP)	PTZ[c]	PDI[d]	0.46	Wasielewski (37e)
xy$_n$	Ru^{II}	PTZ[c]	0.77	Wenger (37f)
fl$_n$	exTTF[a]	C_{60}	0.09	Martín (37g)
FN$_n$	DMJ-An[e]	NI[f]	0.34	Wasielewski (37h)

a) Extended tetrathiafulvalene. b) Tetraphenylporphyrin. c) Phenotiazine. d) Perylene-3,4:9,10-bis(dicarboximide). e) 3,5-Dimethyl-4-(9-anthracenyl)julolidine. f) Naphthalene-1,8:4,5-bis(dicarboximide). Ref 37.

Many different examples along the years have demonstrated that employing covalent bonds to link the different components of a molecular wire structure corresponds to very good performances of conductivities, high rationalization of structure–property relationships[39] and of key parameters, such as the mode of transport.[40]

One step further in molecular electronics was accomplished studying how the introduction of weak bonding forces can influence the electron flow through molecular wire systems. Among the many different non-covalent interactions, the hydrogen bonding (H-bonding) has been the most investigated. One of the first examples, in which hydrogen bonds were shown to control electron transfer was reported by Therien *et al.* for bis-chromophoric systems of zinc(II) and iron(III) porphyrins.[41] Hirsch and co-workers in 2010, studying a non-covalent system constituted by a Hamilton receptor/cyanuric acid motif to assemble metalloporphyrins with C_{60} derivatives, determined a β factor of 0.1 Å^{-1} intermediate between the extremes of covalent *p*-phenyleneethynylene[38b,c,d] and fluorene systems.[38g,h,42] More recently, Martín *et al.* reported hybrid covalent/supramolecular porphyrin–[60]fullerene structures, based on the amidinium-carboxylate H-bond interaction, as highly efficient molecular wires with a remarkably low attenuation factor ($\beta = 0.07 \pm 0.01$ Å^{-1}).[43] The supramolecular systems studied by Hirsch and Martín are shown in Figure 10.

[39] G. J. Ashwell, P. Wierzchowiec, L. J. Phillips, C. J. Collins, J. Gigon, B. J. Robinson, C. M. Finch, I. R. Grace, C. Lambert, P. D. Buckle, K. Ford, B. J. Wood, I. R. Gentle, *Phys. Chem. Chem. Phys.* **2008**, *10*, 1859.

[40] S. H. Choi, C. Risko, M. C. R. Delgado, B. S. Kim, J. L. Brédas, C. D. Frisbie, *J. Am. Chem. Soc.* **2010**, *132*, 4358.

[41] P. J. F. de Rege, S. A. Williams, M. J. Therien, *Science* **1995**, *269*, 1409.

[42] F. Wessendorf, B. Grimm, D. M. Guldi, A. Hirsch, *J. Am. Chem. Soc.* **2010**, *132*, 10786.

[43] S. Vela, S. Bauroth, C. Atienza, A. Molina-Ontoria, D. M. Guldi, N. Martín, *Angew. Chem. Int. Ed.* **2016**, *55*, 15076.
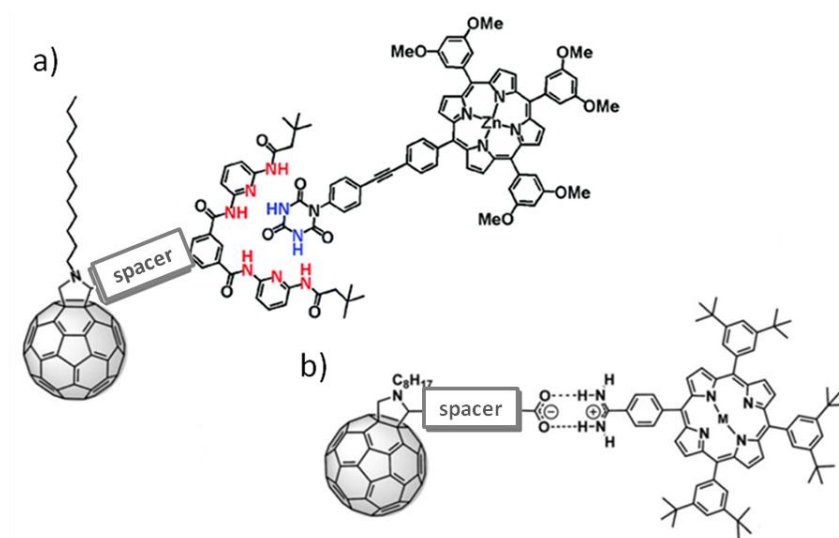
Figure 10: Supramolecular DBA systems from a) Hirsch study (Ref 41) and b) Martín work (Ref. 42).

Anyway, the first purpose in molecular electronics remains the understanding and manipulation of the charge transport phenomenon through single-molecules. Therefore, the obvious direction in the evolution of PET reactions to investigate electron transfer was the substitution of the acceptor and donor moieties with the direct placing of single molecules between two metallic electrodes. UME approach is indeed considered to have more practical applications, because it makes directly use of the molecule as an electrical interconnect between two devices. In this regard single-molecule break junction (BJ) methods, such as the STMBJ, turn out to be suitable techniques for characterizing the conductance of unimolecular junctions.

1.1.5. *Supramolecular Interactions in Single Molecular Junctions*

Significant progress has been made during the past years in many aspects of UME area defining, for example, the dependence of conductance with anchoring groups,[22] molecular length,[44]

---

[44] B. Capozzi, E. J. Dell, T. C. Berkelbach, D. R. Reichman, L. Venkataraman, L. M. Campos, *J. Am. Chem. Soc.* **2014**, *136*, 10486.

electrochemical gating,[45] quantum interference effect,[46] contacts geometries,[47] and the influence of molecular conformation.[48]

Specifically, the technical progress of BJ-methods opens the opportunity to study charge transport phenomena in more complex junction systems. Recent reports revealed the application of these techniques, for example, to the investigation of molecular systems bridged through non-covalent interactions.[49,46b]

Non-covalent interactions are comparatively weaker forces than the covalent ones (Figure 11). Their interactions are based on some peculiar features such as self-assembly, self-organization, molecular recognition, reversibility and tunable strength. Basically, two are the interesting aspects which make these supramolecular interactions appealing with respect to the more stable covalent ones: i) on one side, the high selectivity in the connections developed between building blocks, ii) on the other side, the thermodynamic reversibility, which makes recognition process during the assembly one of the possible finely tuned processes.

---

[45] a) Y. Li, M. Baghernejad, A. G. Qusiy, D.Z. Manrique, G. Zhang, J. Hamill, Y. Fu, P. Broekmann, W. J. Hong, T. Wandlowski, D. Zhang, C. Lambert, *Angew. Chem. Int. Ed*. **2015**, *54*, 13586; b) H. M. Osorio, S. Catarelli, P. Cea, J. B. Gluyas, F. Hartl, S. J. Higgins, E. Leary, P. J. Low, S. Martin, R. J. Nichols, J. Tory, J. Ulstrup, A. Vezzoli, D. C. Milan, Q. Zeng, *J. Am. Chem. Soc.* **2015**, *137*, 14319.

[46] a) C. R. Arroyo, S. Tarkuc, R. Frisenda, J. S. Seldenthuis, C. H. Woerde, R. Eelkema, F. C. Grozema, H. S. J. van der Zant, *Angew. Chem. Int. Ed.* **2013**, *52*, 3152; b) R. Frisenda, V. A. E. C. Janssen, F. C. Grozema, H. S. J. van der Zant, N. Renaud, *Nature Chemistry* **2016**, *8*, 1099.

[47] X. L. Li, J. He, J. Hihath, B. Q. Xu, S. M. Lindsay, N. J. Tao, *J. Am. Chem. Soc*. **2006**, *128*, 2135.

[48] H. Li, M. H. Garner, Z. Shangguan, Q. Zheng, T. A. Su, M. Neupane, P. Li, A. Velian, M. L. Steigerwald, S. Xiao, C. Nuckolls, G. C. Solomon, L. Venkataraman, *Chem. Sci.* **2016**, *7*, 5657.

[49] a) P. T. Bui, T. Nishino, Y. Yamamoto, H. Shiigi, *J. Am. Chem. Soc.* **2013**, *135*, 5238; b) L. Wang, Z. L. Gong , S. Y. Li, W. Hong, Y. W. Zhong, D. Wang, L. J. Wan, *Angew. Chem. Int. Ed.* **2016**, *55*, 1; c) W. Zhang, S. Gan, A. Vezzoli, R. J. Davidson, D. C. Milan, K. V. Luzyanin, S. J. Higgins, R. J. Nichols, A. Beeby, P. J. Low, L. Buyi, L. Niu, *ACS Nano* **2016**, *10*, 5212.
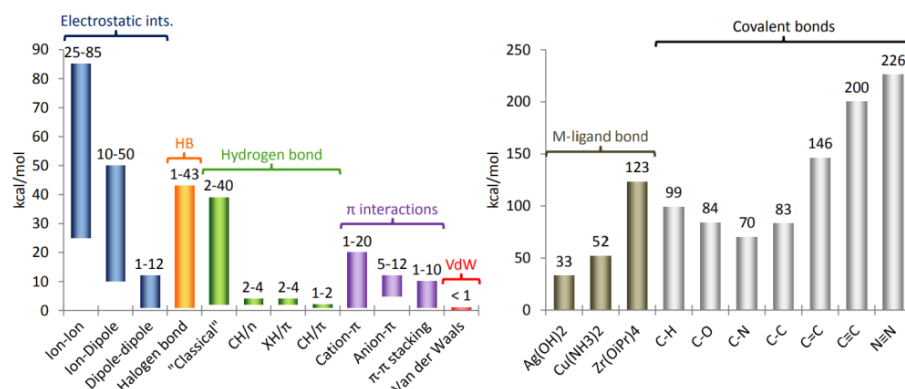
Figure 11: Non-covalent *vs.* covalent bonds strength.

However, the degree of knowledge concerning electron transfer at the single molecule level in non-covalently interacting systems, remains considerably lacking.[50] Therefore, understanding charge transfer within a single supramolecular assembly is a pivotal point for building functional electronic devices, where spontaneous recognition plays a central role in their construction, as well as in conferring unique electronic functionalities.

Building aligned species is of particular interest regarding the development of electronic devices, especially for contacting with the electrodes. In this regard, there are a variety of strategies to obtain efficient molecular wires. The strategy of choice relies on the basis of the type of electro or photoactive moieties to be incorporated, because these units define the wire's electronic properties. Once defined the wire backbone structure, the weak forces can geometrically fine-tune the assemblies.

1.1.5.1.   *π-π Stacking Interactions*

The double stranded organization of DNA and the tertiary structure of proteins are examples of structures stabilized by the intervention of the π-π interactions. Indeed, this kind of connections play a significant role in biological structures and, owing to their large amount of delocalized π electron density, result of special interest in molecular electronics.

---

[50] X. Li, D. Hu, Z. Tan, J. B. Zongyuan, X. Y. Yang, J. Shi, W. Hong, *Top Curr. Chem. (Z)* **2017**, *375*, 42.

Therefore, the understanding of the ET process through π-π stacking is critical in the search for the fabrication of biomolecule-based devices.

In a pioneering work, Wu *et al.* showed that π-π stacking interactions result strong enough to form a molecular junction.[51] Using the mechanically controlled break junction (MCBJ) technique, they studied a series of oligo-phenyleneethynylene (OPE) derivatives. Molecules 1 and 2 possess two active anchoring groups, while the nitrogen atom of the pyridine structure in molecule 3 is hidden, providing a much less probable binding site to the electrode. Molecule 4 directly lacks any efficient second anchoring group (Figure 12).
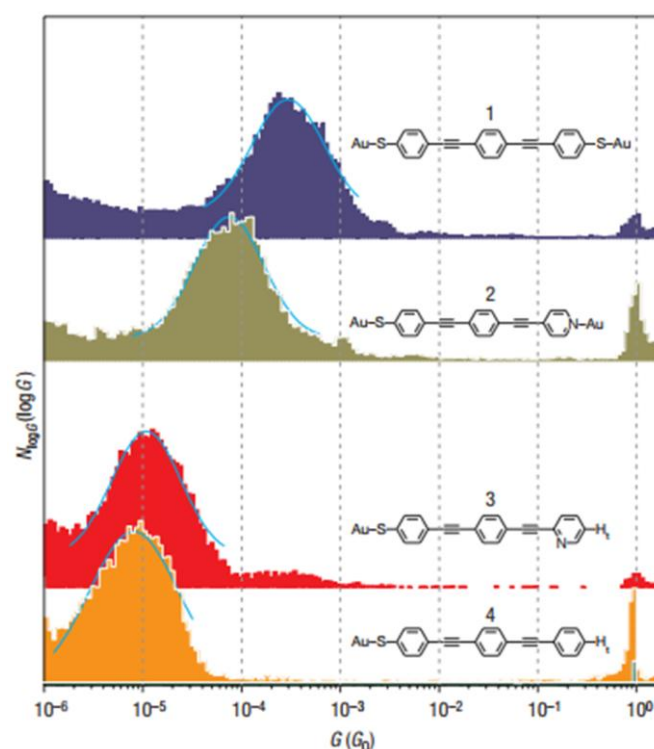
Figure 12: Conductance peak of the corresponding molecules investigated by Wu. Ref 50.

[51] S. Wu, M. T. González, R. Huber, S. Grunder, M. Mayor, C. Schoenenberger, M. Calame, *Nat. Nanotechnol.* **2008**, *3*, 569.

Interestingly, molecules 3 and 4 exhibit a conductance one order of magnitude lower than that of molecules 1 and 2. But even more surprising is that they exhibit an identical magnitude and width in the conductance peak respect to molecules 1 and 2, suggesting that they bind in the junction with a similar probability as molecules with an anchoring group on both ends. Therefore, considering the single anchoring group and the lower conductance, they speculated that the formation of the molecular junctions is ascribed to the π-π stacking interaction between two adjacent molecules.

Further investigations have been performed to prove this natural tendency of aromatic systems to self-assemble and form aggregates. Martin *et al.* demonstrated that the presence of steric hindrance impedes the formation of a stacking arrangement, determining the disappearance of the corresponding conductance peak.[52] González *et al.* investigated the formation of π-π stacked molecular junctions as a function of the environmental conditions, demonstrating that the presence of polar molecules enhance their organization.[53]

Moreover, unique electrical characteristics are exhibited by the inclusion complexes formed when π-π stacked systems (stacked guests) are locked in self-assembled cages (hosts). Using STMBJ technique, Fujii *et al.* observed that inclusion complexes containing two identical aromatics (homocomplex) and different aromatics (heterocomplex) exhibit, the first, a high conductance value, while the second shows two peaks one of which appears at lower conductance.[54] The presence of these two peaks, in the case of the heterocomplex, was attributed to two different electron transport directions at a fixed bias voltage. Statistical analysis of the I-V curves confirmed experimentally that the heterocomplex junction shows rectification properties (Figure 13).

---

[52] S. Martin, I. Grace, M. R. Bryce, C. Wang, R. Jitchati, A. S. Batsanov, S. J. Higgins, C. Lambert, R. J. Nichols, *J. Am. Chem. Soc.* **2010**, *132*, 9157.

[53] M. T. González, E. Leary, R. l. García, P. Verma, M. A. N. Herranz, G. Rubio-Bollinger, N. Martín, N. S. Agraït, *J. Phys. Chem. C* **2011**, *115*, 17973.

[54] S. Fujii, T. Tada, Y. Komoto, T. Osuga, T. Murase, M. Fujita, M. Kiguchi, *J. Am. Chem. Soc.* **2015**, *137*, 5939.
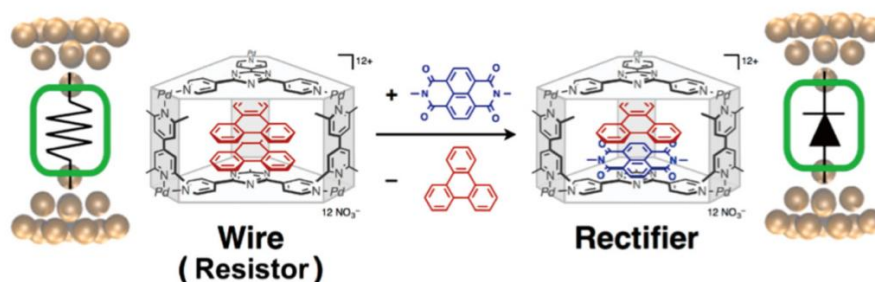
Figure 13: Illustration of chemical structures and molecular junctions of homocomplex (left) and heterocomplex (right). Ref 53.

1.1.5.2.   *Hydrogen Bonding*

Hydrogen bonding is by far the most widely investigated supramolecular interaction. Many are the reasons why this bond results so appealing. Firstly, because the electronic communication through systems connected by such interaction shows a strong and directional component comparable to σ or π bonds.[55] Secondly, because the strength of this connection can be tuned availing of external stimuli that cause the alteration of the transport properties at molecular-scale, influencing their conductance and junction formation.[56] Early investigation of conductance properties at single-molecule level of such interaction was performed in 2013. Employing a STM-based I(t) technique, Nishino showed that the carboxylic dimers interacting through H-bonds exhibit a better conductance than the corresponding alkanes of similar molecular length, even if it decays steeply as the ET pathway becomes longer (Figure 14). [57]

[55] L. Sánchez, M. Sierra, N. Martín, A. J. Myles, T. J. Dale, J. Rebek, Jr., W. Seitz, D. Guldi, *Angew. Chem. Int. Ed.* **2006**, *45*, 4637.

[56] M. Kotiuga, P. Darancet, C. R. Arroyo, L. Venkataraman, J. B. Neaton, *Nano Lett.* **2015**, *15*, 4498.

[57] T. Nishino, N. Hayashi, P. T. Bui, *J. Am. Chem. Soc.* **2013,** *135*, 4592.
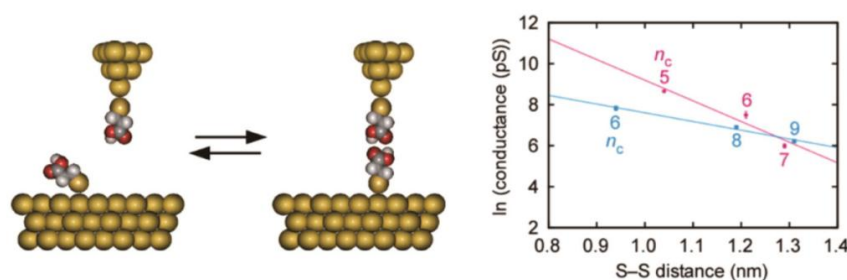
Figure 14: Scheme of the formation of a single molecular junction based on the hydrogen bond interaction between two carboxylic units (right); distance dependence of conductance of molecular junction consisting of H-bonded C_nCOOH dimers (pink) and alkanedithiolates (blue); n_c represents the number of C-atoms in the molecular junction (left). Ref 56.

To investigate the electron transport through multiple hydrogen bonds, Wang *et al.* studied a series of ureido pyrimidinedione (UPy) derivatives (Figure 15).[58] The results of this study show that the thiol terminated quadruple-hydrogen-bonded dimer presents a high conductance value which is comparable to conjugated oligo(phenylene-ethynylene) junctions, while the conductance of the pyridyl and amino terminated dimers result considerably lower, owing to the weaker N–Au bond.
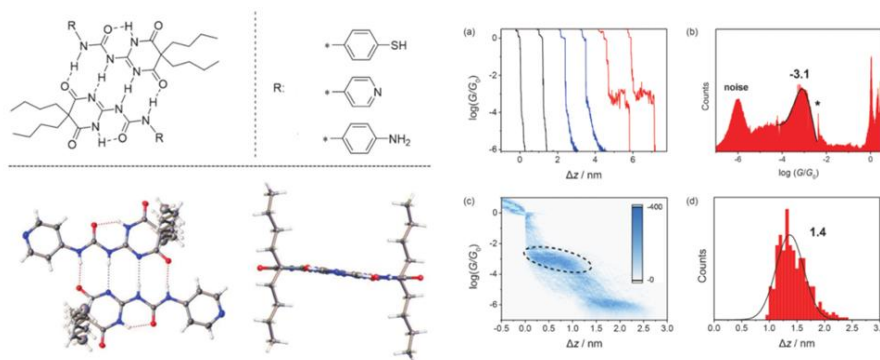
Figure 15: Molecular structures and self-assembly mode of UPy derivatives (left); Single-molecule conductance results from STMBJ experiments for the Upy terminated via thiol groups. Ref 57.

However, hydrogen bonds are fundamental interactions present in biological systems. They preserve, for instance, the double-stranded

[58] L. Wang, Z. L. Gong, S. Y. Li, W. J. Hong, Y. W. Zhong, D. Wang, L. J. Wan, *Angew. Chem. Int. Ed.* **2016**, *55*, 12393.

structure of DNA and its unique characteristics, such as self-recognition and self-assembly, make it a promising material in molecular electronics.[59] With this aim, the understanding of charge transport properties involving the hydrogen bonds of the DNA structure is a matter of crucial relevance. Particularly interesting is the detection of mutations in the double-stranded DNA (dsDNA) structure through the application of electric-based methods. A good example is the work by Hihath *et al.*, in which STMBJ is used to identify the presence of even a single base pair mismatch by evidencing that the conductance of dsDNA can vary as much as one order of magnitude.[60]

1.1.5.3.   *Host–Guest and Charge-Transfer (CT) Interactions*

The wide application that host-guest complexes find in many aspects of life, ranging from biological systems to pharmaceuticals, and chemical sensors, make them considerably attractive. A common host in these complexations is represented by cyclodextrins. These compounds are a group of cyclic glucose oligosaccharides of different diameter, characterized by an amphipathic nature, due to the hydrophobic internal cavity and the hydrophilic outer surface.

On the basis of these attractive characteristics, Kiguchi *et al*., using the STMBJ technique, decided to investigate the conductance properties of a π-conjugated molecular junction covered by a permethylated α-cyclodextrin (PM α-CD) (Figure 16).[61]

---

[59] G. I. Livshits, A. Stern, D. Rotem, N. Borovok, G. Eidelshtein, A. Migliore, E. Penzo, S. J. Wind, R. Di Felice, S. S. Skourtis, J. C. Cuevas, L. Gurevich, A. B. Kotlyar, D. Porath, *Nat. Nanotech.* **2014**, *9*, 1040.

[60] J. Hihath, B. Xu, P. Zhang, N. Tao, *PNAS* **2005**, *102*, 47, 16979.

[61] M. Kiguchi, S. Nakashima, T. Tada, S. Watanabe, S. Tsuda, Y. Tsuji, J. Terao, *Small* **2012**, *8*, 5, 726.
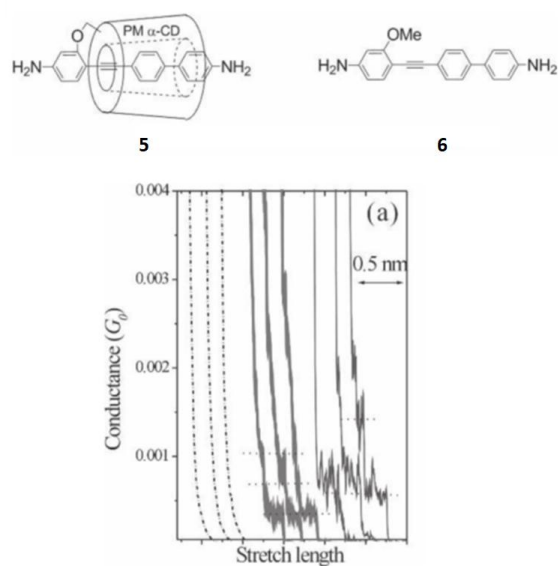
Figure 16: Structures of covered **5** and uncovered **6** molecules, conductance traces of covered (thick line) and uncovered (thin line) molecules. Ref 60.

Kiguchi discovered that inserting a single π-conjugated molecule into a host molecule like CDs is a promising technique. It permits to study the charge transport properties of single-molecule devices suppressing conductance fluctuations with respect to the uncovered π-conjugated molecule.

Charge transfer interactions are of course the main central topic of the field. For this reason, thanks to their electronic versatility, complexes generated from the attractive interaction between donor and acceptor molecules have become currently subject of great interest.

The discovery of tetrathiafulvalene-tetracyano-*p*-quinodimethane (TTF-TCNQ) charge-transfer complex in 1973, and its high electrical conductivity, make it an interesting candidate in the field of molecular electronics.[62] García *et al.* investigated the charge transport of the complex formed between an extended-TTF (ex-TTF) and a tetrafluorotetracyano-*p*-quinodimethane (F_4TCNQ).[63] No conductance

[62] P. W. Anderson, P. A. Lee, M. Saitoh, *Solid State Commun.* **1973**, *13*, 595.

[63] R. García, M. A. Herranz, E. Leary, M. T. González, G. Rubio Bollinger, M. Buerkle, L. A. Zotti, Y. Asai, F. Pauly, J. C. Cuevas, N. Agraït, N. Martín, *Beilstein J. Org. Chem.* **2015,** *11*, 1068.

signal was registered for the ex-TTF, which according to theoretical calculations results under the measurement sensitivity. In contrast, two distinct conductance plateaus were observed for the complex. The higher was attributed to that of F_4TCNQ, while the lower was assigned to the exTTF-F_4TCNQ complex (Figure 17).
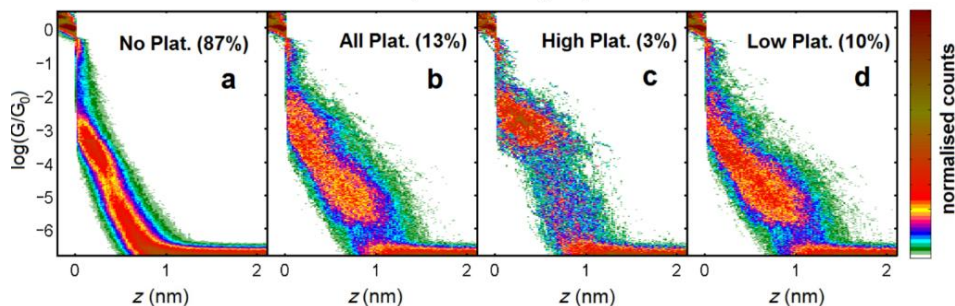
Figure 17: 2D histograms of ex-TTF (a), F_4TCNQ (d), all traces (b) and the ones for CT complex between ex-TTF and F_4TCNQ (c). Ref 62.

Electron acceptor properties of [60]fullerene and donor behavior of porphyrin have made these molecules fundamental building blocks in molecular electronics. Nishino *et al.* investigated, for example, the electronic properties of a single fullerene-porphyrin complex by STM.[64] Functionalizing the tip of the STM with fullerene derivatives, they demonstrated that the interaction with a porphyrin derivative, deposited on a highly oriented pyrolytic graphite (HOPG) substrate, results in asymmetric I-V curves. Therefore, single fullerene-porphyrin complex exhibits an obvious rectifying behavior (Figure 18).
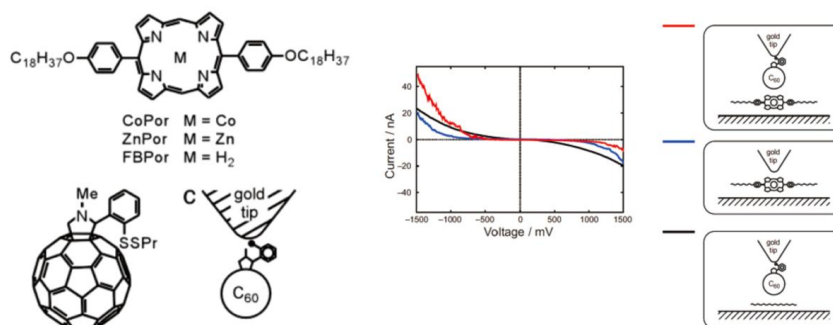
Figure 18: Fullerene-porphyrin complex and their I-V curves. Ref 63.

---

[64] T. Nishino, T. Ito, Y. Umezawa, *PNAS* **2005**, *102* ,5659.

1.1.6. *Single Molecule Switches*

The technical progress of BJ-techniques has also allowed the study of one of the most appealing functional elements in a molecular electronic device, the switch. This electronic element has its molecular correspondent in a compound whose electronic communication can be controlled externally.[65] The interest in these molecules is that their *"on-off"* control could, in principle, introduce relevant applications as, for example, memory elements. Anyway, a molecular functional element with switchable properties, once attached to the electrodes, can preserve or not its functionality. Remarkably, the opposite phenomenon does exist as well. A device whose core is not constituted by a molecule with switchable properties in solution, once pinned to the metal electrodes, can exhibit an unexpected switching activation (Figure 19).
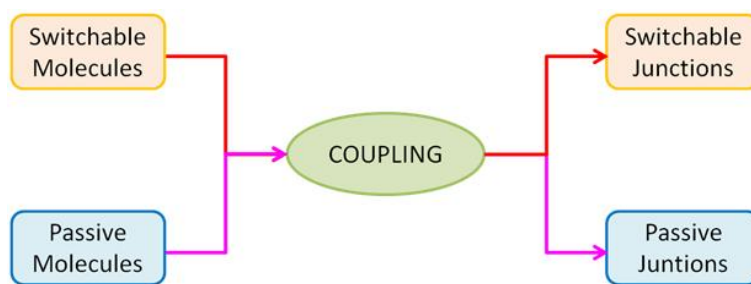
Figure 19: Scheme of how coupling can influence the performance of a molecular device.

Therefore, single molecules in solid-state devices can be divided into: i) *intrinsic switches*, when the molecule preserves its switching ability, ii) *extrinsic switches,*[66] when a non-switching molecule may be activated by contacting with the electrodes. The ability to exist in two distinguishable stable forms and to turn each one into the other, under the effect of some external stimuli, is the main feature of molecular switches. Roughly, two modes of switching can be identified for this conversion mechanism, the conformational and the redox type. In the first case, an isomerization reaction takes place, where the three-dimensional structure of the molecule undergoes fundamental changes. In the second case, a molecule can modify its charge state by taking up

---

[65] J. F. Stoddart, H. M. Colquhoun, *Tetrahedron* **2008**, *64*, 8231.
[66] a) B. de Boer, M. M. Frank, Y. J. Chabal, W. Jiang, E. Garfunkel, Z. Bao, *Langmuir* **2004,** *20*, 1539; b) J. M. Beebe, J. G. Kushmerick, *Appl. Phys. Lett.* **2007**, *90*, 083117.

(or giving up) an electron. Obviously the redox mechanism can include some minor basic structural changes in the molecule, but, of course, the conformational mechanism, on its side, does not involve changing in the molecular charge. A required condition for a useful bistable molecule is that the energy barrier between the two states, ΔE_{act}, is much larger than the thermal energy k_BT (Figure 20).
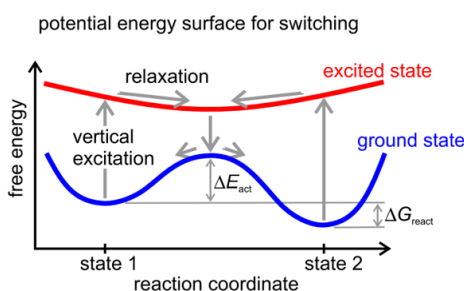
Figure 20: Potential energy surface for switching mechanism between two states.

Therefore, switching from one isomer to the other needs to overcome this barrier and two are the ways that can be taken. The molecule can be brought to an excited state, e.g. by illumination. This would result into a relaxation process over the excited potential energy surface (which mean on the top of the blue curve) and the probabilistic conversion into the other form. Clearly, that this could happen or not is a matter of probability. Alternatively, the probabilities may change noticeably when the molecule is attached to the electrodes. To this purpose, STM techniques become a powerful tool for the selective single molecule manipulation. Indeed, it is possible to directly drive the molecule over the ground state barrier by means of various tip-molecule interactions, such as the electric field, tunneling electrons or tip-molecule interaction forces. Therefore, STM can induce single molecule switching by different mechanisms: dipole switching, spin switching, conformational switching, charge switching, bonds switching, etc.

Liljeroth *et al.* presented an elegant example of conformational switching based on a structural isomerization mechanism.[67] By positioning the tip above a naphthalocyanine and increasing the bias

---

[67] P. Liljeroth, J. Repp, G. Meyer, *Science* **2007**, *317*, 1203.

above the LUMO resonance, the current-induced hydrogen tautomerization of the molecule results in the back and forth switching of the tunneling current between two well defined levels (Figure 21).
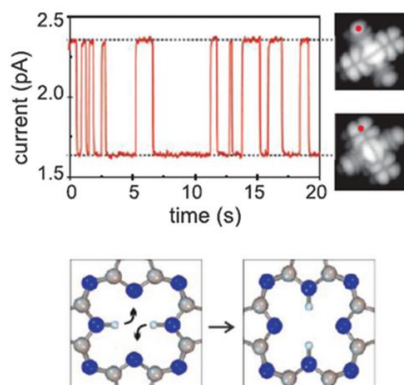
Figure 21: Up:(Left) Current-trace by tip-molecule interaction. (Right) Orbital images showing the orientation of the LUMO. Down: Scheme of the hydrogen tautomerization reaction responsible for the switching. Ref 66.

Wang *et al.*, on the other side, demonstrated a dipole switching mechanism through the conversion of a Sn ion, inside a tin phthalocyanine (SnPc) molecule adsorbed on Ag surface, between two conformations, Sn-up and Sn-down (Figure 22).[68]
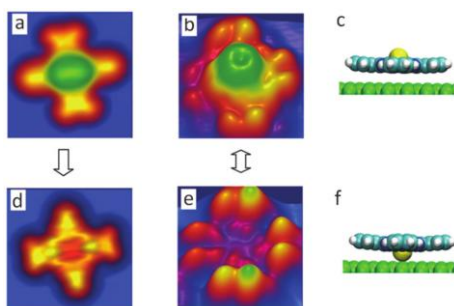
Figure 22: STM images of SnPc. The single arrow between (a) and (d) illustrates the irreversible switching from Sn-up to Sn-down conformations, while the double arrow between (b) and (e) illustrates the reversible switching. (c) and (f) correspond to a schematic representation of Sn-up and Sn-down respectively. Ref 67.

The mechanism postulated by Wang was that this switching occurs via hole attachment. The resonant tunneling from the highest occupied

[68] Y. Wang, J. Kroger, R. Berndt, W. A. Hofer, *J. Am. Chem. Soc.* **2009**, *131*, 3639.

molecular orbital (HOMO) of Sn^{2+} starts generating a transient oxidized Sn^{3+} state, smaller than Sn^{2+}. The applied negative pulse voltage supplies the required energy to move the Sn^{3+} under the substrate surface. Whilst, by applying a positive sample bias, the electron may deposit energy to vibrational degrees of freedom of the molecule thus allowing the backward switching process from Sn^{3+} to Sn^{2+}.

Another fascinating example of a switching process is the one presented by bipyridyl-dinitrooligophenylene–ethynylene dithiol (BPDN) molecule. By using MCBJ, Lörtscher *et al.* showed that it is possible to reversibly control the BPDN switching between two conductance states (Figure 23).[69]
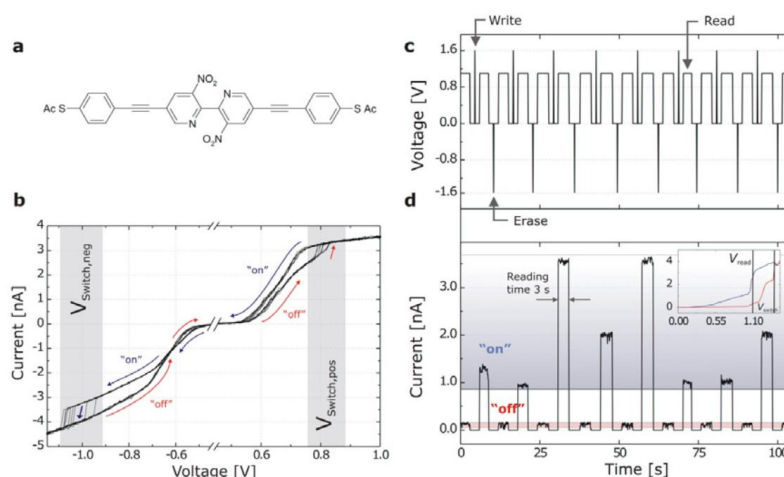
Figure 23: a) BPDN molecule under study with MCBJ. b) Hysteretic IV curves. A positive voltage switches the molecule from the initial OFF state to the ON state, while an applied negative bias reverse the process from ON to OFF state. c) and d) Memory operation based on the hysteretic IV curve. Ref 68.

They demonstrated that by controlling the switching behavior of a single BPDN, this molecule can be used as a memory element to write, read and erase bits by simple voltage pulses. They also performed the control study on a related molecule without the nitro groups demonstrating that it did not show any switching behavior. Anyway, despite the indication of the importance of the presence of the nitro

---

[69] E. Lörtscher, J. W. Ciszek, J. Tour, H. Riel, *Small* **2006**, *2*, 973.

groups, which is the exact mechanism regulating this switching process actually remains unclear.

Obviously, the ideal building blocks desired in molecular electronics are represented by molecules that can be reversibly switched between high and low conductance states. To this purpose, diarylethene (DAE), and derivatives, have always been seen as promising molecular units because of their peculiar structure and high lifetimes of the charge-separated states.[70] Such molecules, in fact, can be reversibly switched between an "on-off" state. The "off" state consists in the open form of the molecule characterized by an interrupted π-conjugated structure. Under UV light irradiation, instead, the open state can be switched to the "on" form corresponding to the closed fully conjugated structure. On the opposite, the backwards process is triggered by visible light. Recently, Sendler *et al.* reported the controlled *in situ* switching of DAE derivatives from their nonconductive to conductive state in contact to gold nanoelectrodes via controlled light irradiation (Figure 24).[71]
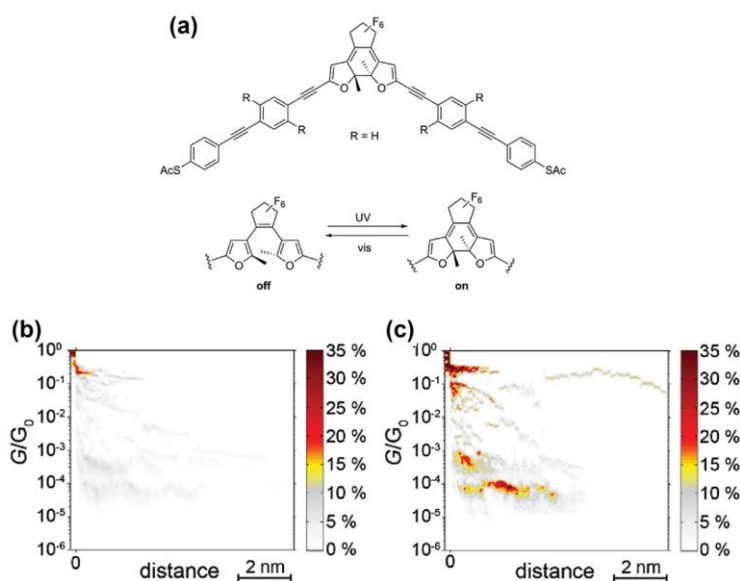
Figure 24: a) Photocromic switching process of the DAE structure designed by Sendler. b) and c) Conductance–distance traces respectively for the open ("off") and closed ("on") form. Ref 70.

[70] S. Castellanos, A. A. Vieira, B. M. Illescas, V. Sacchetti, C. Schubert, J. Moreno, D. M. Guldi, S. Hecht, N. Martín, *Angew. Chem. Int. Ed.* **2013**, *52*, 13985.

[71] T. Sendler, K. Luka-Guth, M. Wieser, W. J. Lokamani, M. Helm, S. Gemming, J. Kerbusch, E. Scheer, T. Huhn, A. Erbe, *Adv. Sci.* **2015**, *2*, 1500017.

They demonstrated that before UV irradiation, no clear and defined conductance plateaus are visible, due to the lack of fully π-conjugated molecular states. But, what happen after irradiation is that they start to observe defined conductance plateaus, which indicates a successful switching "on" of the molecular state.

Another interesting family of molecules which show a peculiar character of sensors and switches is the one formed by crown ethers derivatives. Crown-ether molecules are well known to selectively bind alkali atoms and an always greater variety of structures, belonging to the family of these compounds, is nowadays available and investigated.[72] The only area which remains to be explored is represented by their conductance properties. Anyway, some theoretical studies revealed that by incorporating these structures within wires, any change in electrical conductance of the wire upon binding would lead to discriminating sensing.

A pioneer theoretical work of Liu *et al.* in 2003, by using density functional theory (DFT) calculations showed how the conductance value of a short molecular wire containing a 18-crown-6 molecule connected via sulfur atoms to two long atomic gold wires changes drastically passing from the empty to the full form of the hole (Figure 25).[73]
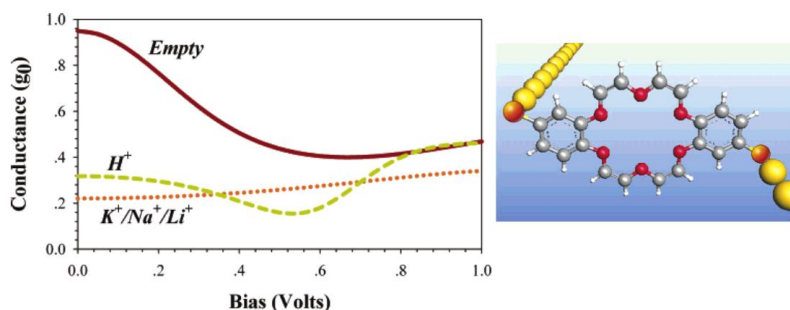
Figure 25: 18-crown-6 conductance values for the empty and complexed with different alkali metals forms. Ref 72.

---

[72] a) M. J. Marsella, T. M. Swager *J. Am. Chem. Soc.* **1993**, *115*, 25, 12214; b) P. V. Bernhardt, E. J. Hayes, *Inorg. Chem.* **2002**, *41*, 2892; c) J. Guo, J. Lee, C. I. Cu, N. C. Gallego, S. T. Pantelides, S. J. Pennycook, B. A. Moyer, M. F. Chisholm, *Nat. Commun.* **2014**, *5*, 5389; d) J. Li, D. Yim, W.D. Jang, J. Yoon, *Chem. Soc. Rev.* **2017**, *46*, 2437.
[73] C. Liu, D. Walter, D. Neuhauser, R. Baer, *J. Am. Chem. Soc.* **2003**, *125* , 13936.

More recently, instead, Ismael *et al.* using a DFT-based approach to quantum transport, studied the sensor potential abilities of single-molecule junctions formed by crown ethers attached to anthraquinone units, pinned to gold electrodes via alkyl chains.[74] Calculations showed that, due to a charge transfer from the ion to the molecular wire, the molecular resonances shift closer to the electrode Fermi energy and the conductance results enhanced by different amounts by changing the complexed alkali metal (Figure 26).
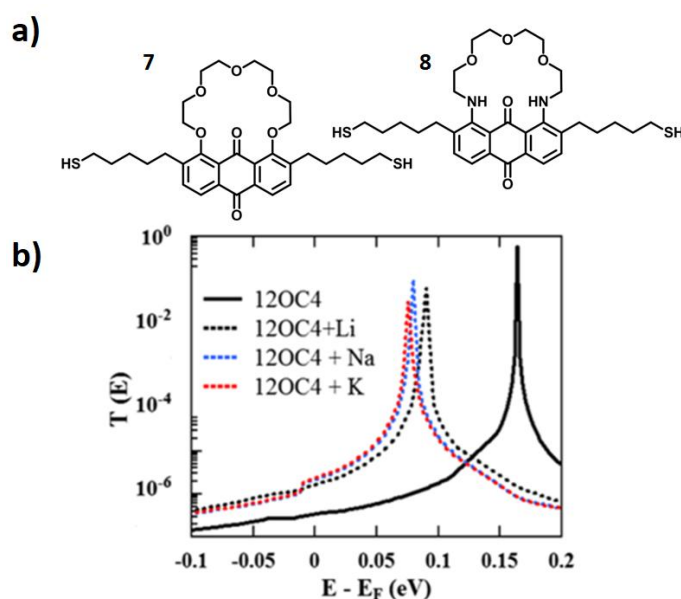
Figure 26: a) Anthraquinone molecular wires containing crown ethers. b) Transmission coefficient T(E) of **7** with different alkali metals. Ref 73.

On the other hand, Ponce *et al*. reported an interesting work studying the effect that a metal coordination has on the conductance of single molecular wires. MCBJ method revealed a variable metal coordination effect depending on the anchoring group. They investigated the conductance properties of a family of rigid, highly conductive ligands using acetylthiols, pyridines and ethynyl groups as anchors. Upon metal coordination, the molecular conductance of thiol and ethynyl

---

[74] A. K. Ismael, A. A. Jobory, I. Grace, C. J. Lambert, *J. Chem. Phys.* **2017**, *146*, 064704.

derivatives decreases, whereas that of pyridine derivatives increases (Figure 27).[75]
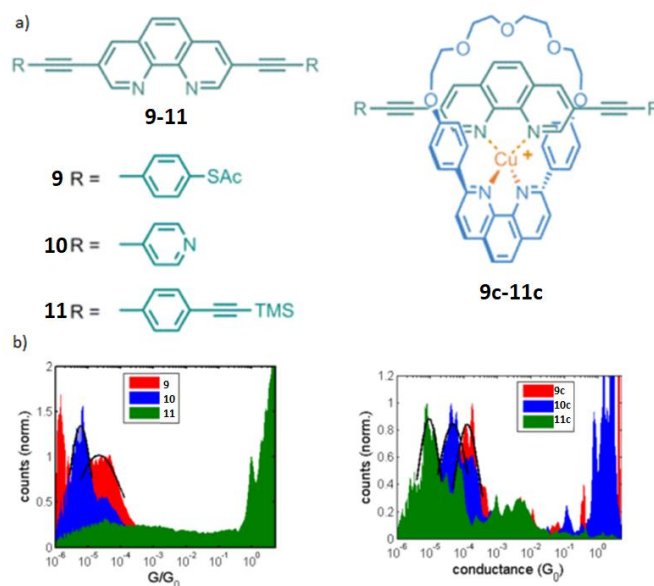
Figure 27: a) Chemical structures of molecular wires **9-11** and complexes **9c-11c**. b) Conductance histograms of the bare and complexed forms. Ref 74.

In conclusion, all the aforementioned experimental and theoretical findings reveal the degree of development achieved in the so-called molecular electronics and represent continuous and important steps toward the achievement of real molecular electronic devices for eventually realistic applications. However, as stated before, we are still far away from this ultimate goal.

---

[75] J. Ponce, C. R. Arroyo, S. Tatay, R. Frisenda, P. Gaviña, D. Aravena, E.Ruiz, H. S. J. van der Zant, E. Coronado, *J. Am. Chem. Soc.* **2014**, *136*, 8314.

3.   Objectives

2. Objectives

Based on the examples discussed in the previous section about the interesting opportunities displayed by non-covalent interactions, the main objective in the first part of this thesis focuses on the development of supramolecular wire structures whose electronic properties can be investigated and potentially exploited to obtain a functional molecular element of a circuit. In order to simplify the approach to this first chapter of the work, the next section is divided in two main parts involving amidinium-carboxylate and crown ethers, respectively, as common chemical functional groups.

- **Part 3.1.** *Amidinium-Carboxylate Based Supramolecular Wires.*

  In this section, we have carried out the synthesis of a new generation of molecular wires sharing the common feature of the amidinium-carboxylate non-covalent interaction as core bridge unit. Our proposal was centered on studying the conductance properties in two target series:

a) *Fullerene dumbbells series*, on one side, constituted by fulleropyrrolidines characterized by various molecular lengths and side chains of different nature (Figure 28).
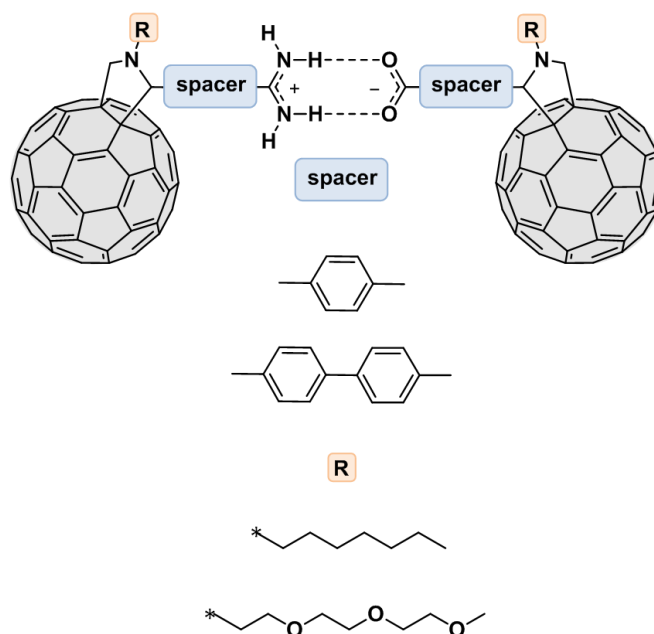
Figure 28: Scheme of the target fullerene dumbbells molecules.

b) *Linear supramolecular wires series*, on the other side, composed by aromatic derivatives characterized by different lengths and anchoring groups (Figure 29).
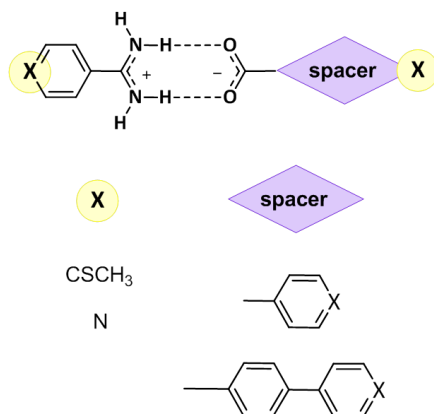
Figure 29: Linear supramolecular wire series based on aromatic compounds

- **Part 3.2.** *Crown Ethers Switching Systems as Supramolecular Wires.*

  This chapter focuses on the synthesis of functionalized linear crown ether structures as supramolecular wires with switching power conferred by the metal complexation. Inspired by the variable effect that a metal coordination has on the conductance of single molecular wires depending on their anchoring group[75] and the well-known potentialities of crown ethers as sensors and switches, we decided to investigate the only area which remained unexplored, their conductance properties.[73] Two consecutives projects have been addressed:

a) *Synthesis of 4,5'-diaminodibenzo[18]crown-6*, on one side, to investigate the electronic properties of a short molecular wire containing a 18-crown-6 ether connected via a primary amino group to two gold electrodes (Figure 30);
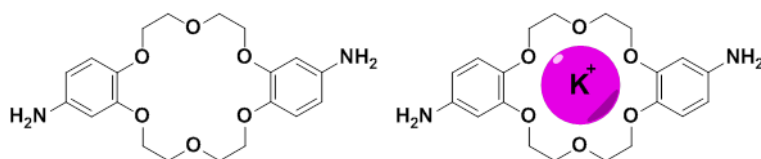
Figure 30: 4,4'-Diaminodibenzo-18-crown-6, (left) empty, and complexed with potassium (right).

b) *Synthesis of oligo(p-phenylene ethynylene) (OPE) and poly(p-phenylene)(PPP) crown ether molecular wires series*, on the other side, to study the effect of a metal coordination on these wire structures, where the crown ether moiety is not directly inserted in the π-conjugated system but laterally connected to the central unit. Different anchoring groups have been proposed to study the variable effect that the anchoring group could have on the conductance upon metal coordination (Figure 31).[75]
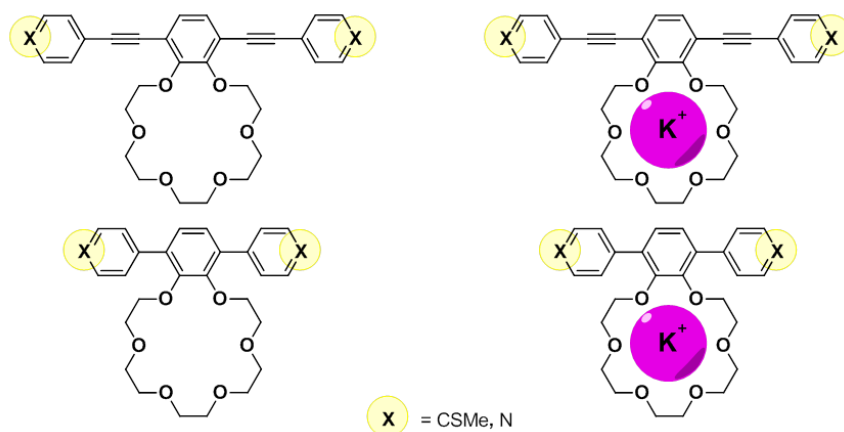
Figure 31: OPE and PPP crown ether wires series, (left) empty, complexed with potassium (right).

4.   Results and Discussion

3. Results and Discussion

3.1. *Amidinium-Carboxylate Based Supramolecular Wires*

Among the many possible ways to introduce hydrogen bonds, the choice of using the amidinium carboxylate salt bridge was dictated by the following different considerations: i) The two-point amidinium-carboxylate binding motif guarantees an extraordinary stabilization introducing a strong component of selectivity and directionality in the charge transfer process. ii) A previous work of our group focused on the efficiency of non-covalent donor-acceptor ensembles, composed by the interaction of a porphyrin-amidine and a fulleropyrrolidine-carboxylic acid.[55] iii) The exceptionally strong electronic coupling deriving from such binding, results in remarkably high values of association constant, even in polar solvents (up to 10^5 M^{-1} in THF), and more efficient formation of longer-lives radical-ion-pair states (~10 μs in THF). iv) A recent investigation of the aforementioned H-bonding motif was also realized in our group in 2016.[43] Interestingly, the molecular wire behaviour of such "supra-system", was described through the determination of its attenuation factor as a function of the growing length of the C_{60}-*p*-phenylene carboxylic acid oligomers. The extraordinary small *β*-value obtained (0.07±0.01 Å^{-1}) is among the lowest *β*-values reported in the literature.

3.1.1. *Fullerene Dumbbells Series*

Dumbbell-type molecules are symmetric compounds characterized by a typical dumbbell shape, where two identical molecular units are bridged through a spacer. Fullerene dimers, in which two [60]fullerene spheres are covalently connected through a molecular electroactive bridge, are therefore perfect example of dumbbell shape molecules. Dumbbells-shape covalent molecular wires based on fullerenes are synthetically achieved by bifunctional cycloaddition reactions to C_{60}, that means, a derivatization of C_{60} with bifunctionalized molecules.[76] The first non-covalent H-bonding C_{60}-dimer was firstly reported independently by Hummelen[77] and Martín.[78]

---

[76] J. L. Segura, N. Martín, *Chem. Soc. Rev.* **2000**, *29*, 13.

[77] M. T. Rispens, L. Sánchez, J. Knol, J. C. Hummelen, *Chem. Commun.* **2001**, *0*, 161.

[78] J. J. González, S. González, E. Priego, C. Luo, D. M. Guldi, J. de Mendoza, N. Martín, *Chem. Commun.* **2001**, *0*, 163.

The compounds proposed in this first part, are non-covalently linked through the two point H-bonding interaction of the functionalized aromatic units of the spacer. Therefore, a stepwise different synthetic strategy requires to be used. However, these compounds own some of the main desirable properties required for the study of molecular wires in a nanoscale approach. Among them, the stiffness, symmetry and linearity of their structures, besides, the visibility on a gold surface for the conductance experiments performed through STM setups, thanks to the bigger size of the fullerene in comparison to other significantly smaller anchoring groups.[11d,79]

3.1.1.1.   *Synthesis of Proton-Donor and Proton-Acceptor Fulleropyrrolidines*

2-Substituted   *N*-methyl-3,4-pyrrolidino[3,4:1,2][60]fullerenes (fulleropyrrolidines) are products easily achievable from the decarboxylation of the iminium salts derived from the condensation of substituted amino acids with different starting aldehydes (Scheme 1).
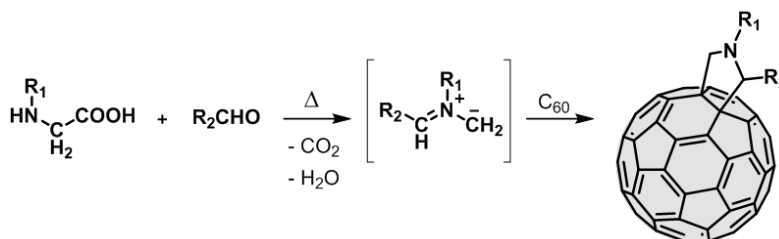
Scheme 1: 1,3-Dipolar cycloaddition of azomethine ylides to C_{60}.

The 1,3-dipolar cycloaddition of azomethine ylides to C_{60}, also known as "Prato's reaction", is among the several successful methodologies employed for the functionalization of fullerenes. It is a site-selective reaction, because the addition occurs only at a 6,6 ring junction.[80] The reaction is easily controlled to get the monoadduct compound, and the starting materials (substituted amino acids and aldehydes) are commercially available or readily synthesized from commercial

---

[79] a) C. A. Martin, D. Ding, J. K. Sørensen, T. Bjørnholm, J. M. van Ruitenbeek, H.S. J. van der Zant, *J. Am. Chem. Soc.* **2008,** *130*, 13198; b) K. Gillemot, C. Evangeli, E. Leary, A. La Rosa, M. T. González, S. Filippone, I. Grace, G. Rubio-Bollinger, J. Ferrer, N. Martín, C. J. Lambert, N. Agraït, *Small* **2013**, *9*, 3812.

[80] M. Maggini, G. Scorrano, M. Prato, *J. Am. Chem. Soc.* **1993**, *115*, 9798.

sources. Another noticeable advantage associated to this powerful methodology is that two functional chains can be simultaneously introduced (R_1 and R_2), offering the possibility to incorporate, in one step, the desired functionalities along with the role of increasing the solubility of the product. When R_2 is not hydrogen, a stereogenic centre is generated at the C_2 position in the pyrrolidine ring. Anyway, this is just a minor drawback, because it can jump out only when either R_1 or R_2 chains contain a chiral group, determining the production of diastereomeric mixtures.

Therefore, taking into account the previous Scheme 1, the desired final compounds were obtained as depicted in their retrosynthetic analysis (Scheme 2).
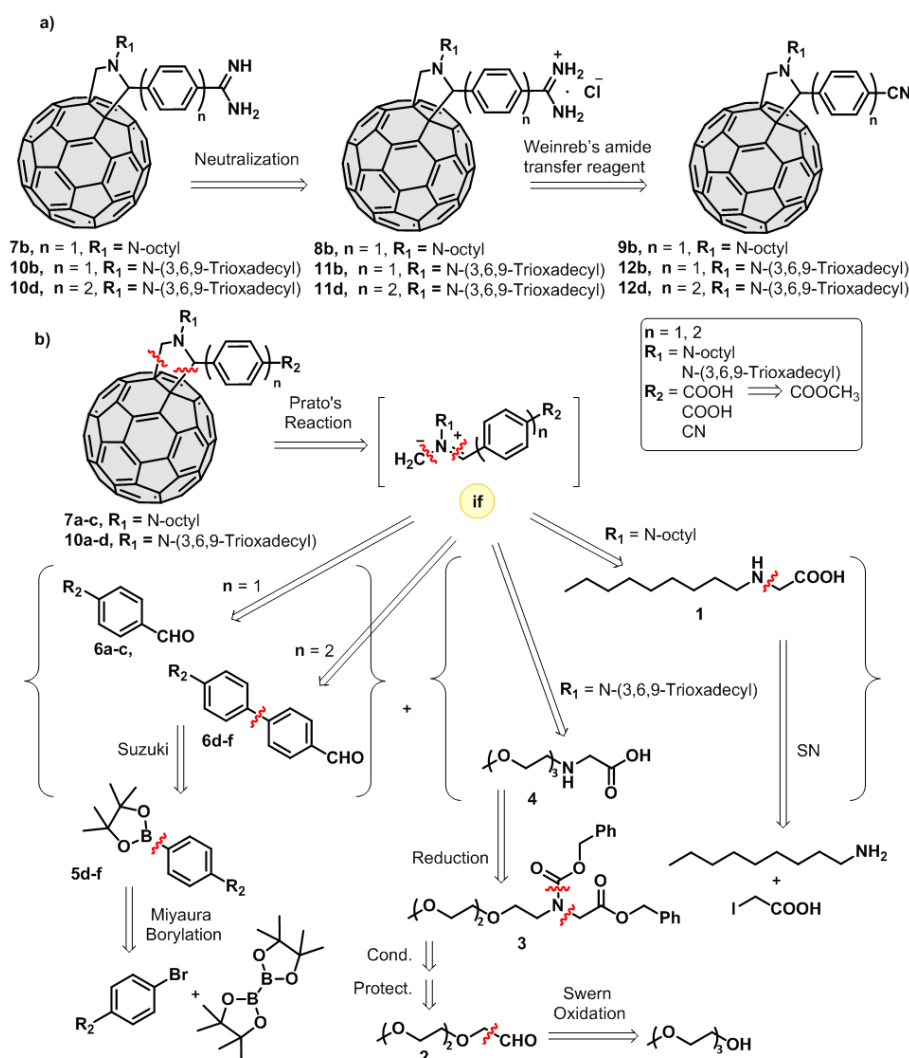
Scheme 2: a) Functional group synthesis of the H-donor fulleropyrrolidines. b) Retrosynthetic analytic chart of the target fullerenes dumbbells molecules.

55

The synthesis of the H-donor and H-acceptor fulleropyrrolidines can be separated in three main building blocks (Figure 32):

a. the side chains (R_1)

b. the skeleton of the spacer (*p*-phenylene backbone)

c. the functional groups (R_2)
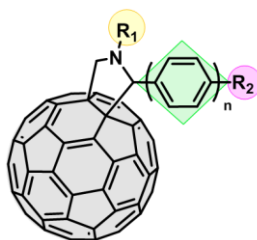
Figure 32: Main building blocks for the fullerene dumbbells.

a. Side Chains

The synthesis of the side chains (R_1) was achieved from the corresponding α-aminoacids: *N*-octylglycine and *N*-(3,6,9-trioxadecyl)glycine (Scheme 3).
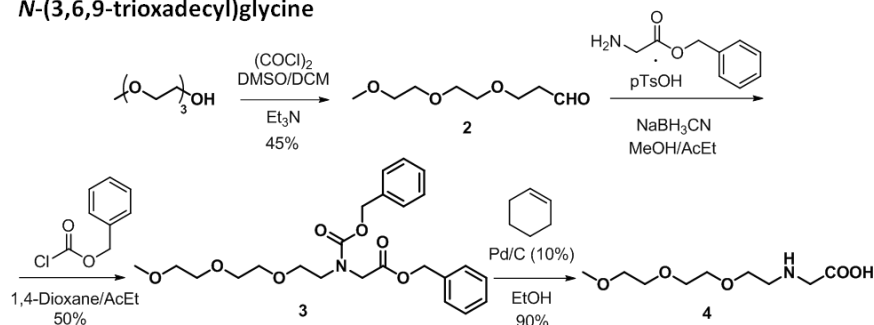
Scheme 3: Synthetic routes to the amino acids containing the side chains (R_1).

Initially, it was decided to synthesize the desired fulleropyrrolidines using a simple apolar-substituted α-amino acid. Hence, the choice was *N*-octylglycine, which is easily achievable in only one synthetic step.

The commercially available α-iodocarboxylic acid can be converted via substitution reaction to the α-amino acid **1**, through nucleophilic attack of commercially available octylamine, through its amino group.

In order to increase the solubility of the final compounds in more polar solvents, it was decided to introduce a more polar appendage consisting in a triethyleneglycol chain. The synthetic pathway employed to obtain the more polar α-amino acid consists in a three steps process. The synthesis starts with a Swern oxidation, reaction where the hydroxy group of the easily available triethyleneglycol monomethyl ether is converted into the aldehyde functionality of **2**. The following condensation of glycine benzyl ester with aldehyde **2** under reductive conditions ($NaBH_3CN$) yielded the *N*-Cbz-N-(3,6,9-trioxadecyl)glycine benzyl ester **3,** which was finally reduced, by hydrogenolysis of the benzyl ester, to the *N*-substituted glycine **4**.[81]

b.   *Spacer Skeleton*

The core structure of the wires consists on a *p*-phenylene backbone of 1 or 2 units. The longer skeleton is extended by a sequence of coupling reactions starting with a Miyaura borylation to obtain the *p*-functionalized phenylboronic acid pinacol esters **5d-f** (Scheme 4).
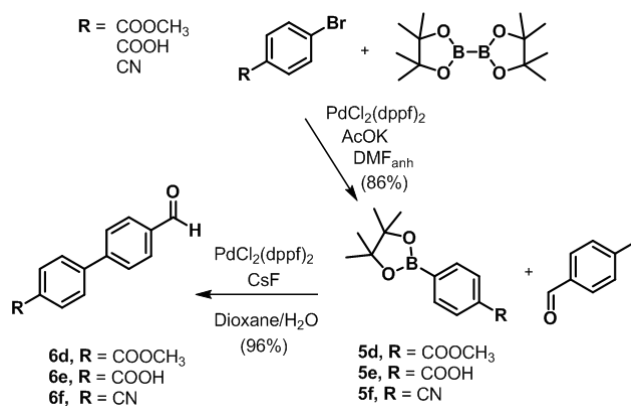
Scheme 4: Synthetic route to the elongation of the *p*-phenylene backbone.

The choice of using boronic esters instead of boronic acids is related to the instability of the latter in not truly anhydrous conditions. They tend

---

[81] T. Da Ros, M. Prato, F. Novello, M. Maggini, E. Banfi, *J. Org. Chem.* **1996**, *61,* 9070.

to trimerize generating cyclic boroxines.[82] Therefore, the commercial starting materials methyl 4-bromobenzoate, 4-bromobenzonitrile and 4-bromobenzoic acid are coupled with bis(pinacolate)diboron to obtain the corresponding phenylboronic acid pinacol esters **5d**-**f**. The latter are then reacted with 4-iodobenzaldehyde in a Pd catalysed Suzuki coupling reaction to obtain the final 4'-formyl-[1,1'-biphenyl]-4-substituted products **6d**-**f**. At this point, compounds **6a**-**f** are employed in the condensation, through Prato's reaction, with *N*-octylglycine **1** or *N*-(3,6,9-trioxadecyl)glycine **4** and C$_{60}$ to give, respectively, the [60]fullerene dumbbells **7a**-**c** and **10a**-**d** (Scheme 5).

6a, R$_2$ = COOCH$_3$
6b, R$_2$ = COOH
6c, R$_2$ = CN
6d, R$_2$ = H$_3$COOC—⟨biphenyl⟩—

6e, R$_2$ = HOOC—⟨biphenyl⟩—

6f, R$_2$ = NC—⟨biphenyl⟩—

7a, R$_1$ = N-octyl, **R$_2$ =** COOCH$_3$
7b, R$_1$ = N-octyl, **R$_2$ =** CN
7c, R$_1$ = N-octyl, **R$_2$ =** H$_3$COOC—⟨biphenyl⟩—

10a, R$_1$ = N-(3,6,9-Trioxadecyl), **R$_2$ =** COOH
10b, R$_1$ = N-(3,6,9-Trioxadecyl), **R$_2$ =** CN
10c, R$_1$ = N-(3,6,9-Trioxadecyl), **R$_2$ =** HOOC—⟨biphenyl⟩—

10d, R$_1$ = N-(3,6,9-Trioxadecyl), **R$_2$ =** NC—⟨biphenyl⟩—
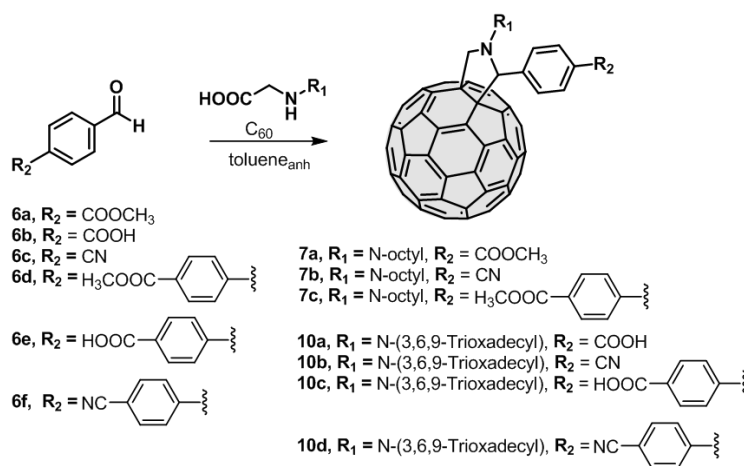
Scheme 5: Fulleropyrrodines' synthesis.

c.   Functional Groups

The 4-(1-octyl-3,4-fulleropyrrolidin-2-yl) methyl ester derivatives **7a,c** were hydrolysed under basic conditions to achieve the respective acid functionalities of the final products **8a,c** (Scheme 6).

---

[82] D. G. Hall, *Boronic Acids: Preparation and Applications in Organic Synthesis and Medicine,* Wiley-VCH Verlag GmbH & Co. KGaA., **2006**.
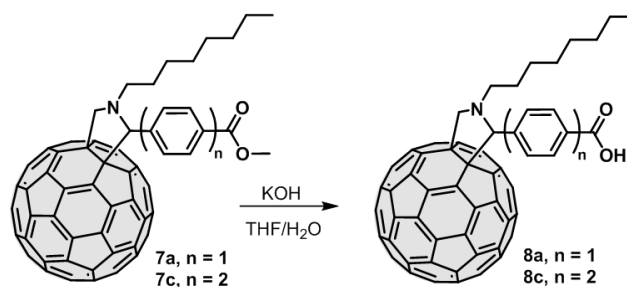
Scheme 6: Hydrolysis of 2-(4-methoxycarbonylphenyl)pyrrolidino[3,4:1,2][60]fullerene.

The nitrile group of fulleropyrrolidines **7b** and **10b,d** also requires a further treatment to give the desired conversion into the final amidine products. This final step consists in an adjustment of Garigipati's method[83] by using the Weinreb's amide transfer reagent (Scheme 7).[84]
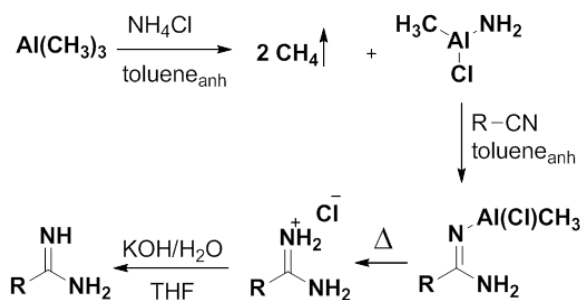
Scheme 7: Amidine synthesis from Weinreb's amide formation.

The active transfer agent is achieved from the interaction of trimethyl aluminium and ammonium chloride in warm anhydrous toluene under evolution of methane. The nitrile group of the fulleropyrrolidines with 1 or 2 phenylene units readily attacks the methylchloroaluminium amide giving rise to the formation of an aluminium complex, which evolves to the amidinium chloride species under heating. The final basic hydrolysis of the latter compounds transforms the salts into the corresponding neutral desired amidines (Scheme 8).

[83] R. A. Garigipati, *Tetrahedron Lett.* **1990**, *31*, 1969.
[84] J. I. Levin, E. Turos, S. M. Weinreb, *Synthetic Communications* **1982**, *12*, 989.
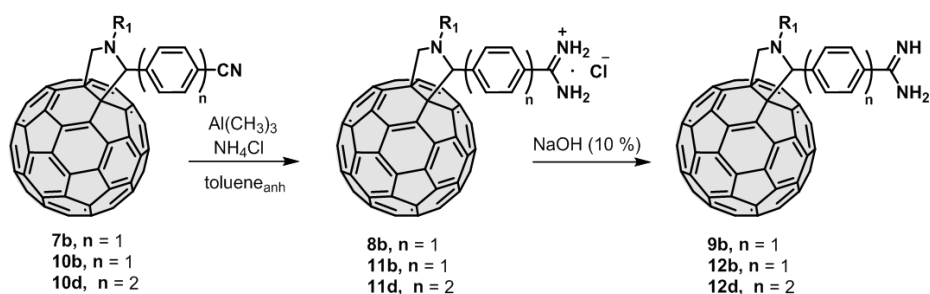
Scheme 8: Synthesis of amidine-containing fulleropyrrolidine derivatives.

All new products were satisfactorily characterized by standard analytical and spectroscopic techniques. A reliable proof for the successful conversion of the nitrile function into the amidinium group is the disappearance of the characteristic band of CN group at 2228 cm^{-1} in the FTIR spectra of compounds **8b** and **10b,d**. Additionally, the appearance of a double peak around 3393 and 3457 cm^{-1}, corresponding to the asymmetric and symmetric stretching bands of primary amines, part of the amidinium group, confirms this conversion. Interestingly, other characteristic features of the amidinium-containing fulleropyrrolidines can be identified. The wagging band of amine group (-NH$_2$) between 649 and 910 cm^{-1}, the scissoring band of the same group at 1646 cm^{-1} and the sp^3 stretching bands of the carbons bonded to hydrogen (C-H) at 2855 and 2923 cm^{-1}, evident identification of the glycolic chain. As an example, the compared FTIR spectra of molecules **10b** and **12b** are shown in Figure 33.
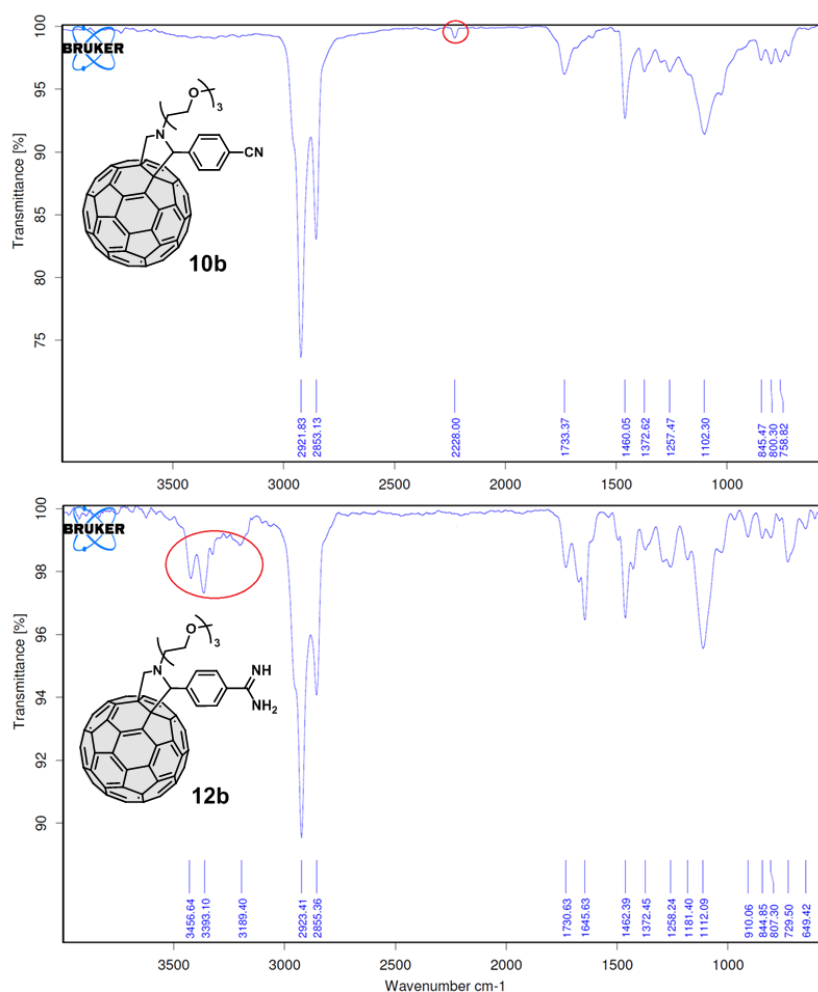
Figure 33: Comparison of FTIR spectra of compounds **10b** and **12b**.

3.1.1.2.   *Formation and Characterization of Supramolecular Ensembles*

Complexation of the supramolecular ensemble was realized starting from the neutral form of the amidinium-containing fulleropyrrolidines. Once converted by basic hydrolysis to the corresponding amidine molecular structures, proton donor compounds **9b** and **12b,d** were complexed with the proton acceptor molecules **8a,c** and **10a,c** (Figure 34).
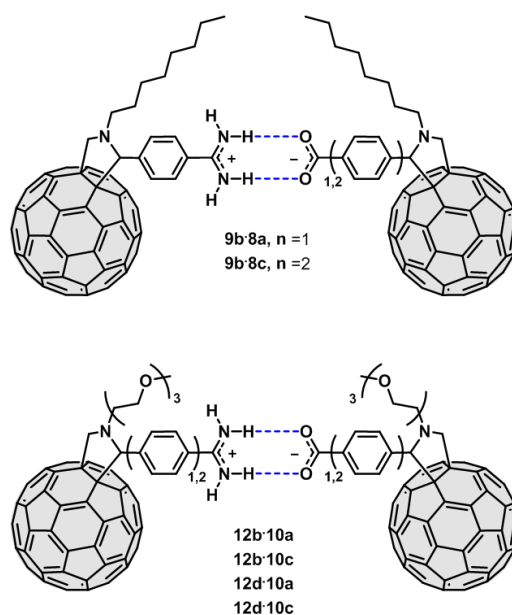
Figure 34: Supramolecular dumbbell-type fulleropyrrolidine complexes
9b·8a,c and **12b,d·10a,c**.

Considering the hydrogens involved in the supramolecular interaction as axial hydrogens (NH_{ax}) and the hydrogens external to the two point connection as equatorial hydrogens (NH_{eq}) then, the creation of the complexes results evidently confirmed by the shift of the amidinic moiety's protons. The clear signature of salt bridge formation is the concentration-dependent downfield shift of amidinium protons involved in hydrogen bonding to carboxylate (NH_{ax} shifts around 0.3 ppm after addition of one equivalent of the carboxylic acid fulleropyrrolidine) and the insensitivity of the chemical shift for the amidinium protons external to the salt bridge (shift of NH_{eq} is smaller than 0.03 ppm). In Figure 35, the qualitative ^{1}H NMR spectra of the isolated molecules **10a** and **12d** and the corresponding supramolecular complex formed at equimolar concentration[85] is shown as representative example.

---

[85] It was firstly recorded the ^{1}H NMR spectra of amidinium half **10a** by preparing a solution of the compound at 10^{-3}M in CHCl$_3$. Following, an equivalent quantity of the carboxylic unit **12d**, corresponding to a 1:1 ratio, was added. The resulting solution of the complex **12d·10a**, at the final concentration of 10^{-3}M in CHCl$_3$, was formed by
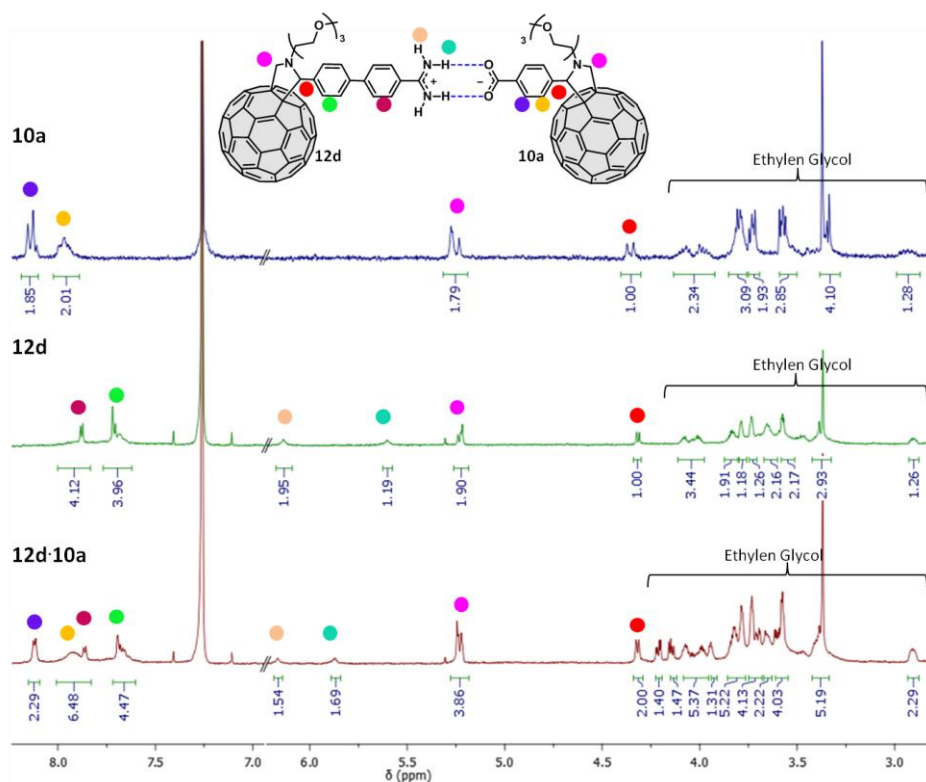
Figure 35: ^{1}H NMR (CDCl$_3$) spectra of **10a** and **12d** together with the corresponding supramolecular complex formed at equimolar concentration **12d·10a.**

Complete assignment of the protons was realized with additional HMQC, COSY and DEPT experiments.

3.1.1.3.   *Supramolecular Ensembles: Physical Characterization*

Physical analysis has allowed a further insight into the characterization of the products and their non-covalent complexes. The morphological study of these supramolecular assemblies on highly ordered pyrolytic graphite (HOPG) supports by drop deposition revealed the sample's structure dependence on its molecular concentration. Specifically, AFM experiments demonstrated the formation of supramolecular aggregates. The size of these aggregates varies increasing the concentration of the

light sonication of the mixture to favour the solubilisation of the proton acceptor moiety into the proton donor solution and finally analyzed.

preformed supramolecular complexes (at 1:1 ratio)[86] which were deposited. Final clusters of variable size between 6 and 20 nm were visible at higher concentration, passing first through the creation of islands of molecules, whose fusion led to one-molecule thickness monolayers (Figure 36).
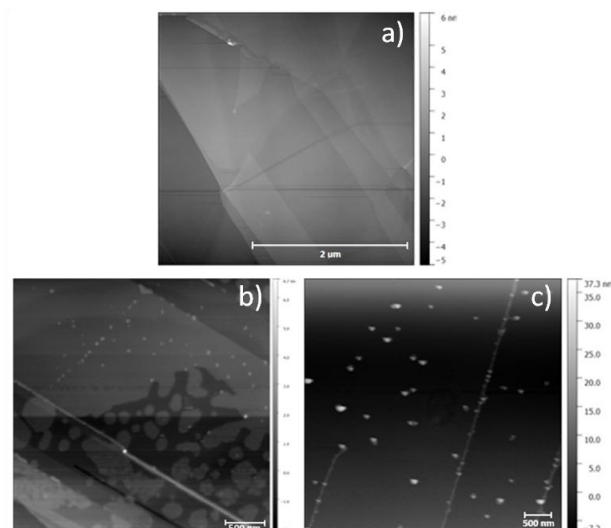
Figure 36: AFM morphological analysis of HOPG blank (a) and AFM imaging of the supramolecular complex **9b·8a** at 10^{-6} M (b) and 10^{-5} M (c) deposited on HOPG.

Due to the limited solubility of the *N*-octylglycine derivatives, it was impossible to perform further analysis related to their conductance properties. This was the main reason why we decided to change the side chain, using the more polar amino acid *N*-(3,6,9-trioxadecyl)glycine. This change produced the desired increase in the solubility of the products, allowing to test their electronic properties as supramolecular hydrogen bonded wires. The conductance properties of these non-covalent ensembles were proved by STMBJ measurements, carried out separately before complexation on the amidinium and

---

[86] The 1:1 solutions of **9b·8a** and **9b·8c** were prepared by mixing the volumes' solutions of the corresponding proton donor and proton acceptor compounds at the final concentration of 10^{-6}M and 10^{-5}M in CHCl$_3$. Each solution of the preformed complexes was deposited by drop casting method on the surface of the HOPG sample. The solvent on the samples was dried by evaporation in a preheated oven at 60°C overnight and then analyzed at AFM.

carboxylate derivatives on the one hand and the whole supramolecular assembly on the other hand (Figure 37).[87]
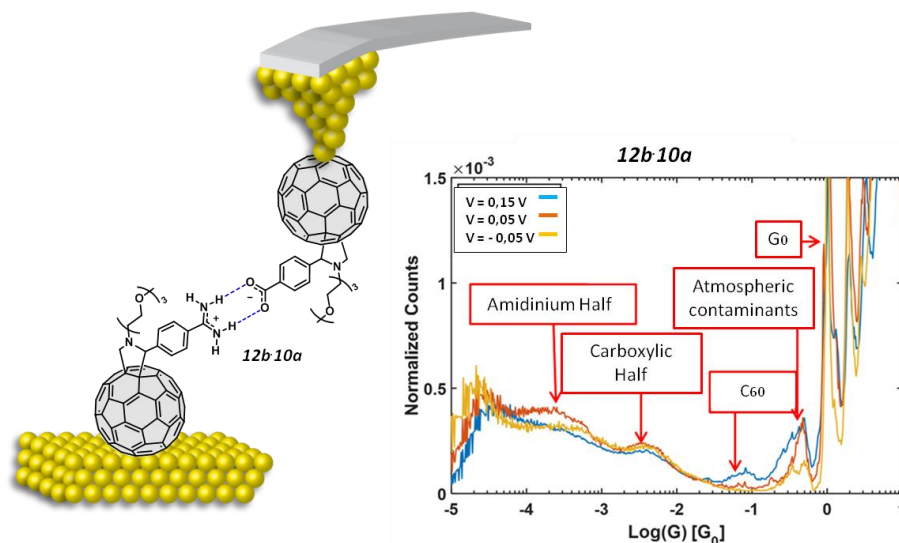
Figure 37: STMBJ of the supramolecular fulleropyrrolidines **12b·10a**. The G_0 peak identifies the conductance of one Au atom between the electrodes.

From the deposition on gold of different samples of diluted solutions of both the amidinium and carboxylate compounds, two conductance peaks could be identified. The first of these conductance peaks, at higher value of G_0, is assigned to the conductance of the C_{60} moiety and the second one, at lower value of G_0, to the molecules connected through the amidine and the carboxylic acid anchoring groups. The STMBJ measurements of the preformed complex (Figure 37) evidenced only the presence of the separated halves (the amidinium and the carboxylate compounds) but not the peak relative to the supramolecular complex itself, probably because the conductance value results lower than the noise cut off of the set up and should, therefore, be smaller than 10^{-5} G_0. Anyway, as visible from Figure 37, the amidinium half **12b** of the complex shows that the conductance associated to the peak

---

[87] The 1:1 solutions of **9b·8a** and **9b·8c** were prepared by mixing the corresponding volumes of the proton donor and proton acceptor compounds at the final concentration of 10^{-6}M in $CHCl_3$. The solution of the separated halves (each one at a concentration of 10^{-6}M in $CHCl_3$) and the preformed complexes were deposited by drop casting method on the surface of a gold sample. The samples were dried by evaporating the solvent in air and then analyzed at STMBJ.

of the functional group is quite high. Therefore, this result interestingly paves the way to the investigation of the amidiunium/amidine functionalities as efficient and unexplored anchoring groups in molecular electronics.

3.1.2. *Linear Supramolecular Wires Series*

This chapter stemmed from the necessity to get a deeper understanding about the two point amidinium-carboxylate interaction as supramolecular alternative connection to the covalent bonding in molecular wires. Therefore, we decided to synthesize really basic systems, whose key strength exactly relies on a linear design to facilitate the investigation and understanding of conductance properties through their wire structure. To this purpose, the initial choice was to use two well-known aurophilic groups, pyridine (Py) and thiomethyl ether (SMe) as the anchoring groups. Physical conductance measurements revealed lately that the pyridine derivatives result inappropriate to study the ET properties by STMBJ, because we were not able to detect neither the signal of the isolated molecules nor the complex.

3.1.2.1.   *Synthesis of Proton-Donor and Proton-Acceptor Moieties for Linear Supramolecular Wires*

The synthesis of the desired products requires just few steps to obtain both the corresponding amidine derivatives and the carboxylic extended structures (Figure 38).
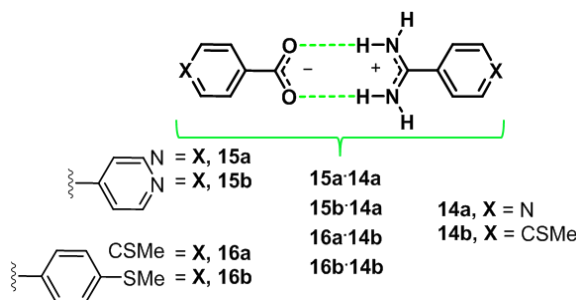
Figure 38: Linear supramolecular wires series **15a,b·14a** and **16a,b·14b**.

Starting from the commercial precursors, 4-(methylthio)benzonitrile and 4-pyridinecarbonitrile, the amidine derivative **14a,b** were obtained through the direct conversion of the nitrile group through its reaction

with the preformed methylchloroaluminium complex, by following the adjusted Garigipati's method[83] previously described for the synthesis of the dumbbells wires series, followed by the neutralization step with NaOH (Scheme 9).
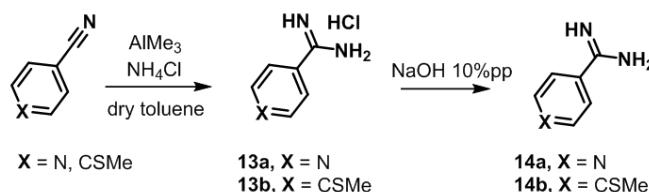
Scheme 9: Amidine synthesis of the pyridine and (methylthio)phenyl derivatives.

On the other side, 4-(methylthio)benzoic acid and isonicotinic acid are products directly available from commercial sources. Furthermore, the spacer structure was easily expanded through a Pd catalysed Suzuki cross-coupling reaction. The potassium pyridine- and (methylthio)phenyl- 4-trifluoroborate salts were coupled with 4-bromobenzoic acid to give the corresponding carboxylic biphenyl derivatives (Scheme 10).
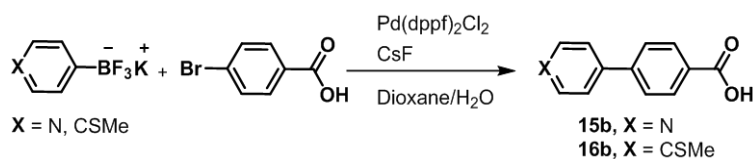
Scheme 10: Suzuki coupling to achieve the carboxylic biphenyl derivatives of both anchoring groups.

The construction of the supramolecular systems was realized in the same way that the formation of fulleropyrrolidine based non-covalent assemblies. The assembly of the tailored molecular building blocks leads to the final desired linear molecular wires (Figure 39).
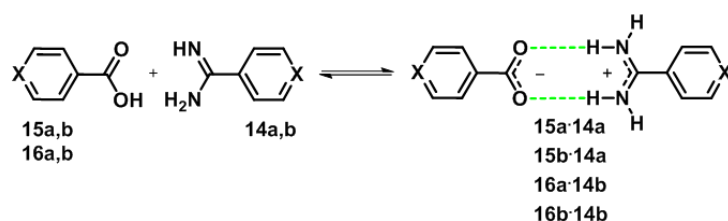
Figure 39: Complexes formed from the pyridine and thiomethylether derivatives.

67

Because it was not possible to study the conductance properties of the supramolecular wire series having pyridines as anchoring groups, only the thiomethyl ether series was completed with the synthesis of an additional compound, which was employed as reference (Figure 40).
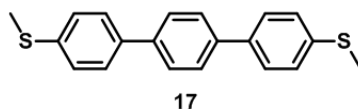
Figure 40: Refence compound **17**.

The 4,4"-bis(methylthio)terphenyl **17** was identified as the most similar covalent compound to compare the conductance of the supramolecular ensemble **16a·14b**. The synthesis was achieved by following one-step procedures.
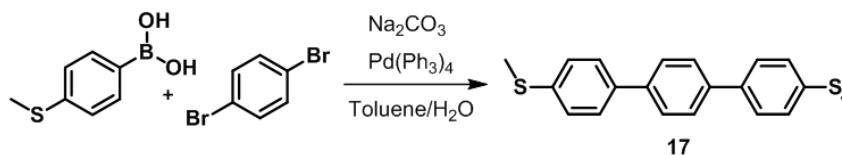
Scheme 11: Synthesis of the reference compounds **17**.

Molecule **17** was obtained by a Suzuki cross-coupling reaction between the commercial products 4-(methylthio)phenylboronic acid and *p*-dibromobenzene[88] (Scheme 11b). All intermediates, reference compounds and final complexed products were unambiguously characterized by standard spectroscopic and analytical techniques (see experimental section).

3.1.2.2.   *Formation and Characterization of Supramolecular Ensembles*

Complexation studies of supramolecular ensembles were carried out by monitoring the changes observed in the chemical shifts (δ) of the proton signals of the amidinium moiety **14b** after addition of increasing quantities of the carboxylic derivatives **16a,b**. Both titration experiments for the formation of the complexes **16a·14b** and **16b·14b**

---

[88] Y. Joseph, A. Peic, X. Chen, J. Michl, T. Vossmeyer, A. Yasuda, *J. Phys. Chem. C* **2007**, *111*, 12855.

perfectly show how the CH resonance of the protons of the aromatic ring close to the amidinium group undergo a downfield shift upon increasing the addition of the carboxylate derivatives. These downfield shifts give evidence of the formation of a positive charge in the amidinium group by interaction with the carboxylate (Figure 41).
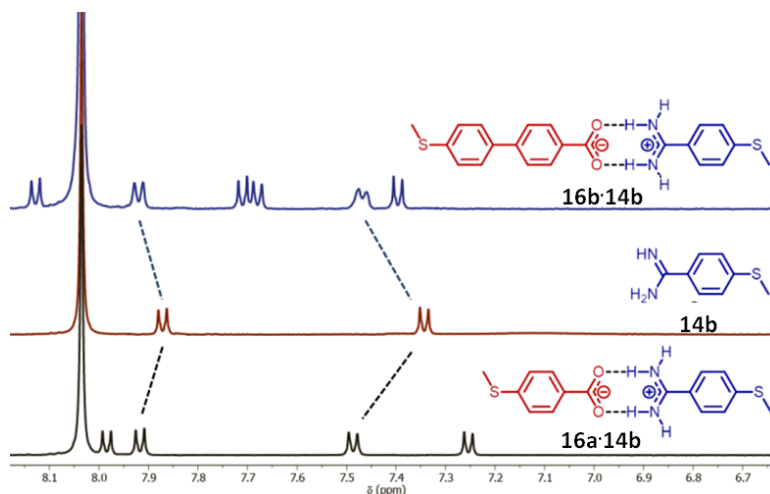
Figure 41: Partial ^{1}H NMR of **14b** (middle) and the 1:1 supramolecular complexes **16a·14b** (down) and **16b·14b** (up) in [D$_7$]DMF.

The titration analyses were conducted at room temperature and/or, in some cases, lowering the temperature below zero Celsius degrees. The decision to decrease the temperature is related to the equilibrium nature of supramolecular forces. In fact, the reduction of molecular vibrational degrees permits to block molecules in their more stable conformation. The determination of the association constant of the complex was carried out by ^{1}H NMR titration experiments. Because of the well-known strength of the amidinium-carboxylate interaction[55] and that, as stated by data from literature,[89] the limit for NMR titration experiments corresponds to around $10^5 \, M^{-1}$, it was necessary to use a solvent whose polarity was high enough to decrease the value of the corresponding association constant. Therefore, the choice of the solvents were [D$_7$]DMF and [D$_6$]DMSO. [D$_7$]DMF qualitative titration experiments show the clear appearance of the signal relative to the amidinium

---

[89] a) C. S. Wilcox, *Frontiers in Supramolecular Organic Chemistry and Photochemistry*, H. J. Schneider and H. Dürr, VCH, Weinheim, 1991, pp. 123–144; b) P. Thordarson *Chem. Soc. Rev.* **2011**, *40*, 1305.

protons involved in the supramolecular interaction. It appears as a broad band changing its width and position with the guest concentration, whose equatorial and axial hydrogen atoms can be resolved by decreasing the temperature to -15 °C (Figure 42).
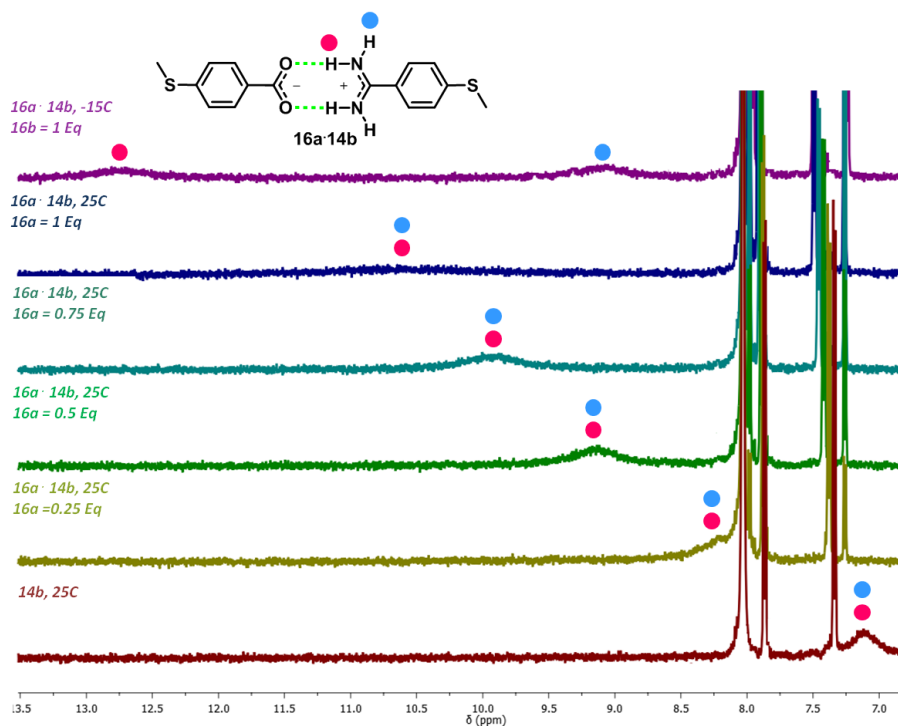
Figure 42: Protons shift and resolution at -15°C of the amidinium moiety of compound **11b** in titration experiments in [D$_7$]DMF for the complex **16a·14b**.

The shift of this broad signal (from ~7.1 to ~9.9 ppm for **16a·14b**), corresponding to the amidinium protons, evidences that the supramolecular interaction is effectively formed. On the other hand, the quantitative titration experiments of the wires complexes **16a·14b** and **16b·14b**, carried out in [D$_6$]DMSO, allowed to determine K$_a$ values $\geq$ 10^4 M^{-1} for both complexes.[90] This result, achieved in so polar solvent, clearly reveals the extraordinary strength of the supramolecular assembly for this specific amidinium-carboxylate units.

---

[90] See in Annex *Titration Section* for more details.

3.1.2.3.   *Supramolecular Ensembles: Physical Characterization*

Since the main interest of this part of the thesis relies on the investigation and understanding of the ET processes in single molecular systems characterized by weak supramolecular interactions, an accurate physical characterization of the final products was carried out. Separate measurements of charge transfer features of the single units and the pre-formed complexes were conducted in ambient conditions by using a made-in-house STM. The molecules and their complexes were deposited on commercial gold over glass substrates, which serve as the first electrode, while the gold tip (freshly cut from a gold wire), acting as the second electrode of the STM, was repeatedly moved vertically (z) in and out of contact with the substrates covered by molecules. Several thousands of individual conductance (G) traces *vs.* tip displacement (z) traces were recorded. Regions of constant conductance (plateaus) at values below 1 G_0 indicating the formation of a stable molecular junction between the STM tip and substrate were identified in these traces. But because this does not occur in all the G *vs.* z traces, in order to discriminate the molecular-junction signature, the traces with plateaus were separated from those without them. The results of the many breaking traces, that complied with the previous criterion, were gathered in a conductance histogram, which presents peaks at the conductance of the most probable configurations, and that is normally considered to be the conductance of a single-molecule junction. Also 2D-histograms of G *vs.* z traces were built giving valuable information about the breaking length, which is related to the length of the molecule. Firstly the amidine half **14b** and the complementary carboxylic unit **16a**, of the short methylthio-containing wire complex **16a·14b** were studied, separately. 1D and 2D conductance histograms were built with approximately a 15-20% of all the recorded traces for both compounds (Figure 43).
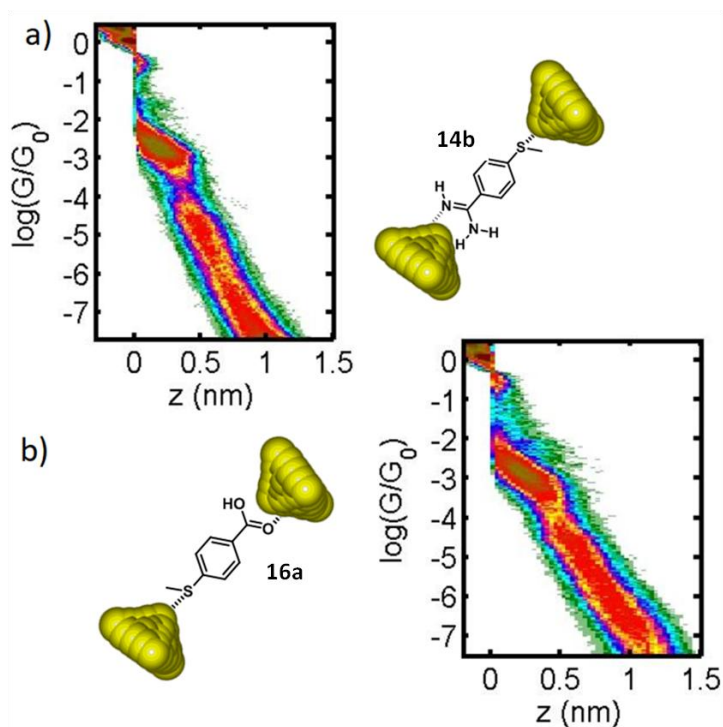
Figure 43: 2D conductance histograms versus relative distance *z* of a) the amidine derivative **14b.** and b) the carboxvlic half **16a.**

While the results for the carboxylic derivative agree with the previously reported in the literature,[91] the results presented here for the amidine compound results again, as for the fulleropyrrolidine supramolecular wires, interestingly high and comparable with the one of the carboxylic unit, which in turn is commonly known to be a good anchoring group. Therefore in the present thesis it is shown for the first time that the amidine group can be as efficient linker to gold as the carboxyl group. Figure 43 clearly shows that the conductance values obtained for both compounds are very similar. In particular, a main conductance value of $\log(G/G_0) = -3.0\pm0.9$ for the carboxylic derivative and $\log(G/G_0) = -2.8\pm0.5$ for the amidine one, where the error is given by the width at half maximum of the peaks observed in the conductance histograms. The typical length of the plateaus for the amidine and carboxylic halves was also determined (0.84 and 0.95 nm, respectively), resulting in good

---

[91] S. Ahn, S. V. Aradhya, R. S. Klausen, B. Capozzi, X. Roy, M. L. Steigerwald, C. Nuckolls, L. Venkataraman, *Phys. Chem. Chem. Phys*. **2012**, *14*, 13841

agreement with the expected theoretical length for each compound of ~0.68 nm. At this point, the measurements carried out on the short methylthio-containing wire complex **16a·14b** evidence the presence of two plateaus of different lengths, one at high and the other at low values of G_0, centered at $\log(G/G_0)$ = -6.1±0.7 and -3±0.4 (Figure 44).
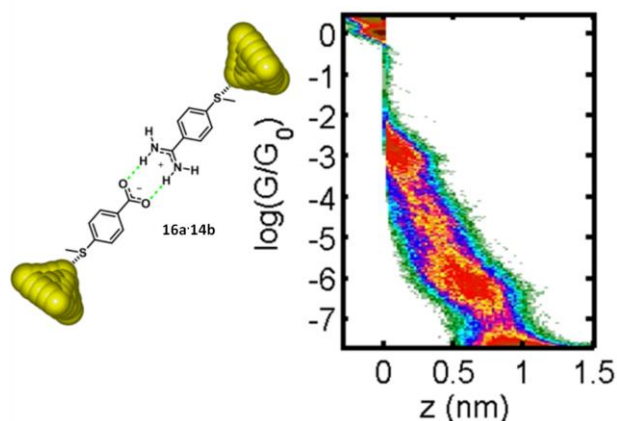
Figure 44: 2D conductance histogram *vs.* relative distance *z* of **16a·14b.**

In order to see these two peaks more clearly, two groups were made with the obtained traces, separating those that have plateaus in the low conductance range (Low-G) from those that do not (High-G). After this separation, the corresponding length distributions for the high and low conductance plateaus were obtained, with typical maximum length values of 0.74 nm (High-G plateaus) and 1.45 nm (Low-G plateaus) (Figure 45).
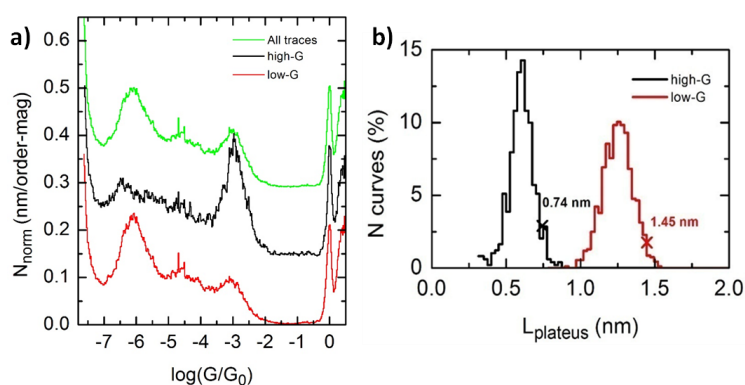
Figure 45: a) All the 1D conductance histogram traces of the complex **16a·14b**, compared with the two separated groups at Low-G and High-G. b) Length distribution of the Low-G and High-G plateaus separately, taking into account the gold retraction after the gold contact breakage.

These results led us to conclude that the low conductance plateaus, almost doubling the length of the shorter plateau, are due to the molecular junctions formed by the whole complex, while the high conductance plateaus can be due to any of the two halves, which would result from the breakage of the complex, which seems to be partially happening when the complex is deposited over the gold STM substrate.

In order to estimate the efficiency for electron conduction of the amidine-carboxylic interaction, the results for the amidine-carboxylic complex **16a·14b** were compared with those for the terphenyl used as reference compound **17** (Figure 46).
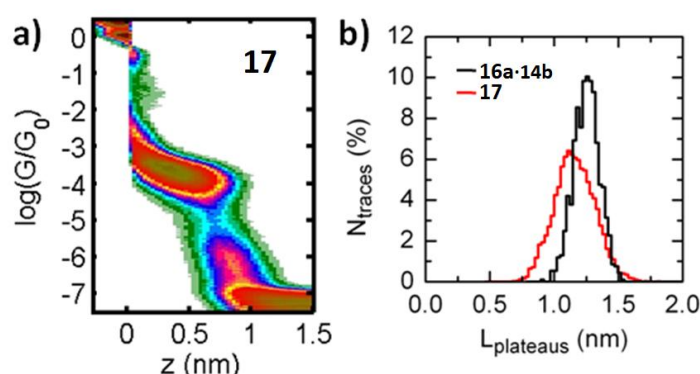
Figure 46: a) 2D conductance histogram *vs.* relative distance z of **17**. b) Plateaus length distribution comparison of molecule **17** with the complex **16a·14b**.

While the length of the plateaus for the amidine-carboxylic complex is only slightly longer, their conductance is more than two orders of magnitude lower, as for compound **17** a conductance of $\log(G/G_0) = -3.7 \pm 0.7$ was obtained. Therefore, the conductance value found for the complex results unexpectedly low respect to the previous studies about CT in supramolecular DBA systems connected by the amidinium-carboxylate interaction.[55,56] A possible explanation for this result can be related to the mixed nature of the linkage in the amidinium-carboxylate interaction, which is not merely based on hydrogen bonding interaction but also on electrostatic forces due to the charge separation. Therefore, this charge separation can, in principle, interrupt the CT process along the wire.

Finally, it was also studied the longer supramolecular complex **16b·14b**. In Figure 47 the 2D histogram for all the traces with plateaus were shown.
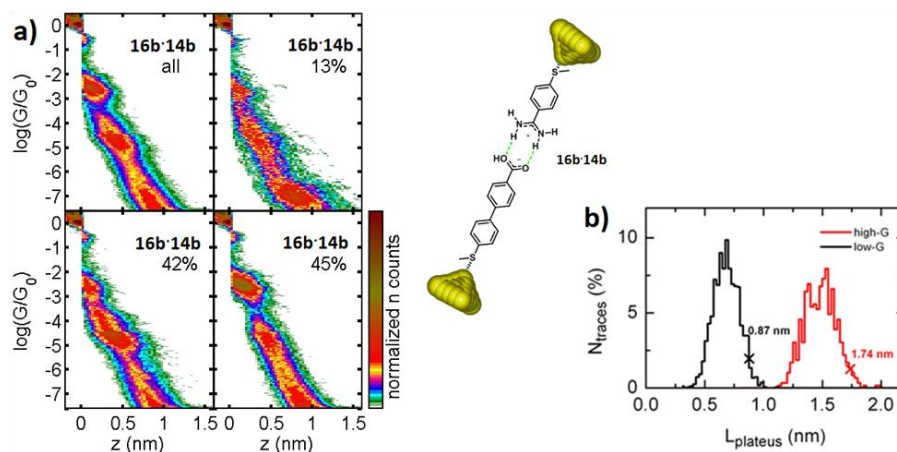
Figure 47: a) 2D histograms versus for **16b·14b** (all histograms present an artifact at -4.5 due to the use of an IV converter with two amplification stages with high gains). b) The length distribution of the Low-G and High-G plateaus, separately, shows the correspondence of the shorter plateaus to conductance of the amidine derivative **14b**.

The highest peak, centered at $\log(G/G_0) = -2.7 \pm 0.4$, are equivalent to those observed in the shorter complex and were assigned to the amidine derivative **14b**. On the other hand, the lowest-G plateaus having a main conductance of $\log(G/G_0) = -7.0 \pm 0.6$ and a typical maximum length of 1.7 nm, were assigned to junctions formed by the whole longer amidine-carboxyl complex **16b·14b**. This reduction of one order of magnitude (from $\sim 10^{-6}G_0$ to $\sim 10^{-7}G_0$) between the short and long complexes corresponds to a calculated decay factor β of 2. This value, compatible with the decay factor reported in the literature for amine-oligophenyl compounds of 1.7 per added phenyl ring,[25] therefore, results in agreement with the elongation of the system. Indeed, when we deposited only the carboxylic part **16b** of the longer complex, the same decay in conductance respect to the carboxylic half **16a** of the short complex **16a·14b** was observed. Figure 48 shows the former plateaus at a mean conductance of $\log(G/G_0) = -4.0 \pm 0.6$.
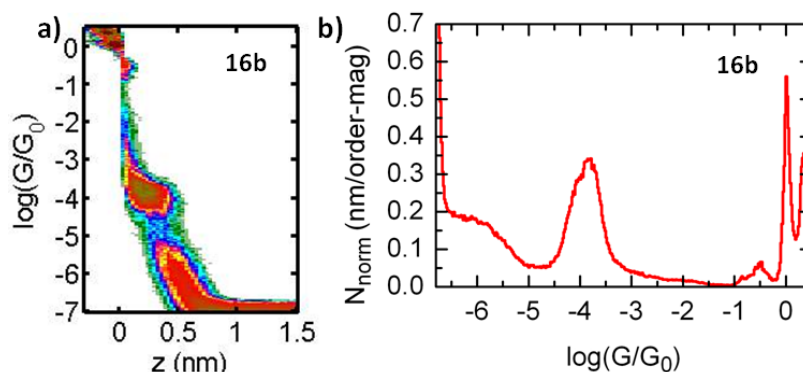
Figure 48: 2D and 1D conductance histograms versus relative distance z of the longer wire complex **16b** (a) and (b), respectively.

Summarizing, the results of low conductance for the methylthio ether complexes discouraged the possibility to further investigate the other pyridine linear wire series. In fact, measurements of the conductance of the complexes formed by the interaction of the pyridine derivatives (**15a·14a** and **15b·14a**) did not afford any results. Due to the smaller size of the compounds in comparison to the methylthio ether analogues and the proved low conductance of the last ones, it resulted extremely difficult for the pyridine appended smaller complexes to identify any plateaus in the STMBJ experiments.

3.1.2.4.   *Theoretical Calculations of Supramolecular Ensembles*

To understand the low and high conductance behaviour of the STMBJ experiments for the different molecular junctions, electronic structure and transport calculations were also performed. Density functional theory (DFT) was used in combination with the non-equilibrium Green's function (NEGF) formalism.[92] DFT+Σ method[93] was also employed, to avoid the self-interaction errors and image charge effects, introduced by DFT at the hybrid molecule-metal interfaces. First, the electronic structure of the molecules **14b** and **16a** and of the complexes **16a·14b** and **16b·14b** were analyzed in the gas phase (Figure 49).

[92] F. Pauly, J. K. Viljas, U. Huniar, M. Häfner, S. Wohlthat, M. Bürkle, J. C. Cuevas, G. Schön, *New J. Phys.* **2008**, *10*, 125019.

[93] S. Y. Quek, L. Venkataraman, H. J. Choi, S. G. Louie, M. S. Hybertsen, J. B. Neaton, *Nano Lett.* **2007**, *7*, 3477.
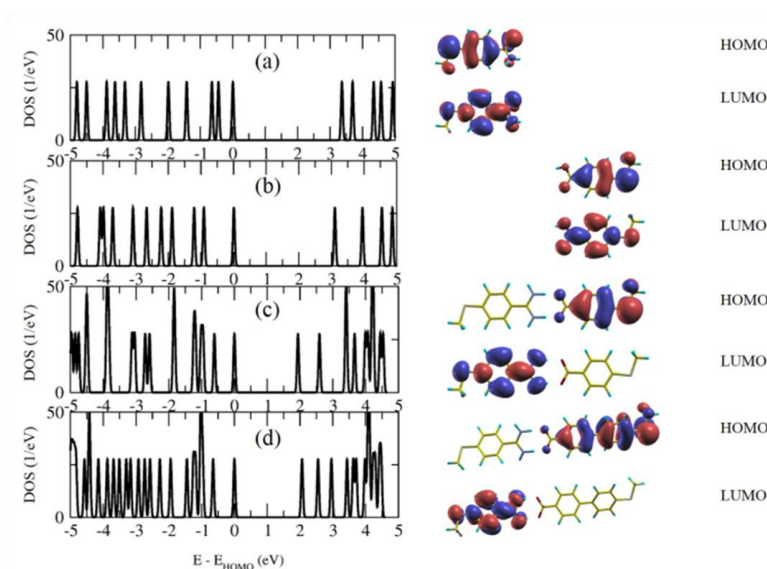
Figure 49: Calculated density of states (DOS) of the free molecules (a) **14b**, (b) **16a**, (c) **16a·14b** and d) **16b·14b**. For each molecule, in addition, the spatial distributions of HOMO and LUMO orbital wave functions were presented. Isosurfaces of positive and negative isovalues are shown in red and blue, respectively.

The calculated HOMO-LUMO gaps at the DFT level were found to be about 3 eV for **14b** and **16a**. These gaps were reduced to about 2 eV in the case of **16a·14b** and **16b·14b**, since the molecular complexes are obviously longer. The calculated binding energy for the assembly **16a·14b**, which forms from **14b** and **16a**, was found to be -0.94 eV. Moreover, it results that the HOMO and LUMO of the short complex **16a·14b** was localized on the **16a** and **14b** parts, respectively.

Next step has consisted in the metal-molecule-metal junctions construction. Here molecules and complexes bridge two Au electrodes. After exploring various possible binding configurations, the lowest energy configurations were determined to be S and N, S and O, S and S, S and S binding to undercoordinated Au atoms on both sides for **14b**, **16a**, **16a·14b** and **16b·14b**, respectively, as shown in Figure 50.
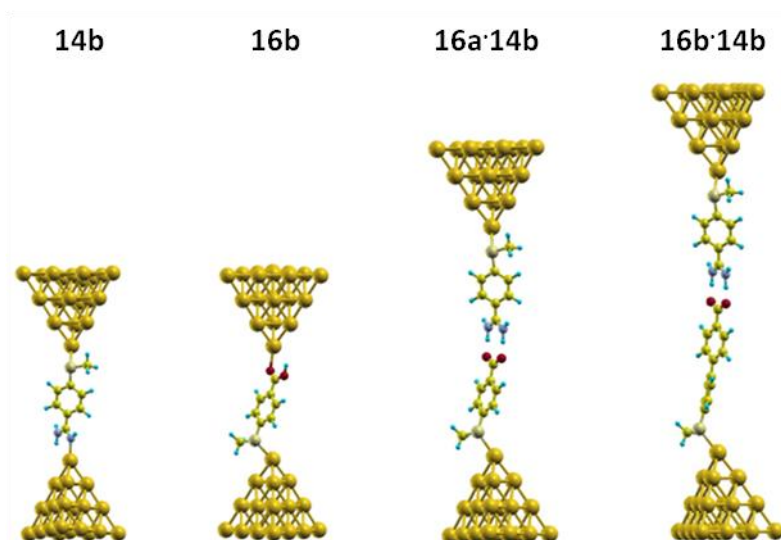
Figure 50: Optimized ground-state geometries of the four different molecular junctions with C in yellow, H in light blue, S in white, N in blue and O in red.

These findings are in agreement with previous studies on carboxylic and methylsulfide molecular junctions.[94] Low conductance values for the molecular junctions formed by the compounds **14b**, **16a**, **16a·14b** and **16b·14b** were derived with the DFT+Σ method. (Table 3)

Table 3: Calculated conductances by DFT and DFT+Σ methods compared with the experimental results.

	G_{DFT}	$G_{DFT+Σ}$	G_{exp}
14b	1.2×10^{-2}	1.2×10^{-3}	10^{-3}
16a	8.8×10^{-3}	4.6×10^{-4}	10^{-3}
16a·14b	2.5×10^{-5}	1.0×10^{-6}	10^{-6}
16b·14b	2.0×10^{-5}	5.0×10^{-7}	10^{-7}

These results suggest a rather big mismatch between the Fermi level of Au and both the HOMO and LUMO levels of the products (Figure 51).

---

[94] D. L. Bao, R. Liu, J. C. Leng, X. Zuo, Y. Jiao, Z. L. Li, C. K. Wang, *Phys. Lett. A* **2014**, *378*, 1290.
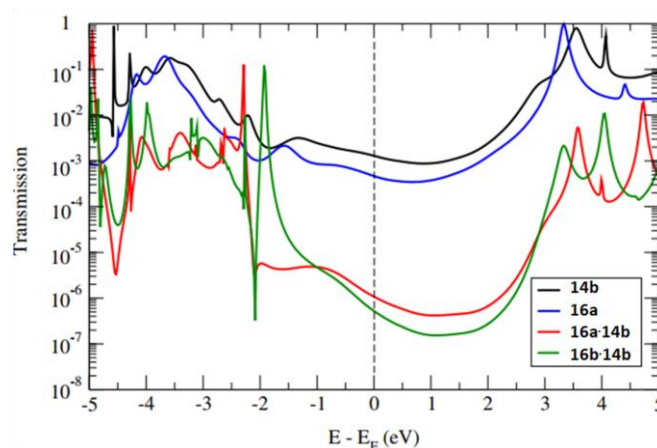
Figure 51: Energy dependent electronic transmission probability relative to EF, calculated by the DFT+Σ method.

These transmission curves evidence that molecular transmission resonances occur far away from the Fermi energy (E_F). While the transmission curves for **14b** and **16a** exhibit a rather similar behaviour, the conductance of **14b** is a factor of about 3 larger than that of **16a**. Visibly, a much lower conductance for the wires complexes **16a·14b** and **16b·14b** is observed. This reduction is attributed to the longer size of the molecular complexes and an off-resonant transport. In Figure 51 it can also be identified a Fano anti-resonance at about -2 eV with respect to the Fermi level for **16b·14b**. This is considered related to an interference effect between a localized molecular orbital and a delocalized one. Overall, the conductance calculated by the DFT+Σ method agrees well with the experimental values, while DFT overestimates the experimental conductances by about one order of magnitude. Therefore, theoretical calculations are in agreement with the experimental study, demonstrating that the high conductance values measured correspond to molecular junctions formed by only one of the two halves (**14b**, **16a**) while the low conductance features, to the molecular junctions formed by the whole complex (**16a·14b** or **16b·14b** respectively).

3.2. *Crown Ethers Switching Systems as Supramolecular Wires*

Crown ethers are ring shape molecular structures containing several ether groups. Their discovery (awarded later in 1987 with the shared Nobel Prize in Chemistry together with Donald J. Cram and Jean-Marie

Lehn) was performed by Charles J. Pedersen in 1967, at DuPont, while he was trying to prepare a complexing agent for divalent cations.[95] Part of his research included the design of a synthetic route toward the bis-phenol depicted in Scheme 12. However, a secondary by-product was obtained as white crystals insoluble in hydroxylic solvents due to incomplete protection of starting catechol.[96]
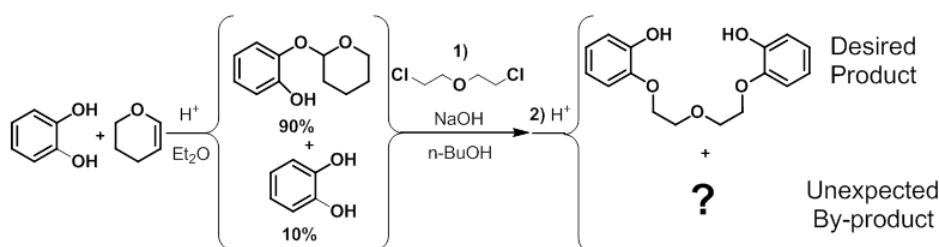
Scheme 12: The first crown ether obtained as by-product.

Luckily, Pedersen further investigated this by-product discovering that it was a biphenol derivative composed by a 18-membered ring able to accommodate cations in the hole located in the centre of the molecule. The molecular model of dibenzo[18]crown-6 (DB18C6) shows in all its evidence the exactitude of the chosen name to define these systems, which, due to their extraordinary ability to surround the bonded cation, behave as a crown do wreathing the head of a king (Figure 52).
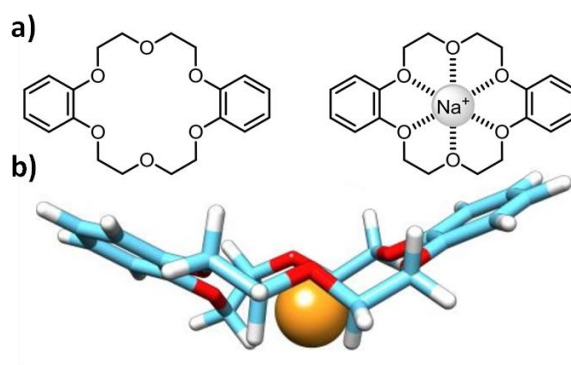
Figure 52: a) The first crown ether synthesized, DB18C6, in its empty and complexed form. b) Molecular model of DB18C6·Na$^+$ complex.

[95] C. J. Pedersen, *J. Am. Chem. Soc.*, **1967**, *89*, 2495.
[96] C. J. Pedersen, *J. Inclusion Phenom.* **1988**, *6*, 337.

Therefore, the most significant property of crown ethers consists in their use as hosts for binding inorganic and organic guests, especially cationic ones.[97] The stability of the formed complexes arises from ion-dipole interactions, when complexing metallic cations, or H-bonds, when complexing ammonium cations. This interaction is maximized when the diameter of the unsolvated ion fits exactly the size of the crown ether. However, complexation can be achieved even if the fit is not optimal. If the crown is too large, it can wrap around the cation or can also complex several ions. While, if the crown is too small, it can forms a sandwich system consisting of two crown ethers per cation.[95] Therefore, our interest focuses clearly in taking advantage of their peculiar ability to create stable but reversible supramolecular structures towards the synthesis of wire systems, characterized by a switching power conferred by this ion-dipole interaction. The substantial aim of this chapter, as these systems are already widely investigated, goes in the direction of studying the only aspect remained unexplored, "*how their CT properties can be modulated by this phenomenon of complexation*".

3.2.1. *Trans-4,5'-diaminodibenzo[18]crown-6*

The first project developed in this direction was the synthesis of a simple short molecular wire containing a 18-crown-6 ether connected via amino groups to two gold electrodes (Figure 53).
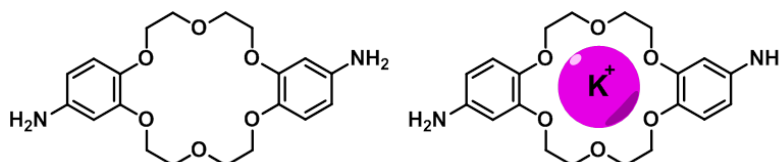
Figure 53: 4,5'-diaminodibenzo[18]crown-6 in its empty and complexed form.

The synthesis of this system was carried out on the basis of a theoretical investigation of 2003 where the same molecular structure, varying just for the anchoring group used, is studied from the point of view of its electronic properties, by complexing with different cations (Li^+, Na^+, K^+ and H^+).[75] This theoretical work found that the cationic

---

[97] C. J. Pedersen, *J. Am. Chem. Soc.* **1967**, *89*, 7017.

binding significantly lowers the conductance in comparison to the empty form of the crown ether, due to quantum mechanical interference effects. Furthermore, a striking insensitivity of conductance to the type of ligand is predicted. A recent theoretical work of Lambert group also demonstrated that the spectrum of responses from molecules with different crown-ether side groups supplies a fingerprint which can be used for discriminating sensing of alkali metals.[74] Therefore we decided to carry out an experimental work to study this conductance switching behavior of crown ethers. We decided to examine the effect of the only flawless fitting K^+ cation, whose ionic radius of 1.38 Å, perfectly accommodates in the cavity of 18C6, having a radius of 1.34-1.43 Å.[98]

3.2.1.1.   *Synthesis of trans-4,5'-diaminodibenzo[18]crown-6*

To achieve the product **18**, a one step reduction from the commercially available *trans*-4,5'-dinitrodibenzo[18]crown-6, using hydrazine hydrate and nickel Raney as the catalyst, allows to get the final product (Scheme 13).
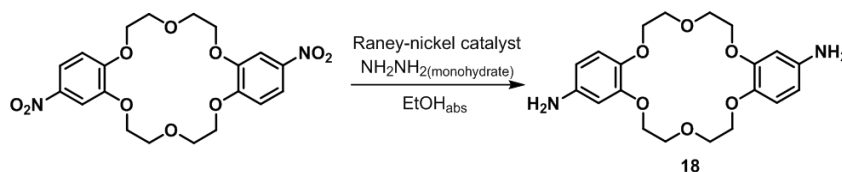
Scheme 13: Synthesis of *trans*-4,5'-diaminodibenzo[18]crown-6

The product was fully characterized by standard spectroscopic and analytical techniques. ^{1}H NMR analysis of **18**, for example, shows a broad signal around δ= 2.74, corresponding to the protons of the amine groups, absent in the starting product. The FTIR spectrum of **18** also showed the characteristic double peaks of primary amines at 3246–3424 cm^{-1} (Figure 54).

---

[98] N. K. Dailey, in R. M. Izatt and J.J. Christensen (Eds.), *Synthetic Multidentate Macrocyclic Compounds*, Academic Press, New York, **1978**, 207.
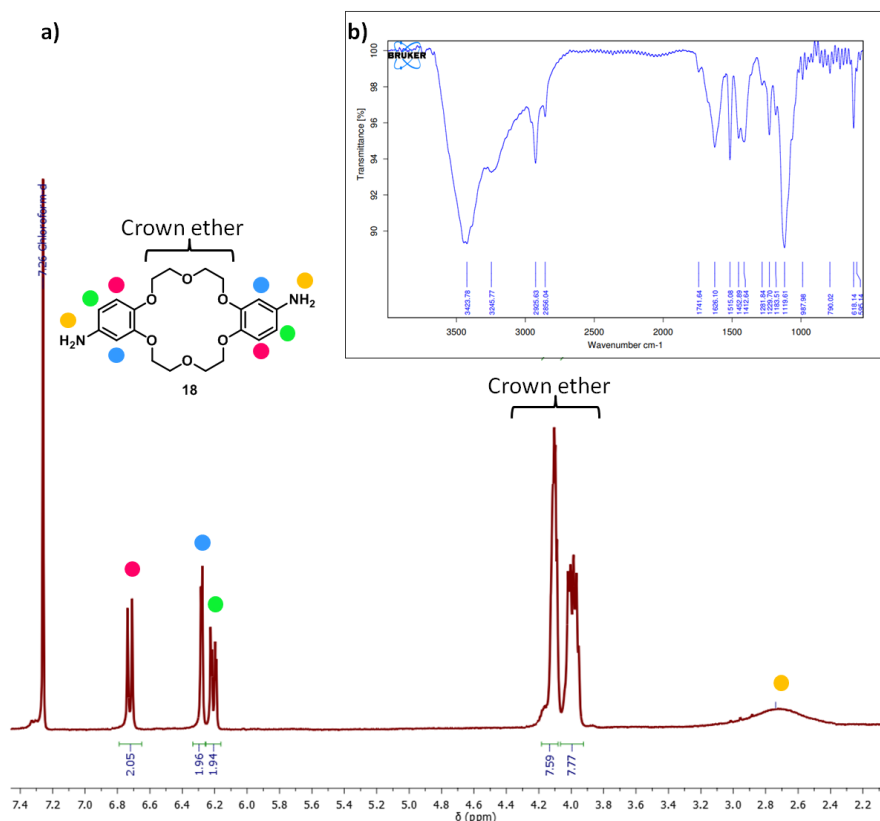
Figure 54: a) ^{1}H NMR spectrum in CDCl$_3$ and b) FTIR spectrum of **18**.

Anyway, once the empty crown ether **18** was analyzed by STMBJ technique, unfortunately, the measurements did not evidence any conductance signal. This finding, unexpected from the theoretical study, was justified attending to the lack of conjugation between the two aromatic systems.

3.2.2. *Oligo-phenylene ethynylene (OPE) and Poly(p-phenylene) (PPP) Crown Ether Molecular Wires Series*

The previous results have prompted us to think about a new design for the development of molecular wires including crown ether moieties as a switching unit. We propose a different molecular organization, where it was avoided that the positioning of the crown ether could interrupt the π-conjugation along the structure. Therefore, we decided to synthesize fully conjugated OPE and PPP derivatives, where the crown ether ring

is located as pendant on the benzene's central unit while at the extremities of the wire structure two well-known anchoring groups, the pyridine and the methylthio ether were used. This design was thought to help in evidencing the variations of conductivity produced by metal coordination on systems whose CT properties are renowned. Moreover, the study of the two different anchoring groups offers the possibility to demonstrate the effect that metal coordination has on molecular conductance for each anchoring group, as shown by Ponce's work.[75]

3.2.2.1.   *Synthesis of OPE and PPP Crown Ether Molecular Wires Series*

The OPE and PPP crown ether molecular wires derivatives were obtained as depicted in their retrosynthetic analysis. (Scheme 14) The key steps towards the OPE (**25a**,**b**)[99] and PPP (**26a**,**b**) derivatives are, respectively, Pd catalyzed Sonogashira reaction from derivatives **24** and **20a**,**b** and a Suzuki coupling from derivatives **24** and the commercial boronic acids of pyridine and 4-methylthio benzene (Scheme 14).

[99] Y. L. Zhao, L. Liu, W. Zhang, C. H. Sue,Q. Li, O. Š. Miljanić, O. M. Yaghi, J. F. Stoddart, *Chem. Eur. J.* **2009**, *15*, 13356.
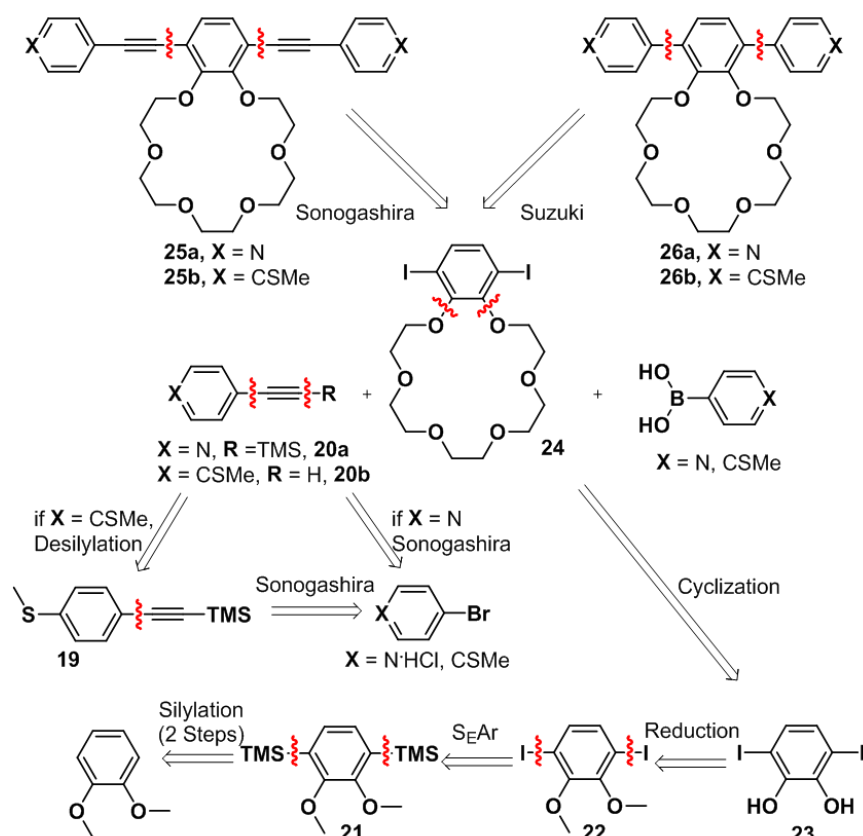
Scheme 14: Retrosynthetic analytic chart of the target OPE and PPP crown ether wires series.

To synthesize the desired OPE and PPP derivatives **25a,b** and **26a,b** it was employed a convergent synthetic route. Important starting materials to these synthesis were 4-[(trimethylsilyl)ethynyl]pyridine (**20a**) and (4-ethynylphenyl)(methyl)sulfane (**20b**) (Scheme 15)**.**

Scheme 15: Synthetic procedure towards 4-[(trimethylsilyl)ethynyl]pyridine **20a** and (4-ethynylphenyl)(methyl)sulfane **20b**.

The products were prepared starting by a Sonogashira coupling reaction from commercial 4-bromopyridine hydrochloride and (4-bromophenyl)(methyl)sulfane, respectively, with trimethylsilylacetylene in a really good yield, according to a similar previously reported procedure.[100] Then, the thiomethyl derivative **19**, differently from compound **20a**, went through a desylilation reaction. The central core of the wire, on the other side, was prepared by a sequence of 5 steps (Scheme 16).[99]
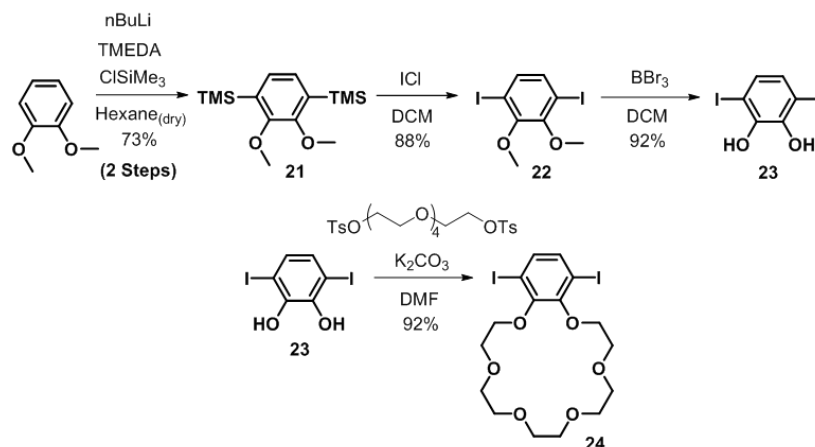
Scheme 16: Synthesis of the wires core structure.

1,4-Bis(trimethylsilyl)-2,3-dimethoxybenzene (**21**) was prepared from 1,2-dimethoxybenzene (veratrol) in two steps. Compound **21** reacted with ICl in DCM giving the *ipso* electrophilic aromatic substitution on the trimethylsilyl positions, to afford 1,4-diiodo-2,3-dimethoxybenzene (**21**). Product **22** was treated with the demethylating agent boron tribromide being reduced to the diol **23**. At this point, the precursor crown ether **24** was prepared through the macrocyclization of the pentaethylene glycol di(*p*-toluenesulfonate) with the diol **23**. Once the central core structure of both wires series (OPE and PPP derivatives) was synthesized, compound **24** was employed to obtain the final products **25a,b** and **26a,b** (Scheme 17).

---

[100] Y. Arakawa, S. Kang, H. Tsuji, J. Watanabe, G. Konishi, *RSC Adv.* **2016**, *6*, 92845.
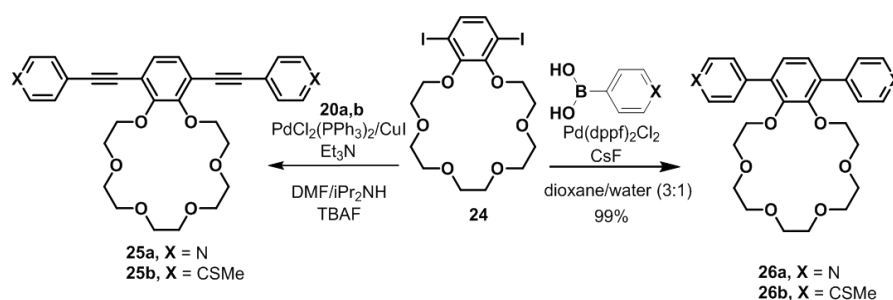
Scheme 17: Synthesis of OPP **25a,b** and PPP **26a,b** crown ether molecular wires series.

Compounds **25a** and **25b** were prepared through a Pd catalysed Sonogashira reaction where **24** is coupled with **20a** and **20b**, respectively. Unfortunately, it was impossible to isolate pure final products, due to the formation of a stable electron donor–acceptor complex between the crown ether and triphenylphosphine oxide (TPPO).[101] On the other side, products **26a** and **26b** were synthesized in high yield by a Suzuki coupling between the molecular central core **24** and side arms represented by two commercial compounds, 4-pyridinylboronic acid and 4-(methylthio)benzeneboronic acid, respectively. All the intermediates and final compounds were unambiguously characterized by the standard analytical and spectroscopic techniques.

3.2.2.2.   *Formation and Characterization of the Complexed PPP Crown Ether Molecular Wires Series*

Treatment of methanol solutions containing the PPP crown ether molecular wires **26a,b** and KSCN, in a 1:l ratio, leads to the formation of the potassium (K$^+$) complexes of the final crown ether compounds, **27a,b** (Scheme 18).
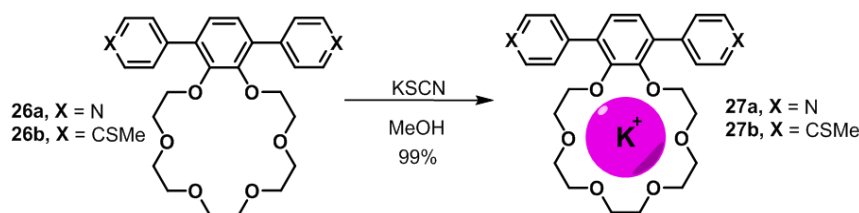
Scheme 18: Synthesis of the K$^+$ complexed PPP crown ether molecular wires **27a**,**b.**

[101] S. Banerjee , P. Dey , S. Basu, *Radiochemistry* **2010**, *52*, 2, 162.

^{1}H NMR experiments visibly reveal the formation of the complex by comparison of the free host signals **26a,b** and its signals after K^{+} complexation (**27a,b**) (Figure 55).
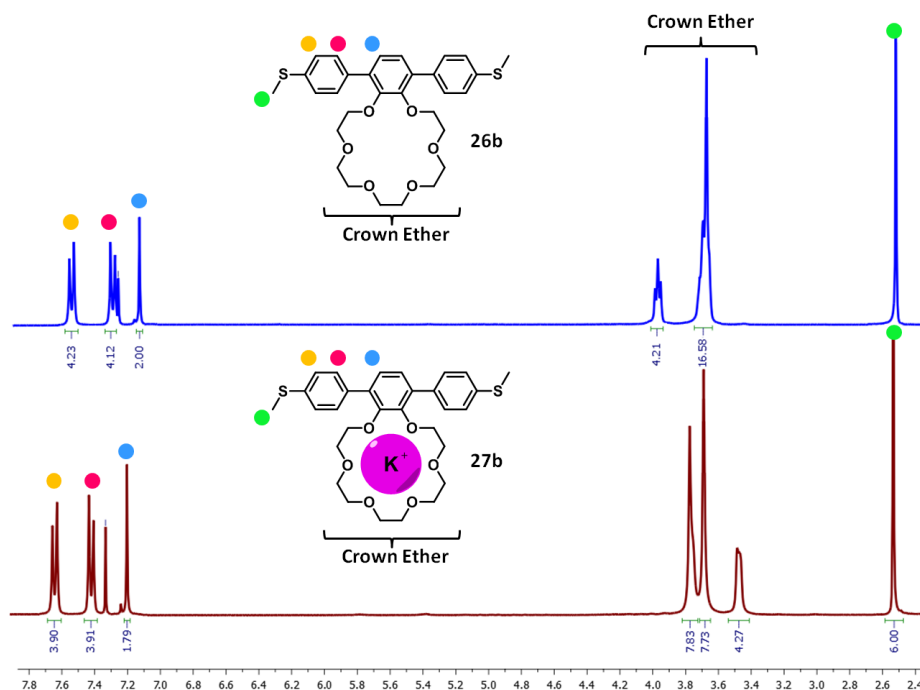
Figure 55: ^{1}H NMR comparison of methylthio ether crown ether derivatives **26b** and its potassium complex **27b**.

The strong upfield shift of the peaks corresponding to the crown ether moiety and the smaller shift of the signals of the aromatic protons of the PPP backbone are a clear indication of the successful complexation of the metal cation.

Further proof that the potassium ion-dipole interaction with the hole of the crown ether occurs effectively was provided by ESI mass spectroscopy (Figure 56).
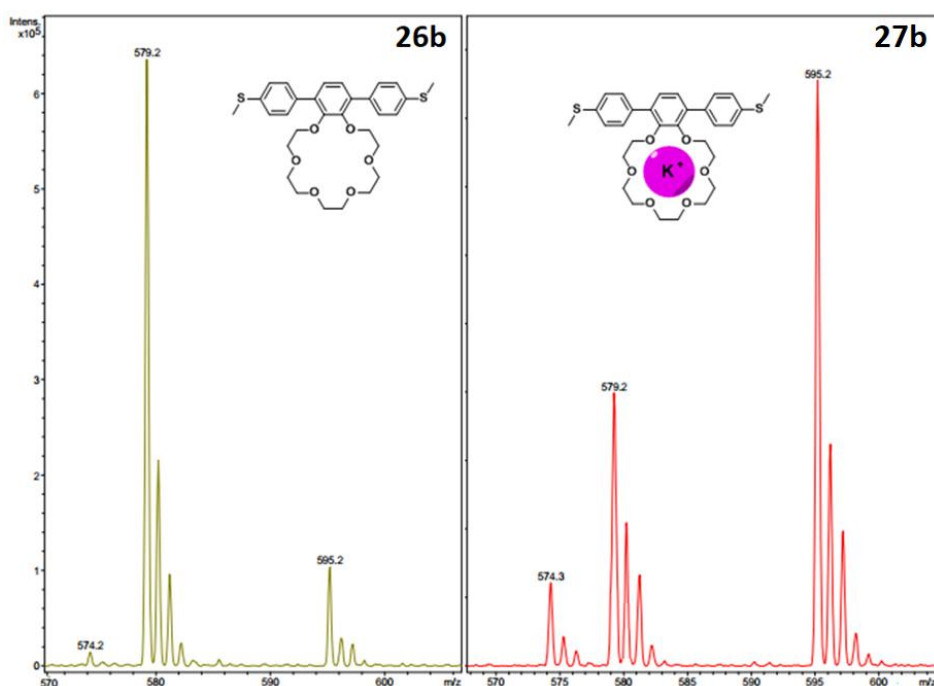
Figure 56: Comparison of the ESI mass spectra of empty **26b** and complexed **27b**.

The appearance of the peak corresponding to the molecule plus the mass of the potassium at m/z 595,2 for the complex **27b** respect to the mass of the empty molecule **26b** plus sodium at 579,2 m/z, which is consequence of the analytical technique itself, guarantees the occurrence of the complexation phenomenon.

3.2.2.3.   *Complexed PPP Crown Ether Molecular Wires Series: Physical Characterization*

The conductance properties of the synthesized systems was investigated by STMBJ technique. The measurements of the free compounds **26a,b** were carried out without any difficulties, corresponding to similar *p*-terphenylene derivatives systems (Figure 57).[25]
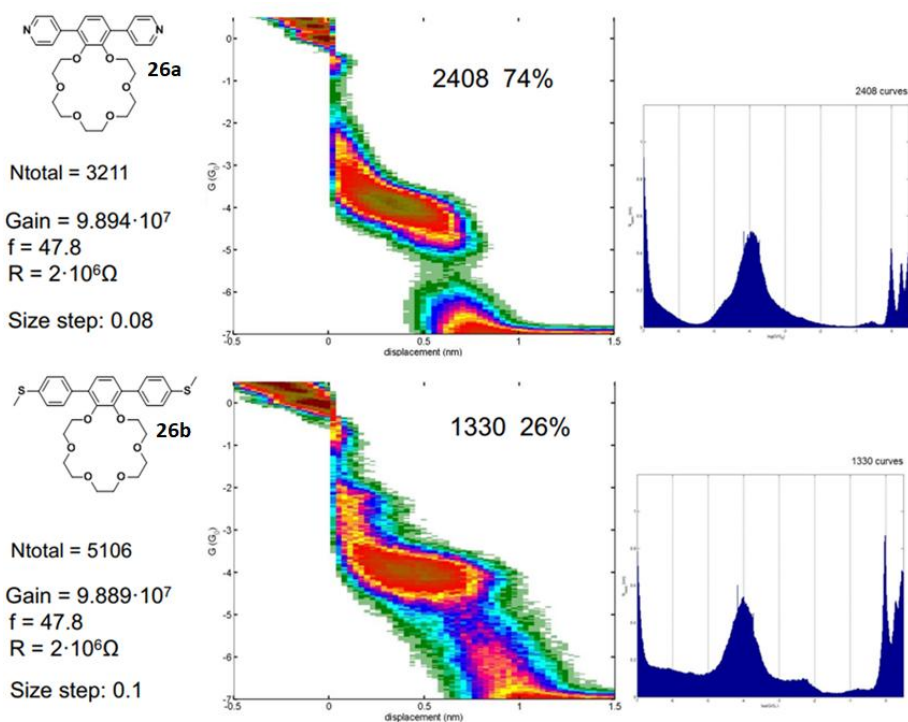
Figure 57: STMBJ of empty PPP crown ether molecular wires **26a** and **26b**.

While the determination of the conductance features of both empty compounds **26a**,**b**, resulting to be around $10^{-4}G_0$, was accomplished without difficulties, the measurements of complexes **27a**,**b** are presenting some experimental problems. Work is currently in progress to try to determine these experimental values.

4. Conclusions

4. Conclusions

The work developed in this first part of the thesis has allowed to further deepen in the knowledge relative to the employment of non-covalent interactions in the formation of systems potentially applicable in the field of molecular electronics.

- ***Amidinium-Carboxylate Based Supramolecular Wires***

Spacers   : [ring structure] $n = 0, 1, 2$

Anchors   : C_{60}, SMe, Py

Electrodes : Gold
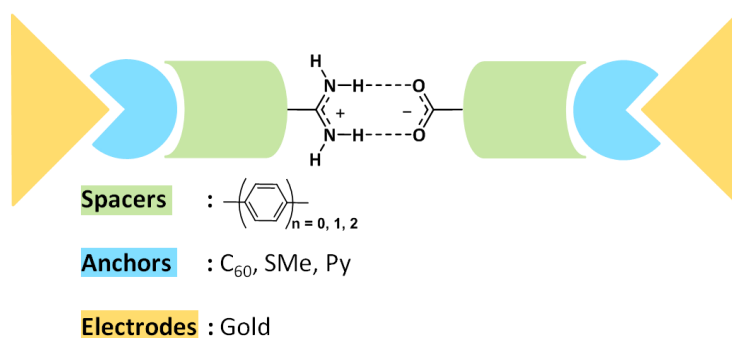
Figure 58: Schematic representation of the supramolecular fulleropyrrolidines dumbbells (**9b·8a,c**; **12b·10a,c** and **12d·10a,c**) and supramolecular linear wires (**15a,b·14a** and **16a,b·14b**).

-The systems developed for this study have strengthened the well-known concept of the formation of highly stable non-covalent complexes based on the two point amidinium-carboxylate binding motif (see determination of the K_a in Appendix).

-The investigation on their electron transfer properties was satisfactorily performed by the use of the STMBJ method, demonstrating that, through H-bonds, the behaviour of these transfer properties exhibits evident dependence on the junction length.

-It also results, from this study, that the amidinium group displays electronics characteristics interesting enough to be further investigated and employed as novel anchoring group.

-However, in spite of the aforementioned properties, and the potentiality of the H-bonding interactions to be employed as switching systems by simply changing the polarity of the solvent, the amidinium-carboxylate salt bridge does not compete with covalent spacers, showing conductance values around two orders of magnitude lower than covalent derivatives of comparable length. The low conductance

values measured for the investigated systems, in fact, clearly evidences that these systems are not suitable to be employed as building blocks for the creation of self-assembling molecular electronic components.

- *Crown Ethers Switching Systems as Supramolecular Wires*
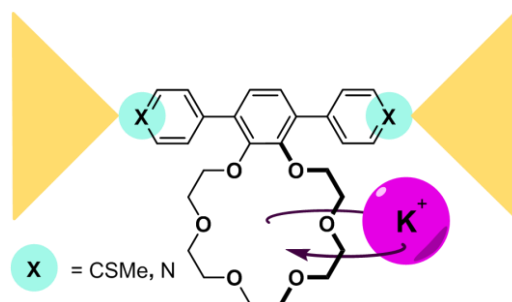
Figure 59: Schematic representation of the wires based on crown ethers switching systems (empty **26a,b** and complexed **27a,b**).

The proposed molecular wires, based on a conjugated backbone structure including dangling crown ethers, were successfully synthesized and fully chemically characterized. Studies on their CT properties to determine the effect of the metal complexation and the different   anchoring   groups,   are   still   in   progress.

5.   Experimental Part

5. Experimental Part

5.1. *General Methods and Techniques*

-*Materials*: Reagents for synthesis were purchased from commercial sources and used without further purification. Solvents were dried and distilled using standard techniques.[102] Those reactions requiring an inert atmosphere were carried out using Argon as source.

-*Analytical thin-layer chromatography (TLC):* was performed using aluminum coated Merck Kieselgel 60 F254 plates to check the evolution of reactions. Visualization was made by UV light ($\lambda = 254$ or 365 nm).

-*Purification of crude reaction mixtures:* was achieved by flash column chromatography or gravity-fed column chromatography using silica gel.

-*NMR spectra:* were recorded on a Bruker DPX-300, Bruker AV-500 or Bruker AVIII-700 at 298 K, using partially deuterated solvents as internal standards. Chemical shifts (δ) are expressed in ppm and are referred to the residual peak of the solvent. Spin multiplicities are reported as singlet (s), doublet (d), triplet (t), quartet (q), multiplet (m) and broad (br), with proton-proton coupling constants (*J*) given in Hz.

-*FTIR spectra:* were recorded on a Bruker TENSOR 27 (ATR device, 7500-370 cm^{-1}). The spectral range was 4000-550 cm^{-1}, with a resolution of 1 cm^{-1}. Spectra of pellets of dispersed samples of the corresponding materials were recorded in dried KBr.

-*Mass spectra:* were realized by the mass spectra services at the Universidad Complutense de Madrid. Electronic Impact measurements (EI) were recorded using a HP 5989A apparatus (70 eV, 200 ºC). MALDI-TOF measurements were recorded utilizing a BRUKER-REFLEX III apparatus (matrix: dithranol, N_2 laser at 337 nm) or Brucker Ultraflex III apparatus (matrix: *trans*-2-[3-(4-*tert*-Butylphenyl)-2-methyl-2-propenylidene]malononitrile (DCTB)).

---

[102] W. L. F. Armarego, C. L. L. Chai, *Purification of Laboratory Chemicals*, Elsevier, **2003**.

-Scanning Tunnel Microscopy (STM):

Measurements of the *Fullerene Dumbbells Series* were performed using a custom built STM setup located in IBM's Noise Free Labs[103].

Measurements of the *Linear Supramolecular Wires* were carried out by the group of Prof. Nicolás Agraït at IMDEA Nanoscience Institute. They were performed using the break-junction technique with a made-in-house scanning tunneling microscope (STM) optimized to work in ambient conditions. Commercial gold over glass substrates (Arrandee) were used, and a freshly cut gold wire as tip. The experiments were performed in air, after immersing the substrates in 1 mM solutions of the compounds in dioxane. A constant bias voltage V of 230 mV was established between the tip and the substrate along the experiments, and a protection 12 MΩ resistor was placed in-series. The current I along the STM substrate-tip circuit was measured with a made-in-house linear current-to-voltage converter with two amplification stages. As gains were used 5×10^8 and 2.5×10^{10} V/A, values which allow to explore a range in conductance G = I/V of 9 orders of magnitude between 10 and 10^{-8} G_0 ($G_0 = 2e^2/h$). Several thousands of G *vs.* z traces were recorded. The criterion used to identify a molecular plateau (regions of constant conductance at values below 1 G_0) was that at any conductance below 0.5 G_0, a displacement Δz larger than 8 Å was needed to produce a change in conductance of $\Delta\log(G/G_0) = 0.1$. As reference, the typical displacement needed for gold-gold tunneling to produce this conductance change in air is 0.2 Å. Using the traces that complied with this criterion, conductance histograms were built by accumulating the number of points measured in fixed $\log(G/G_0)$ intervals along thousands of traces. 2D conductance-distance histograms were built accumulating the number of points measured in fixed $\log(G/G_0)$ and z intervals along the traces. In this case, the position at which the conductance 0.5 G_0 is reached (just after each gold contact is broken) was used as zero for z. In those conductance values where plateaus are frequent in the G vs z traces, there will be a larger number of points recorded, and a peak will form in the conductance histograms.

---

[103] E. Lörtscher, D Widmer, B. Gotsmann, *Nanoscale* **2013**, *5*, 10542.

-Atomic force microscopy (AFM): was performed at IBM Zurich Laboratories, using a VEECO Dimension 3100 instrument under ambient conditions in air. It worked on tapping mode with a PPP-NCHR-W tip (which guarantes radius of curvature below 10 nm taken fresh from the wafer) at a working frequency of 330 KHz. Height and phase images were simultaneously obtained. The samples were prepared by drop-casting on freshly cleaved mica and were dried under ambient conditions for few hours.

5.2. *Proton-Donor and Proton-Acceptor Fulleropyrrolidines*

Synthesis of the amino acids containing the side chains R₁:

N-octylglycine (**1**)[42]
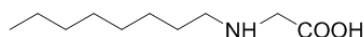
Octylamine (15.12 g, 117 mmol) was dissolved in a mixture of EtOH (15 mL) and water (12 mL). After cooling to 0°C 2-iodoacetic acid (7.44 mg, 40 mmol) was slowly added portionwise. The reaction mixture was stirred overnight allowing reaching room temperature and afterwards poured into 100 mL acetone. The occurring white precipitate was filtered, washed with acetone and dried in vacum.

Yield: 83 %.

^{1}H NMR (300 MHz, D₂O) δ 3.58 (s, 2H), 3.09 – 2.98 (m, 2H), 1.75 – 1.60 (m, 2H), 1.32 (dd, J = 25.9, 11.5 Hz, 10H), 0.85 (t, J = 6.8 Hz, 3H).

3,6,9-Trioxadecanaldehyde (**2**)[81]
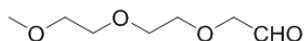
To a solution of oxalyl chloride (3 mL) in dichloromethane (75 mL) under argon and cooled in a dry ice-acetone bath 5 mL of dimethyl sulfoxide in 15 mL of DCM were carefully added. The solution was stirred for 10 min, and then a solution of 5 mL (29.7 mmol) of triethylene glycol monomethyl ether in 30 mL of DCM was added dropwise. The mixture was stirred for 15 min, and then triethylamine (20 mL) was added dropwise over a period of 20 min. The reaction

mixture was left for 30 min at -78 °C and then allowed to reach RT. After a standard workup with a saturated aq NaCl solution, the crude was purified by flash chromatography DCM/MeOH (9:1), affording the aldehyde as a light yellow oil.

Yield: 45 %

^{1}H NMR (300 MHz, CDCl$_3$) δ 9.74 (s, 1H), 4.16 (d, 2H), 3.78 – 3.68 (m, 4H), 3.66 (dd, J = 5.3, 3.4 Hz, 2H), 3.56 (dd, J = 6.2, 3.1 Hz, 2H), 3.38 (s, 3H).

N-Cbz-N-(3,6,9-trioxadecyl)glycine benzyl ester (3)[81]
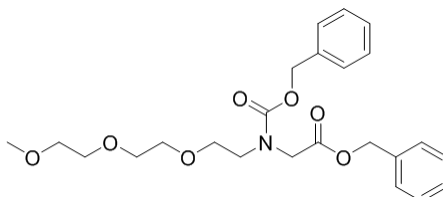
To a solution of aldehyde **2** (250 mg, 1.5 mmol) and glycine benzyl ester 4-toluenesulfonate (1,4 g, 4.09 mmol) in 30 mL of methanol-acetic acid (99:1) sodium cyanoborohydride (319 mg 5.07 mmol) was added in 30 min. The solution was stirred at RT for 2.5 h and then was poured into 75 mL of saturated NaHCO$_3$ solution. The product was extracted with ethyl acetate, the organic phase washed with brine and dried with anhyd Na$_2$SO$_4$, and the solvent was removed in vacuo. The residue aws redissolved in dioxane and treated with benzyl chloroformate (1 g, 5.03 mmol). The *N*-Cbz-*N*-(3,6,9-trioxadecyl)glycine benzyl ester was then purified by column chromatography with AcOEt/petroleum ether (1:1).

Yield: 50 %

^{1}H NMR (300 MHz, CDCl$_3$) δ 7.38 – 7.27 (m, 10H), 5.16 (s, 2H), 5.09 (d, J = 3.2 Hz, 2H), 4.21 (s, 1H), 4.16 (s, 1H), 3.67 – 3.47 (m, 12H), 3.37 – 3.32 (m, 3H).

N-(3,6,9-Trioxadecyl)glycine (4)[81]
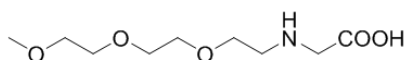
A solution of **3** (390 mg, 0.88 mmol), cyclohexene (6.26 g, 76.21 mmol) and palladium on carbon 10% (196 mg, 1.84 mmol) in 12 mL of EtOH were heated under reflux. The reaction was followed by TLC and after 24h, if it was not completed the same quantities of cyclohexenne and palladium on carbon were added and it was kept under reflux for other 24h. After filtration on celite, the solvent was evaporated under vacuum leaving a dark oil.

Yield: 70%

^{1}H NMR (300 MHz, CDCl$_3$) δ 3.82 (broad t, 2H), 3.70 – 3.50 (m, 12H), 3.38 (s, 3H), 3.20 (broad t, 2H).

FTIR (KBr) υ: 3350, 1650, 1111 cm^{-1}.

Synthesis of the spacer skeleton:

General Procedure for the Synthesis of p-functionalized phenylboronic acid pinacol esters 5d-f [104]

Pd(dppf)Cl$_2$ (0.07 mmol) was added to a mixture of the corresponding aryl bromides (1.4 mmol), bis(pinacolato)diboron (1.5 mmol), and KOAc (402 mmol) in 7 mL of anhyd DMF. The mixture was degassed under argon atm for 1h, then heated at 80°C for 5h. The solvent was removed and the crude material purified by column chromatography on silica gel with Hex/AcOEt (20:1).

4-methoxycarbonylphenylboronic acid pinacol ester (**5d**)[105]
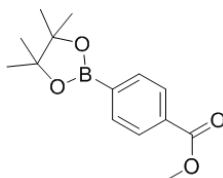
Yield: 86%

^{1}H NMR (300 MHz, CDCl$_3$) δ 8.08 – 7.98 (m, 2H), 7.88 (d, *J* = 8.3 Hz, 2H), 3.94 (s, 3H), 1.37 (s, 12H).

[104] T. Ishiyama, M. Murata, N. Miyaura, *J. Org. Chem.* **1995**, *60*, 23, 7508.
[105] T. Yamamoto, T. Morita, J. Takagi, T. Yamakawa, *Org. Lett.* **2011**, *13*, 5766.

4-cyanophenylboronic acid pinacol ester (5e)[106]
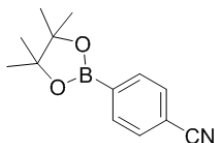
Yield: 92%.

^{1}H NMR (500 MHz, CDCl$_3$) δ 7.87 (d, J = 8.0 Hz, 2H), 7.62 (d, J = 8.0 Hz, 2H), 1.34 (s, 12 H).

4-carboxylphenylboronic acid pinacol ester (5f)[106]
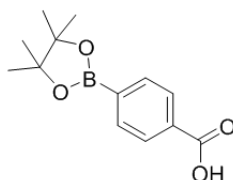
Yield: 74%.

^{1}H NMR (500 MHz, CDCl$_3$) δ 8.09 (d, J = 8.5 Hz, 2H), 7.90 (d, J = 8.0 Hz, 2H), 1.35 (s, 3H).

General Procedure for the Synthesis of 4'-formyl-[1,1'-biphenyl]-4-substituted products 6d-f

A mixture of dioxane/H$_2$0 (90 mL, 3:1) was degassed for 1h under argon atm. Boronates **5d-f** (0.76 mmol) and 4-iodobenzaldehyde (3.8 mmol) were added and the solution was heated to 80°C. After 30 min, Pd(dppf)Cl$_2$ (0.038 mmol) and CsF (2.28 mmol) were added and the mixture was kept at 80ºC for 16 h. The reaction was washed with water and extracted with DCM (3 x 20 mL). The organic phase was dried over MgSO$_4$ and the solvent was removed under reduced pressure. The crude product was purified by column chromatography on silica gel with Hex/DCM (1:1).

---

[106] P. Li, C. Fua, S. Ma, *Org. Biomol. Chem*. **2014**, *12*, 3604.

methyl 4'-formyl-[1,1'-biphenyl]-4- carboxylate (6d)[107]
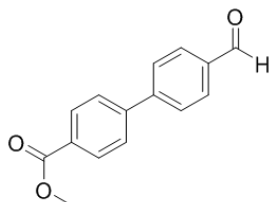
Yield: 96%

^{1}H NMR (300 MHz, CDCl$_3$) δ 10.10 (s, 1H), 8.16 (d, J = 8.2 Hz, 2H), 8.00 (d, J = 8.2 Hz, 2H), 7.81 (d, J = 8.3 Hz, 2H), 7.72 (d, J = 8.2 Hz, 2H), 3.97 (s, 3H).

4'-formyl-[1,1'-biphenyl]-4-carbonitrile (6e)[108]
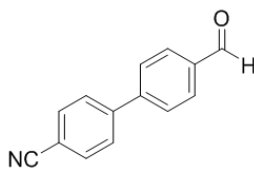
Yield: 93%.

^{1}H NMR (300 MHz, CDCl$_3$) δ 10.11 (s, 1H), 8.02 (d, J = 8.4 Hz, 2H), 7.86 – 7.68 (m, 6H).

4'-formyl-[1,1'-biphenyl]-4-carboxylic acid (6f)[109]
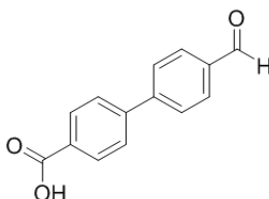
Yield: 74%.

[107] Y. L. Zhao, Y. Li, S. M. Li, Y. G. Zhou, F. Y. Sun, L. X. Gao, F. S. Han, *Adv. Synth. Catal.* **2011**, *353*, 1543.

[108] J. I. Urgel, D. Ecija, W. Auwärter, D. Stassen, D. Bonifazi, J. V. Barth, *Angew. Chem. Int. Ed.* **2015**, *54*, 6163.

[109] T. Fujimori, P. Wirsching, K. D. Janda, J. Comb. Chem. **2003**, *5*, 625.

^{1}H NMR (300 MHz, Acetone-d$_6$) δ 10.13 (s, 1H), 8.17 (d, J = 8.2 Hz, 2H), 8.07 (d, J = 8.3 Hz, 2H), 7.99 (d, J = 8.4 Hz, 2H), 7.92 (d, J = 8.3 Hz, 2H).

Synthesis of the Amidinium-Carboxylate Fulleropyrrolidines:

***General Procedure for the Synthesis of fullerene derivatives* 7a-c and 10a-d**

To a solution of C$_{60}$ (0.25 mmol) in 80 mL of toluene aldehydes **6d-f** (0.25 mmol) were added togheter with *N*-octylglycine **1** or *N*-(3,6,9-trioxadecyl)glycine **4** (0.75 mmol). The mixture was heated under reflux for 3h. After cooling, the solvent was removed under reduced pressure. The crude material was purified by column chromatography on silica gel with CS$_2$, and then eluted with Tol/MeOH (9:1). The compounds dissolved in DCM and precipitated by addition of methanol, were recovered as brown solids (racemic form).

***4-(N-Octyl-3,4-fulleropyrrolidin-2-yl)benzoic acid methyl ester* (7a)**
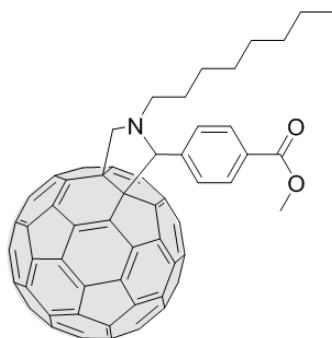
Yield: 38%

^{1}H NMR (300 MHz, CDCl$_3$) δ 8.10 (d, J = 8.4 Hz, 2H), 7.92 (s, 2H), 5.15 (s, 2H), 4.17 (d, J = 9.6 Hz, 1H), 3.91 (s, 3H), 3.20 – 3.09 (m, 1H), 2.60 – 2.42 (m, 1H), 1.94 – 1.79 (m, 2H), 1.51 – 1.17 (m, 10H), 0.88 (s, 3H).

^{13}C NMR (125 MHz, CDCl$_3$) δ 171.92 165.04, 164.61,   155.75, 155.22, 153.43, 153.14, 152.60, 152.08, 145.72, 144.38, 143.85, 143.62, 143.03, 140.93, 140.41, 138.84, 136.14, 135.09, 132.99, 128.58, 125.82, 125.03, 80.76, 75.52, 67.30, 28.22, 27.89, 26.94, 23.37, 23.20,23.04, 22.88, 22.72, 22.56, 21.18, 14.62

4-(1-Octyl-3,4-fulleropyrrolidin-2-yl)benzonitrile (**7b**)
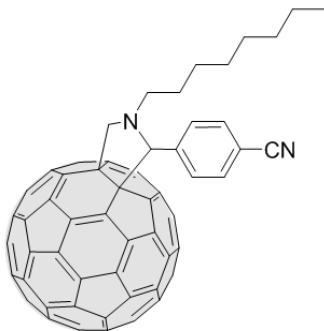
Yield: 35%

^{1}H NMR (300 MHz, CD$_3$OD) δ 8.11 (s, 2H), 7.87 (d, *J* = 8.4 Hz, 2H), 5.22 (s, 1H), 5.17 (d, *J* = 9.4 Hz, 1H), 4.21 (d, *J* = 9.4 Hz, 1H), 2.70 – 2.59 (m, 1H), 2.22 – 2.09 (m, 1H), 1.99 – 1.83 (m, 2H), 1.73 – 1.18 (m, 10H), 0.89 (s, 3H).

^{13}C NMR (125 MHz, CDCl$_3$) δ 154.17, 152.95, 147.80, 147.76, 146.76, 146.66, 146.64, 146.61, 146.58, 146.42, 146.40, 146.09, 146.03, 145.99, 145.89, 145.82, 145.80, 145.76, 145.72, 145.67, 145.64, 145.17, 144.97, 144.86, 144.76, 143.62, 143.47, 143.17, 143.07, 143.05, 143.01, 142.68, 142.64, 142.60, 142.59, 142.50, 142.47, 142.39, 142.28, 142.23, 142.13, 141.99, 140.69, 140.38, 139.94, 137.58, 136.80, 136.42, 135.94, 132.89, 130.54, 119.03, 112.81, 82.37, 76.57, 69.28, 67.17, 53.79, 32.33, 30.01, 29.71, 28.61, 27.93, 23.12, 14.57.

ESI_POS: m/z theoretical for C$_{76}$H$_{22}$N$_2$O$_3$ 736.29 exp [M+H]$^+$ 737.35.

FTIR (KBr) υ: 2923, 2853, 2798, 2229, 1676, 1607, 1501, 1460, 1299, 1264, 1213, 1178, 1113, 1020, 754 cm^{-1}.

***4'-(1-Octyl-3,4-fulleropyrrolidin-2-yl)biphenyl-4-carboxylic   acid
methyl ester* (7c)**[110]
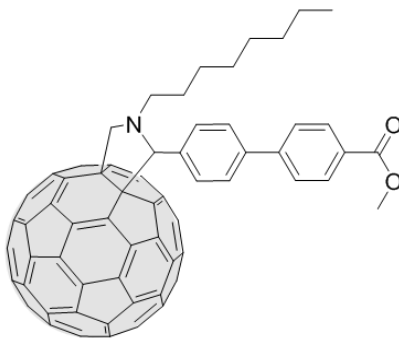
Yield: 26%

^{1}H NMR (300 MHz, CDCl$_3$) δ 8.10 (d, J = 8.5 Hz, 2H), 7.91 (s, 2H),
7.71 (d, J = 8.5 Hz, 4H), 5.14 (s, 2H), 4.17 (d, J = 10.1 Hz, 1H), 3.95
(s, 3H), 3.25 – 3.99 (m, 1H), 2.61 – 2.47 (m, 1H), 1.90 – 1.86 (s, 2H),
1.69 – 1.12 (m, 10H), 0.92 (s, 3H).

***4'-(N-(3,6,9-Trioxadecyl)glycine-3,4-fulleropyrrolidin-2-yl)benzoic
acid* (10a)**
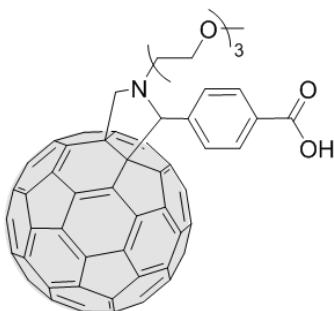
Yield: 22%

^{1}H NMR (300 MHz, CDCl$_3$) δ 8.15 (d, J = 8.3 Hz, 2H), 7.98 (s, 2H),
5.27 (d, J = 12.6 Hz, 2H),), 4.37 (d, J = 10.4 Hz, 1H), 4.18 – 3.90 (m,
2H), 3.77 (m, 6H), 3.59 (m, 2H), 3.37 (m, 4H), 2.94 (m, 1H).

---

[110] M. Segura, L. Sánchez, J. de Mendoza, N. Martín, D. M. Guldi *J. Am. Chem. Soc.*
2003, *125*, 49, 15093.

^{13}C NMR (125 MHz, CDCl$_3$) δ 168.95, 147.32, 146.31, 146.25, 146.21, 146.11, 145.97, 145.72, 145.74, 145.52, 145.46, 145.3, 145.33, 144.72, 143.13, 142.64, 142.56, 142.21, 142.14, 141.86, 141.72, 140.63, 139.11, 137.33, 137.05, 136.51, 136.01, 135.58, 133.51, 132.69, 132.14, 131.53, 131.33, 130.07, 128.75, 128.61, 127.01, 125.79, 125.58, 123.06, 79.83, 73.66, 70.10, 69.94, 69.51, 65.41, 60.81, 57.81, 54.02.

ESI_POS: m/z theoretical for C$_{76}$H$_{23}$NO$_5$ 1029.1576 exp [M+H]$^+$ 1030.1690.

FTIR (KBr) υ: 2923, 2854, 1715, 1694, 1610, 1460, 1424, 1375, 1289, 1251, 1206, 1109, 853, 755 cm^{-1}.

4'-(N-(3,6,9-Trioxadecyl)glycine-3,4-fulleropyrrolidin-2-yl) benzonitrile (10b)
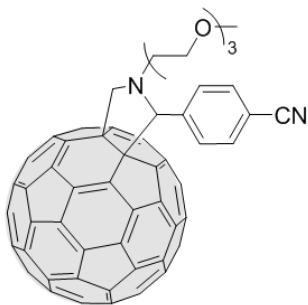
Yield: 25%

^{1}H NMR (300 MHz, CDCl$_3$) δ 7.98 (d, J = 7.3 Hz, 2H), 7.73 (d, J = 8.5 Hz, 2H), 5.23 (d, J = 10.6 Hz, 2H), 4.34 (d, J = 9.7 Hz, 1H), 4.10 – 3.93 (m, 2H), 3.87 – 3.68 (m, 6H), 3.58 (m, 2H), 3.43 – 3.30 (m, 4H), 2.99 – 2.86 (m, 1H).

^{13}C NMR (175 MHz, CDCl$_3$) δ 146.77, 146.64, 146.61, 146.58, 146.46, 146.21, 146.03, 145.99, 145.89, 145.78, 145.77, 145.73, 145.70, 145.67, 145.64, 145.17, 144.97, 144.90, 144.86, 144.76, 144.14, 143.62, 143.01, 142.68, 142.64, 140.63, 139.11, 136.51, 135.58, 133.51, 132.69, 132.14, 131.33, 130.24, 130.07, 129.02, 128.61, 127.01, 125.98, 125.58, 119.12, 110.59, 79.83, 75.66, 70.10, 69.94, 69.71, 65.02, 61.81, 58.39, 54.05.

ESI_POS: m/z theoretical for $C_{76}H_{22}N_2O_3$ 1010.1630 exp $[M+H]^+$ 1011.2.

FTIR (KBr) υ: 2853, 2228, 1733, 1460, 1372, 1257, 1102, 845, 800, 758 cm^{-1}.

4'-(N-(3,6,9-Trioxadecyl)glycine-3,4-fulleropyrrolidin-2-yl)biphenyl-4-carboxylic acid (10c)[110]
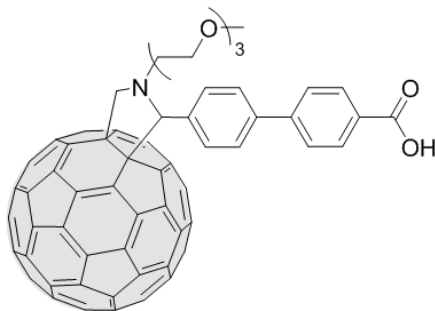
Yield: 48%

^{1}H NMR (300 MHz, CDCl$_3$) δ 8.14 (d, J = 8.4 Hz, 2H), 7.98 – 7.88 (m, 3H), 7.73 (m, 3H), 5.25 (s, 2H), 4.35 (s, 1H), 4.11 – 4.03 (m, 2H), 3.85 – 3.71 (m, 6H), 3.59 (m, 2H), 3.38 (m, 4H), 2.95 – 2.90 (m, 1H).

^{13}C NMR (175 MHz, CDCl$_3$) δ 168.95, 146.44, 146.32, 146.25, 146.11, 146.00, 145.68, 145.46, 145.39, 145.10, 145.02, 144.95, 144.85, 144.39, 144.23, 144.11, 143.29, 143.24, 143.23, 143.14, 142.57, 141.6, 141.5, 141.44, 140.88, 140.63, 140.34, 140.32, 140.07, 139.67, 139.11, 138.63, 137.11, 136.51, 135.58, 133.51, 132.69, 132.14, 131.33, 130.33, 130.27, 130.07, 129.47, 128.61, 127.37, 127.11, 127.01, 125.79, 125.00, 79.83, 73.66, 70.10, 69.94, 67.51, 63.41, 62.81, 57.81, 53.02.

ESI_POS: m/z theoretical for $C_{82}H_{27}NO_5$ 1105.1889 exp $[M+H]^+$ 1106.1942.

FTIR (KBr) υ: 2923, 2853, 2798, 2229, 1676, 1607, 1501, 1460, 1299, 1264, 1213, 1178, 1113, 1020, 754 cm^{-1}.

4'-(N-(3,6,9-Trioxadecyl)glycine-3,4-fulleropyrrolidin-2-yl)biphenyl-4-cyano (**10d**)
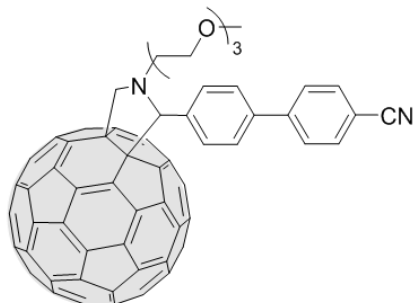
Yield: 15%

^{1}H NMR (300 MHz, CDCl$_3$) δ 7.93 (s, 2H), 7.71 (s, 4H), 7.66 (d, *J* = 8.4 Hz, 2H), 5.24 (d, *J* = 6.2 Hz, 2H), 4.34 (d, *J* = 9.7 Hz, 1H), 4.13 – 3.97 (m, 2H), 3.86 – 3.70 (m, 6H), 3.58 (m, 2H), 3.38 (m, 4H), 2.91 (m, 1H).

^{13}C NMR (75 MHz, CDCl$_3$) δ 146.74, 146.55, 146.53, 146.47, 146.23, 146.03, 145.61, 145.44, 145.39, 145.32, 145.27, 145.24, 144.93, 144.86, 144.83, 144.76, 143.91, 142.28, 141.68, 140.73, 140.67, 140.63, 140.34, 139.11, 136.81, 135.08, 133.78, 133.11, 132.69, 132.14, 131.33, 130.43, 130.33, 130.07, 128.92, 127.37, 127.01, 125.99, 125.50, 119.12, 115.67, 79.13, 73.65, 70.10, 69.94, 69.51, 65.41, 60.81, 57.81, 53.82.

ESI_POS: m/z theoretical for C$_{82}$H$_{26}$N$_2$O$_3$ 1086.1943 exp [M+H]$^+$ 1087.0954.

FTIR (KBr) υ: 2922, 2854, 2225, 1740, 1462, 1110, 826, 762 cm^{-1}.

General Procedure for the hydrolysis to obtain compounds **8a,c**

To a sample of 15 mg of the fullerene derivatives **7a,c** in THF (5 mL) at room temperature KOH 10% (40 mL) was added. The reaction was heated under reflux for 3 h. Then, HCl (3 mL) was added to neutralize and a precipitate was formed. The precipitate was filtered and washed with water (20 mL), methanol (20 mL) and ethyl ether (20 mL) affording the corresponding carboxylic acids **8a,c**.

4-(1-Octyl-3,4-fulleropyrrolidin-2-yl)benzoic acid (8a)[110]
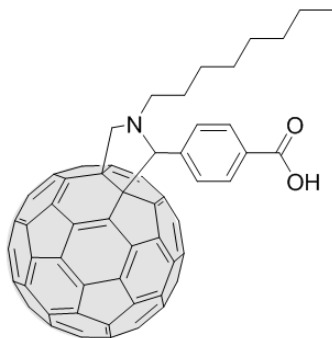
Yield: 94%

^{1}H NMR (300 MHz, CDCl$_3$) δ 8.16 (d, *J* = 8.4 Hz), 7.96 (br s, 2 H), 5.16 (d, *J* = 9.2 Hz, 1 H), 5.15 (s, 1 H), 4.17 (d, *J* = 9.2 Hz, 1 H), 3.20 (m, 1 H), 2.57 (m, 1 H), 2.00 (m, 2 H), 1.42-1.27 (m, 10 H), 0.92 (m, 3 H).

4'-(1-Octyl-3,4-fulleropyrrolidin-2-yl)biphenyl-4-carboxylic   acid (8c)[110]
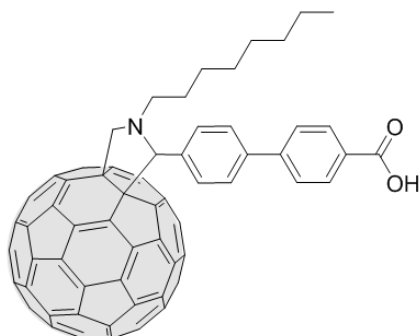
Yield: 72%

^{1}H NMR (300 MHz, CDCl$_3$) δ 8.16 (d, *J* = 8.4 Hz, 2 H), 7.93 (br s, 2 H,), 7.74 (m, 4 H,), 5.14 (d, *J* = 9.0 Hz, 1 H,), 5.13 (s, 1 H,), 4.17 (d, *J* = 9.0 Hz, 1 H,), 3.32 (m, 1 H,), 2.63 (m, 1 H,), 2.01 (m, 2 H,), 1.90 (m, 2 H,), 1.70-1.26 (m, 8 H,), 0.90 (t, *J* = 8.4 Hz, 3 H).

General Procedure for the Synthesis of the amidinium fulleropyrrolidine derivatives **8b and 11b,d**

Aluminium amide complex (1 M):

Under scrupulously anhydrous conditions, NH_4Cl (0.39 mmol), previously desiccated overnight in a heater at 80°C, was added to 0.2 mL of dry toluene. The suspension was cooled at -79°C and argon/vacuum cycles were repeated 3-5 times. After warming to room temperature, the mixture was cooled to 0°C and a solution of $AlMe_3$ in hexane (2M, 0.2 mL) was slowly added. When the addition was completed, the reaction mixture was allowed to warm to RT and was further stirred for 2 h under argon, until gas evolution had ceased.

Amidinium formation:

A solution of **7b** or **10b,d** (0.03 mmol) in dry toluene (1 mL), after 3-5 argon/vacuum cycles at -79°C, was allowed to warm at RT and then heated at 90°C. The previously formed aluminium amide complex was added under argon atm and the resulting solution was stirred for 78h. The heating was discontinued and the reaction solution quenched with MeOH. After evaporation of the solvent under reduced pressure, the compound was purified by column chromatography on silica gel DCM/MeOH (9:1).

4-(1-Octyl-3,4-fulleropyrrolidin-2-yl)benzamidine hydrochloride **(8b)**
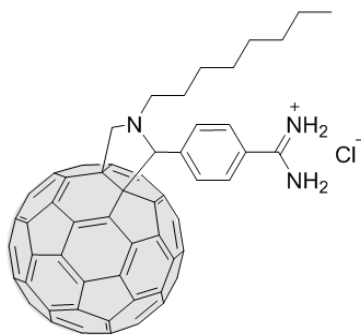
Yield: 62%

^{1}H NMR (300 MHz, CD_3OD) δ 8.09 (s, 2H), 7.87 (d, *J* = 7.5 Hz, 2H), 5.22 (s, 1H), 5.17 (d, *J* = 9.5 Hz, 1H), 4.21 (d, *J* = 9.0 Hz, 1H), 2.64 (s, 2H), 1.99 (s, 2H), 1.27 (m, 10H), 0.89 (s, 3H).

^{13}C NMR (75 MHz, CDCl$_3$) δ 154.23, 153.02, 147.41, 147.26, 146.56, 146.46, 146.21, 146.19, 146.09, 146.03, 145.99, 145.95, 145.84, 145.81, 145.74, 145.69, 145.67, 145.61, 145.07, 144.88, 144.81, 144.72, 143.54, 143.27, 143.12, 143.01, 142.68, 142.64, 142.60, 142.59, 142.40, 142.37, 142.29, 142.28, 141.99, 140.63, 139.11, 138.73, 136.51, 135.58, 133.51, 132.69, 132.14, 131.47, 131.33, 130.07, 130.01, 128.61, 127.01, 125.99, 125.79, 125.58, 79.83, 65.41, 60.81, 54.84, 31.64, 29.06, 28.95, 27.89, 27.55, 22.93, 14.01.

MALDI-TOF: *m/z* theoretical for C$_{77}$H$_{28}$ClN$_3$ 1029.1972 exp [M-Cl]$^+$ 995.2147.

FTIR (KBr) υ: 3367-2990, 2763, 2328, 1713, 1430, 1312, 1217, 1198, 795, 789, 754 cm^{-1}.

4'-(N-(3,6,9-Trioxadecyl)glycine-3,4-fulleropyrrolidin-2-yl) benzamidine hydrochloride (**11b**)
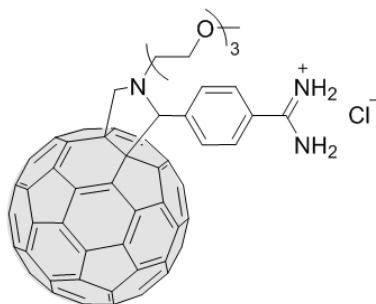
Yield: 20%

^{1}H NMR (300 MHz, CDCl$_3$) δ 8.05 – 7.94 (m, 2H), 7.73 (d, *J* = 8.5 Hz, 2H), 5.23 (d, *J* = 10.5 Hz, 2H), 4.34 (d, *J* = 9.8 Hz, 1H), 4.09 – 3.93 (m, 2H), 3.76 (m, 6H), 3.58 (m, 2H), 3.37 (m, 4H), 2.98 – 2.91 (m, 1H).

^{13}C NMR (75 MHz, CDCl$_3$) δ 146.71 146.64, 146.63, 146.54, 146.67, 146.41, 146.13, 145.99, 145.89, 145.78 145.70 145.67, 145.64, 145.17, 144.97, 144.86, 144.76, 143.94, 143.62, 143.01, 142.68, 142.64, 141.63, 140.21, 139.03, 138.23, 136.11, 135.99, 132.51, 132.49, 132.14, 131.57, 130.33, 130.07, 130.01, 128.61, 127.01, 125.99, 125.79, 125.58, 79.83, 72.76, 71.50, 69.84, 69.63, 65.71, 60.05, 57.81, 54.52.

MALDI-TOF: *m/z* theoretical for $C_{76}H_{26}ClN_3O_3$ 1063.1663 exp [M-Cl]$^+$ 1028.2097.

FTIR (KBr) υ: 3421-3087, 2923, 2855, 1730, 1621, 1459, 1426, 1382, 1168, 1114, 855, 718, 575, 526 cm^{-1}.

4'-(N-(3,6,9-Trioxadecyl)glycine-3,4-fulleropyrrolidin-2-yl)biphenyl-4-amidine hydrochloride (11d)
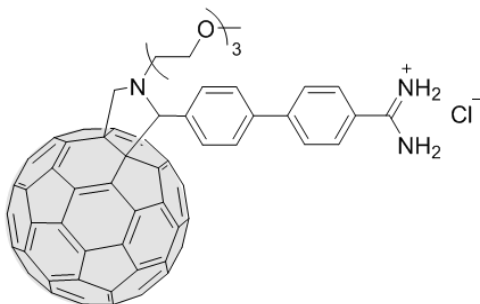
Yield: 18%

^{1}H NMR (700 MHz, CDCl$_3$) δ 7.90 (d, *J* = 8.2 Hz, 4H), 7.79 – 7.64 (m, 4H), 5.26 (d, *J* = 13.5 Hz, 2H), 4.36 (d, *J* = 9.7 Hz, 1H), 4.07 (d, 2H), 3.88 – 3.48 (m, 8H), 3.40 (s, 4H), 2.94 (s, 1H).

^{13}C NMR (175 MHz, CDCl$_3$) δ 146.71 146.64, 146.63, 146.54, 146.67, 146.41, 146.13, 145.99, 145.89, 145.78 145.70 145.67, 145.64, 145.17, 144.97, 144.86, 144.76, 143.94, 143.62, 143.01, 142.68, 142.64, 141.63, 140.21, 139.03, 138.23, 136.11, 135.99, 132.51, 132.49, 132.14, 131.57, 130.33, 130.07, 130.01, 128.61, 127.01, 125.99, 125.79, 125.58, 79.83, 72.76, 71.50, 69.84, 69.63, 65.71, 60.05, 57.81, 54.52.

MALDI-TOF: *m/z* theoretical for $C_{82}H_{30}ClN_3O_3$ 1139.1976 exp [M-Cl]$^+$ 1104.3109.

FT-IR (KBr): 3326-2890, 2826, 2802, 2325, 1699, 1482, 1342, 1112, 750 cm^{-1}.

General Procedure for the neutralization to obtain the amidine derivatives **9b** *and* **12b,d**

The amidinium salt derivative **8b** or **11b,d** (10 mg) was washed with an aq solution of NaOH (10%) and extracted with CHCl$_3$ (3 x 30 mL). The organic phase was dried over MgSO$_4$ and the solvent removed under reduced pressure to obtain the corresponding neutral forms **9b** and **12b,d**.

4-(1-Octyl-3,4-fulleropyrrolidin-2-yl)benzamidine **(9b)**
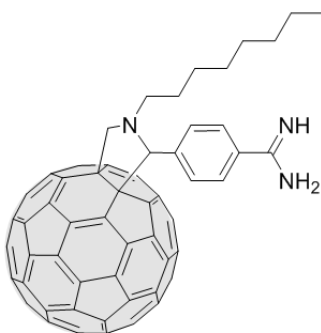
Yield: 72%

^{1}H NMR (300 MHz, CD$_3$OD) δ 8.11 (s, 2H), 7.67 (d, *J* = 7.5 Hz, 2H), 5.16 (s, 1H), 5.07 (d, *J* = 9.5 Hz, 1H), 4.01 (d, *J* = 9.5 Hz, 1H), 2.84 (s, 2H), 2.04 (s, 2H), 1.32 (m, 10H), 0.93 (s, 3H).

FTIR (KBr) υ: 3332, 2986, 2763, 2328, 1713, 1430, 1312, 1217, 1198, 795, 789, 754, 574 cm^{-1}.

4'-(N-(3,6,9-Trioxadecyl)glycine-3,4-fulleropyrrolidin-2-yl) benzamidine **(12b)**
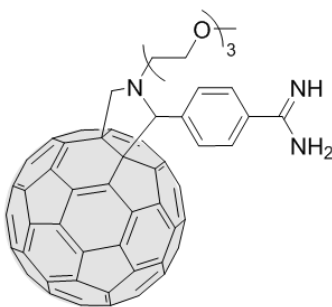
Yield: 80%

^{1}H NMR (300 MHz, CDCl$_3$) δ 8.01 (m, 2H), 7.73 (d, J = 8.4 Hz, 2H), 5.60 (d, J = 10.2 Hz, 2H), 4.54 (d, J = 9.6 Hz, 1H), 4.11 – 3.93 (2m, 2H), 3.46 (m, 6H), 3.28 (m, 2H), 3.07 (m, 4H), 2.78 – 2.71 (m, 1H).

FTIR (KBr) υ: 3456, 3393, 2923, 2855, 1730, 1645, 1462, 1372, 1258, 1181, 1112.09, 910, 844, 807, 729, 649 cm^{-1}.

4'-(N-(3,6,9-Trioxadecyl)glycine-3,4-fulleropyrrolidin-2-yl)biphenyl-4-amidine (**12d**)
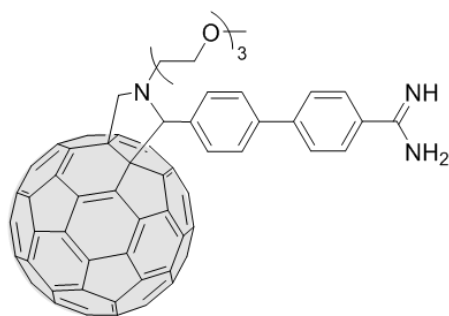
Yield: 68%

^{1}H NMR (300 MHz, CDCl$_3$) δ 7.88 (d, J = 8.6 Hz, 4H), 7.79 – 7.58 (m, 4H), 5.26 (s, 1H), 5.23 (s, 1H), 4.34 (d, J = 9.5 Hz, 1H), 4.02 (s, 2H), 3.49 (s, 4H), 3.37 (s, 8H), 2.97 – 2.86 (m, 1H).

FT-IR (KBr) υ: 3103, 3026, 2920, 1942, 1857, 1604, 1494, 1459, 1379, 1178, 1080, 1029, 895, 724, 692 cm^{-1}.

General Procedure for the formation of the amidinium-carboxylate complexes **9b·8a,c** *and* **12b,d·10a,c**

To a solution of the amidine derivatives **9b** and **12b,d** (1 mmol) in hot CHCl$_3$ (5 mL) the corresponding carboxylic acids **8a,c** and **10a,c** (1 mmol) were added. The resulting solution was stirred for 1h and then, warmed to room temperature, the solvent was dried under vacuum giving the corresponding complexes **9b·8a,c** and **12b,d·10a,c**.

115

5.3. *Linear Supramolecular Wires*

Synthesis of the Proton Donor and Proton Acceptor Moieties:

For the synthesis of the amidine moieties **14a,b** of the supramolecular linear wires, see the General Procedure to obtain the amidinium fulleropyrrolidine derivatives and their neutralization in the previous section (*General Procedure for the hydrolysis,* p. 92).

4-pyridinecarboamidine hydrochlorid (13a)
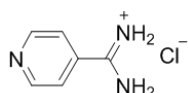
Yield: 99%

^{1}H NMR (300 MHz, DMSO-d$_6$) δ 6.93-6.87 (m, 2H), 6.18-6.10 (m, 2H).

^{13}C NMR (75 MHz, CD$_3$OD) δ 170.12, 149.27, 135.28, 123.43.

FTIR (KBr) υ: 3367-2860, 1692, 1592, 1558, 1483, 1414, 1355, 1222, 749, 685 cm^{-1}.

4-pyridinecarboamidine (14b)
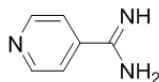
Yield: 98%

^{1}H NMR (300 MHz, DMSO-d$_6$) δ 8.90-8-86 (dd, J = 4.5, 1.6 Hz, 2H), 7.78-7.74 (dd, J = 4.5, 1.6 Hz, 2H).

^{13}C NMR (75 MHz, CD$_3$OD) δ 165.32, 150.84, 144.69, 122.91.

FTIR (KBr) υ: 3352, 3186, 2926, 2856, 1678,1620, 1551, 1513, 1463, 1407, 1262, 1219, 1067, 998, 847, 757, 617.

4-(methylthio)benzamidine hydrochloride (13b)
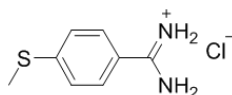
Yield: 99%

^{1}H NMR (300 MHz, CD$_3$OD) δ 6.76 – 6.70 (m, 2H), 6.16 – 6.04 (m, 2H), 2.58 (m, 3H).

^{13}C NMR (75 MHz, CD$_3$OD) δ 169.93, 139.53, 128.77, 126.76, 124.05, 14.78.

FTIR (KBr) υ: 3350-2859, 1740, 1677, 1599, 1532, 1479, 1431, 1370, 1263, 1219, 1090, 833, 754, 608 cm^{-1}.

4-(methylthio)benzamidine (14b)
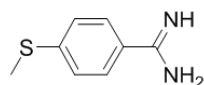
Yield: 90%

^{1}H NMR (300 MHz, CD$_3$OD) δ 7.72 – 7.60 (m, 2H), 7.36 – 7.22 (m, 2H), 2.51 (s, 3H).

^{13}C NMR (75 MHz, CD$_3$OD) δ 167.37, 144.69, 131.87, 128.36, 126.58, 14.95.

FTIR (KBr) υ: 3417, 3237, 2925, 2855, 1672, 1599, 1555,1480, 1409, 1158, 1028, 1013, 731, 718, 733, 675, 645 cm^{-1}.

General Procedure for the synthesis of the carboxylic biphenyl derivatives 15b and 16b

Potassium pyridine or (methylthio)phenyl 4-trifluoroborate salts (2.6 mmol) and 4-bromobenzoic acid (4.2 mmol) were added to a mixture of dioxane/H$_2$0 (3:1) previously degassed for 1h. The stirring solution was heated at 80°C and Pd(dppf)Cl$_2$ (0.13 mmol) and CsF (7.8 mmol) were added after 30 minutes. The temperature was maintained at 80°C overnight under argon atm. The crude was washed with water and extracted with DCM (3 x 20 mL). The organic phase was dried over MgSO$_4$ and the solvent was removed under reduced pressure. The crude product was purified by column chromatography on silica gel with DCM/MeOH (9:1). The product extracted from the column chromatography was further purified by recrystallization from pyridine to obtain the carboxylic biphenyl derivative 15b and from MeOH to achieve 16b.

4-(pyridin-4-yl)benzoic acid (**15b**)
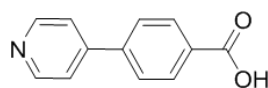
Yield: 80%

^{1}H NMR (500 MHz, DMSO-d$_6$): δ 8.67 (dd, 2H, 1.53 Hz, 4.57 Hz), 8.06 (dd, 2H, 1.83 Hz, 6.72 Hz), 7.92 (dd, 2H, 1.83 Hz, 6.72 Hz), 7.76 (dd, 2H, 1.53 Hz, 4.57 Hz).

^{13}C NMR (175 MHz, DMSO-d$_6$): δ 166.90, 150.33, 145.96, 141.24, 131.26, 130.08, 127.11, 121.46.

ESI_POS: m/z theoretical for C$_{12}$H$_9$NO$_2$ 199.06 exp [M+H]$^+$ 200.51.

FTIR (KBr) υ: 2431, 1700, 1604, 1403, 1317, 1296, 1180, 1073, 1006, 828, 733, 742, 701, 668, 519 cm^{-1}.

4'-(methylthio)-[1,1'-biphenyl]-4-carboxylic acid (**16b**)
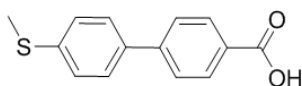
Yield:72%

^{1}H NMR (300 MHz, CDCl$_3$) δ 8.16 (d, *J* = 10.2 Hz, 2H), 7.68 (d, *J* = 9.9 Hz, 2H), 7.57 (d, *J* = 9.6 Hz, 2H), 7.35 (d, *J* = 10.0 Hz, 2H), 2.54 (s, 3H).

^{13}C NMR (125 MHz, CDCl$_3$) δ 168.95, 140.88, 138.90, 135.19, 130.27, 129.47, 128.03, 127.72, 127.11, 16.53.

FTIR (KBr) υ: 3059, 2925, 2852, 1643, 1589, 1439, 1398, 1312, 1176, 1125, 1087, 956, 843, 816, 718, 578, 541 cm^{-1}.

Synthesis of the Reference Compounds for Linear Supramolecular Wires:

4,4''-bis(methylthio)-1,1':4',1''-terphenyl (**17**)[88]
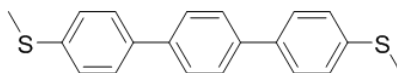
A mixture of Toluene/H$_2$O (15 mL / 2 mL) was degassed for 1h. 4-(methylthio)phenylboronic acid (500 mg, 2.98 mmol) and *p*-dibromobenzene (280.7 mg, 1.19 mmol) were added and heated to 95°C under argon atm. After 30 minutes, Na$_2$CO$_3$ (630.6 mg, 5.95 mmol) together with Pd(Ph$_3$)$_4$ (13.87 mg, 0.012 mmol) as a catalyst were added and the temperature was kept overnight. The reaction mixture was cooled down to room temperature before MeOH was added. The mixture was filtered and the precipitate was washed with deionized water and HCl solution (0.5 M) to get rid of the unreacted NaCO$_3$, followed by another washing step with deionized water and finally with MeOH. The precipitate was dried with P$_2$O$_5$ under vacuum. It was purified by column chromatography on SiO$_2$ with hexane/DCM (1:1) as the eluent to obtain **17** as a white solid.

Yield: 55%

^{1}H NMR (300 MHz, CDCl$_3$) δ 7.64 (s, 4H), 7.57 (d, *J* = 8.3 Hz, 4H), 7.34 (d, *J* = 8.3 Hz, 4H), 2.53 (s, 6H).

***General Procedure for the formation of the amidinium-carboxylate complexes* 15a,b·14a and 16a,b·14b**

To a solution of the amidine derivatives **14a,b** (1 mmol) in hot MeOH (5 mL) the corresponding carboxylic acids **15a,b** or **16a,b** (1 mmol) were added. The resulting solution was stirred for 1h and then, warmed to room temperature. The solvent was dried under vacuum giving the corresponding complexes **15a,b·14a and 16a,b·14b**.

5.4. *Crown Ethers Switching Systems*

Synthesis of trans-4,5'-diaminodibenzo[18]crown-6:

***trans-4,5'-diaminodibenzo[18]crown-6* (18)**[111]

---
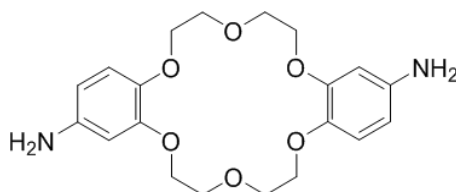
[111] B. R. Pandya, Y. K. Agrawal, *Dyes and Pigments* **2002**, *52*, 161.

A mixture of *trans*-4,5'-dinitrodibenzo[18]crown-6 (0.99 g, 2.2 mmol), Raney nickel (1.5 g) and anhyd ethanol (100 mL) was stirred under reflux as hydrazine hydrate (0.40 g, 8.0 mmol) was added over 20 min. The reflux was continued for 2 h to ensure complete removal of ammonia and the hot mixture was filtered to recover the catalyst. Excess solvent was removed under reduced pressure and on cooling, obtaining product **19**.

Yield: 60%

^{1}H NMR (300 MHz, CDCl$_3$) δ 6.72 (d, J = 8.4 Hz, 2H), 6.28 (d, J = 2.4 Hz, 2H), 6.21 (dd, J = 8.4, 2.5 Hz, 2H), 4.10 (dd, J = 4.9, 2.9 Hz, 8H), 4.07 – 3.92 (m, 8H).

Synthesis of the "arms" of the OPE and PPP Crown Ether Molecular Wires Series:

trimethyl((4-(methylthio)phenyl)ethynyl)silane (**19**)[100]
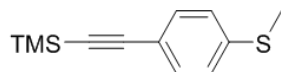
4-bromophenylmethylsulfide (2 g, 8.7 mmol) ws dissolved in DMF (80 mL) and diisopropylamine (20 mL). Under argon atm, trimethylsilylacetylene (1.29 g, 13.1 mmol), P(PPh$_3$)$_4$ (0.5 g, 0.44 mmol), and CuI (0.04 g, 0.44 mmol) were added to the solution. The mixture was then stirred under Ar at 80°C for 48 h. The solvent was then removed in vacuum and the residue dissolved in DCM (50 mL) before being washed with water (2 x 20 mL) and brine (20 mL). The organic phase was then dried over MgSO$_4$. After the solvent was removed in vacuum, column chromatography on SiO$_2$ with hexane/DCM (3:1) was carried out to provide the product **19** as a yellow solid.

Yield: 94%

^{1}H NMR (300 MHz, CDCl$_3$) δ 7.76 – 7.78 ppm (d, J = 8.7 Hz, 2H), 7.50 – 7.52 (d, J = 8.7 Hz, 2H), 2.39 (s, 3H), 0.26 (s, 9H).

4-((trimethylsilyl)ethynyl)pyridine (**20a**)[100]
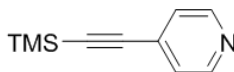
A mixture of 4-bromopyridine hydrochloride (3.00 g, 15.4 mmol), $PdCl_2(PPh_3)_2$ (271 mg, 0.39 mmol), and CuI (74 mg, 0.39 mmol) was placed in a 100 mL three-neck round-bottom flask. The flask was flushed with argon, and degassed diisopropylamine (30 mL) was added into the flask while stirring at 40 °C, followed by the addition of (trimethylsilyl)acetylene (4.44 mL, 30.9 mmol). After 12 h, the reaction mixture was diluted with water (1 mL), extracted with DCM, dried over $MgSO_4$, and filtered. The solvent was removed under reduced pressure and the crude oil was purified by column chromatography, eluting with a hexane/ethyl acetate (89:11) mixture to collect the product. After removal of the solvent, the product was obtained as a dark brown oil.

Yield: 94%

^{1}H NMR (300 MHz, $CDCl_3$) δ 8.56 (d, J = 5.2 Hz, 2H), 7.30 (dd, J = 4.6, 1.4 Hz, 2H), 0.31 – 0.22 (m, 9H).

(4-ethynylphenyl)(methyl)sulfane (20b)[100]
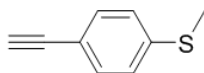
Compound **19** (0.81 g, 3.49 mmol) was dissolved in a mixture of MeOH (50 mL) and DCM (50 mL), and K_2CO_3 (2.42 g, 17.5 mmol) was added. The reaction mixture was purged with Ar flow for 15 min and stirred at room temperature for 2 h. Most of solvents were removed under reduced pressure and water (50 mL) was added to the reaction mixture. The mixture was extracted with Et_2O (2 x 50 mL), and then the combined organic extracts were washed with brine (3 x 50 mL). The combined organic extracts were then dried over $MgSO_4$ and filtered, and the solvent was evaporated in vacuum. Column chromatography on SiO_2 with hexane/DCM (3:1) was carried out to afford the product **20b**.

^{1}H NMR (300 MHz, $CDCl_3$) δ 7.96 – 7.99 (d, J = 8.7 Hz, 2H), 7.53–7.55 (d, J = 8.7 Hz, 2H), 3.92 (s, 3H), 3.23 (s, 1H).

Synthesis of the core structure of the OPE and PPP Crown Ether Molecular Wires Series:

(2,3-dimethoxyphenyl)trimethylsilane[99]
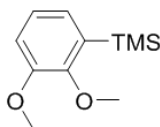
Veratrol (2.5 g, 18.09 mmol) was dissolved in a mixture of dry hexane (6.25 mL) and TMEDA (2.5 mL). nBuLi (1.6 M in hexane, 12.5 mL, 20 mmol) was added dropwise at room temperature. The reaction was stirred at room temperature for 28 h and cooled to -78°C. ClSiMe$_3$ (2.81 mL) was slowly added and the reaction mixture was allowed to warm to room temperature over 5 h. H$_2$O was added and the reaction mixture was extracted with hexane. The organic layer was separated and dried over MgSO$_4$. Solvent was removed in vacuum and the residue was purified by flash chromatography on SiO$_2$ with hexane/DCM (10:1) to give the product as a colourless oil.

Yield: 73%

^{1}H NMR (300 MHz, CDCl$_3$) δ 6.97 (t, *J* = 7.6 Hz, 1H), 6.87 (ddd, *J* = 7.6, 5.6, 1.7 Hz, 2H), 3.78 (d, *J* = 0.8 Hz, 6H), 0.25 (s, 9H).

(2,3-dimethoxy-1,4-phenylene)bis(trimethylsilane) (**21**)[99]
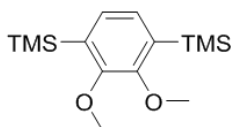
(2,3-dimethoxyphenyl)trimethylsilane (2.76 g, 13.14 mmol) was dissolved in TMEDA (2.5 mL) and cooled to 0°C. nBuLi in hexane (1.6 M, 12.5 mL, 20 mmol) was added dropwise. The reaction mixture was stirred at room temperature for 28 h and then cooled to -78°C. After ClSiMe$_3$ (2.81 mL) was added dropwise, the reaction mixture was warmed to room temperature over 5 h. H$_2$O was added and the reaction mixture was extracted with hexane. The organic layer was separated and dried over MgSO$_4$. Solvent was removed in vacuum and the residue was purified by flash chromatography on SiO$_2$ with hexane/DCM (10:1) to give the product as a colourless oil.

Yield: 58%

^{1}H NMR (300 MHz, CDCl$_3$) δ 7.11 (s, 2H), 3.83 (s, 6H), 0.29 (s, 18H).

1,4-diiodo-2,3-dimethoxybenzene (**22**)[99]
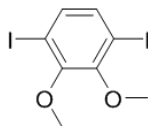
Compound **21** (2.18 g, 7.73 mmol) was dissolved in DCM (11.5 mL) and the solution was cooled to 0°C. A solution of ICl (2.58 g, 15.92 mmol) in DCM (11.5 mL) was slowly added. The reaction mixture was warmed to room temperature, stirred for 30 min, and quenched with an aq solution of Na$_2$S$_2$O$_3$. The organic layer was separated and dried over MgSO$_4$. The solvent was removed in vacuum and the crude product was purified by flash chromatography on SiO$_2$ with hexane/DCM (10:1) to give the product as a yellowish oil that slowly solidify.

Yield: 88%

^{1}H NMR (300 MHz, CDCl$_3$) δ 7.24 (s, 2H), 3.87 (s, 6H).

3,6-diiodobenzene-1,2-diol (**23**)[99]
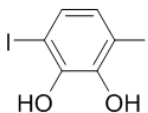
Compound **22** (2.65 g, 6.79 mmol) was dissolved in DCM (29.5 mL) and the solution was cooled to -78°C. BBr$_3$ (31.17 mL, 7.81 g, 31.17 mmol) was added and the reaction mixture was warmed to room temperature and stirred for 14 h. The reaction was poured into ice/H$_2$O and the mixture was extracted with EtOAc. The organic layer was separated and dried over MgSO$_4$. The solvent was removed in vacuum and the residue was purified by flash chromatography on SiO$_2$ with DCM to afford **23** as a white solid.

Yield: 92%

^{1}H NMR (300 MHz, CDCl$_3$) δ 7.00 (s, 2H), 5.62 (s, 2H).

1,4-diiodiobenzene-2,3-[18]crown-6 (**24**)
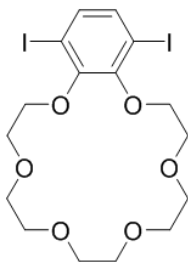
Compound **23** (500 mg, 1.38 mmol) was solubilised into anhyd THF under argon atm. NaH (828 mg, 34.5 mmol) was added and after H_2 evolution has ceased, Cs_2CO_3 (273.93 mg, 1.42 mmol) was added to the mixture and the reaction was refluxed for 30 minutes. After this time, a solution of pentaethylene glycol di(*p*-toluenesulfonate) (798.12 mg, 1.46 mmol) was added dropwise during 1h. After the addition, the reaction mixture was stirred for 78h, cooled to room temperature, and filtered to remove the salts. The solvent was evaporated in vacuum and the residue was purified by flash chromatography on silica with DCM/acetone (9:1) to afford the product as a white solid.

Yield: 20%

^{1}H NMR (300 MHz, CDCl$_3$) δ 7.23 (s, 2H), 4.19 (t, *J* = 4.9 Hz, 4H), 3.96 (t, *J* = 4.9 Hz, 4H), 3.79 – 3.71 (m, 8H), 3.68 (s, 4H).

^{13}C NMR (75 MHz, CDCl$_3$) δ 152.55, 135.70, 93.34, 73.16, 71.04, 70.80, 70.47.

ESI_POS: *m/z* theoretical for $C_{16}H_{22}I_2O_6$ 563,9506 exp [M+Na]$^+$ 586.9398.

Synthesis of the final PPP Crown Ether Molecular Wires Series:

General Procedure to obtain the PPP Derivatives **26a,b**

A round bottom flask charged with 1,4-diiodobenzene-2,3-18-crown-6 (0.053 mmol) and pyridineboronic acid or (4-(methylthio)-phenyl)boronic acid (0.159 mmol) were deoxygenated for 1h while simultaneously deoxygenating the mixture dioxane/H$_2$0 (90 mL, 3:1). After that time, solvents were added to the solids and the mixture was heated to 80°C. After 30 minutes, always under argon atm, Pd(dppf)Cl$_2$

(0.003 mmol) and CsF (0.159 mmol) were added and the reaction was stirred overnight. Cooled to room temperature, the reaction mixture was extracted with chloroform and dried over MgSO$_4$. The solvent was then evaporated in vacuum and the residue purified by column chromatography on silica with CH$_3$Cl/acetone (9:1) to afford the corresponding final products **26a** and **26b**, respectively as yellowish and grey powders.

1,4-di(pyridine-4-yl)benzo[18]crown-6 (**26a**)
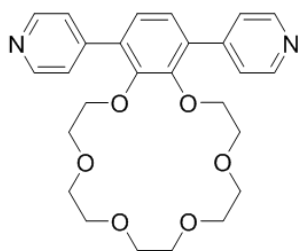
Yield: 99%

^{1}H NMR (300 MHz, CDCl$_3$) δ 8.67 (s, 4H), 7.55 (d, *J* = 5.4 Hz, 4H), 7.22 (s, 2H), 4.03 (t, *J* = 5.0 Hz, 4H), 3.82 – 3.57 (m, 16H).

^{13}C NMR (75 MHz, CDCl3) δ 150.88, 149.99, 145.97, 134.58, 125.88, 124.38, 73.61, 71.32, 71.09, 70.96, 70.59.

FT-IR (KBr) υ: 3033.27, 2924.79, 2864.30, 1724.87, 1596.54, 1545.85, 1514.97, 1464.81, 1437.44, 1404.58, 1354.92, 1318.38, 1214.39, 1118.31, 1045.52, 999.63, 947.14, 810.08, 755.41, 719.59, 623.00 cm^{-1}.

ESI_POS: m/z theoretical for C$_{26}$H$_{30}$N$_2$O$_6$ 466,2104 exp [M+Na]$^+$ 489.2

1,4-bis(4-(methylthio)phenyl)-benzo[18]crown-6 (**26b**)
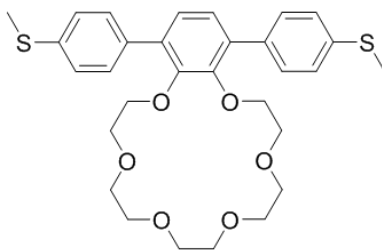
Yield: 98%

^{1}H NMR (300 MHz, CDCl$_3$) δ 7.54 (d, J = 8.3 Hz, 4H), 7.29 (d, J = 8.3 Hz, 4H), 7.15 (d, J = 9.0 Hz, 2H), 3.98 (dd, J = 12.6, 7.6 Hz, 4H), 3.84 – 3.57 (m, 16H), 2.53 (s, 6H).

^{13}C NMR (75 MHz, CDCl$_3$) δ 150.36, 137.55, 134.99, 134.82, 129.79, 126.21, 125.60, 77.16, 72.82, 70.94, 70.81, 70.78, 70.44, 15.86.

FT-IR (KBr) υ: 2923.28, 2868.92, 1737.58, 1597.04, 1508.37, 1468.32, 1432.97, 1388.38, 1353.14, 1304.09, 1243.58, 1210.90, 1116.82, 1050.21, 1014.64, 946.79, 808.15 cm^{-1}.

ESI_POS: m/z theoretical for C$_{30}$H$_{36}$O$_6$S$_2$ 556,1953exp [M+Na]$^+$ 579.2.

General Procedure to form the complexes **27a,b**

Compound **26a** or **26b** (0.018 mmol) and KSCN (0.018 mmol) were dissolved in hot methanol (60°C) for 3h, under stirring. Cooled to room temperature, the solution was filtered and the solvent was evaporated to recover the complexed products **27a,b**.

Complex 27a
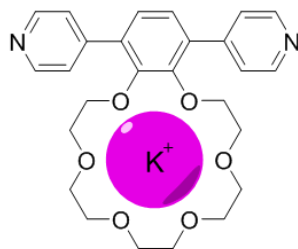
Yield: quantitative

^{1}H NMR (300 MHz, CDCl$_3$) δ 8.72 (d, J = 3.2 Hz, 4H), 7.60 (d, J = 5.4 Hz, 4H), 7.23 (s, 2H), 3.87 (s, 4H), 3.70 (d, J = 10.7 Hz, 12H), 3.58 (d, J = 4.2 Hz, 4H).

^{13}C NMR (75 MHz, CDCl$_3$) δ 150.19, 149.84, 145.38, 134.20, 126.54, 124.06, 77.16, 73.68, 73.38, 70.45, 70.26.

ESI_POS: *m/z* theoretical for C$_{26}$H$_{30}$N$_2$O$_6$ 466.2 exp [M+K]$^+$ 505.4.

Complex 27b
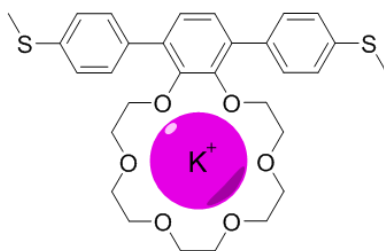
Yield: quantitative

^{1}H NMR (300 MHz, CDCl$_3$) δ 7.56 (d, *J* = 8.3 Hz, 4H), 7.35 (d, *J* = 8.3 Hz, 4H), 7.13 (s, 2H), 3.71 (d, *J* = 25.2 Hz, 16H), 3.47 (d, *J* = 3.3 Hz, 4H), 2.54 (s, 6H).

^{13}C NMR (75 MHz, CDCl$_3$) δ 148.60, 138.55, 134.50, 134.03, 129.27, 126.73, 126.39, 69.84, 68.66, 68.37, 15.50.

ESI_POS: *m/z* theoretical for C$_{30}$H$_{36}$O$_6$S$_2$ 556,1953 exp [M+K]$^+$ 595.2

.

6. Appendix

6. Appendix

6.1. *NMR titration experiments*

In a typical experiment, a solution of the amidine compound **14b** at 1×10^{-3} M was utilized as solvent in the preparation of the guests solutions (**16a** or **16b**) at 1×10^{-2} M, to ensure working at constant concentration of the host. Increasing amounts of **16a** or **16b** solutions (1×10^{-2} M in [D$_6$]DMSO) were added up to a total of 3 molar equivalents to the host solution of **14b** (1×10^{-3} M in [D$_6$]DMSO) and ^{1}H NMR spectra were recorded at room temperature on a Bruker DPX-300. Determination of the binding constants for the complexes formed by interaction between **14b** and **16a** or **16b** was carried out by the calculator *Bindfit* of the website *supramolecular.org*. The calculator operates by accepting a preformatted excel document with host and guest concentrations at each titration point together with the appropriate signals (e.g., for NMR the chemical shifts). The user, at this point, has to provide an initial guess for the binding constant and the calculator performs a non-linear regression on the given data using the corresponding exact binding equation implemented on the server. In our case, it was chosen to use the curve-fitting algorithm Nelder-Mead and the binding isotherm for a simple 1:1 equilibrium[89b] (Equation 2):

$$[G] = \frac{1}{2}\left\{\left(G_0 - H_0 + \frac{1}{K_a}\right) - \sqrt{\left(G_0 - H_0 + \frac{1}{K_a}\right)^2 + 4\frac{G_0}{K_a}}\right\}$$

Equation 2: Binding isotherm for a 1:1 equilibrium.

Here, G is the guest concentration (**16a** and **16b**, respectively), G$_0$ the "initial" guest concentration, H refers to the host concentration (**14b**), H$_0$ to the "initial" host concentration and K_a represents the association constant.

The binding fit program allowed to determine values of K$_a$ > 10^4 M^{-1} for both complexes. These binding constants were confirmed using Sigma Plot software by fitting the proton signals to a 1:1 association model and, again, in both cases K$_a$ > 10^4 M^{-1} were obtained. Therefore, more diluted solutions were considered necessary to get a more exact value of K. However, attempts with more diluted samples, always

taking into account the sensitivity's limits of the NMR technique, did not allowed to get the proper ^{1}H NMR spectra.

16a·14b
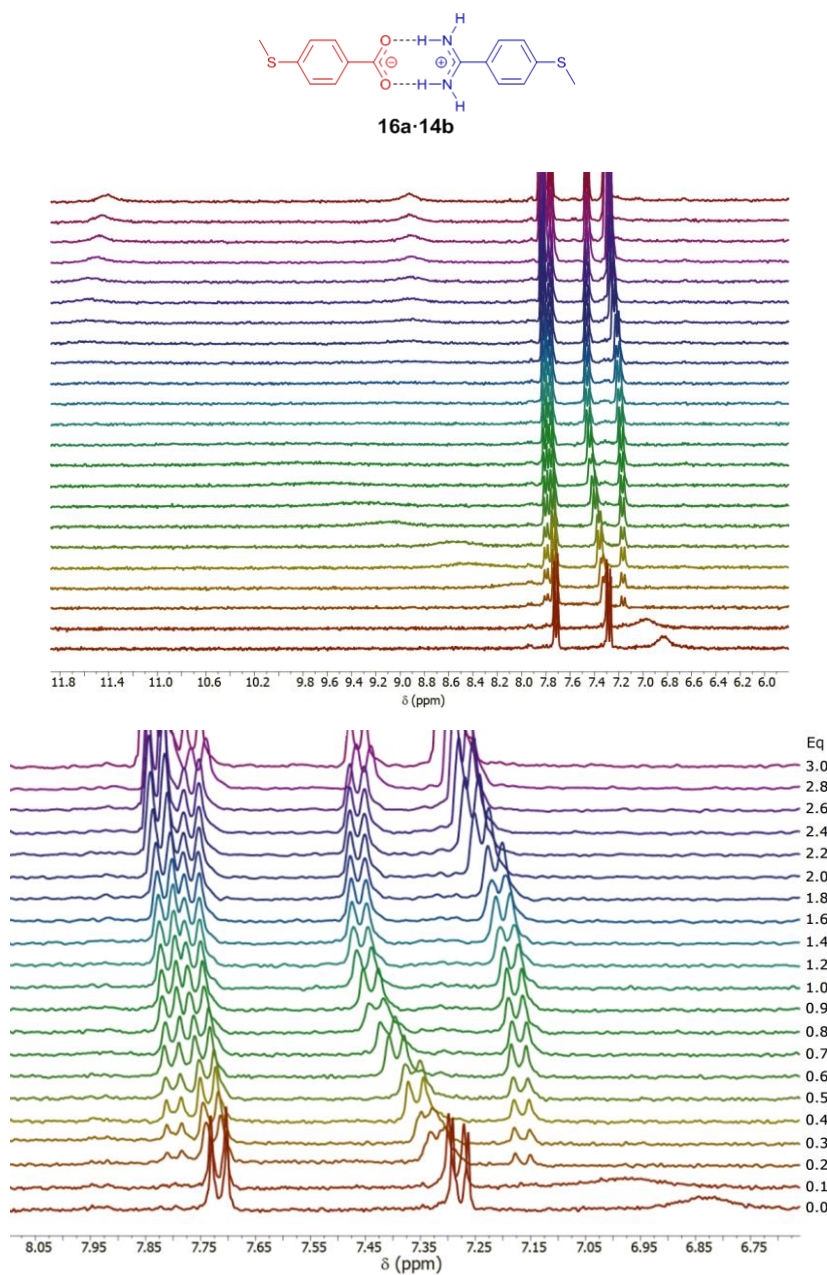
Figure 60: NMR titration of a dilute solution of **14b** (1×10^{-3} M) in [D_6]DMSO with increasing concentration of **16a** in [D_6]DMSO (0; 2.66×10^{-4}; 5.27×10^{-4}; 7.85×10^{-4}; 1.04×10^{-3}; 1.29×10^{-3}; 1.54×10^{-3}; 1.81×10^{-3}; 2.07×10^{-3}; 2.32×10^{-3}; 2.57×10^{-3}; 3.10×10^{-3}; 3.61×10^{-3}; 4.13×10^{-3}; 4.63×10^{-3}; 5.17×10^{-3}; 5.68×10^{-3}; 6.19×10^{-3}; 6.69×10^{-3}; 7.21×10^{-3} and 7.73×10^{-3} M).

16b·14b
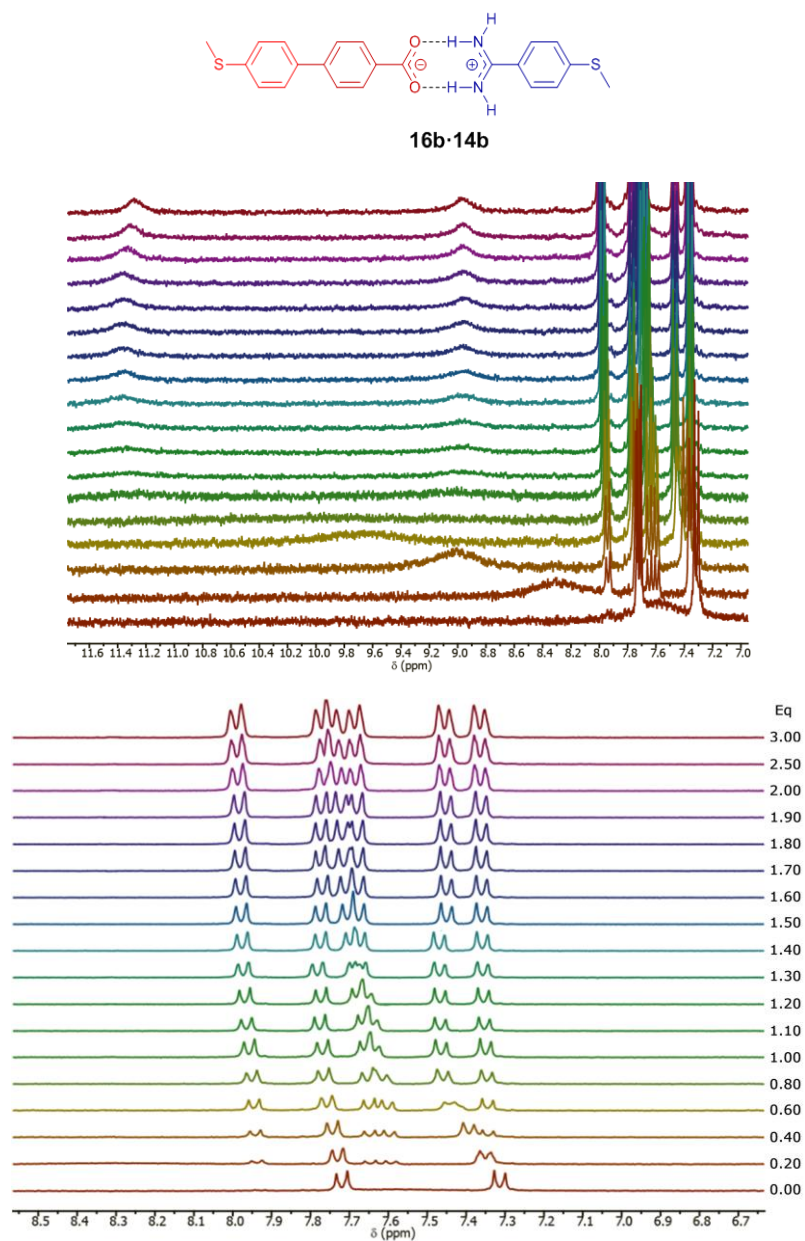
Figure 61: NMR titration of a dilute solution of **14b** (1×10^{-3} M) in [D$_6$]DMSO with increasing concentration of **16a** in [D$_6$]DMSO (0; 8.43×10^{-5}; 1.7×10^{-4}; 2.56×10^{-4}; 3.42×10^{-4}; 4.28×10^{-4}; 4.71×10^{-4}; 5.14×10^{-4}; 5.57×10^{-4}; 6.00×10^{-4}; 6.43×10^{-4}; 6.86×10^{-4}; 7.30×10^{-4}; 7.73×10^{-4}; 8.16×10^{-4}; 8.59×10^{-4}; 1.07×10^{-3} and 1.29×10^{-3}).

Chapter 2.

7. Background

7. Background

7.1. *Carbon Nanostructures*

Although widely distributed, carbon is not really particularly abundant in nature. Actually, this atom constitutes only about 0.025 percent of Earth's crust.[112] However, from all the elements contained in the Periodic Table, it is the only one able to provide the basis for life on our planet, forming more compounds than all the other elements combined. It exists in a wide variety of nanostructures embracing different allotropic forms characterized by an ample amount of shapes and sizes (Figure 62).
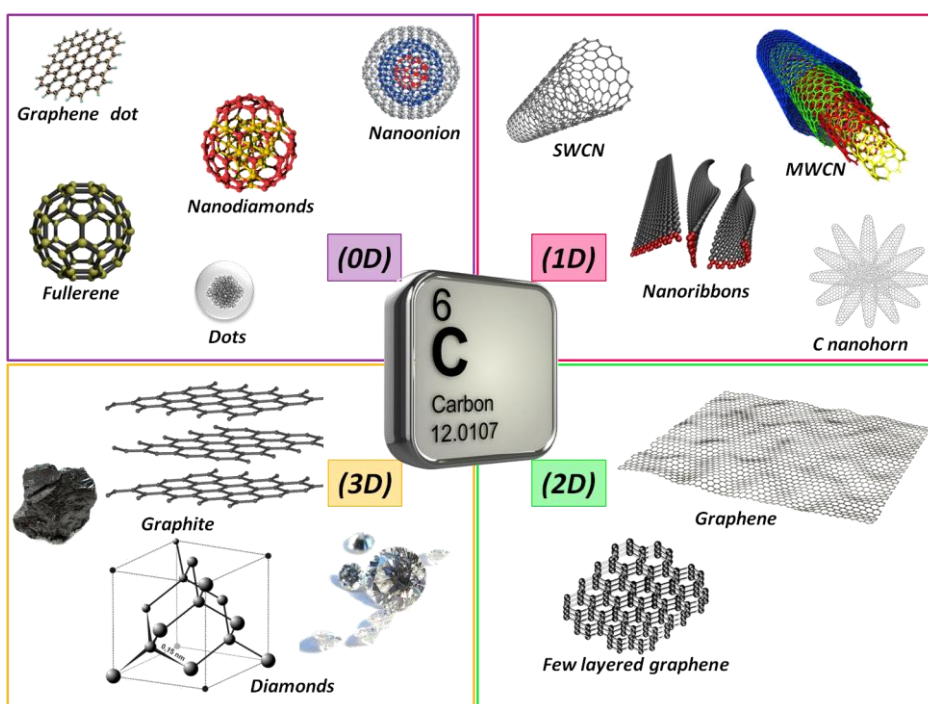
Figure 62: Allotropes and nanoforms of carbon.

For a long time, diamond and graphite represented the only known allotropes of carbon. This situation changed in 1985 with the serendipitous discovery of fullerenes, observed for the first time by H. Kroto, R. Smalley and R. Curl, who received in 1996 the Nobel Prize in

---

[112] HyperPhysics, Georgia State University, Abundance of Elements in Earth's Crust.

Chemistry for this finding.[113] The advent of fullerenes opens the beginning of a discovering era for other amazing carbon nanostructures, such as carbon dots (CDs), carbon nanotubes (CNTs), and graphene as well as other less-explored carbon nanoforms such as graphene quantum dots (GQDs), nanodiamonds, carbon nanoonions, carbon nanohorns, etc. (Figure 62).

A most interesting finding is that this structural diversity, guaranteed by sp^3-, sp^2-, and sp-hybridized carbon networks, results in sheer endless chemical and physical properties.

7.1.1.   *[60]Fullerene: Structure and Properties*

After the fortunate discovery of fullerenes by H. Kroto, R. Smalley and R. Curl in 1985, the first successful preparation of these zero-dimensional structures in macroscopic quantities, by evaporation and recondensation of graphite, was reported five years later by Krätschmer and Huffman.[114] The fullerenes, of which the smallest stable and most prominent is C_{60}, are carbon structures built up of fused pentagons and hexagons. The pentagons are the units responsible for providing curvature to the structure, since a network consisting only by hexagons is planar (see graphene).

Specifically, C_{60}, with an outer diameter of 10.34 Å,[115] is made up of a spherical network of sixty structurally equivalent sp^2-hybridized carbon atoms. The shape of this molecule corresponds to a football (or soccer ball or, more technically, an I_h-symmetrical truncated icosahedron) composed of 12 isolated pentagons and 20 hexagons and two different type of bonds. The bonds at the junctions of two hexagons, [6,6] bonds, are shorter (1.37 Å) than the bonds at the junctions of a hexagon and a pentagon, [5,6] bonds (1.45 Å) (Figure 63).

[113] H. W. Kroto, J. R. Heath, S. C. O'Brien, R. F. Curl, R. E. Smalley, *Nature* **1985**, *318*, 162.

[114] W. Kratschmer, L. D. Lamb, K. Fostiropoulos, D. R. Huffman, *Nature* **1990**, *347*, 354.

[115] a) C. S. Yannoni, P. P. Bernier, D. S. Bethune, G. Meijer, J. R. Salem, *J. Am. Chem. Soc.* **1991**, *113*, 3190; b) M. S. Dresselhaus, G. Dresselhaus, P. C. Eklund, *Science of Fullerenes and Carbon Nanotubes*, Academic Press, San Diego, **1996**.
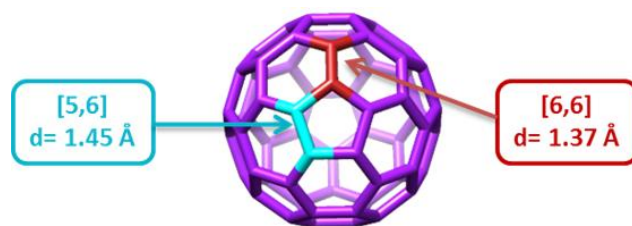
Figure 63: [60]fullerene structure showing the differenttypes of bonds.

This bond-length alternation in C_{60} shows that the double bonds are located in the [6,6] junctions and there are no double bonds in the pentagonal rings. Due to the curvature of the molecule, each σ-bond presents an intermediate hybridization of $sp^{2.3}$ in between the hybridizations of graphite (sp^2) and diamond (sp^3).[116] Therefore, [60]fullerene behaves as an electron deficient polyene, with the most reactive positions located in the [6,6] bonds. The driving force of the reactivity of fullerenes is due to the release of strain energy stemming from the saturation of one or more double bonds.

The stability of C_{60} has been demonstrated through the isolated pentagon rule (IPR), developed by H. Kroto in 1987.[117,118] It says that the local tension enhances with the number of shared bonds between two pentagon rings, leading to less stable molecules. Owing to this rule, the easier fullerenes to be formed will be those in which pentagons are separated by rings of hexagons.[118]

The [6,6] bonds in the C_{60} cage, due to their shorter length respect to the [5,6] bonds, are considered as double bonds. The six-membered rings, therefore, resemble the rarely encountered cyclohexatriene molecule, with localised multiple bonds, while five-membered rings are topologically related to the [5]radialene.[119] The non-aromaticity in the six-membered fragments of the [60]fullerene cage is a consequence of the substantial deviation of the double bond geometry from the normal planar one, which means a pyramidalization effect. This

[116] R. C. Haddon, *Acc. Chem. Res*. **1992**, *25*, 127.

[117] T. G. Schmalz, W. A. Seitz, D. J. Klein, G. E. Hite, *Chem. Phys. Lett*. **1986**, *130*, 203.

[118] H. W. Kroto, *Nature* **1987**, *329*, 529.

[119] A. Hirsch, *Fullerenes and Related Structure,* Top Curr. Chem. 199, Springer, Berlin Heidelberg New York Springer, **1999**.

pyramidalization is the reason for the appearance of properties non-typical of arenes.[120] In spite of considerable pyramidalization of multiple bonds, the six-membered rings maintain a planar geometry, mainly due to the rigidity of the [60]fullerene spherical structure. This blocked-pyramidization induced strain determines the high reactivity of fullerenes compared to other carbon forms.

Fullerene C_{60} is a good electron acceptor.[121,122,123] Theoretical calculations of the molecular orbital levels of C_{60} show a triply degenerated LUMO comparatively low in energy.[124] It allows the reversible addition of up to six electrons in solution.[125] Cyclic voltammetry (CV) measurements of C_{60} solutions also supported its facile and stepwise reversible reduction.[126]

All the reductions are one-electron transfer processes and are favored by the small reorganization energy of [60]fullerene.[121] However, the reduction potentials are strongly dependent on the nature of the solvent, the electrolyte and the temperature. The six electron acceptor reversible capability of [60]fullerene comes out in experiments at -10°C in a solution of acetonitrile:toluene (Figure 64).[127]

---

[120] A. L. Balch, M. M. Olmstead, *Chem. Rev.* **1998**, *98*, 2123.

[121] D. M. Guldi, *Chem. Commun.*, **2000**, *5*, 321.

[122] D. M. Guldi, M. Prato, *Acc. Chem. Res*. **2000**, *33*, 695.

[123] N. Martín, L. Sánchez, B. Illescas, I. Pérez, *Chem. Rev*. **1998**, *98*, 2527.

[124] a) C. A. Reed, R. D. Bolskar, *Chem. Rev*. **2000**, *100*, 1075; b) A. D. J. Haymet, *Chem. Phys. Lett*. **1985**, *122*, 421; c) P. D. Hale, *J. Am. Chem. Soc*. **1986** *108*, 6087.

[125] a) F. Arias, Q. Xie, Y. Wu, Q. Lu, S. R. Wilson, L. Echegoyen, *J. Am. Chem. Soc*. **1994**, *116*, 6388; b) P.M. Allemand, A. Koch, F. Wudl, Y. Rubin, F. Diederich, M. M. Alvarez, S. J. Anz, R. L. Whetten, *J. Am. Chem. Soc*. **1991**, *113*, 1050.

[126] R. E. Haufler, J. Conceicao, L. P. F. Chibante, Y. Chai, N. E. Byrne, S. Flanagan, M. M. Haley, S. C. O'Brien, C. Pan, *J. Phys. Chem*. **1990**, *94*, 8634.

[127] Q. Xie, E. Pérez-Cordero, L. Echegoyen, *J. Am. Chem. Soc*. **1992**, *114*, 3978.
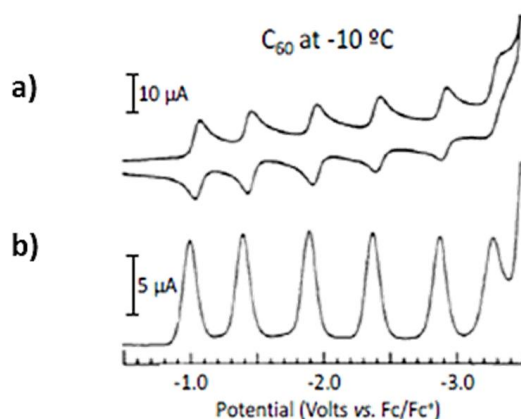
Figure 64: Cyclic voltammogram (a) and square wave voltammogram (b) of C_{60} with TBAPF$_6$ as supporting electrolyte, at −10° C in toluene:acetonitrile 4:1 at 100 mV/s (V vs Fc/Fc$^+$). Ref 128.

The oxidation process, as Haddon *et al*. predicted,[128] is an extremely difficult process, but in 1993 Echegoyen *et al*. were able to measure the first electrochemically irreversible oxidation of C_{60} at 1.26 V (*vs* Fc/Fc$^+$, TBAPF$_6$, 1,1,2,2-tetrachloroethane, 100 mV/s).[129]

These pronounced redox activity and excellent electronic properties have led to a notable breakthrough in synthetic electron donor-acceptor systems, using C_{60} as an outstanding electron acceptor. Especially, under optimal conditions, the small reorganization energies provide an optimal charge-separation kinetics and a decelerated charge-recombination rate. Thus, donor-acceptor arrays containing fullerene have been proposed as models for artificial photosynthetic mimics and as energy storage systems.[130] Also, thanks to this property, C_{60} or its derivatives may be employed as acceptor components in photovoltaic devices as well as in organic electronics.

7.1.1.1. *[60]Fullerene: Chemical Reactivity*

Because C_{60} does not possess any kind of functionalization, but double bonds, its reactivity is driven by the transformation of more strained *sp*^{2} into *sp*^{3} carbon atoms. This simple consideration shows the great

---

[128] R. C. Haddon, L. E. Brus, K. Raghavachari, *Chem. Phys. Lett*. **1986**, *125*, 459.

[129] Q. Xie, F. Arias, L. Echegoyen, *J. Am. Chem. Soc*. **1993**, *115*, 9818.

[130] H. Imahori, Y. Sakata, *Eur. J. Org. Chem*. **1999**, *1999*, 2445.

difference between the reactivity of fullerenes and the classical planar aromatic systems.

The [60]fullerene chemical behaviour is comparable to an electron poor polyolefin. The driving force of its chemical reactivity is the reduction of the strain energy stored in the spherical carbon framework.

Regarding the solubility, [60]fullerene is soluble in aromatic solvents and in carbon disulfide. In polar and H-bonding solvents such as acetone, tetrahydrofuran or methanol, C_{60} is essentially insoluble. Therefore, chemical functionalization is the key to fully exploit its vast potential, providing the possibility of combining its unique properties with those of other compounds, while increasing its solubility.

Among all known organic reactions, the nucleophilic addition and the cycloaddition reactions have been widely employed to modify fullerenes for further practical applications.

a) *Nucleophilic Additions*

Nucleophiles of different nature, based on carbon, nitrogen, phosphorous or oxygen, give a wide variety of nucleophilic addition reactions to [60]fullerene. By the initial attack of a nucleophile to C_{60}, the intermediate $Nu_nC_{60}^{n-}$ is formed. This intermediate is stabilized by: (a) the addition of electrophiles E^+, for example H^+ or carbocations to give $C_{60}E_nNu_n$ species, (b) the addition of neutral electrophiles EX such as alkyl halogenides to give $C_{60}E_nNu_n$, (c) intramolecular addition to yield methanofullerenes and cyclohexenefullerenes, or by (d) oxidation to obtain compounds of type $C_{60}Nu_2$ (Scheme 19).
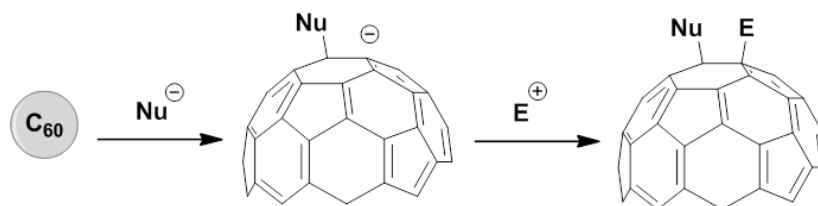
Scheme 19: General mechanism of the nucleophilic addition to [60] fullerene.

Although many isomers are possible for additions, the preferred mode of addition is 1,2. The addition pattern changes according to the size of the added groups. For a combination of sterically demanding addends,

1,4 additions and even 1,6 additions can take place alternatively or exclusively.[119,131]   Given the large number of reactive double bonds in the molecule, polyadditions are frequent in the chemistry of fullerenes.

b) *Cycloaddition Reactions*

Cycloaddition is the most employed reaction in fullerenes chemistry since it leads to stable adducts avoiding the formation of isomeric mixtures, very frequent in nucleophilic addition reactions.

A large variety of cycloaddition reactions have been carried out with C_{60} and the complete characterization of the products, mainly monoadducts, have greatly increased our knowledge of fullerenes chemistry. These chemical transformations provide a powerful tool for the functionalization of the fullerene sphere, because almost any functional group can be covalently linked to C_{60} (Scheme 20).
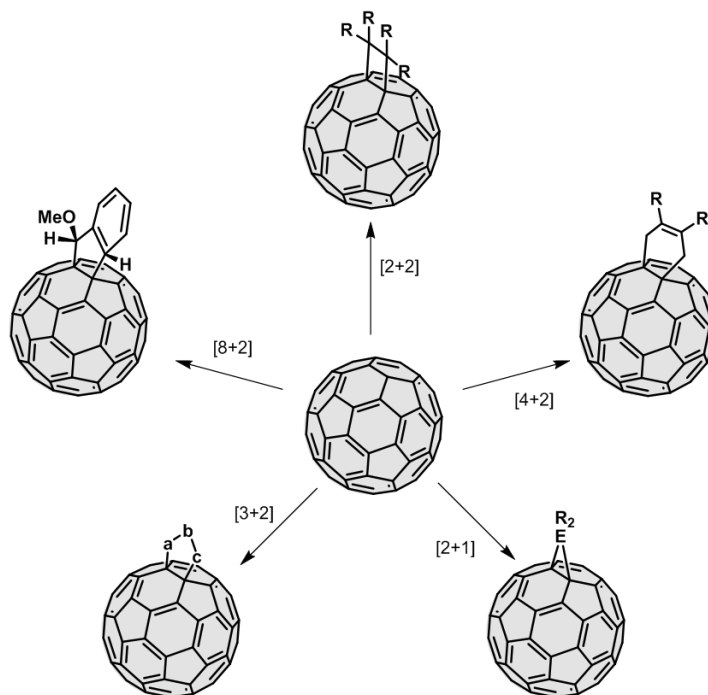
Scheme 20: Schematic representation of cycloaddition reactions on [60]fullerene.

---

[131] M. S. Meier, R. G. Bergosh, M. E. Gallagher, H. P. Spielmann, Z. Wang, *J. Org. Chem.* **2002**, 67, 5946.

7.1.1.2.   *[60]Fullerene: Applications*

The possibility to chemically modify the structure of C_{60} opened the doors to the many possible investigation lines involving this molecule, as well as to its real commercial applications. Sporting goods, such as badminton rackets with fullerenes in the polymer matrix composite, and cosmetics, such as the Vitamin C_{60} skin creams, are only some suggestive examples made available to consumers in select markets (Figure 65).

Figure 65: a) and b) Advertisements of cosmetic products based on [60]fullerene. c) Racket frames incorporating nanoclays with fullerenes.

However, fullerenes research has mainly been focused in the fields of organic electronics and bioscience in the search for potential applications.

Molecular electronics is a research area where the outstanding properties of fullerenes, in particular their electrochemical and photophysical properties (favouring the separation of the charges while avoiding a fast recombination)[132,11m] find application for the construction of molecular electronic devices such as transistors and rectifiers. Organic field effect transistors (OFETs) and photodetectors performance has been increased indeed due to the n-type semiconducting properties of fullerenes based on C_{60}, C_{70} along with

---

[132] a) R. A. Marcus, *J. Chem. Phys. I* **1956**, 24, 966.

C$_{84}$.[133] A recent work of Qiu *et al.* showed, for example, that the degree of rectification current of mixed-monolayers of alkanethiolates in tunneling junctions can be controlled by the amount of fullerene incorporated, reaching a maximum value of 940 at 1 V.[134]

[60]Fullerene and its derivatives have also found wide application in the nowadays important sector of environment sustainability. Solar cells, alternatives to fossil fuels and water purification systems, are some of the possible uses to which fullerenes are dedicated. In fact, (6,6)phenyl C$_{61}$ butyric acid methyl ester (PC$_{61}$BM) and (6,6)phenyl C$_{71}$ butyric acid methyl ester (PC$_{71}$BM) acceptors still remain the cornerstone of all fullerene derivatives for photovoltaic (PV) studies.[135] For example, recently, Chen *et al.* reported a record high power conversion efficiency (PCE) of ~10% for a bulk heterojunction (BH) organic solar cell, obtained for the PTB7-Th polymer with PC$_{71}$BM acceptor.[136] Fullerene employment as hydrogen gas storage devices for electric vehicles is another interesting green application due to its unique molecular structure, which potentially can be chemically and reversibly hydrogenated and de-hydrogenated.[137] C$_{60}$H$_{36}$ isomers, characterized approximately by 5% of hydrogen content, have been developed experimentally.[138] According to theoretical calculations, a C-H bond is 68 kcal/mol, which is about 15 kcal/mol weaker than a C-C bond (83 kcal/mol).[137] This means that, under heating, the C-H bond will break faster than the C-C bond, making fullerene hydrides able to give off hydrogen while preserving their structure. Carbon nanomaterials, including fullerenes, have also been proposed for the development of a range of new bio-technologies, including degradation of a probe organic compound by *in situ* generation of reactive oxygen

[133] a) P. H. Wöbkenberg, D. D. C. Bradley, D. Kronholm, J. C. Hummelen, D. M. de Leeuw, M. Cölle, T. D. Anthopoulos, *Synthetic Metals* **2008**, *158*, 468; b) K. Shibata, Y. Kubozono, T. Kanbara, T. Hosokawa, A. Fujiwara, Y. Ito, H. Shinohara, *Appl. Phys. Lett.* **2004**, *14*, 84, 2572.

[134] L. Qiu, Y. Zhang, T. L. Krijger, X. Qiu, P. van't Hof, J. C. Hummelen, R. C. Chiechi, *Chem. Sci.* **2017**, *8*, 2365.

[135] a) P. Hudhomme, *EPJ Photovolt.* **2013**, *4*, 40401; b) Y. He, Y. Li, *Phys. Chem. Chem. Phys.* **2011**, *13*, 1970; c) S. Vidal, M. Izquierdo, W. Kit Law, K. Jiang, S. Filippone, J. Perles, H. Yan, N. Martín, *Chem. Commun.* **2016**, *52*, 12733.

[136] J. D. Chen, C. Cui, Y. Q. Li, L. Zhou, Q. D. Ou, *Adv. Mater.* **2015**, *27*, 1035.

[137] J. C. Withers, R. O. Loutfy, T. P. Lowe, *Fullerene Sci. Technol.* **1997**, *5*, 1.

[138] A. A. Peera, L. B. Alemany, W. E. Billups, *Appl. Phys. A* **2004**, *78*, 995.

species (ROS), new strategies for microbial disinfection, and the inhibition of bio-film development on membrane surfaces.[139]

Recently there has been much interest in studying possible biological activities of fullerenes with the aim of using them in medicine. Having unique electronic properties and the possibility to access to a full set of functionalization tools to improve solubility in physiological media, fullerenes become attractive candidates for diagnostic, therapeutic and theranostic applications. Their powerful antioxidant and radical scavenger properties have led to investigate their potential in a wide variety of biological activities including multiple sclerosis,[140] neurodegenerative,[141] anti-HIV activity,[142] anti-Ebola activity,[143] cancer,[144] radiation exposure,[145] ischemia,[146] osteoporosis,[147] general inflammation[148] and selective antimicrobial agents against bacteria, just to name a few.[149]

[139] S. R. Chae, E. M. Hotze, M. R. Wiesner, *Water Sci Technol.* **2013**, *67*, 11, 2582.

[140] A. S. Basso, l. D. Frenke, F. J. Quintana, F.A. Costa-Pinto, S. Petrovic-Stojkovic, L. Puckett, A. Monsonego, A. Bar-Shir, Y. Engel, M. Gozin, H. L. Weiner, *J. Clin. Invest.* **2008**, *118*, 1532.

[141] L. L. Dugan, D. M. Turetsky, C. Du, D.Lobner, M. Wheeler, C. R. Almli, C. K. F. Shen, T. Y. Luh, D. W. Choi, T. S. Lin, *PNAS* **1997**, *94*, 9434.

[142] S. Bosi, R. T. Da, G. Spalluto, J. Balzarini, M. Prato, *Bioorg. Med. Chem. Lett.* **2003**, *13*, 4437; b) S. Marchesan, R. T. Da, G. Spalluto, J. Balzarini, M. Prato, *Bioorg. Med. Chem. Lett.* **2005**, *15*, 3615.

[143] a) A. Muñoz, D. Sigwalt, B. M. Illescas, J. Luczkowiak, L. Rodríguez-Pérez, I. Nierengarten, M. Holler, J. Remy, K. Buffet, S. P. Vincent, J. Rojo, R. Delgado, J. Nierengarten, N. Martín, *Nat. Chem.* **2016**, *8*, 50; b) B. M. Illescas, J. Rojo, R. Delgado, N. Martín, *J. Am. Chem. Soc* **2017***, 139*, 6018.

[144] C. S. Berger, J. W. Marks, R. D. Bolskar, M. G. Rosenblum, L. J. Wilson, *Transl. Oncol.* **2011**, *4*, 350.

[145] B. Daroczi, G. Kari, M. F. McAleer, J. C. Wolf, U. Rodeck, A. P. Dicker. *Clin*. *Cancer Res.* **2006**, *12*, 7086.

[146] Y. L. Lai, P. Murugan, K. C. Hwang, *Life Sci.* **2003**, *72*, 1271.

[147] K. A. Gonzalez, L. J. Wilson, W. Wu, G. H. Nancollas, *Bioorg. Med. Chem.* **2002**, *10*, 6, 1991.

[148] A. Dellinger, Z. Zhou, R. Lenk, D. Macfarland, C. L. Kepley, *Exp. Dermatol.* **2009**, *18*, 1079.

[149] N. Tsao, T. Y. Luh, C. K. Chou, T. Y. Chang, J. J. Wu, C. C. Liu, H. Y. Lei, *J. Antimicrob. Chemother.* **2002**, *49*, 641.

7.1.2. *Graphene: Structure and Properties*

Graphite, the most abundant natural carbon allotrope due to its thermodynamic stability at ambient temperature and pressure, is characterized by a network of sp^2 hybridized carbons for each single layer, which in turn corresponds to graphene structure. Each atom is bonded to other three, forming hexagons that are fused throughout the layer. The layers are separated by a distance of 3.35 Å and linked by van der Waals interactions generated by the delocalization of π-orbitals. This delocalization generates conjugated π-electrons that are responsible of the electronic properties of graphite. Graphite is anisotropic because of the nature of this binding forces, it presents good electrical and thermal conductivity through the layers and it is a poor electrical and thermal conductor in the perpendicular direction.[150]

Although graphene can be considered the mother for all the different allotropes (i.e. fullerenes can be obtained from graphene with the introduction of pentagons,[151] carbon nanotubes by rolling graphene along a given direction and reconnecting the carbon bonds,[152] etc.) and it has been presumably produced every time someone writes with a pencil, it was "curiously" isolated *only* 440 years after its invention (Figure 66).[153]

[150] D. D. L. Chung, *J. Mater. Sci.* **2002**, *37*, 1475.

[151] W. Andreoni, *The Physics of Fullerene-Based and Fullerene-Related Materials*, Springer, Berlin, **2000**.

[152] a) R. Saito, G. Dresselhaus, M. S. Dresselhaus, *Physical Properties of Carbon Nanotubes*, Imperial College Press, London, **1998**; b) J. C. Charlier, X. Blase, S. Roche, *Rev. Mod. Phys.* **2007**, *79*, 677.

[153] K. S. Novoselov, A. K. Geim, S. V. Morozov, D. Jiang, Y. Zhang, S. V. Dubonos, I. V. Gregorieva, A. A. Firsov, *Science* **2004**, *306*, 666.
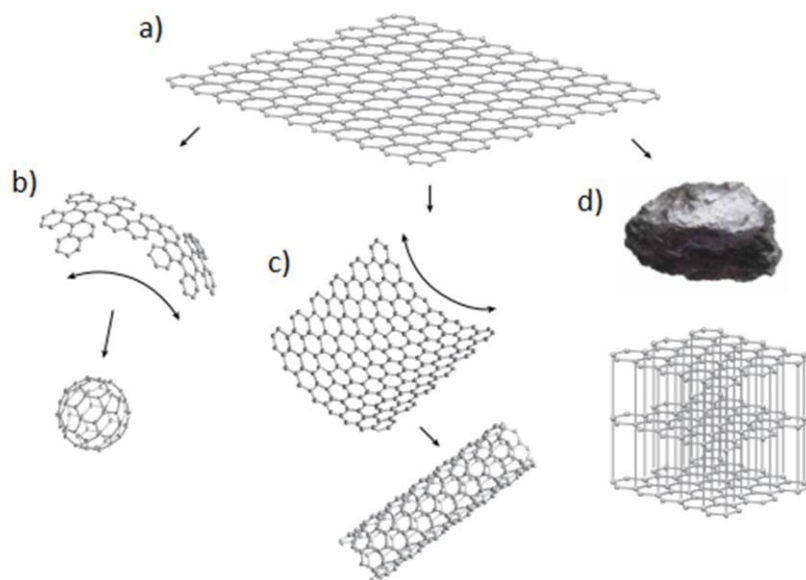
Figure 66: Allotropes of carbon: a) 2-D graphene, b) 0-D fullerene, c) 1-D carbon nanotube, d) 3-D graphite.

In general, graphene can be thought of as composed of benzene rings stripped out from their hydrogen atoms.[154] In fact, it is a two-dimensional material consisting of a single-atom-thick sheet of sp^2-hybridized carbon atoms arrayed in a honeycomb pattern, which means that is a single atomic layer of graphite. It is the world's thinnest, strongest, and stiffest material. It is also furnished by peculiar features such as high flexibility and brittleness at the same time, or impermeability to gases.[153] However, from the application viewpoint, what really makes graphene the most promising of all carbon nanostructured allotropes is the displaying of superior characteristics of electronic, mechanical, optical, and transport nature. These include ambipolar field effect,[155] superlative mechanical strength,[156] large specific surface area,[157] high transparency,[158,159] and high thermal

---

[154] L. Pauling, *The nature of the chemical bond and the structure of molecules and crystals: an introduction to modern structural chemistry,* Cornell University Press., Ithaca, NY, **1939**.

[155] K. S. Novoselov, A. K. Geim, S. V. Morozov, D. Jiang, M. I. Katsnelson, I. V. Grigorieva, S. V. Dubonos, A. A. Firsov, *Nature* **2005**, *438*, 197.

[156] C. Lee, X. D. Wei, J. W. Kysar, J. Hone, *Science* **2008**, *321*, 385.

[157] M. D. Stoller, S. J. Park, Y. W. Zhu, J. H. An, R. S. Ruoff, *Nano Lett.* **2008**, *8*, 3498.

conductivity.[160] Moreover, electrons can move through graphene sheets as if they have no mass and cover submicrometer distances thanks to ballistic transport quantum effects.[161]

Until its isolation, it was expected that graphene, as two dimensional material, could not exist because of thermodynamic instability.[162,163] Nevertheless, these materials are stabilized by deformations in the third dimension. Even if it is always being considered as a planar material, A. Geim and K. Novoselov reported that graphene layers present intrinsic corrugations and can exist without a substrate.[164] Real graphene, in fact, exhibits edges that have either a zigzag or an armchair arrangement (Figure 67).[165]
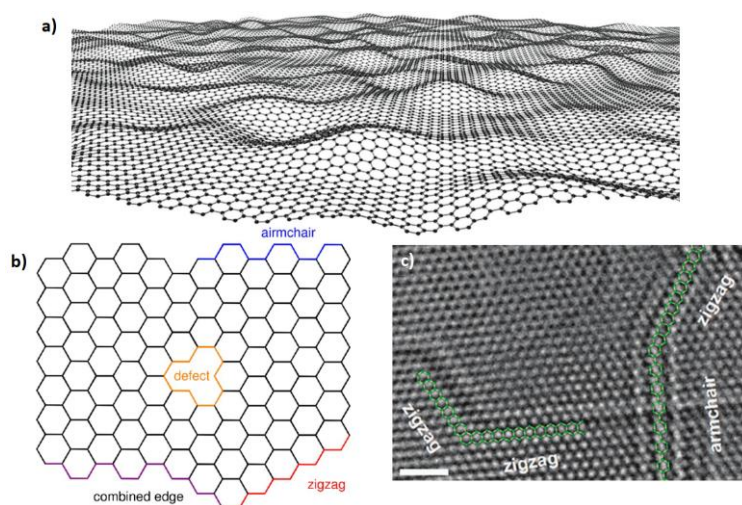
Figure 67: a) Corrugation of graphene surface; b) graphene's sheet with zig-zag and armchair edges and c) integrated TEM-STM system image showing either zigzag and armchair edges.

[158] A. Reina, X. Jia, J. Ho, D. Nezich, H. Son, V. Bulovic, M. S. Dresselhaus, J. Kong, *Nano Lett.* **2009**, *9*, 30.

[159] R. R. Nair, P. Blake, A. N. Grigorenko, K. S. Novoselov, T. J. Booth, T. Stauber, N. M. R.Peres, A. K. Geim, *Science* **2008**, *320*, 1308.

[160] A. A. Balandin, S. Ghosh, W. Bao, I. Calizo, D. Teweldebrhan, F. Miao, C. N. Lau, *Nano Lett.* **2008**, *8*, 902.

[161] A. K. Geim, *Science* **2009**, *324*, 1530.

[162] R. E. Peierls, *Ann. Inst. Henri Poincare* **1935**, *5*, 177.

[163] L. D. Landau, *Phys. Z. Sowjetunion* **1937**, *11*, 26.

[164] J. C. Meyer, A. K. Geim, M. I. Katsnelson, K. S. Novoselov, T. J. Booth, S. Roth, *Nature* **2007**, *446*, 60.

[165] L. Yan, Y. B. Zheng, F. Zhao, S. Li, X. Gao, B. Xu, P. S. Weiss, Y. Zhao, *Chem. Soc. Rev.* **2012**, *41*, 97.

Although a two dimensional material is considered a one atom thick layer, graphene is defined as two dimensional when it contains up to ten layers. So, depending on its structure, it could be classified in three different types: single layer, bilayer and few-layer graphene.[166]

In general, carbon has led to several technological revolutions, from the industrial one, with energy production by burning carbon, in the 19th century[167], to the revolution in manufacturing industry, in the 20th century, with the introduction of plastics based on carbon.[168] So, why might graphitic carbon not be a key component of a third technological revolution in the 21st century?

After all, the number of publications on this topic keeps growing with no sign of slowing down, and the reasons are multiple. First, its unique set of properties can be exploited in many areas. Second, it is an inherently sustainable and economical technology due to its abundance on earth. Third, as planar material results compatible with the established production technologies and integrable with conventional materials, such as Si. Graphene and its relative materials are a perfect example of transferable technology to the industry, in fact, a significant number of global patents around graphene have been filed since 2004 (Figure 68).[169]
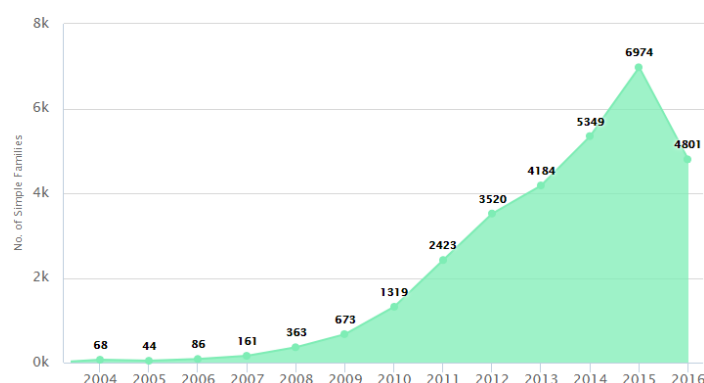
Figure 68: Filing trends in Graphene during the last 15 years. Ref 170.

---

[166] A. K. Geim, K. S. Novoselov, *Nat. Mater.* **2007**, *6*, 183.

[167] E. Hobsbawm, *The Age of Revolution: Europe 1789-1848*, Weidenfeld&Nicolson Ltd., **1962**.

[168] H. G. Elias, *Plastics, General Survey, Ullmann's Encyclopedia of Industrial Chemistry*, Wiley-VCH, Weinheim, **2005**.

[169] *Patent Analysis Report on Graphene*, PatSeer Pro, **2017**.

A very diverse range of applications was found for graphene, including characterization,[170] polymer composites,[171] transparent displays,[172] transistors,[173] capacitors,[174] solar cells,[175] biosensors,[176]conductive inks,[177] windows,[178] saturable absorbers,[179] photodetectors,[180] tennis rackets.[181] However, overall, the graphene patent space comprises patent filings in two main sectors: electronics (e.g. use of graphene for displays, transistors and computer chips) and synthesis (e.g. production of graphene by chemical vapour deposition (CVD), exfoliation, chemical, electrochemical, thermal, or photocatalytic reduction of graphene oxide, etc.).

In spite of the great application potential of this material and its derivatives, the competitiveness of graphene in the field of semiconductors and sensors is decreased by the intrinsic zero band gap nature of its pristine form.[182] Therefore, if the initial research efforts were mainly focused on the development of new synthetic routes enabling an effective production of well-defined sheets (such as micromechanical cleavage,[153] chemical vapor deposition,[158] graphitization of silicon carbide,[183] anodic bonding,[184] unzipping of

---

[170] A. Colli, S. A. Awan, A. Lombardo, T. J. Echtermeyer, T. S. Kulmala, A. C. Ferrari, *US 20130162333*, **2013**.

[171] O. Rozhin, A. Ferrari, W. I. Milne, *US 20100003528*, **2010**.

[172] Y. Woo, S. A. Seo, D. Kim, H. Chung, *US 20110089403*, **2011**.

[173] T. Kobayashi, EP 2393107, **2013**.

[174] L. Song, A. Zhamu, J. Guo, B. Z. Jang, *US 7623340*, **2009**.

[175] S. M. Yoon, W. M. Choi, H. J. Shin, J. Y. Choi, *EP 2439779*, **2014**.

[176] G. Owen, *GB 2471672*, **2011**.

[177] a) B. Z. Jang, A. Zhamu, *US 20100000441*, **2008**; b) R. Murphy, O. Rozhin, A. C. Ferrari, J. Robertson, W. I. Milne, *US 20070275230*, **2007**; c) F. Torrisi, T. Hasan, F. Bonaccorso, A. C. Ferrari, *WO 2014064432 A1, 2014*.

[178] H. Andersson, *US 20110311029*, **2011**.

[179] O. Rozhin, A. Ferrari, W. I. Milne, *US 8323789 B2*, **2007**.

[180] P. Avouris, M. B. Steiner, M. Engel, R. Krupke, A. C. Ferrari, A. Lombardo, *US 20130107344 A1*, **2013**.

[181] H. Lammer, *US 20100125013*, **2010**.

[182] a) K. S. Kim, Y. Zhao, H. Jang, S. Y. Lee, J. M. Kim, K. S. Kim, J. H. Ahn, P. Kim, J.Y. Choi, B. H. Hong, *Nature* **2009**, 457, 706. b) A. H. C. Neto, F. Guinea, N. M. R. Peres, K. S. Novoselov, A. K. Geim, *Rev. Mod. Phys.* **2009**, *81*, 109.

[183] K. V. Emtsev, A. Bostwick, K. Horn, J. Jobst, G. L. Kellogg, L. Lay, J. L. McChesney, T. Ohta, S. A. Reshanov, J. Röhrl, E. Rotenberg, A. K. Schmid; D. Waldmann, H. B. Weber, T. Seyller, *Nat. Mater.* **2009**, *8*, 203.

carbon nanotubes,[185] organic synthesis,[186] reduction of graphene oxide,[187] polymer-coated graphene,[188] liquid phase exfoliation of graphite,[189] electrochemical exfoliation of graphite,[190] graphite intercalation,[191] and ball-milling processing of graphite)[192] the number of research projects aimed at the functionalization of graphene has increased drastically. Understandably, chemical functionalization is the required first step in order to get graphene able to be handled for further conversion to practical applications.[161,193,194] This previous step is also useful to overcome other disturbing limits of pristine graphene such as its strong tendency to aggregate due to electrostatic forces, the strong π-π interactions between individual sheets and its intrinsic insolubility in organic solvents. Specifically, the chemical approach to graphene modification permits to open a gap between its conduction band and its valence band, at the Brillouin zone corners[195] (Figure 69).

[184] A. Balan, R. Kamar, M. Boukhicha, O. Beyssac, J. C. Bouillard, D. Taverna, W. Sacks, M. Marangolo, E. Lacaze, R. Gohler, W. Escoffier, J. M. Poumiroi, A. Shukla, *J. Phys. D: Appl. Phys.* **2010**, *43*, 374013.

[185] D. V. Kosynkin, A. L. Higginbotham, A. Sinitskii, J. R. Lomeda, A. Dimiev, K. Price, J. M. Tour, *Nature* **2009**, *458*, 872.

[186] X. Yang, X. Dou, A. Rouhanipour, L. Zhi, H. J. Räder, K. Müller, *J. Am. Chem. Soc.* **2008**, *130*, 4216.

[187] Y. Zhu, S. Murali, M. D. Stoller, K. J. Ganesh, W. Cai, P. J. Ferreira, A. Pirkle, R. M. Wallace, K. A. Cychosz, M. Thommes, D. Su, E. A. Stach, R. S. Ruoff, *Science* **2011**, *332*, 1537.

[188] X. Li, X. Wang, L. Zhang, H. Dai, *Science* **2008**, *319*, 1229.

[189] Y. Hernandez, V. Nicolosi, M. Lotya, F. M. Blighe, Z. Y. Sun, S. De, I. T. McGovern, B. Holland, M. Byrne, Y. K. Gun'ko, J. J. Boland, P. Niraj, G. Duesberg, S. Krishnamurthy, R. Goodhue, J. Hutchison, V. A. C. Scardaci, J. Ferrari, N. Coleman, *Nat. Nanotechnol.* **2008**, *3*, 563.

[190] J. Lu, J. Yang, J. Wang, A. Lim, S. Wang, K. P. Loh, *ACS Nano* **2009**, *3*, 2376.

[191] C. Valles, C. Drummond, H. Saadaoui, C. A. Furtado, M. He, O. Roubeau, L. Ortolani, M. Monthioux, A. Pénicaud, *J. Am. Chem. Soc.* **2008**, *130*, 15802.

[192] V. Léon, M. Quintana, M. A. Herrero, J. L. G. Fierro, A. de la Hoz, M. Prato, E. Vázquez, *Chem. Commun.* **2011**, *47*, 10936.

[193] J. Park, W. H. Lee, S. Huh, S. H. Sim, S. B. Kim, K. Cho, B. H. Hong, K. S. J. Kim, *Phys. Chem. Lett.* **2011**, *2*, 841.

[194] J. Park, S. B. Jo, Y. J. Yu, Y. Kim, J, W. Yang, W. H. Lee, H. H. Kim., B. H. Hong, P. Kim, K. Cho, K. S. Kim, *Adv. Mater.* **2012**, *24*, 407.

[195] H. X. Wang, Q. Wang, K. G. Zhou, H. L. Zhang, *Small* **2013**, *9*, 1266.
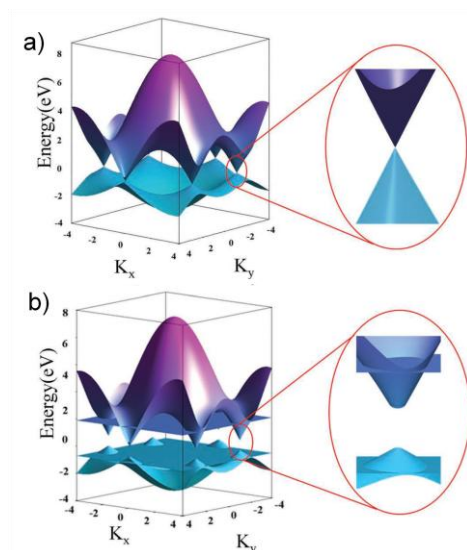
Figure 69: a) Zero band-gap of graphene, b) band-gap opening by chemical modification.

To carry out this opening, there are four kinds of methods: heteroatom doping,[196] electrostatic field tuning,[197] cutting graphene into nanoribbons[198] and chemical modification (Figure 69b).[199]

Therefore, functionalization schemes confer an additional element of control over the nanomaterial properties by various covalent and non-covalent interaction methods of organic and inorganic molecules.[200]

[196] M. L. Mueller, X. Yan, B. Dragnea, L. S. Li, *Nano Lett.* **2011**, *11*, 56.

[197] T. Ohta, A. Bostwick, T. Seyller, K. Horn, E. Rotenberg, *Science* **2006**, *313*, 951.

[198] L. Jiao, L. Zhang, X. Wang, G. Diankov, H. Dai, *Nature* **2009**, *458*, 877.

[199] H. Liu, Y. Liu, D. Zhu, *J. Mater. Chem.* **2011**, *21*, 3335.

[200] a) Z. Sun, D. K. James, J. M. Tour, *J. Phys. Chem. Lett.* **2011**, *2*, 2425; c) M. Quintana, E. Vazquez, M. Prato, *Acc. Chem. Res.* **2013**, *46*, 138; d) K. P. Loh, Q. Bao, P. K. Ang, J. Yang, *J. Mater. Chem*. **2010**, *20*, 2277; e) K. Dirian, M. A. Herranz, G. Katsukis, J. Malig, L. Rodríguez-Pérez, C. Romero-Nieto, V. Strauss, N. Martín, D. M. Guldi, *Chem. Sci.* **2013**, *4*, 4335; f) G. Bottari, M. Á. Herranz, L. Wibmer, M. Volland, L. Rodríguez-Pérez, D. M. Guldi, A. Hirsch, N. Martín, F. D'Souza, T. Torres, *Chem. Soc. Rev*. **2017**, *46*, 4464.

7.1.2.1.   *Graphene: Chemical Reactivity*

In contrast to fullerenes and CNTs which exhibit a curved surface, graphene is planar and, therefore, it is considerably less reactive.[201] The covalent functionalization of graphene implies a conversion from sp^2 to sp^3 carbons, the saturation of double bonds generates tetrahedral sp^3 carbon atoms protruding out of the plane, resulting in a strong strain. However, this tension significantly decreases when the tetrahedral geometry is formed in the carbon atoms located at the edge. Therefore, the major reactivity of graphene can be located at the edge carbon atoms. Moreover, from molecular orbitals considerations, the carbon atoms at zigzag borders seem to be the most reactive positions.[202] Graphene, depending on the production method, can also present a different number of defects due to the absence of some sp^2 carbon atoms or the presence of carbons with tetrahedral hybridization. The consequence is obviously an enhanced reactivity of the material because of the chemical activation of the atoms surrounding the structural imperfection.[203]

The major part of reviews are dedicated to the reactivity of graphene based on the chemical transformation of readily available graphene oxides.[204] Graphene oxide (GO) is a chemically modified graphene layer. The modification consists in the introduction of epoxide, hydroxyl, carbonyl and carboxyl groups by oxidative treatment of graphite.[205] This treatment consists in the initial intercalation of the

[201] S. Ryu, M. Y. Han, J. Maultzsch, T. F. Heinz, P. Kim, M. L. Steigerwald, L. E. Brus, *Nano Lett.* **2008**, *8*, 4597.

[202] a) K. Nakada, M. Fujita, G. Dresselhaus, M. S. Dresselhaus, *Phys. Rev. B: Condens. Matter Mater. Phys.* **1996**, *54*, 17954; b) D. E. Jiang, B. G. Sumpter, S. Dai, *J. Chem. Phys.* **2007**, 126, 134701; c) R. Sharma, N. Nair, M. S. Strano, *J. Phys. Chem. C* **2009**, *113*, 14771.

[203] X. Gao, Y. Wang, X. Liu, T. L. Chan, S. Irle, Y. Zhao, S. B. Zhang, *Phys. Chem. Chem. Phys.* **2011**, *13*, 19449.

[204] a) D. R. Dreyer, S. Park, C. W. Bielawski, R. S. Ruoff, *Chem. Soc. Rev.* **2010**, 39, 228; b) D. Chen, H. Feng, J. Li, *Chem. Rev.* **2012**, 112, 6027; c) F. Li, X. Jiang, J. Zhao, S. Zhang, *Nano Energy* **2015**, *16*, 488; d) W. L. Xu, C. Fang, F. Zhou, Z. Song, Q. Liu, R. Qiao, M. Yu, *Nano Lett.* **2017**, *17*, 2928.

[205] a) A. Lerf, H. He, M. Forster, J. Klinowski, *J. Phys. Chem. B* **1998**, *102*, 4477; b) D. C. Marcano, D. V. Kosynkin, J. M. Berlin, A. Sinitskii, Z. Sun, A. Slesarev, L. B. Alemany, W. Lu, J. M. Tour, *ACS Nano* **2010**, *4,* 8, 4806; b) J. Chen, B. Yao, C. Li, G. Sh, *Carbon* **2013**, *64*, 225.

graphite planes with acid, followed by oxygenation and final delamination of the final more hydrophilic material. Anyway, the major drawbacks of this method are that GO retains significant levels of defects and possess uncontrolled geometrical shapes due to the harsh oxidation conditions.

On the other side, stands out the opportunity to directly functionalize the pristine graphene. Obviously, respect to GO, the pristine material possesses a lower reactivity due to the planarity of its structure. Specifically, the chemistry of pristine graphene can be divided in two main approaching types: supramolecular and covalent.

The non-covalent functionalization is a physical process that takes advantage of the adsorption of molecules[200f,206] (that can also be characterized by photo- and/or electroactive moieties) onto the graphene surface, through van der Waals forces, electrostatic interactions, hydrogen bonding, coordination bonds, π-π interactions or electron transfer processes, to benefit from eventually induced new properties. The main advantage of this technique is that graphene's π-natural structure remains unaffected.

Covalent Functionalization of Graphene

When organic molecules are covalently attached on the graphene surface, its extended aromatic character is perturbed, enabling the control of its electronic properties. To functionalize the *pristine* material covalently different methodologies were developed, the major part of which were already part of the arsenal of chemical reactions previously used for the functionalization of related fullerenes and carbon nanotubes (Figure 70).[207]

---

[206]a) V. Georgakilas, M. Otyepka, A. B. Bourlinos, V. Chandra, N. Kim, K. C. Kemp, P. Hobza, R. Zboril, K. S. Kim, *Chem. Rev.* **2012**, *112*, 6156; b) A. Ciesielski, P. Samorì, *Adv. Mater.* **2016**, *28*, 6030.

[207] a) R. R. Nair, W. Ren, R. Jalil, I. Riaz, V. G. Kravets, L. Britnell, P. Blake, F. Schedin, A. S. Mayorov, S. Yuan, M. I. Katsnelson, H. Ming Cheng, W. Strupinski, L. G. Bulusheva, A. V. Okotrub, I. V. Grigorieva, A. N. Grigorenko, K. S. Novoselov, A. K. Geim, Small, **2010**, *6*, 2877; b) S. Sarkar, E. Bekyarova, S. Niyogi, R. C. Haddon, *J. Am. Chem. Soc.* **2011**, *133*, 3324; c) X. Zhong, J. Jin, S. Li, Z. Niu, W. Hu, R. Li, J. Ma, *Chem. Commun*. **2010**, *46*, 7340; d) E. K. Choi, I. Y. Jeon, S. Y. Bae, H. J. Lee, H. S. Shin, L. Daib, J. B. Baek, *Chem. Commun.* **2010**, *46*, 6320; e) S. P. Economopoulos, G. Rotas, Y. Miyata, H. Shinohara, N. Tagmatarchis, *ACS Nano* **2010**, *4*, 7499; f) L. H. Liu, M. M.
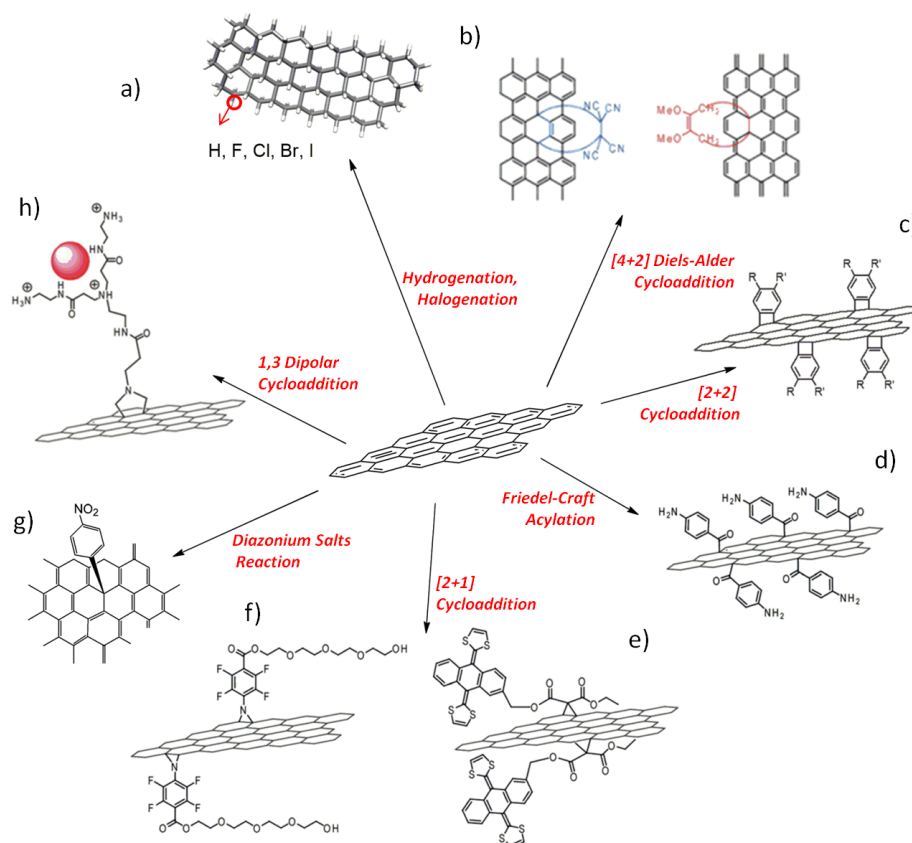
Figure 70: Schematic representation of the principal reactions on pristine graphene. Ref 208.

The first covalent reaction conducted on the pristine material produced the so called "graphane", in which the honeycomb structure of graphene is modified by the covalent attachment of a hydrogen atom for each knot of the lattice.[208] However, this first hydrogenation process, carried out in a cold hydrogen plasma flow, resulted in the production of a high number of defects. Less imperfections were observed with the radiofrequency catalytic chemical vapour deposition

Lerner, M. Yan, *Nano Lett.* **2010**, *10*, 3754; g) E. Bekyarova, M. E. Itkis, P. Ramesh, C. Berger, M. Sprinkle, W. A. de Heer, R. C. Haddon, *J. Am. Chem. Soc*. **2009**, *131*, 1336; h) M. Quintana, A. Montellano, A. E. del Rio Castillo, G. Van Tendeloo, C. Bittencourt, M. Prato, *Chem. Commun*. **2011**, *47*, 9330; i) L. Rodríguez-Pérez, M. Á. Herranz, N. Martín, *Chem. Commun.* **2013**, *49*, 3721.

[208] A. Savchenko, *Science* **2009**, *323*, 589.

(rf-cCVD) method used later by Biris group.[209] While, other groups, using the wet-chemical method based on a Birch reduction, obtained a slowdown of the process which permits to reduce the competitive process of H_2 evolution.[207a,210] Halogenated analogues of graphane were also obtained by different approaches.[211] From theoretical calculations, the fluorinated derivative seems to be the more stable between the five graphene derivatives (graphane, graphene fluoride, bromide, chloride, and iodide).[211a] However, hydrogenated and halogenated graphene derivatives result without any exclusion highly insulator.

Considering the low reactivity of graphene, particularly suitable to fulfil the task of functionalizing by covalent attachments are the thermal and/or photoinduced radical additions. One of the first examples was carried out on FLG by employing the photodecomposition of benzoyl peroxides.[212] Surely, the most widely used technique to functionalize the pristine surface of graphene consists in the use of the aryl radicals obtained from aryl diazonium salts. This reaction, which is exactly the functionalization method used in this second chapter of the present thesis, is a powerful tool that provides interesting intermediates to introduce further functional groups by simply changing the substituents in the benzene ring. After the use of this reaction to chemically modify the external surface of CNTs

[209] L. Zheng, Z. Li, S. Bourdo, F. Watanabe, C. C. Ryersonb, A. S. Biris, *Chem. Commun.* **2011**, *47*, 1213.

[210] R. A. Schafer, J. M. Englert, P. Wehrfritz, W. Bauer, F. Hauke, T. Seyller, A. Hirsch, *Angew. Chem. Int. Ed*. **2013**, *52*, 754.

[211] a) R. R. Nair, W. Ren, R. Jalil, I. Riaz, V. G. Kravets, L. Britnell, P. Blake, F. Schedin, A. S. Mayorov, S. Yuan, M. I. Katsnelson, H. Ming Cheng, W. Strupinski, L. G. Bulusheva, A. V. Okotrub, I. V. Grigorieva, A. N. Grigorenko, K. S. Novoselov, A. K. Geim, *Small* **2010**, *6*, 2877; b) H. L. Poh, P. Šimek, Z. Sofer, M. Pumera, *Chem. Eur. J.* **2013**, *19*, 2655.

[212] H. Liu, S. Ryu, Z. Chen, M. L. Steigerwald, C. Nuckolls, L. E. Brus, *J. Am. Chem. Soc.* **2009**, *131*, 17099.

(Scheme 22),[213] Tour and collaborators also went a step further employing the same reaction on different GO derivatives.[214]
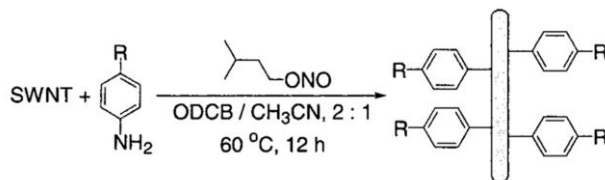
Scheme 22: Covalent functionalization of single wall carbon nanotubes (SWNT) by diazonium salts performed by Tour's group. Ref 214.

The aryl radicals of the Tour's reaction derives from the thermal decomposition of *in situ* generated diazonium salts by action of isoamyl nitrite on aniline derivatives. The suggested mechanism for this reaction, still not completely clear, involves three main steps (Scheme 23):[215]

---

[213] J. L. Bahr, J. Yang, D. V. Kosynkin, M. J. Bronikowski, R. E. Smalley, J. M. Tour*, J. Am. Chem. Soc.* **2001**, *123*, 6536.

[214] a) J. R. Lomeda, C. D. Doyle, D. V. Kosynskin, W. F. Hwang, J. M. Tour, *J. Am. Chem. Soc.* **2008**, *130*, 16201; b) Z. Jin, J. R. Lomeda, B. K. Price, W. Lu, Y. Zhu, J. M. Tour, *Chem. Mater.* **2009**, *21*, 3045.

[215] M. E. Lipińska, S. L. H. Rebelo, M. F. R. Pereira, J. A. N. F. Gomes, C. Freire, J. L. Figueiredo, *Carbon* **2012**, *50,* 3280.
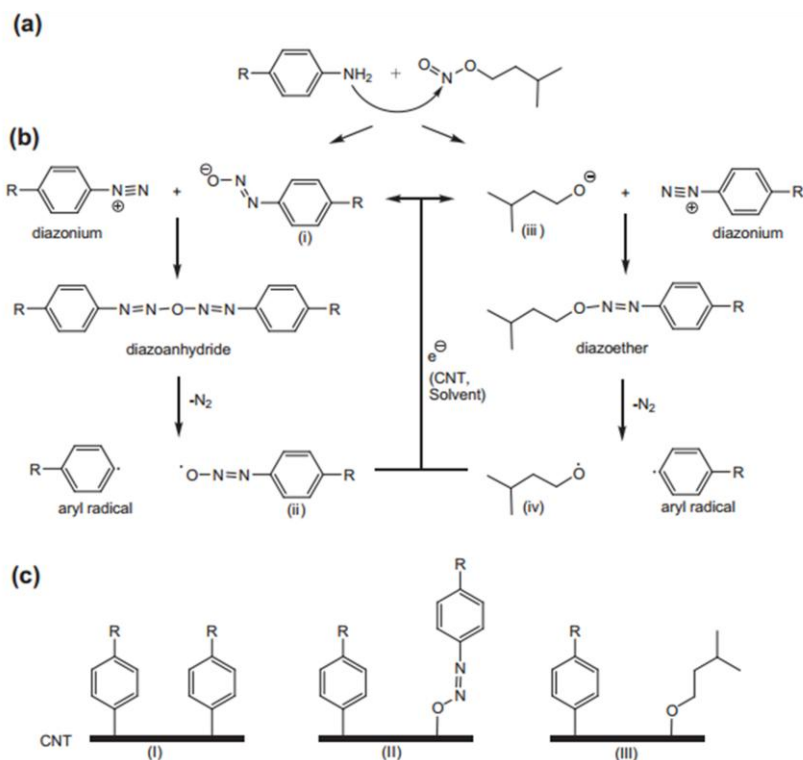
Scheme 23: Proposed mechanism for Tour's reaction: (a) diazotization reaction; (b) formation of aryl radicals and of oxygen radicals that reinitiate the cycle; and (c) recombination of radicals with CNT. Ref 216.

a) the aniline derivatives attack nitrite group, giving the diazonium species plus the diazotate (i) and the alcoxide (iii) species (which can also be formed);

b) the anionic species (i) and (iii) react with the diazonium salts leading to diazoanhydride and diazoether, respectively. At this point, the formed intermediates undergo a rapid thermal decomposition releasing nitrogen and generating the aryl radicals;

c) finally these species readily react with the curved surface of CNTs or the planar one of graphene forming a carbon-radical structure, which in turn can react with other radicals.

However, due to the radical nature of the reaction other associated paths can also take place.[215] The first reaction performed involving diazonium salts functionalization on pristine graphene was carried out by Haddon (Scheme 24).[207g]
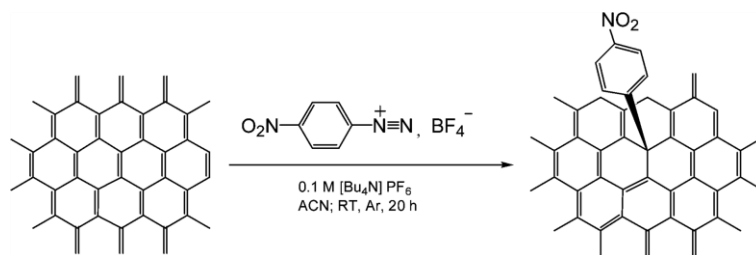
Scheme 24: Haddon's functionalization of pristine graphene by nitrophenyldiazonium salts. Ref 208g.

Nitrophenyldiazonium salts were employed as radical initiators determining changes in the electronic structure and transport properties of the graphene surface from near-metallic to semiconducting. However, another group arrived to the opposite conclusion studying exactly the same reaction. They claimed that the material, after the modification, exhibits a higher conductivity than its original pristine form resulting from the charge transfer effect of nitrophenyl groups (Figure 71).[216]
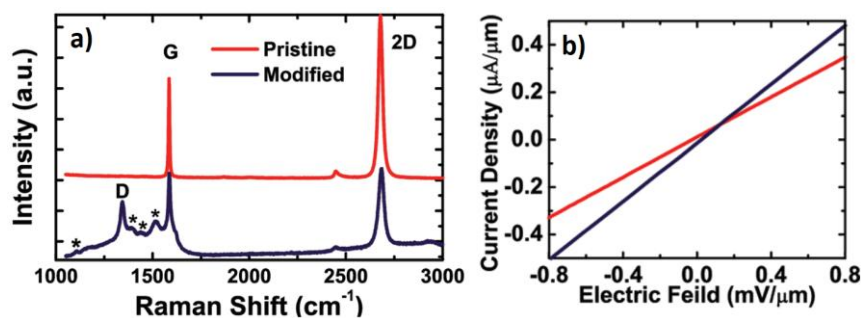
Figure 71: Raman spectra of pristine and modified graphene, where the asterisks correspond to the peaks introduced by nitrophenyl groups (a) and I/V curve of pristine and modified graphene respectively (b). Ref 217.

Hirsch *et al.*[217] developed a wet chemical approach based on the functionalization of graphene layers derived from an exfoliation process of bulk graphite by activation with a liquid Na/K alloy. The positive potassium cations intercalate the negative charged graphite

[216] P. Huang, H. Zhu, L. Jing, Y. Zhao, X. Gao, *ACS Nano* **2011**, *5*, 7945.

[217] J. M. Englert, C. Dotzer, G. Yang, M. Schmid, C. Papp, J. M. Gottfried, H. P. Steinruck, E. Spiecker, F. Hauke, A. Hirsch, *Nat. Chem.* **2011**, *3*, 279.

layers enhancing the interlayer distance. At this point the successful reaction with the radicals generated from aryl diazonium salts is testified by the temperature increase and the liberation of nitrogen. Interestingly, once the negative charged graphene was functionalized the hindrance of the groups present on the surface avoids the π-π stacking reaggregation process. Another example of prevented reaggregation process of graphene layers, mediated by diazonium salts functionalization, was reported by Tour's group.[218] In this process, thermally expanded graphite is reacted *in situ* with 4-bromophenyl diazonium salts. After a mild sonication in DMF, the exfoliation of functionalized, especially at the edges, FLGs takes place. This particular higher degree of edge's functionalization is motivated considering the low internal surface exposure of graphite during the reaction. The diazonium salts functionalization, depending on the substituent of the aryl rings, results also particularly useful to be coupled with other reactions. An interesting example is furnished by the so called "click reaction", the Cu(I)-catalyzed Huisgen [3+2] cycloaddition between azide and alkyne moieties.[219] Its combination with the diazonium salts reaction on graphene, due to the retaining of the conjugation of the formed triazole ring, results extremely suitable for studying the charge transport properties of different molecular architectures derived from the grafting of chemically or physically active molecules (Figure 72).[219c,220]

---

[218] Z. Sun, S. Kohama, Z. Zhang, J. R. Lomeda, J. M. Tour, *Nano Res.* **2010**, *3*, 117.

[219] a) F. Amblard, J. H. Cho, R. F. Schinazi, *Chem. Rev.* **2009**, *109*, 4207; b) H. C. Kolb, M. G. Finn, K. B. Sharpless, *Angew. Chem. Int. Ed*. **2001**, *40*, 2004; c) Z. G. L. C. Paulus, A. J. Hilmer, S. Shimizu, M. S. Strano, *Chem. Mater.* **2011**, *23*, 3362.

[220] a) H. X. Wang, K. G. Zhou, Y. L. Xie, J. Zeng, N. N. Chai, J. Li, H. L. Zhang, *Chem. Commun.* **2011**, *47*, 5747; b) M. Castelaín, G. Martínez, P. Merino, J. A. Martín-Gago, J. L. Segura, G. Ellis, H. J. Salavagione*, Chem. Eur. J.* **2012**, *18*, 4965.
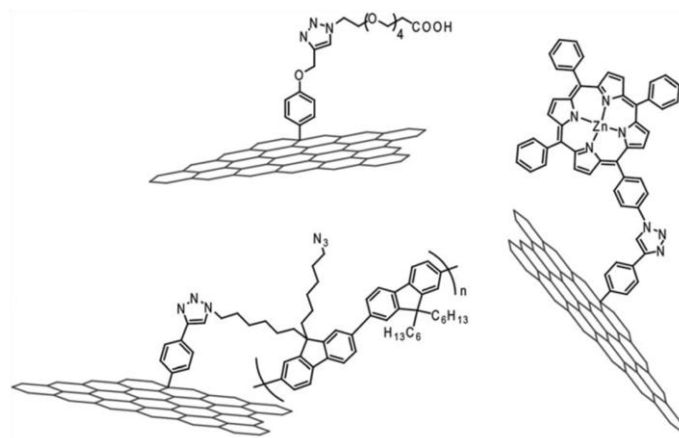
Figure 72: Representation of different graphene materials obtained by using Cu(I)-
catalyzed Huisgen 1,3-dipolar cycloaddition reactions. Ref 220c and 221.

A good alternative to the aryl diazonium salt covalent modification of
graphene edges was the Friedel–Crafts acylation reaction.[207d] The
reaction is carried out in a mild viscous acid medium, a mixture of
polyphosphoric acid (PPA) and phosphorus pentoxide (P_2O_5), and
allows the protonation of the graphitic surface favouring its
delamination. The 4-aminobenzoic acid, generating *in situ* carbonium
ions, becomes capable of attacking the defects of the graphite edges.
This functionalization, enhancing the solubility of graphite, allows in
this way the further penetration of the viscous medium which leads,
eventually, to the isolation of exfoliated graphene.

Another useful possibility to create covalent interactions with the
pristine carbon lattice relies on the cycloaddition processes. The
graphene reactivity in these reactions and more specifically in the
Diels−Alder cycloaddition is attributable to the particular peculiarity of
graphene of degeneracy of the electronic states at the Dirac point. The
states close to the Fermi level may give rise to either an antisymmetric
or symmetric graphene orbital, making graphene able to act as both
donor and acceptor (diene and dienophile) within the frontier molecular
orbital (FMO) theory.[221] 1,3-Dipolar cycloadditions of azomethine
ylides "*in situ*" generated by thermal condensation of aldehydes and α-
amino acids, [2+1] cycloadditions of thermo-derived nitrenes

---

[221] K. Fukui, *Theory of Orientation and Stereoselection*, Springer-Verlag, Berlin,
Germany, **1970**.

164

bromomalonates in the presence of a base and [2+2] cycloadditions of arynes derivatives can be generically considered additions of dienophiles to the sp^2 carbon-carbon bonds of the graphene structure. The [4+2] Diels-Alder cycloaddition reaction makes the only exception, because graphene results able to behave, as diene and dienophile. To prove the efficiency of this reaction, various types of graphene were employed (epitaxial graphene, exfoliated graphene and highly orientated pyrolitic graphite), together with different dienes (9-methylanthracene and 2,3-dimethoxy-1,3-butadiene) and dienophiles (tetracyanoethylene and maleic anhydride).[207b,222] However, different reaction conditions, such as the substrate used, the graphene type and temperature, result to strongly affect the degree of surface functionalization.[207b,222] As a representative example, Quintana *et al.*[207h] demonstrated that the reactive sites of graphene vary depending on the type of covalent chemical modification performed. Making use of the selective binding of gold nanoparticles to the amino groups, Quintana compared the selectivity of the 1,3 dipolar cycloaddition *versus* the amidation reaction on exfoliated graphene. It was observed that, while the 1,3-dipolar cycloaddition occurs indiscriminately all over the graphene surface, with the amidation reaction, on the other side, the functional groups were deposited mainly at the edges of the graphene layers. (Figure 73)

---

[222] S. Sarkar, E. Bekyarova, R. C. Haddon, *Acc. Chem. Res.* **2012**, *45*, 673.
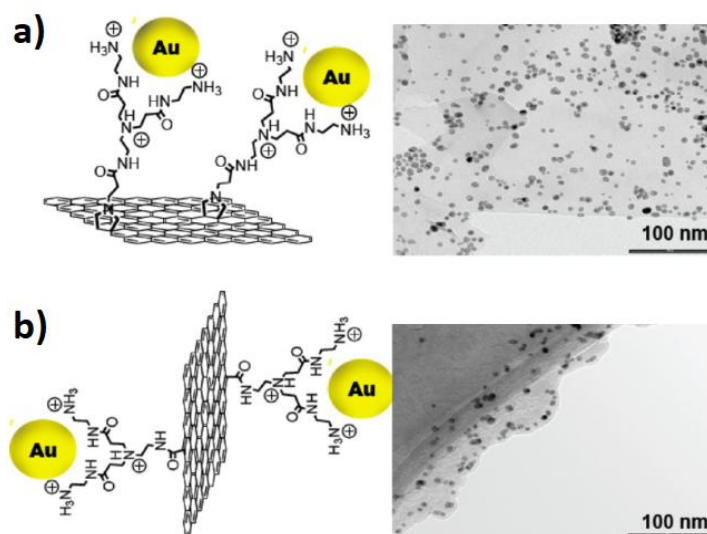
Figure 73: Graphene layers functionalized with Au nanoparticles on the left and TEM photographs of the corresponding composites on the right of the a) 1,3-dipolar cycloaddition and b) the amidation reaction. Ref 208h.

Other interesting example, which shows one of the few attempts to carry out a [2+2] cycloaddition reaction on graphene, is furnished by the recent work of García *et al.*[223] The synthesis of a hybrid all-carbon nanostructure via a C_{60}-aryne building block is described (Figure 74).
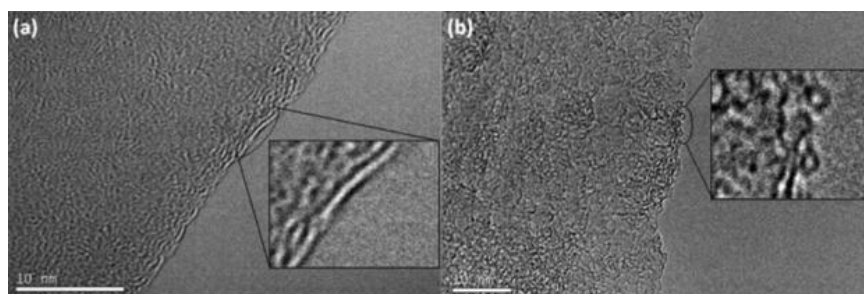
Figure 74: TEM images of pristine FLG (a) and FLG-C_{60} nanoconjugates. Ref 224.

In conclusion, the chemical modification of pristine graphene, by the covalent attachment of different functionalities, induces expected changes in its original properties. The resulting solubility of this

---

[223] D. García, L. Rodríguez-Pérez, M. A. Herranz, D. Peña, E. Guitián, S. Bailey, Q. Al-Galiby, M. Noori, C. J. Lambert, D. Pérez, N. Martín, *Chem. Commun*. **2016**, *52*, 6677.

hybrids improves in both polar and apolar media if hydrophilic[224] or hydrophobic[214a,225] precursors are employed, respectively. Improved mechanical and thermal properties have been detected in polymeric matrix which make use of graphene as a filler.[226] Moreover, a lot of different modifiers, ranging from synthetic[227] and natural[228] polymers to relatively small organic or inorganic molecules,[229] could be incorporated in the graphene composites to achieve better electrical and photoelectrical properties. These latter properties, together with its many other advantageous characteristics and the always better control of the techniques at the base of its chemical manipulation, rise the interest and expectation towards its still comparatively rare industrial applications. A field which may receive a significant boost by the development of graphene based materials is, for example, the flexible and stretchable electronics area, including semiconducting channels for high-speed transistor and logic circuits, transparent electrodes for flexible energy-harvesting devices, touch panels, rollable displays, and sensing materials for tactile sensors.[230]

---

[224] a) F. Liu, J. Y. Choi, T. S. Seo, *Chem. Commun.* **2010**, *46*, 2844; b) J. Liu, W. Yang, L. Tao, D. Li, C. Boyer, T. P. Davis, *J. Polym. Sci., Part A: Polym. Chem*. **2010**, *48*, 425; c) D. W. Lee, T. Kim, M. Lee*, Chem. Commun.* **2011**, *47*, 8259.

[225] a) J. F. Shen, Y. H. Hu, C. Li, C. Qin, M. X. Ye, *Small* **2009**, *5*, 82; b) E. Y. Choi, T. H. Han, J. Hong, J. E. Kim, S. H. Lee, H. W. Kim, S. O. Kim, *J. Mater. Chem*. **2010**, *20*, 1907.

[226] a) M. A. Rafiee, J. Rafiee, Z. Wang, H. Song, Z. Z. Yu, N. Koratkar, *ACS Nano* **2009**, *3*, 3884; b) E. R. Margine, M. L. Bocquet, X. Blase, *Nano Lett.* **2008**, *8*, 3315.

[227] Q. Bao, H. Zhang, J. Yang, S. Wang, D. Y. Tang, R. Jose, S. Ramakrishna, C. T. Lim, K. P. Loh, *Adv. Funct. Mater*. **2010**, *20*, 782.

[228] Q. Yang, X. Pan, F. Huang, K. Li, *J. Phys. Chem. C* **2010**, *114*, 3811.

[229] a) Y. Xu, H. Bai, G. Lu, C. Li, G. Shi, *J. Am. Chem. Soc.* **2008**, *130*, 5856; b) M. Quintana, K. Spyrou, M. Grzelczak, W. R. Browne, P. Rudolf, M. Prato, *ACS Nano* **2010**, *4*, 3527; c) Q. Su, S. Pang, V. Alijani, C. Li, X. Feng, K. Mullen, *Adv. Mater.* **2009**, *21*, 3191.

[230] a) N. Petrone, I. Meric, J. Hone, K. L. Shepard, *Nano Lett.* **2012**, *13*, 121; b) D. Kuzum, H. Takano, E. Shim, J. C. Reed, H. Juul, A. G. Richardson, J. de Vries, H. Bink, M. A. Dichter, T. H. Lucas, D. A. Coulter, E. Cubukcu, B. Litt, *Nat. Commun*. **2014** , *5* , 5259; c) J. Li, J. Liang, L. Li, F. Ren, W. Hu, J. Li, S. Qi, Q. Pei, *ACS Nano* **2014**, *8*, 12874; d) B. Zhu, Z. Niu, H. Wang, W. R. Leow, H. Wang, Y. Li, L. Zheng, J. Wei, F. Huo, X. Chen, *Small* **2014** , *10*, 3625.

7.1.2.2.   *Graphene- and Graphene Oxide-Based-C$_{60}$ Hybrid Materials*

Both non-covalent stacking and covalent functionalization of graphene with photosensitizers are expected to shift the Fermi level. This shift results in the opening of an electronic gap between the valence and the conduction band of this material, thus allowing the formation of efficient D-A systems. In these nanoconjugates, graphene can play a dual role, either as electron donor or electron acceptor, depending on the relative energy levels of the interacting species. Porphyrins (P) and phthalocyanines (Pc) have been widely employed as organic photosensitizers in the creation of either covalent or non-covalent graphene-based D-A hybrids.[231] Recently, instead, a great interest has been rising towards the development of novel graphene-based composite nanomaterials integrating C$_{60}$ and its derivatives, widely known in literature as well established molecules for organic photovoltaics applications.[135,136,232] The easiest way to form hybrid materials combining the properties of both carbon allotropes, was to use GO derivatives, due to the presence on their surface of several organic functionalities which could serve as anchoring groups for further chemical functionalization.

X. Y. Zhang *et al.*, for example, prepared covalent GO-based-C$_{60}$ hybrid materials using fulleropyrrolidine[233] and fullerenol.[234] The nonlinear optical properties (NLO) of the new hybrids were investigated revealing an enhanced performance with respect to its parent species (C$_{60}$ and graphene) for both nanocomposites, which can

---

[231] a) T. Skaltsas, S. Pispas, N. Tagmatarchis, *Chem. Eur. J.* **2013**, *19*, 9286; b) Y. Xu, Z. Liu, X. Zhang, Y. Wang, J. Tian, Y. Huang, Y. Ma, X. Zhang, Y. Chen, *Adv. Mater.* **2009**, *21*, 1275; c) J. Malig, N. Jux, D. Kiessling, J. J. Cid, P. Vázquez, T. Torres, D. M. Guldi, *Angew. Chem. Int. Ed.* **2011**, *50*, 3561; d) L. Brinkhaus, G. Katsukis, J. Malig, R. D. Costa, M. Garcia-Iglesias, P. Vázquez, T. Torres, D. M. Guldi, *Small* **2013**, *9*, 2348; e) M. E. Ragoussi, J. Malig, G. Katsukis, B. Butz, E. Spiecker, G. de la Torre, T. Torres, D. M. Guldi, *Angew. Chem. Int. Ed*. **2012**, *51*, 6421.

[232] T. Zhuang, X. F. Wang, T. Sano, Z. Hong, Y. Yang, J. Kido, *Appl. Phys. Lett*. **2013**, *103*, 203301.

[233] X. Y. Zhang, Y. Huang, Y. Wang, Y. F. Ma, Z. F. Liu, Y. S. Chen, *Carbon* **2009**, *47*, 1, 334.

[234] Z. B. Liu, Y. F. Xu, X. Y. Zhang, X. L. Zhang, Y. S. Chen, J. G. Tian, *J. Phys. Chem. B* **2009**, *113*, 29, 9681.

be at least partially attributable to the photoinduced electron transfer mechanism between the graphene sheet and C_{60} (Figure 75).[234, 235]
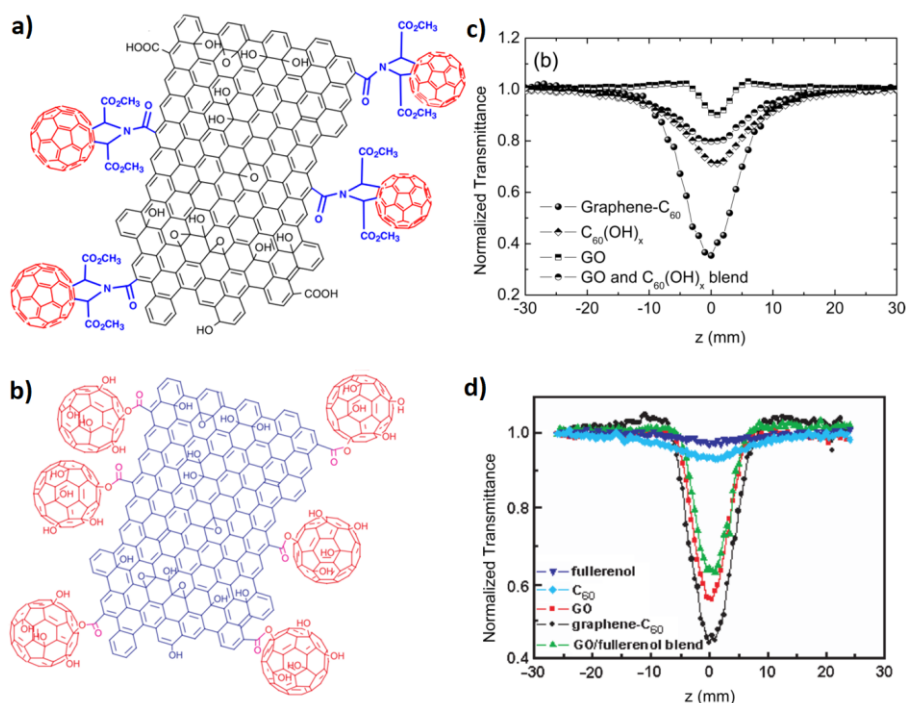
Figure 75: (a) and (b) GO-based-C_{60} hybrid materials using fulleropyrrolidine and fullerenol, respectively.(c) Open-aperture Z-scan curves of Graphene-C_{60}, pyrrolidine fullerene, graphene oxide, and fulleropyrrolidine/graphene oxide blend with (1:1 w/w) for 5 ns pulsed laser at 532 nm. (d) Open aperture Z-scan results of fullerenol in DMF, C_{60} in toluene, GO, Graphene-C_{60} and GO/fullerenol blend with the same concentration of 0.1 mg/mL for 5 ns pulsed laser at 532 nm. The graphene-C_{60} has the largest dip among the transmittance curves of these materials, indicating that it has the best NLO effect. Ref 235 and 236.

In these two attempts, fullerene was only grafted on the edge of graphene, instead, Y. Zhang *et al*. presented an effective route to simultaneously exfoliate and functionalize graphene. Fullerene molecules were innovatively inserted in between graphene layers of GO via the Fisher esterification of the hydroxyl groups on graphene

---

[235] X. Y. Zhang, Z. B. Liu, Y. Huang, X. J. Wan, J. G. Tian, Y. F. Ma, Y. S. Chen, *J. Nanosci. Nanotechnol.* **2009**, *9*, 10, 5752.

oxide with the carboxyl groups in (1,2-methanofullerene C_{60})-61-carboxylic acid (Figure 76).[236]
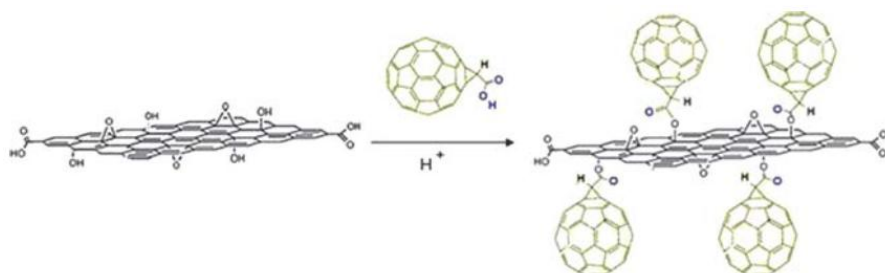
Figure 76: Functionalization of the graphene oxide *via* Fisher esterification. Ref 237.

All the previous works showed the versatility of the many functional groups present on the surface of GO to synthesize GO-based-C_{60} hybrid materials. Although less-studied, some examples of all-carbon hybrids based on the functionalization of pristine graphene have also been reported. Yu *et al*., for example, developed a simple method to achieve a relatively "cleaner" all-carbon hybrid, by using n-BuLi to lithiate graphene, then made to react with C_{60} by nucleophilic addition (Figure 77).[237]
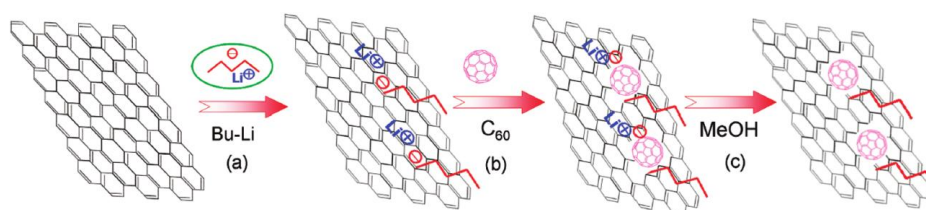
Figure 77: Schematic representation of grafting C_{60} onto graphene through lithiation reaction with n-butyllithium. Ref 238.

These C_{60}-grafted graphene nanosheets employed as electron acceptors in poly-(3-hexylthiophene)-based BH solar cells resulted to significantly improve the electron transport, and hence the overall device performance, whose PCE is of ~1.22%. On the other side, García *et al*. carried out the synthesis of a new really-all-carbon hybrid

---

[236] Y. Zhang, L. Ren, S. Wang, A. Marathe, J. Chaudhuri, G. Li, *J. Mater. Chem.* **2011**, *21*, 5386.

[237] D. Yu, K. Park, M.Durstock, L. Dai, *J. Phys. Chem. Lett*. **2011**, *2*, 1113.

nanoconjugate by the generation of a [60]fullerene-benzyne building block and its further chemical cycloaddition reaction with exfoliated graphene.[223]

7.2. *Thermopower Measurements In Molecular Junctions*[238]

The thermopower and the conductance (G) are characteristic properties of molecular junctions which serve to characterize the electronic transport. The importance of thermopower measurements is due to two main reasons: i) it provides complementary information to the conductance about the electronic structure and transport properties of a junction at molecular scale, and ii) the control of these processes paves the way to the development of new environmentally friendly organic based thermoelectric devices, which can convert directly heat into electricity with high efficiency for energy-harvesting applications or nanoscale cooling systems. The thermoelectric properties of a molecular junction depend on the combination of the charge transport and the thermal transport.

Consider a temperature difference (ΔT) applied between two metal electrodes. Due to the Seebeck effect a voltage difference (ΔV), proportional to the temperature difference, is generated in the nanoscale junction (Figure 78).
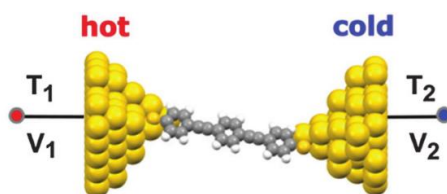
Figure 78: Thermovoltage measurement in a molecular junction.

This is expressed as:

$$\Delta V = S \Delta T$$

[238] L. Rincón-García, C. Evangeli, G. Rubio-Bollingerac, N. Agraït, *Chem. Soc. Rev.* **2016**, *45*, 4285.

Where *S* is the aforementioned *thermopower* (or *Seebeck coefficient)*. Therefore, the electrical current flowing into a junction is the sum of the bias-induced current and the temperature-induced current:

$$I = G\Delta V + G\Delta TS$$

This electrical current depends on the transmission probability for an electron, at the Fermi level, to cross from the left-side electrode to the right-side electrode. Because this transmission probability is a function of the electron energy, which in turn depends on the electronic structure of the molecule (molecular orbitals), it is modified by the coupling to the electrodes. The alignment of the HOMO and the LUMO with respect to the Fermi level is crucial for the transport properties of the junction. The sign of thermopower is governed by which molecular orbital is closer to the Fermi level:

- S > 0, when the electrons below the Fermi level have a larger transmission probability than those above (the movement occurs from the cold to the hot electrode and the Fermi level is closer to the HOMO);

- S < 0, when the electrons above the Fermi level have a larger transmission probability than those below (the movement occurs from the hot to the cold electrode and the Fermi level is closer to the LUMO) (Figure 79).
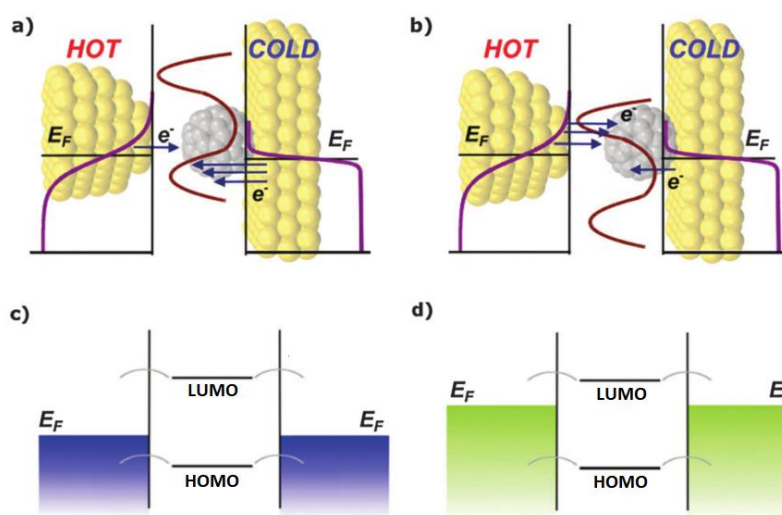
Figure 79: For higher transmission probability below the Fermi level (a), the transport takes place through the HOMO (c) determining a positive sign for S and conversely (b and d).

172

The most widely used method to study the transport processes in molecular junctions is the break junction technique. Specifically, the recent development of a useful STMBJ-based technique permits to measure simultaneously, during the entire evolution of the molecular junction, both conductance and thermopower.[239] In this technique, the movement of the STM tip during its approach and retraction is halted at short time intervals for a few milliseconds and the voltage is ramped to collect hundreds of IV curves for each approaching-retracting cycle.

The thermopower S can be measured from such IV curves, since, when there is no temperature difference between the electrodes, IV curves cross the origin. However, if there is a temperature difference between the electrodes a voltage is generated due to the Seebeck effect, and the IV curves are offset by $\Delta V = S\Delta T$ (see above). By monitoring ΔT in real time during the acquisition of the IV curves, and the measurement of ΔV, such as in Figure 80c, the thermopower S can be determined.
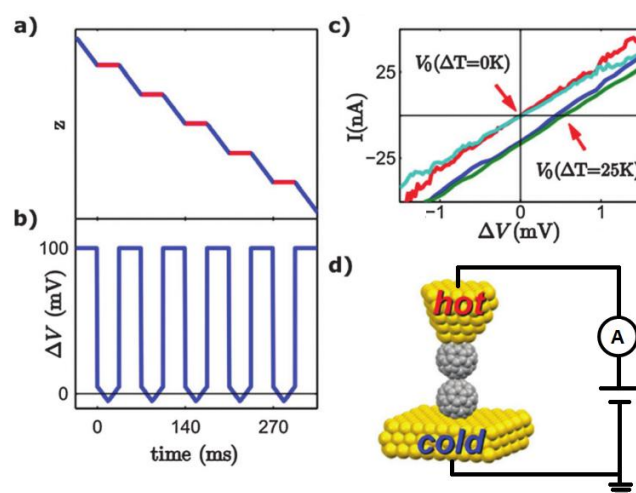
Figure 80: Tip displacement z (a) and bias voltage applied (b) at the molecular junction as a function of time. Experimental IV curves showing the voltage offset due to the temperature difference (c) and schematic representation of the setup (d).

The thermopower measurements of any given junctions although remarkably stable, can be submitted to some fluctuations due to factors such as the contact geometry, the orbital hybridization and the

[239] C. Evangeli, K. Gillemot, E. Leary, M. T. González, G. Rubio-Bollinger, C. J. Lambert, N. Agraït, *Nano Lett.* **2013**, *13*, 2141.

intramolecular interactions which induce variation in the alignment of the orbitals of the molecules with respect to the Fermi level of the electrodes.[240] Different studies also demonstrated that the value of S varies linearly with the length of the molecule.[241] It increases or decreases depending on the nature of the molecular backbone (presence of electron-donating or electron-withdrawing groups,[240] as well as of π-conjugated units or alkyl chains,[242] etc.). Furthermore, tunability of the thermopower can be achieved, with little influence on the conductance, by changing the anchoring group.[242,243] Indeed, the nature of the anchoring group is mainly responsible for the sign of S and, therefore, of the type of transport (p- or n-type, corresponding to transport through the HOMO and the LUMO, respectively). Another important factor which affects the thermopower is the metal constituting the electrodes, since different level alignment of the molecular orbitals can be induced depending on the different work functions of the metal.[242,244,245]

In table 4, the conductance G and the thermopower S, obtained for some molecular junctions, are presented to illustrate typical values and how they vary depending on the factors mentioned above.

[240] J. A. Malen, P. Doak, K. Baheti, T. D. Tilley, A. Majumdar, R. A. Segalman, *Nano Lett.* **2009**, 9, 3406.

[241] P. Reddy, S. Y. Jang, R. A. Segalman, A. Majumdar, *Science* **2007**, 315, 1568.
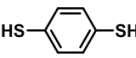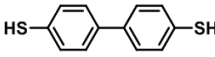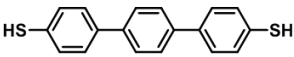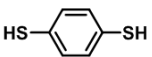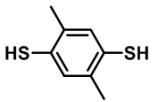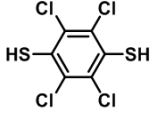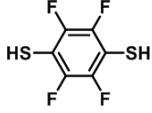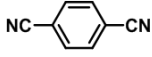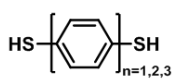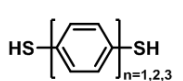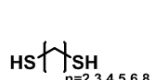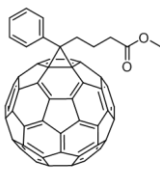
[242] a) J. A. Malen, P. Doak, K. Baheti, T. D. Tilley, R. A. Segalman, A. Majumdar, *Nano Lett.* **2009**, 9, 1164; b) W. B. Chang, C. K. Mai, M. Kotiuga, J. B. Neaton, G. C. Bazan, R. A. Segalman, *Chem. Mater.* **2014**, 26, 7229.

[243] J. R. Widawsky, P. Darancet, J. B. Neaton, L. Venkataraman, *Nano Lett.* **2012**, 12, 354.

[244] K. Baheti, J.A.Malen, P. Doak, P. Reddy, S. Y. Jang, T. D. Tilley, A. Majumdar, R. A. Segalman, Nano Lett. **2008**, 8, 715.

[245] S. K. Yee, J. A. Malen, A. Majumdar, R. A. Segalman, *Nano Lett.* **2011**, 11, 4089.

Table 4: Typical values of conductance and thermopower for some molecular junctions.

Molecule	$G(G_0)$	$S, \Delta S (\mu V \cdot K^{-1})$	Ref.
HS–⟨benzene⟩–SH		8.7 ± 2.1	
HS–⟨biphenyl⟩–SH		12.9 ± 2.2	A. Majumdar (242)
HS–⟨terphenyl⟩–SH		12.9 ± 2.2	
HS–⟨benzene⟩–SH	1.05×10^{-2}	7.2 ± 0.2	
HS–⟨methyl-benzene⟩–SH	1.19×10^{-2}	8.3 ± 0.3	
HS–⟨tetrachloro-benzene (Cl, Cl, Cl, Cl)⟩–SH	7.6×10^{-3}	4.0 ± 0.6	R. A. Segalman (241)
HS–⟨tetrafluoro-benzene (F, F, F, F)⟩–SH	8.7×10^{-3}	5.4 ± 0.4	
NC–⟨benzene⟩–CN		-1.3 ± 0.5	
HS–⟨benzene⟩$_{n=1,2,3}$–SH		8.7 ± 0.2 / 12.9 ± 2.2 / 14.2 ± 3.2	
HS–⟨benzene⟩$_{n=1,2,3}$–SH		2.3 ± 0.3 / 4.9 ± 1.9 / 6.4 ± 0.4	A. Majumdar (243a)
HS–(CH$_2$)$_n$–SH, $n=2,3,4,5,6,8$		6.8 ± 0.2 / 5.5 ± 0.1 / 5.2 ± 0.4 / 4.9 ± 0.2 / 3.3 ± 0.1 / 2.4 ± 0.4	
C$_{60}$ fullerene	~7.1×10^{-4} / ~2.5×10^{-4} / ~2.0×10^{-3}	-8.9 ± 2.2 / -14.5 ± 1.2 / -29.62 ± 3.4	
PCBM (phenyl-C$_{61}$-butyric acid methyl ester)	~1.3×10^{-3} / ~2.5×10^{-3}	-7.6 ± 3.2 / -16.4 ± 1.6 / -30.0 ± 2.6	R. A. Segalman (246)
C$_{70}$ fullerene	~6.3×10^{-4} / ~6.3×10^{-4} / ~1.6×10^{-3}	-8.4 ± 1.9 / -20.1 ± 1.4 / -33.1 ± 8.8	

# 8.	Objectives

8. Objectives

8.1. *Graphene On Surface (GOS)-Based Materials*

As mentioned before, fullerenes are known to have been largely employed as electron acceptors in DBA systems[133,134] and graphene has demonstrated outstanding potential properties for electronic applications.[11d,161,184,185] However, to enhance this applicability and make it able to be handled, its chemical manipulation is required.

In this optic and because of the less number of studies dedicated to the functionalization of the pristine material, due to its lower reactivity than GO, this second chapter of the present thesis has been conceived to study the properties exhibited by carbon nanohybrids based on covalently modified pristine graphene with fullerene derivatives. Specifically, the design of the target nanocomposites was formulated with the aim to get novel heterojunctions where, changing the connection position between the spacer and the graphene layer, would be possible to investigate the modification of the electron transfer path and the thermopower properties by use of a conductive atomic force microscope (c-AFM). The synthesized three covalent GOS-based hybrids (**GOS1**, **GOS2** and **GOS3**) are diphenylmethanofullerenes appended materials. The fullerene moiety, acting as anchoring group, is covalently attached to a silica-supported single layer graphene (SLG), which acts as the second electrode of the c-AFM, through a bridging spacer, constituted by a diphenylmethane unit. This bridge unit can form a covalent bond with the monolayer through just one or both aromatic rings, using two possible attaching positions, *para* and *meta* (Figure 81).
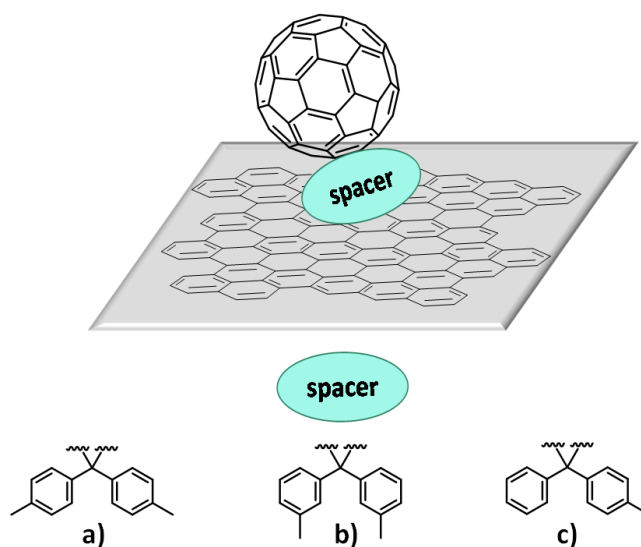
Figure 81: GOS-based materials: (a) **GOS1**, (b) **GOS2** and (c) **GOS3**.

In **GOS1** and **GOS2** both phenyl units of the fullerene derivatives are connected to the pristine graphene monolayer but differ from each other by the position of the linkage. **GOS1** is a *p*-substituted fullerene derivative, while **GOS2** is bonded through the *m*-positions. On the other side, **GOS1** and **GOS3** are both linked through the *p*-positions of the rings, but differ from each other by the number of rings employed to form this covalent interaction. **GOS3**, in fact, is attached by just one unit of the diphenylmethane moiety to the pristine graphene sheet and was employed as reference material.

9. Results and Discussion

9.1. *Retrosynthetic Analysis of the GOS-Based Materials*

As discussed in the background, the covalent modification of pristine graphene, enhancing its properties (like opening its band gap, tuning conductivity, and improving solubility and stability), represents a necessary, very challenging and important research field to make it available for industrial applications. Anyway, a general problem, specifically related to the functionalization of neutral graphene is that, being characterized by a planar structure, results to be a rather chemically inert system. It is not surprising, therefore, that the covalent functionalization of pristine graphene requires mostly reactive species (such as radicals, nitrenes, carbenes, and arynes) that can form covalent adducts with the sp^2 carbons in its structure.

In this context, in this second part of the present thesis, it was decided to use the diazonium chemistry to activate, by covalent modification, the structure of a graphene monolayer. The design of the target materials was structured in two main parts, the synthesis of the diamino-diphenylmethano[60]fullerene derivatives and following, their chemical insertion on the graphene monolayer. These methano[60]fullerene derivatives were thought to act as precursors for the *in situ* generation of the diazonium salts, during the functionalization process, *via* Tour's reaction.[213] The selected diamino-diphenylmethano[60]fullerene building blocks and their further radical addition to graphene, resulted in the synthesis of the three aforementioned new all-carbon hybrid materials.

GOS1, **GOS2** and **GOS3** were obtained as depicted in their retrosynthetic analysis (Scheme 25).
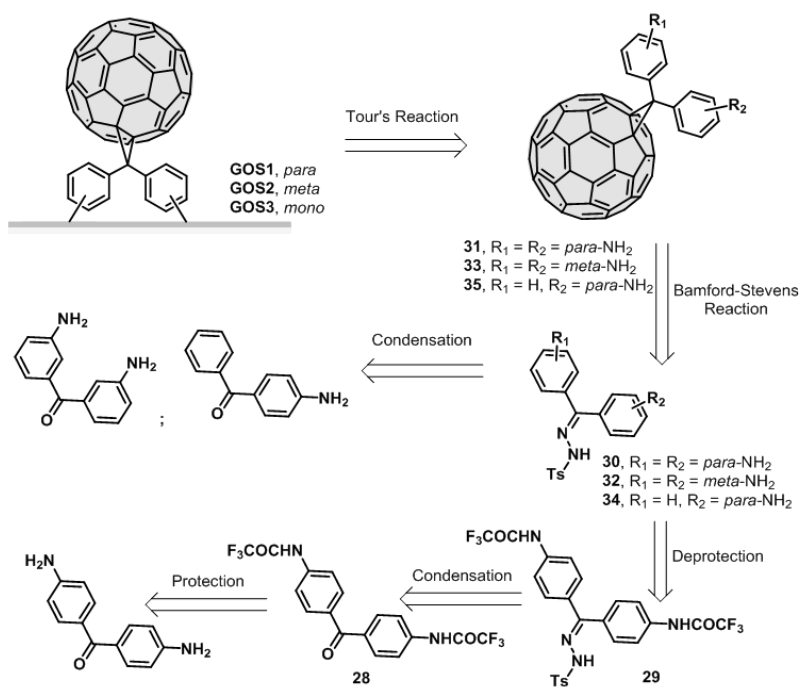
Scheme 25: Retrosynthetic analytic chart of the GOS-based materials.

9.1.1. *Synthesis of the Diamino-Diphenylmethano[60]Fullerene Building Blocks*

Functionalization of [60]fullerene was carried out through a Bamford-Stevens reaction,[246] which takes place through the *in situ* generation of intermediate diazocompounds.[247] Specifically, to justify the reaction product, two possible mechanisms were postulated (Scheme 26): (a) a 1,3-dipolar cycloaddition on a [6,6] bond of C_{60} to form a pyrazoline which is thermally unstable and loses nitrogen rapidly to give the thermodynamically most stable product, the [6,6]-closed methanofullerene, or (b) the direct extrusion of nitrogen followed by [2+1] cycloaddition reaction of the resulting carbene in a [5,6] bond of C_{60} to form the product of kinetic control, the [5,6]-open fulleroid. Conversion of the [5,6]-open fulleroid to the [6,6]-isomer is accomplished by heating as well as by photoexcitation.[248]

---

[246] W. R. Bamford, T. S. Stevens, *J. Chem. Soc*. **1952**, 4735.

[247] R. Gómez, J. L. Segura, N. Martín, *Org. Lett*. **2005**, *7*, 717.

[248] R. A. J. Janssen, J. C. Hummelen, F. Wudl, *J. Am. Chem. Soc*. **1995**, *117*, 544.
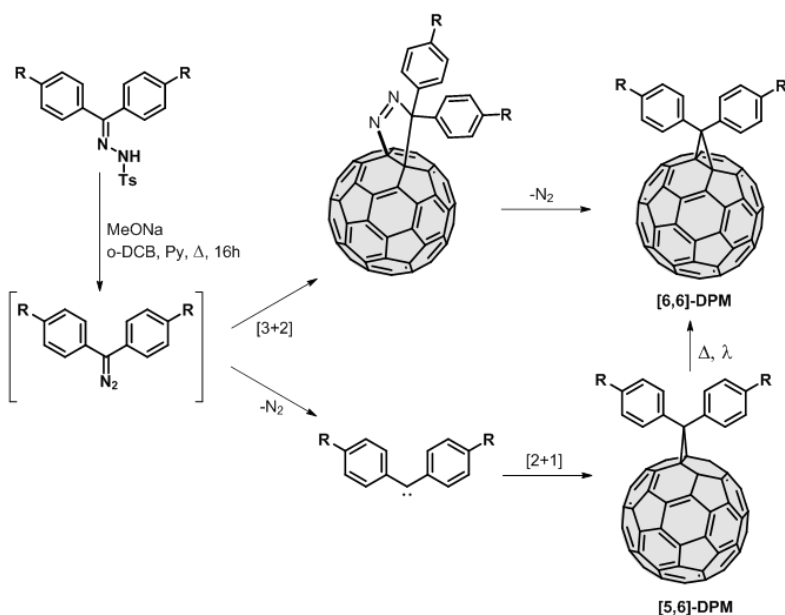
Scheme 26: Cyclopropanation reaction by: 1,3-dipolar cycloaddition to form [6,6]-diphenylmethanofullerenes (DPMs) or by insertion of a carbene to obtain the [5,6]-fulleroid.

However, the first step towards the synthesis of the desired diphenylmethano[60]fullerene structures **31**, **33** and **35** consists in a condensation reaction to get the target tosylhydrazones. While product **30** requires a protection/deprotection strategy,[247] a straightway synthetic path was followed to achieve hydrazones **32** and **34** (Scheme 27).
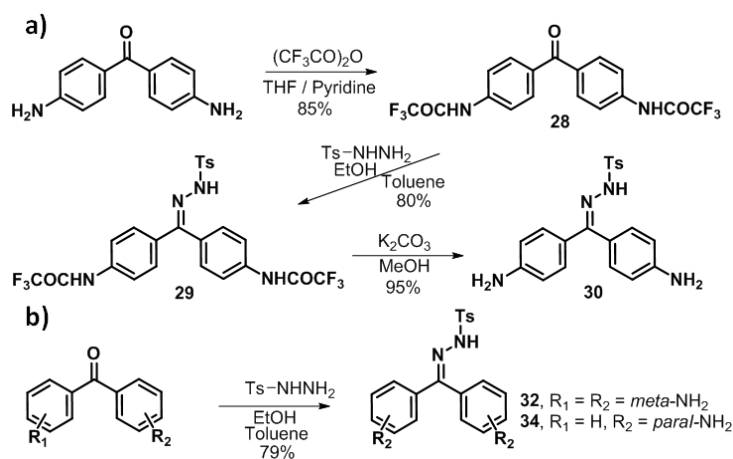
Scheme 27: Synthesis of the target tosylhydrazone moieties **30** by protection/deprotection strategy (a) and **32** and **34** by direct approach (b).

185

These syntheses were started from commercially available 4,4'-diaminobenzophenone, 3,3'-diaminodibenzophenone and 4-aminobenzophenone, respectively. 3,3'-Diaminobenzophenone and 4-aminobenzophenone were directly condensed with *p*-tosylhydrazine in ethanol to afford the corresponding tosylhydrazones **32** and **34**. On the other side, 4,4'-diaminobenzophenone was initially reacted with trifluoracetic anhydride to afford the corresponding *N*-protected diamido compound **28**, then it was treated with *p*-tosylhydrazine to yield the corresponding *p*-tosylhydrazone **29** under mild conditions. At this point, the hydrolysis of the trifluoroacetamido-diphenyl tosylhydrazone **29** with potassium carbonate afforded the corresponding diamino-*p*-tosylhydrazone **30**. Thus, these sequential steps of protection and deprotection to obtain the 4,4'-diaminodiphenyltosylhydrazone **30** can be attributed to the increasing electron density in the carbonyl group due to the presence of two electron-donor amino groups in the *p*-position of the starting product.

Following, the treatment of these derivatives (**30**, **32** and **34**) with sodium methoxide in the presence of pyridine and [60]fullerene in refluxing *o*-dichlorobenzene (*o*-DCB) affords the final building blocks **31**, **33** and **35** (Scheme 28).
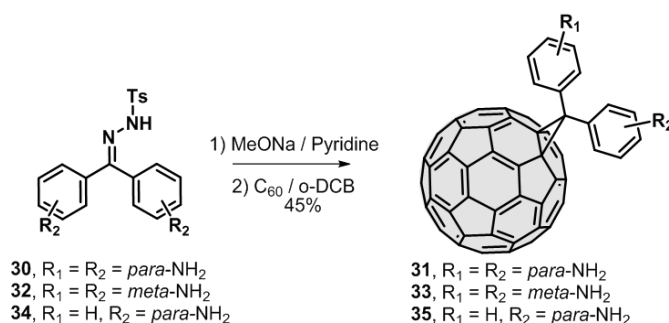
Scheme 28: Synthetic route to the desired methano[60]fullerene building blocks.

As aforementioned, although both [6,6]-closed and [5,6]-open isomers could be expected from this cycloaddition reaction, the high temperature at which the reaction proceeds allows to control the exclusive formation of the thermodynamically more stable [6,6]-closed isomer.^{1}H NMR and ^{13}C NMR allow to confirm the formation of the only [6,6]-closed isomers. As example, the comparison between the [1]H

NMR spectra of tosylhydrazone **32** and the corresponding 3,3'-diaminodiphenylmethano[60]fullerene **33** is shown in Figure 82.
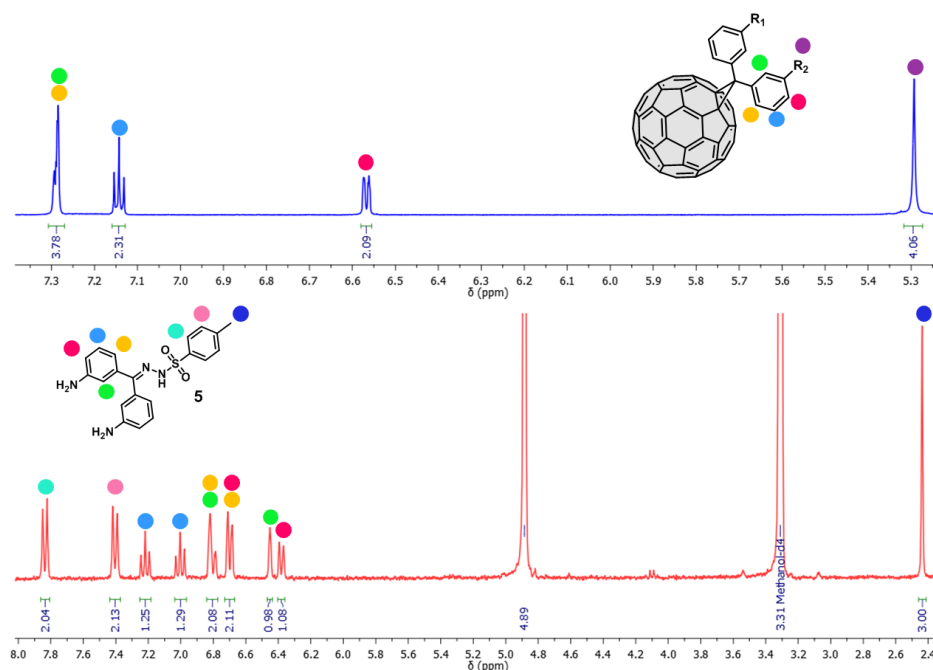
Figure 82: ^{1}H NMR of tosylhydrazone **32** (down) and the corresponding 3,3'-diamino diphenylmethanofullerene **33** (up).

All the synthesized products were satisfactorily characterized either by standard analytical and spectroscopic techniques.

9.1.1.1.   *Tour's Reaction to the GOS-Based Materials*

As discussed in the background, radical species are really useful compounds to overcome the inert character of graphene, allowing its chemical modification. To this purpose, the so called Tour's reaction is an appropriate way to guarantee the introduction of different compounds with a variety of possible functionalities on the surface of the graphene layer. As shown in the background, the active species in the Tour's reaction are aryl radicals derived from the *in situ* generated diazonium salts. Thus, a fundamental prerequisite in employing this reaction is the presence of arylamino groups in the designed starting products. In this way, the arylamino groups can react with the activating isoamyl nitrite leading to the formation of diazonium salts (see Scheme 23 in the previous section **7.1.2.1.**).

The functionalization process with derivatives **31**, **33** and **35** was carried out not only on supported single layer graphene (Graphene On Surface, GOS), but also previously on exfoliated-FLGs, thus permitting to test their chemical reactivity. The synthesis of the graphene-fullerene covalent aggregates is described in Scheme 29.
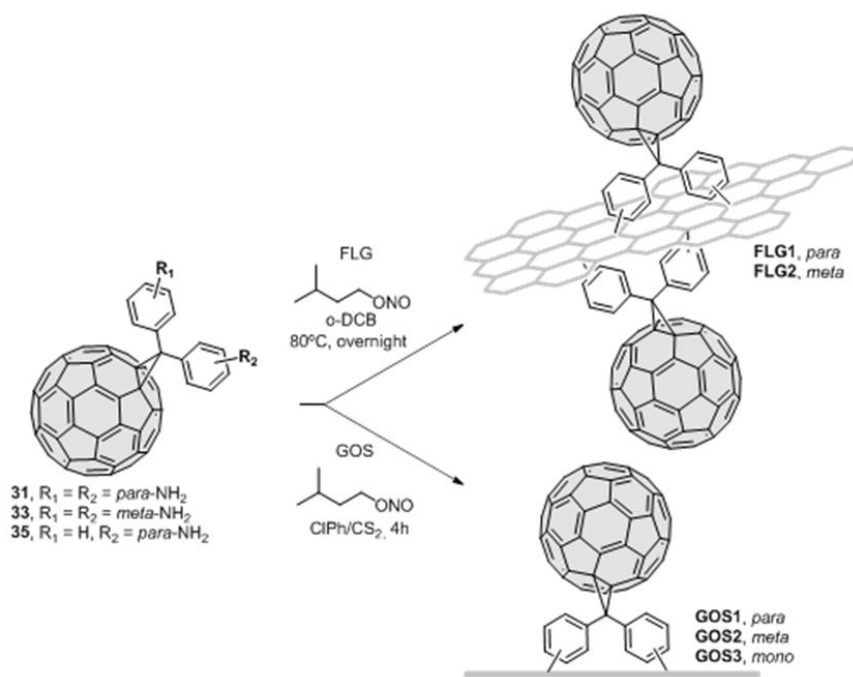
Scheme 29: Tour's reaction on FLG and GOS.

Pristine FLGs are obtained through graphite exfoliation in *o*-DCB following Colleman's method with high degree of purity.[189] Such FLGs suspension in *o*-DCB is immediately reacted with the fullerene derivatives **31** and **33** *via* aryl diazonium chemistry in the presence of isoamyl nitrite following the well-established procedure reported by Tour,[213] providing the **FLG1** and **FLG2** materials, respectively.

On the other side, to successfully functionalize the single layer graphene with the synthesized building blocks, different conditions were tested. When the functionalization of copper supported (Cu-supported-)GOS was tried, each experimental reaction condition used resulted inadequate to the purpose.

At first, because of the malleability of the copper surface, it was thought to use a special expressly designed reaction equipment (Figure 83).
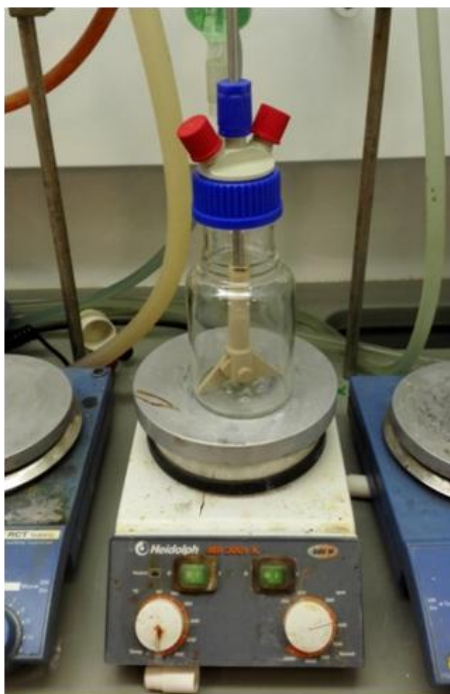
Figure 83: Special reactor expressly designed.

The employed glass vessel was characterized by a mechanical stirrer blade directly connected to the plug on the top and four glass peaks at its bottom. Our principal aim was, by positioning the Cu-supported-GOS at the center of these four peaks, to favour the agitation of the solvent preventing, on the other side, the shifting of the Cu-surface. The reaction was carried out in *o*-DCB at 90°C for 8 hours, and at the end of this time, the Cu-supported-GOS was recovered in its initial position but, unfortunately, it was not possible to prove the functionalization process due to its folding, in turn attributed to the maybe too strong solvent's stirring.

In a second functionalization sequence, it was decided to slightly change the reaction conditions. It was employed a 1:1 mixture of *N*-methylpyrolidone (NMP) with CS_2, while some drops of trifluoroacetic acid acted as catalytic agent. The first to permit gaining a perfect

solubilization of the molecule and the second one to promote the formation of the aryl radicals. The functionalization was carried out using again Cu-supported-GOS at different reaction temperature (90°C and 60°C) and times (8 and 6 hours). Moreover to prevent the former folding of the Cu-supports, providing agitation without direct stirring of the solvent, another "unconventional" system was developed (Figure 84).

Figure 84: "Unconventional" system to avoid the folding of the Cu-supports.

Round bottom flasks, filled with the reaction mixture, were positioned on the top of glass vials containing magnetic stirrers. However, in all cases with different reaction times, the Cu-supported-GOS resulted partially corroded. It results probably due to the combination of the acid, even if in catalytic quantities, with the organosulfur compound, which induce the formation of cuprous sulfides and following hydrogen sulfide which induce the formation of cuprous sulfides and following

hydrogen sulfide which increase the corrosion process of the metal surface.[249]

Decisive solution to get out of this impasse situation, overcoming all the different encountered problems, was to carry out the reaction at milder conditions, using graphene deposited single layers on less sensible and more inert supports, such as silica. Reaction times and temperatures were reduced to 4 hours and room temperature. Moreover, it was decided to eliminate the stirring from the solution and to compare the chemical modification of two SiO_2/Si-supported-GOS by functionalization in different conditions (Figure 85).
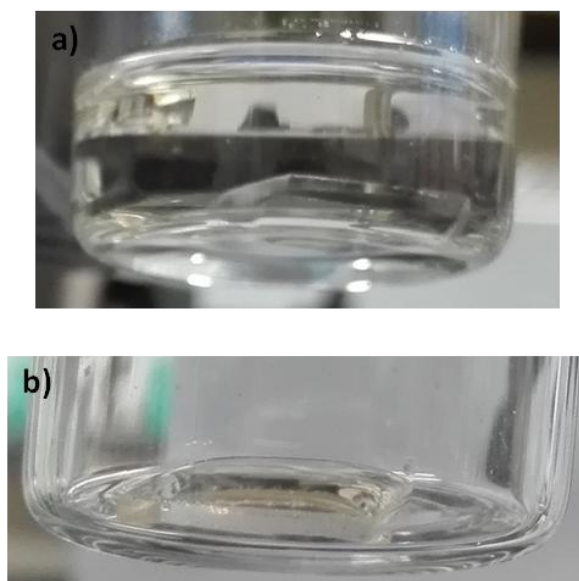
Figure 85: Graphene's functionalization on silica support by: (a) immersion in the reaction mixture and (b) exposure to contact angle formation through the mixture and the graphene covered face of the silica support.

A support was directly dipped in the reaction mixture, while on the surface of the other SiO_2/Si-supported-GOS a single drop of the reaction mixture was deposited forming a contact angle. Finally, to our delight, the reaction conditions, in both cases, did not compromise the

[249] a) A. Fateh, M. Aliofkhazraei, A. R. Rezvanian, Review of corrosive environments for copper and its corrosion inhibitors. *Arabian Journal of Chemistry,* **2017**, doi:10.1016/j.arabjc.2017.05.021; b) L. R. Lewand "The Role of Corrosive Sulfur in Transformers and Transformer Oil", Proceedings of the Sixty-Ninth Annual International Conference of Doble Clients, Insulating Materials Session, **2002**.

single layer graphenes, which were recovered undamaged together with their SiO_2/Si supports. Therefore, when using GOS as starting graphene material, the corresponding aryl diazonium salts were previously generated by adding isoamyl nitrite to a solution of **4**, **6** or **8** and subsequently drop casted on the GOS surface, in a procedure slightly modified respect the Tour's one.[213]

9.2. *GOS-Based Materials Characterization*

Several techniques were used as characterization tools for the synthesized graphene-based materials. Raman spectroscopy is, for instance, a powerful instrument for the identification of graphene doping and imperfections. In fact, the chemical introduction of covalently attached species on its surface effectively corresponds to the creation of defects, being responsible for the substantial rehybridation of the *sp^2* carbons into *sp^3* lattice atoms. Therefore, Raman studies on either FLGs and GOS, before and after chemical treatment, confirm the successfulness of the functionalization process. All aggregates present an increase in the D band associated with a higher defect degree on the nanomaterials. This increase is related presumably with the *sp^3* carbon centers produced on the basal plane by the aryl attack of the diphenylmethanofullerene derivatives **31**, **33** or **35**. The ratio with the G band (I_D/I_G) is a way to quantify the covalent functionalization of those materials. According to this criterion, in our measurement we found a high degree of functionalization for **FLG2** with an I_D/I_G of 0.29 compared with the 0.14 obtained for **FLG1** when the reaction was carried out with dispersion of FLG (Figure 86).
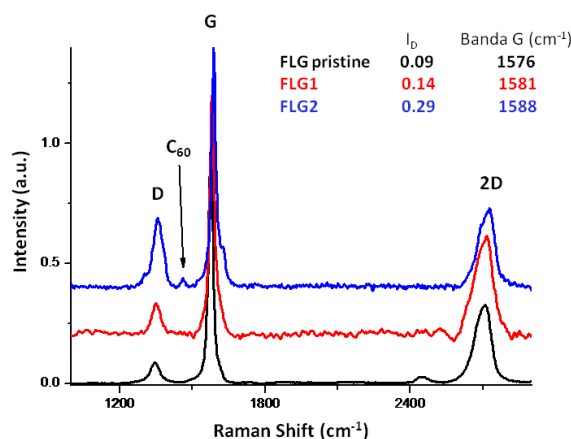
Figure 86: Raman spectra of pristine FLG (black), **FLG1**(red) and **FLG2** (blue) under 532 nm laser excitation wavelength.

An analogous behavior is found with the graphene deposited on silica surface where an I_D/I_G ratio of 0.54 for **GOS2** is the highest among the three different samples being 0.26 and 0.23 the values obtained for **GOS1** and the reference hybrid **GOS3** respectively (Figure 87). Moreover, a new peak around 1457 cm^{-1} is clearly observed for all fullerene aggregates which can be assigned to the pentagonal pinch mode [$A_g(2)$] of C_{60}.[250] Thus, these evidences confirms the covalent attachment of **31**, **33** or **35** on the FLG or GOS.
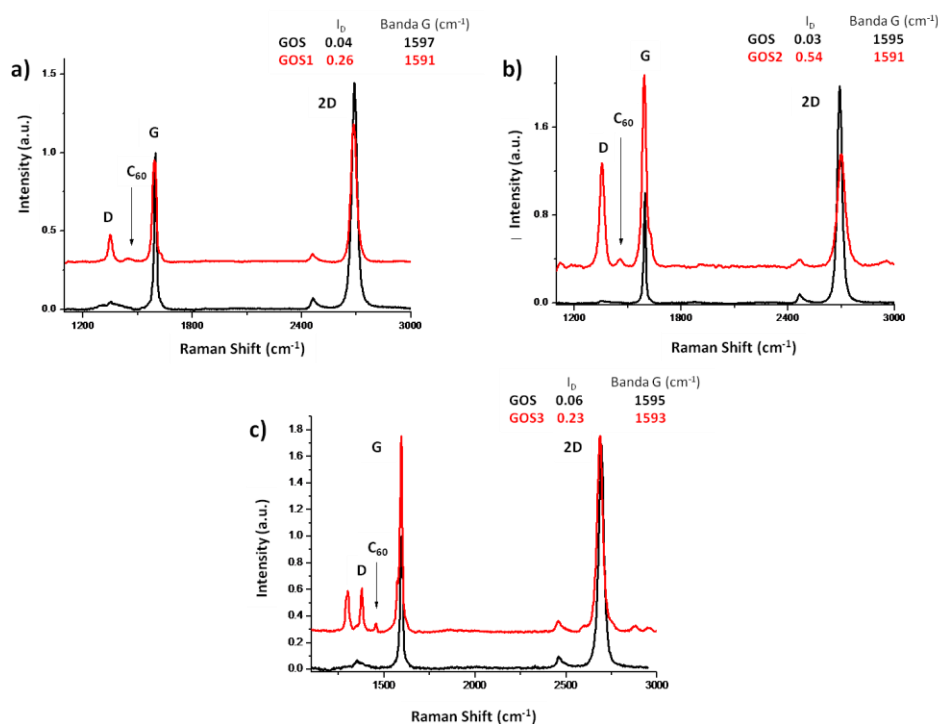
Figure 87: Raman spectra of pristine GOS in black and in red **GOS1** (a), **GOS2** (b) and **GOS3** (c), under 532 nm laser excitation wavelength.

Thermogravimetric analysis (TGA) under inert atmosphere was only carried out on the FLG derivatives to estimate the degree of surface functionalization (Figure 88).

[250] J. Guan, X. Chen, T. Wei, F. Liu, S. Wang, Qi. Yang, Y. Lua, S. Yang, *J. Mater. Chem. A* **2015**, 3, 4139.
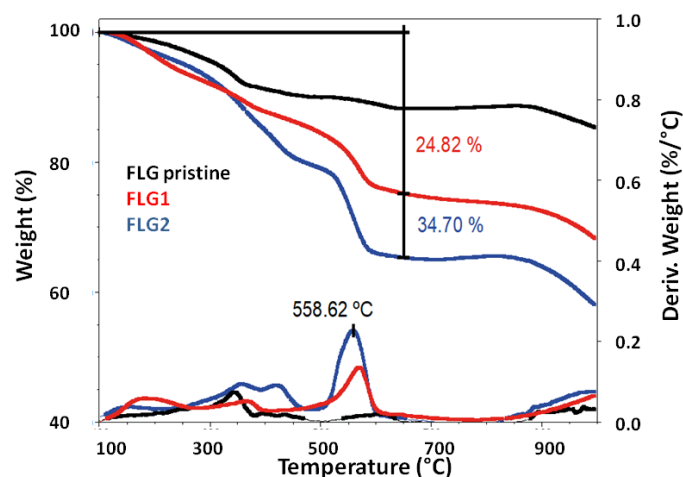
Figure 88: TGA analysis under inert conditions of exfoliated FLG (black), and the nanoconjugates **FLG1** (red) and **FLG2** (blue).

Pristine FLG shows high thermal stability until 800ºC degrees with a slight weight loss due to some physisorbed solvent molecules used in the exfoliation process. For both FLG-C_{60} covalent compounds, two weight loss processes were observed. The first weight loss step can be assigned to the thermal detaching of the attached C_{60} moiety followed by the second weight loss where the C_{60} is decomposed. The total weight loss for **FLG2** (34.70 %) is significantly higher compared to the **FLG1** (24.80 %) which can be interpreted as a higher degree of functionalization. The average molar content can be estimated for **FLG1** in 1 organic molecule per 224 carbon atoms and for **FLG2** in 1 organic molecule per 139 carbon atoms.

The diphenylmethano[60]fullerene **31** reacted with FLGs in absence of the radical initiator isoamyl nitrite, was used as control reaction, to further prove the real occurrence of a covalent modification and not just a supramolecular interaction between the fullerene derivatives and the graphene layer. Thermogravimetric analysis of the sample, indeed, revealed that the mass loss of the control reaction **FLG+31** (grey line) is smaller than the covalent functionalized product **FLG1** (red line) but similar to the weight loss of the isolated molecule **31** (blue line) (Figure 89).
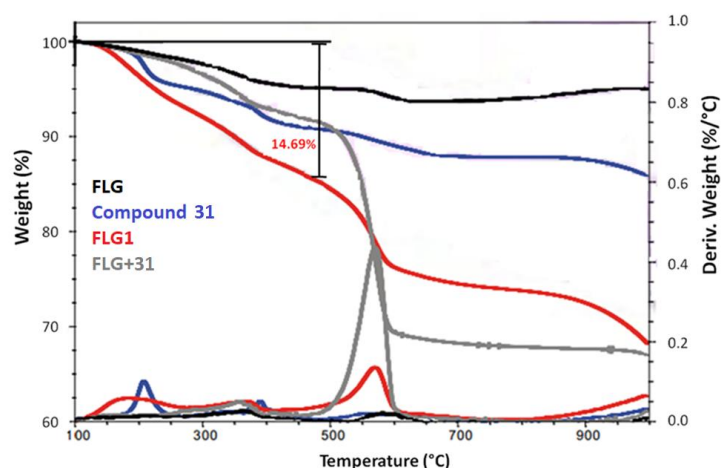
Figure 89: TGA analysis under inert conditions of the control reaction **FLG+31** (grey) compared with the exfoliated FLG (black), the isolated molecule **31** (blue)

The meaning of this result was further supported by the Fourier-transform infrared spectroscopy (FTIR) by which the characteristic peak for the fullerene moiety was observed in derivative **FLG1**. Figure 90 shows the FTIR spectroscopy comparison of the **FLG1**, obtained by following the reported procedure that employs isoamyl nitrite, with the result of the control reaction in its absence, **FLG+31**.
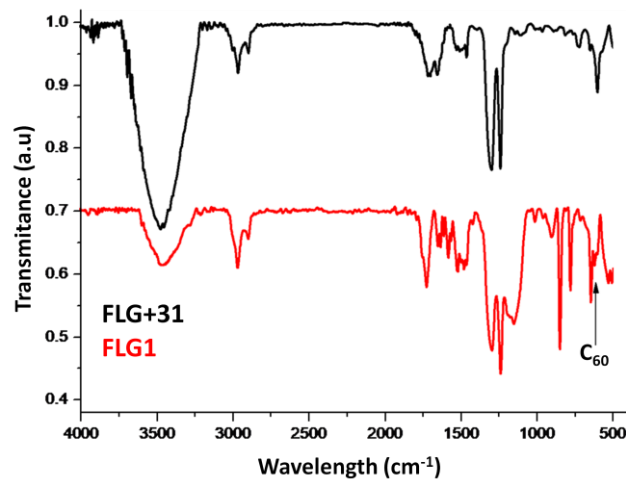
Figure 90: FTIR spectra of **FLG1** (red) compared to **FLG+31** (black).

Among the characteristic peaks are the skeletal in plane vibrations of graphene at 1581 cm^{-1} as well as some vibrational peaks at 2928 and

2857 cm^{-1}, that could be related to aliphatic carbon atoms. But more important are the characteristic vibrational peaks of pristine C$_{60}$ shown around 1454 and 525 cm^{-1} for the covalent **FLG1** that are not present for the control reaction **FLG+31**. These peaks are also present in the FTIR spectroscopy of the organic molecules **31**, **33** and **35**.

As further evidence, X-ray photoelectron spectroscopy (XPS) analysis was recorded for **FLG1** and **FLG2**. The survey spectra of **FLG1** exhibit a main C 1s component together with two more signals assigned to O 1s and N 1s (Figure 91).
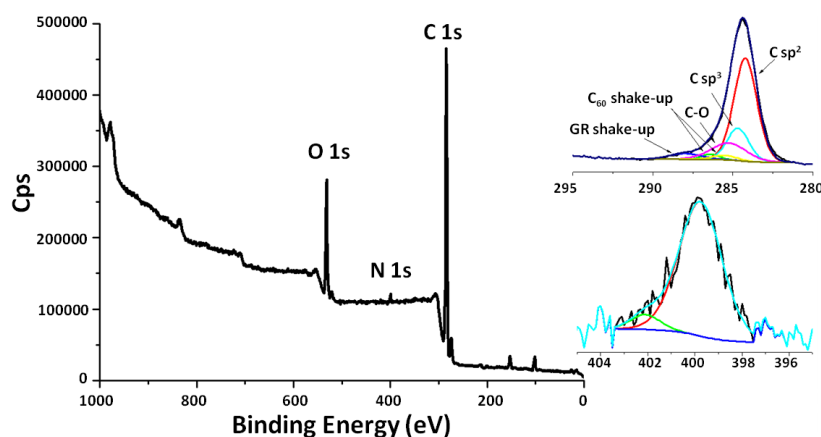
Figure 91: XPS spectra of **FLG1** with inset of the high resolution spectra of C 1s (up) and N 1s (down).

The 12% oxygen contribution observed for **FLG1** is the same obtained for pristine FLG, indicating that no extra oxygen atoms are covalently anchored on the FLG surface during the radical addition reaction with **31**. However for both **FLG1** and **FLG2** the N 1s peak could be related to unreacted amine groups that are still present in the organic molecule being the high resolution spectra of N 1s made up of only one component. The high resolution C 1s core level spectrum of both materials **FLG1** and **FLG2** presents, besides the four expected components (photoelectrons emitted from sp^2 carbon atoms, sp^3 carbon atoms, oxidized carbon atoms in the C–O bonds and the π–π* shake up

structure of graphene sheets) two new contributions that could be assigned to C 1s shake-up satellite peaks of C_{60}.[250,251]

Interestingly, from the transmission electron microscopy (TEM) analysis of **FLG1** and **FLG2** it can be recognized some spherical species at their edges (Figure 92).
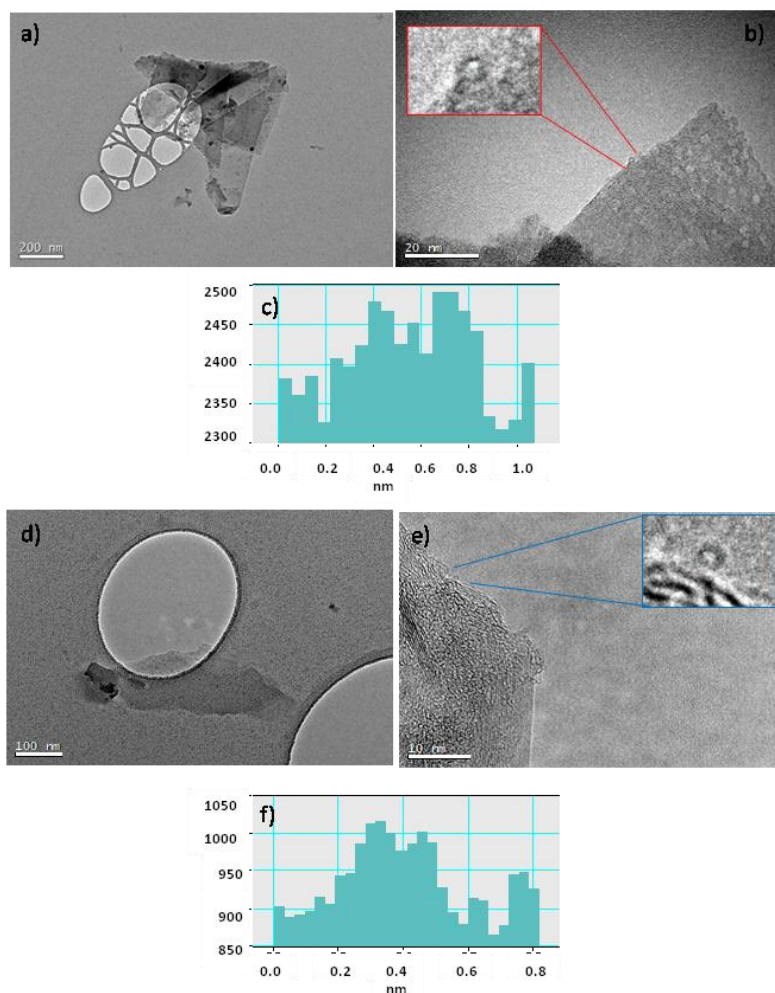
Figure 92: TEM micrographs of **FLG1** with scale bar 200 nm (a), 20 nm (b) and representative image of the width profile of the fullerene attached to the aggregate (c). TEM micrographs of **FLG2** with scale bar 100 nm (d), 10 nm (e) and representative image of the width profile of the fullerene attached to the aggregate (f).

[251] C. Enkvist, S. lunell, B. Sjögren, S. Svensson, P. A. Brühwiler, A. Nilsson, A. J. Maxwell, N. Martensson, *Phys. Rev. B: Condens. Matter Mater. Phys.* **1993**, *48*, 14629.

Under identical conditions, the same spherical forms are not observable in pristine FLG TEM micrographs. Thus, the round shape nanoforms could be attributed to the covalently attached organic molecules based on C_{60}, since their diameter (~1 nm) is compatible with the reported diameter for C_{60}.[236,252]

9.3. *Physical Characterization*

At first, the morphological characterization of all the novel graphene hybrids materials synthesized reveals the presence of molecular islands, with a height of ~1.2 nm, that partially cover the graphene sheet (Figure 93). Visible are also the characteristic folds of bare graphene, which are known to occur during the transfer process of CVD-graphene from copper.
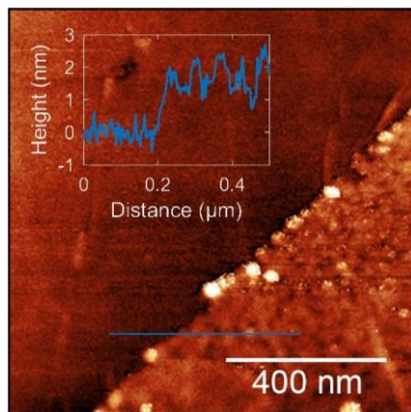
Figure 93: AFM image of **GOS2** on SiO_2/Si

The thermoelectric properties of these graphene-base novel hybrids were determined in ambient conditions by probing these islands through the use of a Pt-coated (Multi75-G from BudgetSensors) AFM tip, while the graphene layer, that is held at high temperature, acts as the opposing electrode. The Pt-coated tip was placed into gentle contact (~30 nN) with the substrate and held still through a feedback loop controller. Figure 94 shows a schematic representation of the measuring technique.

---

[252] X. Zhang, Z. Zhi, Y. Huang, X. Wan, J. Tian, Y. Ma, Y. Chen, *J. Nanosci. Nanotech*. **2009**, *9*, 5752.
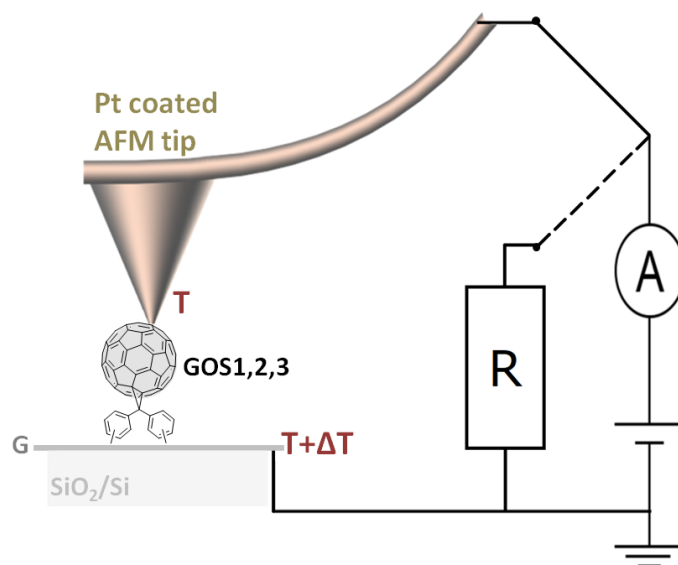
Figure 94: Schematic of the c-AFM setup used.

As demonstrated in the background, this allows to measure, through a generated non-zero tip-substrate temperature difference (ΔT), IV curves in which the thermoelectric voltage shows up as a voltage-offset (ΔV),[253] that can be related to the Seeback coefficient (S). To facilitate a precise voltage reading, a disconnection of the c-AFM from the voltage source and following connection to a resistor allowed to perform the zero-calibration in short time intervals. At this point, the thermopower S and the conductance G were determined. To obtain statistically significant values for S, more than 600 IV curves at several different points on all samples were recorded for either the empty area, corresponding to the bare graphene layer, and the molecule islands. The result is shown in S-histograms, where S was determined to be the mean of the distribution with an error that is the standard error (Figure 95).

---

[253] L. Dobusch, M. M. Furchi, A. Pospischil, T. Mueller, E. Bertagnolli, A. Lugstein, *Appl. Phys. Lett.* **2014**, 105, 253103.
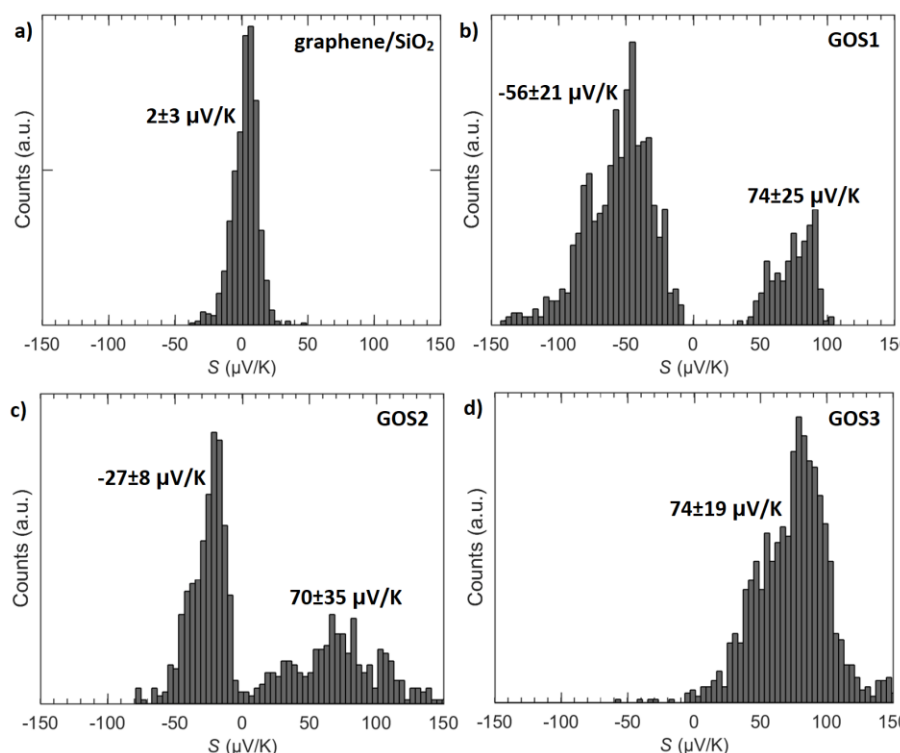
Figure 95: Histograms showing the thermopower values for the SiO_2/Si-supported graphene monolayer (a) and all the nanocomposites, **GOS1** (b), **GOS2** (c) and **GOS3** (d).

Figure 95a shows a histogram of S measured with the tip in contact with the graphene. Since the thermal conductivity of graphene is high and the electrical contact is low-resistive, the thermal gradient, in this case, is not at the tip/graphene junction but has a strong lateral extension. The S value of 2 ± 3 µV/K determined here results, therefore, in good agreement with other experiments where the in-plane thermopower of graphene is found to be positive and <10 µV/K.[254] On the other side, Figure 95b-d shows the S histograms measured when the tip is in contact with a graphene area covered by a molecular island. Interestingly, it is found that when the force with which the tip is pushed towards the surface is increased, the tip can jump into contact with the graphene and the thermopower of graphene, as shown in

---

[254] a) M. Buscema, M. Barkelid, V. Zwiller, H. S. J. van der Zant, G. A. Steele, A. Castellanos-Gomez, *Nano Lett.* **2013**, *13*, 358; b) J. Wu; H. Schmidt, K. K. Amara, X. Xu, G. Eda, B. Özyilmaz, *Nano Lett.* **2014**, *14*, 2730.

Figure 95a, is measured. For the mono-linked G-based-C_{60} hybrid (**GOS3**, Figure 95d) a *S* value of 74±19 µV/K is found, which has to be considered exceptionally high in comparison with the values reported for other molecules.[238] The histograms corresponding to the thermopower measured for the *p*- and *m*-linked diphenylmethanofullerenes (**GOS1** and **GOS2**, respectively) on their molecular islands evidence the appearance of two peaks, but it has to be noted that for each sample, the single approach in a given area only gives values that correspond to one of the peaks. The value of the positive peak, 74±25 µV/K for **GOS1** and 70±35 µV/K for **GOS2**, results in striking agreement with the high value of S found for **GOS3**. This correspondence, also supported by the previously reported XPS analysis of **GOS1** and **GOS2**, suggests that the link of one of the aryl units of the *p*- or *m*-diphenylmethano[60]fullerene may have not formed, giving rise to the presence of mono-linked G-based-C_{60} hybrids on these samples. It was suggested, therefore, that the peak at 74 µV/K can be assigned to the mono linked graphene derivative, and therefore the thermopower corresponding to the *p*-(**4**) and *m*-(**6**) molecules doubly graphene-connected, corresponds to the peaks at -56±21 µV/K and -27±8 µV/K, respectively. These high quantum thermopower values suggest great promise for molecular/graphene composite materials in thermoelectric applications, while the change in thermopower polarity with the number of anchoring groups implies potential for **GOS1** and **GOS2** to be used in more complex device architectures.

9.4. *Theoretical Calculations*

With the aim of understanding the change in sign and magnitude of the Seebeck coefficient, observed as a function of different bonding geometries between the fullerene derivatives **31**, **33** and **35** and the graphene sheet substrate, theoretical calculations were carried out.

The energetics and resulting conformations of the fullerene derivatives **31**, **33** and **35** bonding to a graphene surface via activated aryl radicals were obtained from the SIESTA[255] implementation of density functional theory where the van der Waals density functional (vdW-

---

[255] J. M. Soler, E. Artacho, J. Gale, A. García, J. Junquera, P. Ordejón, D. Sánchez Portal, *J. Phys. Condens. Matter.* **2002**, *14*, 2745.

DF) was employed.[256] The vdW-DF used in SIESTA is applicable to arbitrary geometries[257] and to ensure accuracy the inter atomic forces were relaxed to optimize the geometry. Once the conformer geometries were optimized, the mean field Hamiltonian and overlap matrices, derived from SIESTA, were used to calculate the electronic and thermoelectronic properties using the quantum transport code GOLLUM (Figure 96).[258]
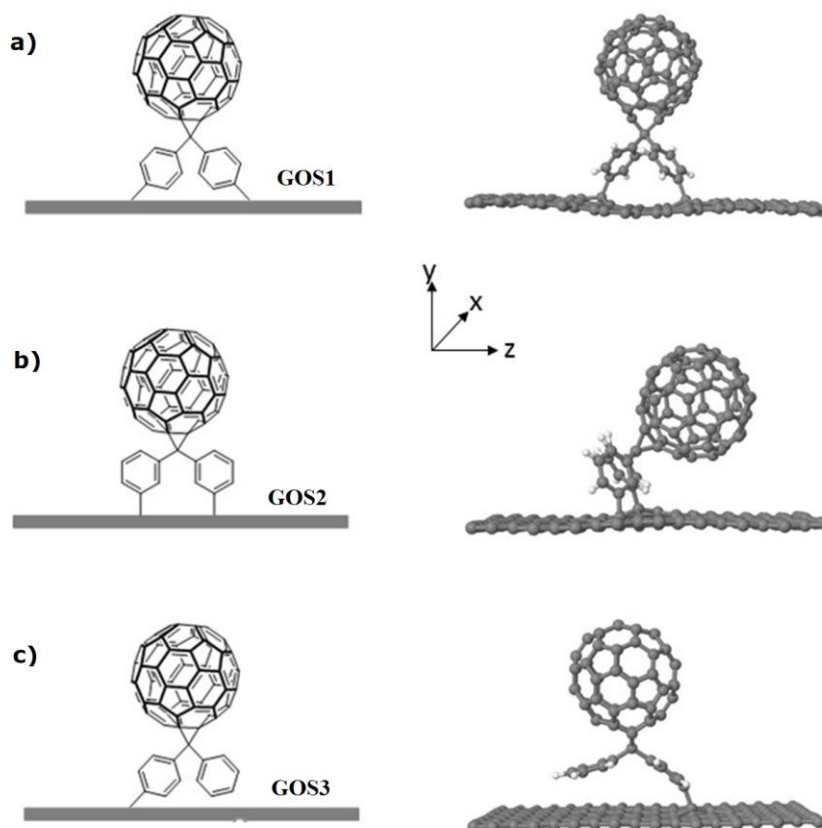
Figure 96: On the left, the synthesized a) **GOS1**, b) **GOS2** and c) **GOS3**. On the right, the relaxed geometries from the theoretical calculations. The graphene sheet with 216 carbon atoms is periodic in both the in-plane x,z directions.

[256] a) M. Dion, H. Rydberg, E. Schröder, D. C. Langreth, B. I. Lundqvist, *Phys. Rev. Lett*. **2004**, *92*, 246401; b) D. C. Langreth, M. Dion, H. Rydberg, E. Schröder, P. Hyldgaard, B. I. Lundqvist, *J. Quantum Chem.* **2005**, *101*, 599.

[257] H. B. Jansen, P. Ross, *Chem*. *Phys*. *Lett*. **1969**, *3*, 140.

[258] J. Ferrer, C. J. Lambert, V. M. García-Suárez, D. Z. Manrique, D. Visontai, L. Oroszlany, R. Rodríguez-Ferradás, I. Grace, S. W. D. Bailey, K. Gillemot, *New J. Phys*. **2014**, *16*, 093029.

The calculations realized by carefully placing the reactive aryl units close to the pristine graphene surface and replacing the C_{60} with two hydrogen atoms and reducing the graphene sheet to 96 atoms to save computation time, lead to successfully carrying out the modeled Tour reaction using SIESTA. After many randomly distributed initial starting configurations the calculations show that randomly placing the dibenzyl units over the surface results in over 60% detachment and no covalent bonding observed. Once the relaxed configurations of **GOS1,2,3** (in absence of the [60]fullerene moiety) have been found, the C_{60} is reattached and the graphene sheet is doubled in size to contain 216 carbon atoms. The system is again relaxed using the bonded conformations.

To model the STM junction a gold tip is constructed and the most energetically favourable tip to fullerene derivatives **31**, **33** and **35** geometry is found. This is shown in Figure 97 where the Au-C bond is shown to form two legs of length d = 2.5 Å placed equidistantly between two carbon atoms on the C_{60} unit forming the edge of a pentagonal ring.
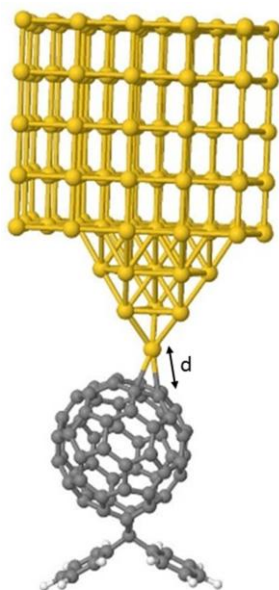
Figure 97: The gold STM tip model showing the most energetically favourable geometry to form the STM gold tip and C_{60} geometry.

Finally, the relaxed geometry for the hybrid nanocomposites systems **GOS1,2,3** shown in Figure 96 were furnished of the STM tip and the resulting structures are shown in Figure 98.
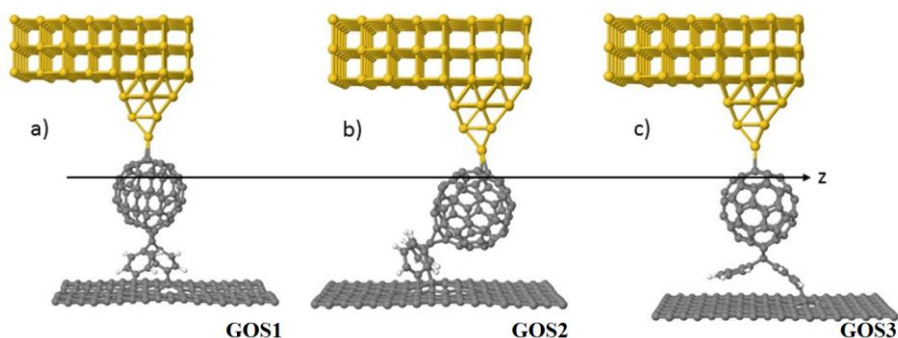
Figure 98: The modelled STM experimental set up to measure the electronic and thermoelectrical properties of **GOS1,2,3**.

SIESTA then calculates the Hamiltonian of these relaxed structures without further conjugate gradient relaxation. This Hamiltonian and the overlap matrices are then used by the transport code GOLLUM to calculate the transmission coefficients T(E) from which the thermoelectric properties are obtained.

The thermopower is calculated as a function of energy for a given temperature dictated by the experimental conditions, in this case 300K. The sign and magnitude of the thermopower are controlled by modulating the contact between the graphene sheet and the benzyl units due to the quantum mechanical effects at the molecular level, for example the sign is given by the negative of the slope of logT(E) at a given energy.

At this stage the robustness of the STM tip and C_{60} contact location was investigated. Locating the tip on the C_{60} surface at a number of possible pentagon edge sites produced little change in the transmission peaks justifying the decision to use one location and one set of transmission data for each calculation.

The calculated values of the Seebeck coefficient S(μV/K) at 300K result in good agreement with the observed values, if the energy is selected, and are shown in Table 5.

Table 5: Comparison between the values of the Seebeck coefficient S(μV/K) at an energy of -0.44 eV, calculated at 300K, and the correspondingt values experimentally determined.

	S_{calc} (300 K)	S_{exp}
GOS1	-56 μV/K	-48,5 μV/K
GOS2	-27 μV/K	-29,6 μV/K
GOS3	74 μV/K	23,8 μV/K

As demonstrated from Table 5, the values of the Seebeck coefficient, calculated at an energy of -0.44 eV, generally follow the trend of the experimental results, showing, moreover, surprising agreement with them for **GOS1** and **GOS2**, while the calculated S value for **GOS3** seems to divert. However, taking into account the histograms of the Seebeck coefficient within the HOMO-LUMO gap, which is defined to lie between -0.5 and -0.2 eV (Figure 99), and considering the most probable values, the results change. On one side, **GOS1** and **GOS2** maintain their good agreement with the experimental data, in fact, both calculated results of the Seebeck coefficient are negative and included in a range of 25-50 μV/K, while on the other side, **GOS3** now shows that the thermopower displays a high probability to assume positive values above 50 μV/K.
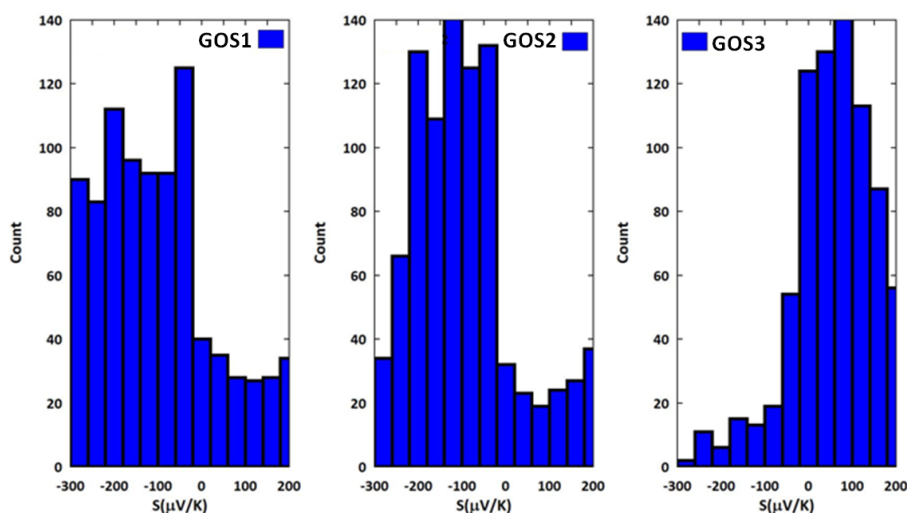
Figure 99: Histograms of the Seebeck coefficient within the HOMO-LUMO gap.

These results, therefore, suggest that combining density functional theory calculations with thermoelectric characterization experiments consists in a valid method for searching and investigating different type of hybrid materials, which could enhance thermoelectric performances.

9. Results and Discussion

10. Conclusions

10. Conclusions

The second chapter of the present thesis has illustrated a simple design approach to achieve high thermoelectric performance materials based on novel covalently attached graphene-molecule composites.
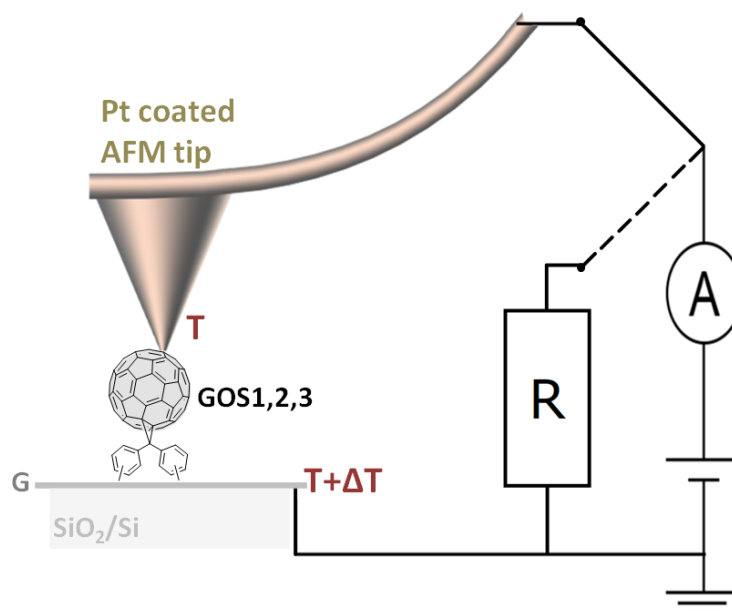
Figure 94: Thermoelectric properties determination on GOS-based materials.

The thermoelectric properties of these new hybrids were successfully characterized through c-AFM by employing the graphene layer as second electrode to test the connected molecular units. The synthesized novel GOS-materials display superior values of thermopower when compared with metal-molecule-metal arrangements. Interestingly, the stemming conclusion from our charge transport studies is that even minimal structural changes in the linked molecules can produce notable variation in the measured thermoelectricity. Moreover, the magnitude and the polarity of thermopower is conditioned by the nature of the anchoring groups and the DFT method reveals itself to be a well-established and efficient simulation technique to produce reliable predictions.

Therefore, with the present thesis work, it is proudly demonstrated that:

- The combination of the density functional theory calculations with the thermoelectric characterization experiments results into an effective way of searching for other material combinations which enhances the thermoelectric performances;

- The fullerene covalently anchored graphene derivatives **GOS1** and **GOS2**, generating exceptionally high quantum thermopowers, pave the way to the potential introduction of 2D organic materials in thermoelectric applications operating at ambient conditions, without the necessity of using rare-earth or heavy elements.

11. Experimental Part

11.Experimental Part

11.1. *General Methods and Techniques*

-*Materials*: Reagents for synthesis were purchased from commercial sources and used without further purification. Solvents were dried and distilled using standard techniques.[102] Those reactions requiring an inert atmosphere were carried out using argon as source. The graphite used for graphene exfoliation was purchased from TIMCAL (TIMREX SFG15, ρ = 2.26 g/cc, particle size = 8.80 μm, surface area = 9.50 m^2/g, ash $\leq$ 0.100%, interlaminar distance = 0.3354-0.3358 nm). Vacuum filtrations of graphene materials were carried out with polycarbonate track etched (PCTE) (pore size = 0.2 μm, Φ = 47 cm) and polytetrafluoroethylene (PTFE) (pore size = 0.2 μm, Φ = 47 cm) membranes.

-*Raman spectra:* were recorded on a NT-MDT in Via Microscope at room temperature using an exciting laser source of 532 nm.

-*Thermogravimetric analyses (TGA):* were carried out with a thermobalance TA-TGA-Q-500 under N_2 or air atmosphere, depending on the sample. The sample ($\approx$ 0.5 mg) was introduced inside a platinum crucible and equilibrated at 100ºC followed by a 10 ºC/min ramp between 100 and 1000 ºC.

-*XPS analysis:* were carried out using a SPECS GmbH (PHOIBOS 150 9MCD) spectrometer operating in the constant analyzer energy mode. A nonmonochromatic aluminium X-ray source (1486.61 eV) was used with a power of 200 W and voltage of 12 kV. Pass energies of 75 and 25 eV were used for acquiring both survey and high resolution spectra, respectively. Survey data were acquired from kinetic energies of 1487 - 400 eV with an energy step of 1 eV and 100 ms dwell time per point. The high resolution scans were taken around the emission lines of interest with 0.1 eV steps and 100 ms dwell time per point. SpecsLab Version 2.48 software was used for spectrometer control and data handling. The semi-quantitative analyses were performed from the C 1s (284.3 eV) signal. The samples were introduced as pellets of 8 mm diameter.

-*Transmission electron microscopy (TEM):* was performed on a JEOL JEM 2100, with an acceleration voltage of 200 kV equipped with a

camera CCD ORIUS SC1000 (model 832) and the microanalysis were performed by XEDS (OXFORD INCA). The samples were dispersed in *o*-DCB and dropped onto a holey carbon copper grid (200 mesh), the solvent was removed in a vacuum oven during 48 hours.

-Conductive Atomic force microscopy (c-AFM): was performed under ambient conditions using Cervantes Fullmode AFM from Nanotec Electronica SL working on tapping mode at a working frequency of ~70 kHz to obtain height images. The samples of SiO_2/Si-supported-SLGs were analyzed as provided after the chemical reaction and following treatment.

11.2. GOS-Based Materials

Synthesis of Amino Functionalized Diphenylmethano[60]Fullerene Building Blocks:

Protection step

4,4'-(trifluoroacetamido)benzophenone (28)[247]
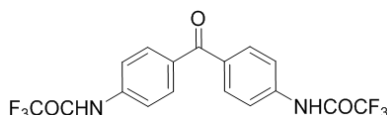
A solution of 4,4'-diaminobenzophenone (848 mg, 4 mmol) in 15 mL of dry THF, 12 mL of trifluoroacetic anhydride and a few drops of dry pyridine were refluxed for 4h under argon atm. After cooling to room temperature, the reaction was quenched by cautiously adding methanol and water and extracted with DCM. The organic phase was dried over $MgSO_4$ and the solvent was then evaporated under reduced pressure. The residue was purified by column chromatography on silica gel with hexane/ethyl acetate (7:3), yielding a white solid.

Yield: 85%

^{1}H NMR (300 MHz, CD$_3$OD) δ 7.98 – 7.73 (m, 8H).

General Procedure for the Condensation to obtain *p*-tosylhydrazones 29, 32 and 34

Under argon atm, a solution of **28**, 3,3′-diaminobenzophenone or 4-aminobenzophenone (3.81 mmol) and *p*-tosylhydrazide (3.81 mmol) in 50 mL of toluene and 7 mL of EtOH was refluxed for 24 h. After

cooling to room temperature, the solvent was evaporated and the crude purified by column chromatography, eluting with hexane/AcOEt (1:1) to obtain *p*-tosylhydrazones **29**, **32** and **34**.

4,4'-(trifluoroacetamido)benzophenone-p-tosylhydrazone (**29**)[247]
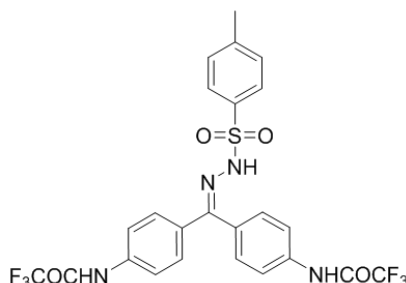
Yield: 80%

^{1}H NMR (300 MHz, CD$_3$OD) δ 7.94 (d, *J* = 8.1 Hz, 2H), 7.83 (d, J = 9.3 Hz, 2H), 7.61 (d, *J* = 9.3 Hz, 2H), 7.47 (d, *J* = 8.1 Hz, 2H), 7.33 (d, *J* = 8.7 Hz, 2H), 7.21 (d, *J* = 8.7 Hz, 2H), 2.42 (s, 3H). .

3,3'-diaminobenzophenone-p-tosylhydrazone (**32**)
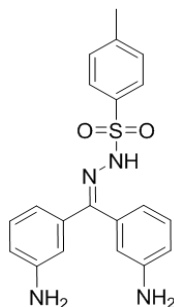
Yield: 79%

^{1}H NMR (300 MHz, CD$_3$OD) δ 7.84 (d, *J* = 8.2 Hz, 2H), 7.41 (d, *J* = 8.0 Hz, 2H), 7.23 (t, *J* = 7.8 Hz, 1H), 7.01 (t, *J* = 7.7 Hz, 1H), 6.81 (d, *J* = 8.1 Hz, 2H), 6.70 (d, *J* = 7.9 Hz, 2H), 6.46 (s, 1H), 6.39 (d, *J* = 7.5 Hz, 1H), 2.44 (s, 3H).

^{13}C NMR (125 MHz, MeOD) δ 159.75, 147.27, 141.65, 140.93, 139.97, 138.16, 129.30, 128.99, 128.27, 118.65, 117.82, 115.23, 21.52.

MALDI-TOF: m/z theoretical for C$_{77}$H$_{25}$NO$_5$ 380.13, exp M$^+$ 380.83.

FTIR (KBr) υ:3451, 3383, 2924, 2854, 1924, 1624, 1489, 1452, 1381, 1324, 1240, 1165, 1091, 1051, 1016, 900, 790, 701, 670, 582, 548 cm^{-1}.

4-aminobenzophenone-p-tosylhydrazone (34) [247]
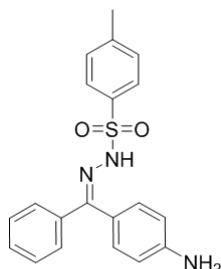
Yield: 83%

^{1}H NMR (300 MHz, CDCl$_3$) δ 7.86 (d, _J_ = 8.3 Hz, 2H), 7.45 (d, _J_ = 7.8 Hz, 2H), 7.26 (m, 5H), 6.93 (d, _J_ = 8.5 Hz, 2H), 6.75 (d, _J_ = 8.5 Hz, 2H), 3.95 (s, 2H), 2.43 (s, 3H).

Deprotection step

4,4'-diaminobenzophenone-p-tosylhydrazone (30) [247]
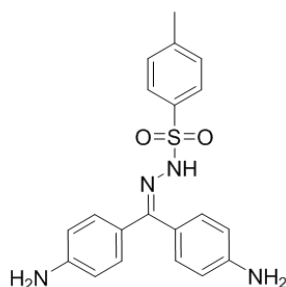
A solution of **2** (500 mg, 0.873 mmol) in 30 mL of MeOH was treated with 20 mL of an aq solution of K$_2$CO$_3$ (10%) and stirred for 24 hours at room temperature. The mixture was extracted with DCM, the organic phase dried over anhyd   MgSO$_4$ and the solvent evaporated under reduced pressure. The residue was then purified by column chromatography on silica gel, DCM/MeOH (9:1), to yield a yellowish solid.

Yield: 95% ^{1}H NMR (300 MHz, CDCl$_3$) δ 7.82 (d, _J_ = 8.3 Hz, 2H), 7.75 (d, _J_ = 8.3 Hz, 2H), 7.54 (d, _J_ = 8.3 Hz, 2H), 7.39 (d, _J_ = 8.3

Hz, 2H), 7.08 (d, J = 9.02 Hz, 2H), 6.91 (d, J = 9.02 Hz, 2H), 2.45 (s, 3H).

General Procedure for the Bamford-Stevens reaction to obtain the diphenylmethano[60]fullerenes **31**, **33 and 35**

To a solution of **30**, **32** or **34** (0.315 mmol) in 8 mL of dry pyridine, sodium methoxyde (0.315 mmol) was added under argon atm. After stirring at room temperature for 15 minutes, a solution of [60]fullerene (0.227 mmol) in 20 mL of *o*-DCB was added at once and the mixture was heated at 180°C for 18 h. After cooling to room temperature, the solvent was stripped away in a rotary evaporator and the remaining solid purified by column chromatography on silica gel, eluting first with CS_2 and then with toluene/AcOEt (8:2) to afford **31**, **33** and **35** as brown solids.

p-diaminodiphenylmethano[60]fullerene (**31**)[247]
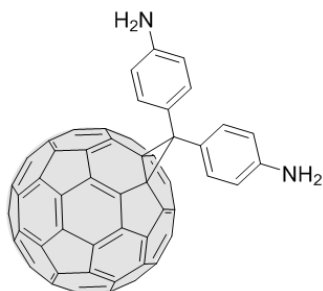
Yield: 45%

^{1}H NMR (300 MHz, DMSO-d$_6$) δ 7.91 – 7.82 (d, 4H), 6.73 – 6.65 (d, 4H).

m-diaminodiphenylmethano[60]fullerene (**33**)
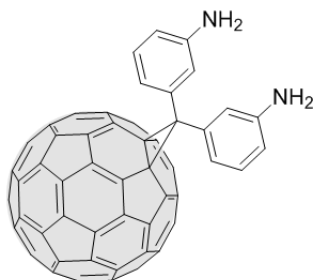
Yield: 30%

^{1}H NMR (300 MHz, DMSO-d$_6$) δ 7.29 (dd, J = 1.9 Hz, 4H), 7.14 (t, J = 8.0 Hz, 2H), 6.57 (d, J = 8.6 Hz, 2H), 5.31 (s, 4H).

^{13}C NMR (175 MHz, DMSO) δ 149.30, 148.64, 145.35, 144.64, 144.53, 144.32, 144.16, 144.01, 143.65, 143.38, 142.40, 142.37, 142.12, 141.84, 141.63, 140.17, 139.54, 137.42, 129.17, 128.25, 118.63, 116.30, 113.64, 79.69, 59.56, 39.52.

MALDI-TOF: m/z theoretical for C$_{77}$H$_{25}$NO$_5$ 916.10, exp M$^+$ 916.16.

FTIR (KBr) υ: 3451, 3385, 2923, 2854, 1611, 1489, 1456, 1382, 1312, 1277, 1162, 862, 771, 697, 569, 525 cm^{-1}.

p-aminodiphenylmethano[60]fullerene (35)[247]
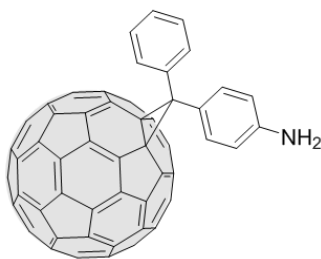
Yield: 22%

^{1}H NMR (300 MHz, CDCl$_3$) δ 8.07 (d, J= 8.64 Hz, 2H), 7.86 (d, J= 8.64 Hz, 2H), 7.47– 7.44 (m, 2H), 7.40 – 7.33 (m, 1H), 6.76 (d, J = 8.5 Hz, 2H), 3.77 (s, 2H).

11.3.   _Synthesis of FLG-Covalent Hybrids_

Chemical exfoliation of graphite:

Graphite flakes (100 mg) were dispersed in _o_-DCB (100 mL) and sonicated at room temperature during 150 minutes in a low-power sonication bath, to obtain homogeneous aggregates. The dispersion was then centrifuged at 500 rpm for 45 minutes. After this process, the decanted supernatant was isolated with a Pasteur pipette and stored in solution.

***General Procedure for the Tour's reaction to obtain* FLG1 *and* FLG2**

50 mL of exfoliated graphene suspensions in *o*-DCB were reacted with a 5 mL solution of the corresponding methano[60]fullerene **31** or **33** (0.065 mmol) in *o*-DCB. The solution was sonicated while deoxigenating with argon for 90 minutes. Isoamyl nitrite (0.26 mmol) was slowly added to the reaction mixture and heated at 70ºC for 24 hours under inert atm. The final product was sequentially washed in a 0.1 μm size PTFE membrane several times with *o*-DCB, DCM and MeOH.

FLG1
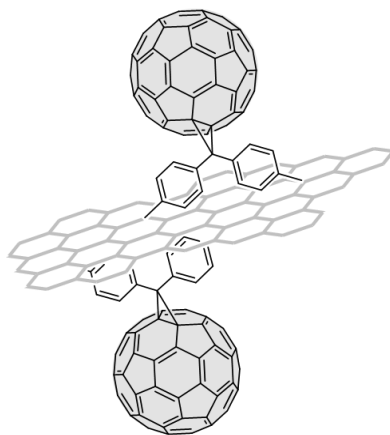
FTIR (KBr) υ: 2928, 2857, 1655, 1579, 1444, 1402, 1157, 1068, 756, 525 cm^{-1}.

TGA: weight loss and temperature desorption (organic anchoring groups): 24.82%, 650 °C.

Raman: $I_D/I_G = 0.14$;

XPS: % atomic: C (284.6 eV) = 87.2, O (531.6eV) = 12.1, N (399.6eV) = 0.65.

FLG2
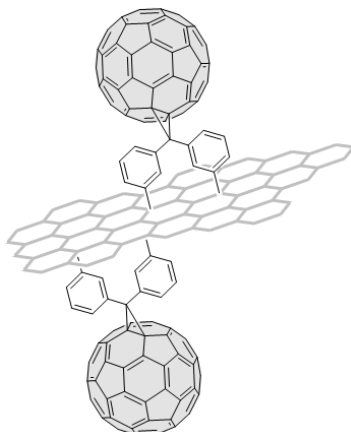
FTIR (KBr): 2928, 2857, 1653, 1579, 1454, 1401, 1038, 784, 525 cm^{-1}.

TGA: weight loss and temperature desorption (organic anchoring groups): 34.70 %, 650 °C.

Raman: $I_D/I_G = 0.29$.

XPS: % atomic: C (284.6 eV) = 80.21, O (532.6 eV) = 19.1, N (399.6 eV) = 0.7.

11.4.   *Synthesis of the Covalent GOS-Based Materials*

General Procedure for the Tour's reaction to obtain **GOS1**, **GOS2**, **GOS3**

A 10^{-4} M solution of the corresponding methano[60]fullerene **31**, **33** or **35** (0.008 M) in chlorobenzene/CS$_2$ (1:1) was deoxygenated for 1 hour. Isoamyl nitrite in a catalytic quantity was slowly added to the reaction mixture that was subsequently drop casted (one drop) onto the GOS. The material was maintained at room temperature under inert atm for 4 hours and subsequently washed several times with *o*-DCB, DCM and MeOH.

GOS1

Raman: $I_D/I_G = 0.26$;

GOS2
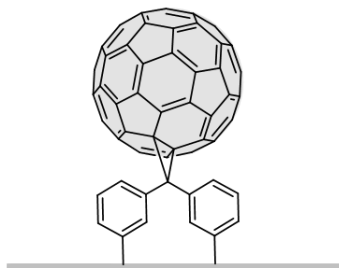
Raman: $I_D/I_G = 0.54$.

GOS3

Raman: $I_D/I_G = 0.23$

11.5. *Control Reaction on FLG*

50 mL of exfoliated graphene suspensions in *o*-DCB sonicated and deoxigenated with argon for 90 minutes were reacted with a 5 mL solution of the corresponding methano[60]fullerene **31** (0.065 mmol) in *o*-DCB. The mixture was heated at 70ºC for 24 hours under inert atm. The final product was washed in a 0.1 μm size PTFE membrane several times with *o*-DCB, DCM and MeOH.

FLG-Control

FTIR (KBr) υ: 2900, 1638, 1579, 1454, 1384, 1157, 1060, 632, 506 cm^{-1}; TGA: weight loss and temperature desorption (organic anchoring groups): 14.69 %, 650 °C.

Summary

Summary

Introduction

The field of molecular electronics, based on the use of single molecules or nanoscale collections of single molecules as electronic components, has represented, and still now represents, a seductive playground for scientists where there is still much to do. Over the past decade, experiments and theory have allowed to greatly enhance the comprehension of the working principles at the base of molecular junctions. Thus, the interest has shifted over other less known, investigated or understood, aspects involving structural or theoretical challenges. So far, most of research efforts in this field were mainly devoted to the investigation of the electrical conductance of covalently conjugated molecular wires. Now, instead, more complex structures (i.e. based on supramolecular systems), less known features (namely, the thermoelectric properties of these systems) and hybrid materials begin to grab the scientific attention of the area.

Chapter 1.

Objectives

A new generation of molecular wires characterized by weak intermolecular forces in their core unit has been designed, synthesized and studied.

On one hand, the salt bridge connection between the amidinium and carboxylate groups was exploited to the development of a set of supramolecular systems with different length, structure and anchoring groups to get a better knowledge of the charge transfer properties of non-covalently linked molecular wires:

Amidinium-Carboxylate Based Supramolecular Wires:

   a) *Fullerene dumbbells series*

   b) *Linear supramolecular wires series*

On the other hand, instead, it was taken advantage of the ion-dipole interaction, which origins between a metallic cation and a crown ether cavity, to study the variable effect that a metal coordination has on the conductance of single molecular wires depending on their anchoring group:

Crown Ethers Switching Systems as Supramolecular Wires:

    a)   *4,5'-diaminodibenzo[18]crown-6*

    b)   *OPE and PPP crown ether molecular wires series*

Results and Discussion

Amidinium-Carboxylate Based Supramolecular Wires:

    a)   *Amidinium-Carboxylate Based Fullerene Dumbbells Series*

The synthesis of a new family of non-covalent fullerene dumbbells characterized by the two-point supramolecular interaction between the amidinium and carboxylate groups has been carried out.
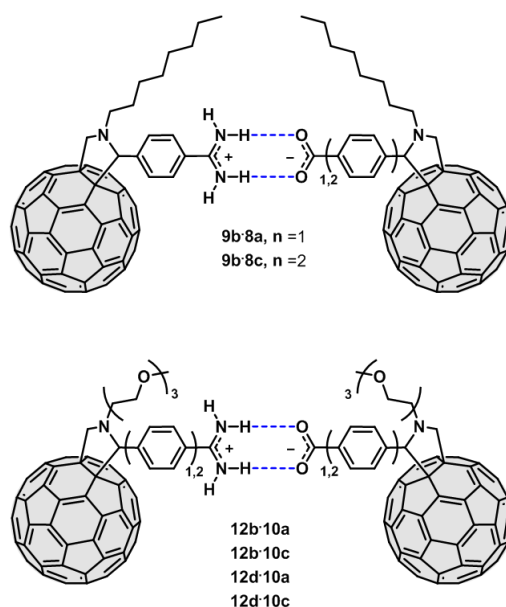
Figure S1: Supramolecular dumbbell-type fulleropyrrolidine complexes, **9b·8a,c** and **12b,d·10a,c**.

The clear signature of salt bridge formation is the concentration-dependent downfield shift of the amidinium protons involved in the hydrogen bonding to the carboxylate observed in ^{1}H NMR experiments.

It was carried out the morphological study of these supramolecular assemblies as a function of their increasing concentrations and it was demonstrated that initially occurs the formation of molecules islands. Subsequently, blend to led to the creation of one-molecule thickness

monolayers and finally, at the highest concentration degree, on the top of these monolayers, supramolecular aggregates tend to be formed.

Their electronic properties, as supramolecular hydrogen-bonded wires, were proved by STMBJ measurements, which evidenced that the corresponding conductance value was probably too low to be detected by the noise cut off of the set up, because only the peaks of the separated halves were visible.

b) Amidinium-Carboxylate Based Linear Supramolecular Wires

To go deeper about the two point amidinium-carboxylate interaction as supramolecular alternative connection to the covalent bonding in molecular wires, simple systems, based on a linear design, were synthesized to facilitate the investigation and understanding of conductance properties through their supramolecular structure.

Figure S2: Linear supramolecular wires series **15a,b·14a** and **16a,b·14b**.

The synthesis of a control compound (**17**) was also carried out to compare the conductance of the supramolecular ensemble **16a·14b** with the most similar covalent analogous.

Figure S3: Refence compound **17**.

The qualitative ^{1}H NMR titration experiments clearly demonstrated the formation of the supramolecular complexes, showing a broad band corresponding to the signal of the amidinium protons involved in the non-covalent interaction, modifying its width and position as a function

of the guest concentration. The quantitative experiments, on the other hand, allowed to determine K_a values superior to 10^4 M^{-1} for all the complexes.

The STM measurements revealed three main results: i) the pyridine derivatives have demonstrated inadequate to be investigated, resulting the conductance values of either, both halves and the complexes, impossible to be detected. ii) It was shown for the first time that the amidine group can be as efficient linker to gold as the carboxyl group, infact the conductance values obtained for both separated halves of the short thiomethyl ether complex derivative result very similar between them. iii) The mixed nature of the amidinium-carboxylate salt bridge connection, based on hydrogen bonding interaction and electrostatic forces, which are due to the charge separation, can be, in principle, considered the responsible for the interruption of the CT process along the wire. Interruption which result into a conductance value of the whole short thiomethyl ether complex derivative unexpectedly more than two orders of magnitude lower of the terphenyl used as reference compound (**17**).

Crown Ethers Switching Systems:

    a)   *4,5'-diaminodibenzo[18]crown-6*

The synthesis and the full characterization of the 4,5'-diaminodibenzo[18]crown-6 was successfully carried out.
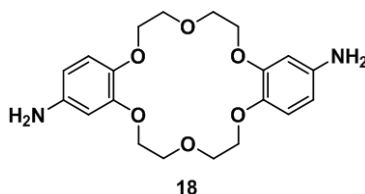
Figure S4: 4,5'-diaminodibenzo[18]crown-6.

However, it resulted impossible to detect the conductance signal corresponding to the empty molecule, probably due to the lack of direct conjugation between the crown ether structure and the aromatic rings. Therefore, the study of the complexed molecules was not attempted.

b) OPE and PPP crown ether molecular wires series

On the basis of the previous result, it was planned the synthesis of OPE and PPP derivatives, where the crown ether ring was located as pendant on the benzene's central unit, in order to avoid that its positioning could interrupt the π-conjugation along the wire structure. While the PPP derivatives were successfully synthesized and characterized, the OPE derivatives crown ether wires, unfortunately, were synthesized as irreversible complexes of TPPO.
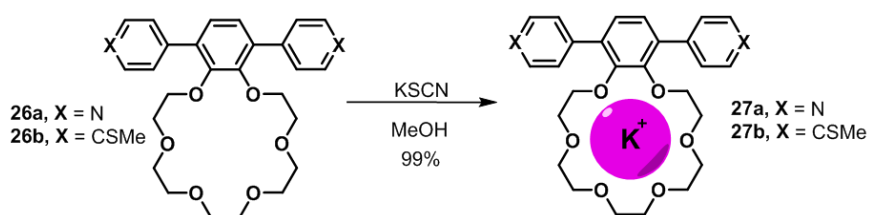
Figure S5: Synthesis of the K$^+$ complexed PPP crown ether molecular wires **27a,b.**

The CT study through the STMBJ technique of the free compounds **26a**,**b** showed, without any surprise, conductance values really similar to *p*-terphenylene based systems. On the other side, instead, the determination of the electronic properties of the complexed PPP crown ether wires is currently underway.

Conclusions

It was accomplished the synthesis of novel supramolecular wires, based, on one side, on the amidinium-carboxylate salt bridge while, on the other, on the ion-dipole interaction of a cation with the cavity of a crown ether. The non-covalent interaction between the two-point amidinium-carboxylate connection was further investigated, also from the point of view of its conductance properties. The low values of conductance observed in comparison to the covalent reference compound could be justified by a combination of supramolecular forces and strong charge separation. The electronic properties of the synthesized PPP crown ether derivatives are currently underway.

Chapter 2.

Objectives

Synthesis of Graphene On Surface (GOS)-Based Materials

Taking into account the well-known electronic properties of the [60]fullerene and the outstanding and interesting characteristics demonstrated by the graphene sheet, novel junctions based on the combination of those features into nanohybrid structures of covalently modified pristine graphene with fullerene derivatives were developed. Specifically, the design of the target nanocomposites was formulated with the aim of studying the thermoelectric properties of hybrid wire systems whit different connection between the spacer and the graphene layer.

Results and Discussion

The synthesis of the graphene composites **GOS1,2,3**, and the control hybrids **FLG1,2**, was achieved following few fundamental steps, and their chemical, physical and theoretical characterization was positively carried out.
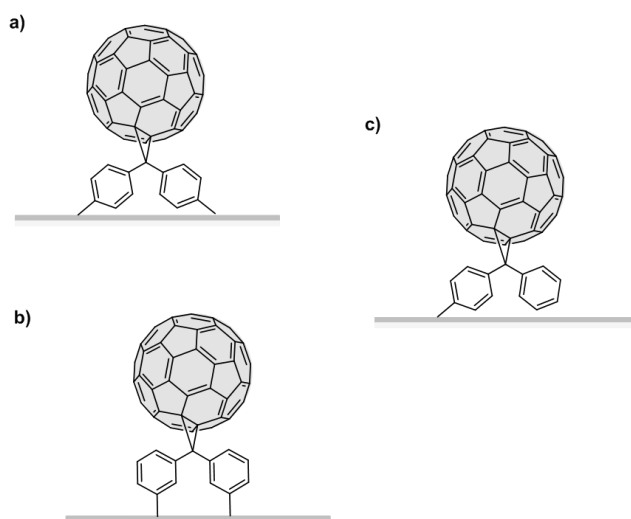
Figure S6: Graphene On Surface (GOS)-Based Materials: a) **GOS1**, b) **GOS2** and c) **GOS3.**

The successfulness of the functionalization process was confirmed by:

- Raman studies on either FLGs and GOS, before and after chemical treatment, which clearly have shown the increase of the D band associated with a higher defect degree on the nanomaterials.

- Thermogravimetric analysis (TGA), only carried out on the FLG derivatives, which has allowed to estimate the degree of surface functionalization as 1 organic molecule per 224 carbon atoms for **FLG1** and 1 organic molecule per 139 carbon atoms for **FLG2**.

- FTIR by which the characteristic vibrational peaks of pristine C_{60} around 1454 and 525 cm^{-1} could be observed in all the covalently functionalized FLGs derivatives.

- XPS analysis, which has evidenced a main C 1s component together with two more signals corresponding to O 1s and N 1s, which, respectively, were assigned to the atmospheric oxygen and the unreacted amine groups, still present in the organic molecule.

- TEM analysis has allowed to recognize, at their edges, some spherical species not observable in pristine FLG TEM micrographs. These spherical forms were attributed to the covalently attached organic molecules based on C_{60}, since their diameter (~1 nm) is compatible with the reported diameter for C_{60}.

- AFM analysis of the novel GOS-based materials also has revealed the presence of molecular islands, partially covering the graphene sheet, which have a height of ~1.2 nm (in good agreement with the size of a fullerene moiety).

- By c-AFM measurements, the thermoelectric properties of the nanohybrids materials synthesized were revealed as surprisingly high respect to other organic molecules. Moreover, it was possible to ascribe the positive S value, of the two which each GOS show (the positive around 74 µV/K and the other negative at -56±21 µV/K and -27±8 µV/K, for **GOS1** and **GOS2**, respectively), to the presence of fullerene derivatives which have reacted with just one of the two amine's legs. This because, it results in perfect agreement with the value of thermopower derived for the mono-linked G-based-C_{60} hybrid (**GOS3**).

Conclusions

Novel molecular/graphene composite materials, were synthesized. The high quantum thermopower values derived for **GOS1** and **GOS2** suggest great promise for these hybrid materials in thermoelectric applications, and, moreover, the change in the thermopower polarity with the number of anchoring groups makes them candidates to be potentially used in more complex device architectures.

Resumen

Resumen

Introducción

El campo de la electrónica molecular, basado en el uso de moléculas individuales o un conjunto de ellas como componentes de dispositivos electrónicos, ha representado, y todavía representa, un área de trabajo seductora para los científicos en la que todavía hay mucho por hacer. Durante la última década, el desarrollo de procedimientos experimentales junto con la parte teórica han permitido mejorar en gran medida la comprensión de los principios básicos de las uniones moleculares. Por lo tanto, el interés se ha dirigido hacia otros aspectos menos conocidos, investigados o entendidos, que implican desafíos estructurales o teóricos. Hasta ahora en este campo, la mayoría de los esfuerzos en investigatión se han dedicado al estudio de la conductancia eléctrica de cables moleculares conjugados covalentemente. Ahora, en cambio, estructuras más complejas (por ejemplo, basadas en sistemas supramoleculares), características menos conocidas (como las propiedades termoeléctricas de estos sistemas) y nuevos materiales híbridos comienzan a captar la atención científica del área.

<u>Chapter 1.</u>

Objectivos

Se diseñó, sintetizó y estudió una nueva generación de cables moleculares caracterizados por fuerzas intermoleculares no covalentes en su unidad central.

Por un lado, la conexión del puente salino entre los grupos amidinio y carboxilato se aprovechó para desarrollar un conjunto de sistemas supramoleculares con diferentes longitudes, estructura y grupos de anclaje de modo que se obtuviese un mejor conocimiento de las propiedades de transferencia de carga de los cables supramoleculares:

Cables Supramoleculares Basados en la Unión Amidinio-Carboxilato:

a) *Serie de derivados de fullereno tipo dumbbells*

b) *Serie de cables supramoleculares lineales*

Por otro lado, en cambio, se aprovechó la interacción ion-dipolo, que se origina entre un catión metálico y una cavidad de éter corona, para estudiar el efecto variable que la coordinación del metal tiene sobre la

conductancia de cables moleculares individuales, dependiendo de su grupo de anclaje:

Interruptores Moleculares Basados en Éteres Corona:

a) *4,5'-diaminodibenzo[18]corona-6*

b) *Serie de cables moleculares derivados de éter corona sobre esqueletos de OPE y PPP*

Resultados y discusión

Cables Supramoleculares Basados en la Unión Amidinio-Carboxilato:

a) *Serie de derivados de fullereno tipo dumbbell caracterizados por el enlace amidinio-carboxilato*

Se ha llevado a cabo la síntesis de una nueva familia de derivados de fullereno de tipo duumbbells caracterizados por la interacción supramolecular de dos puntos entre los grupos amidinio y carboxilato.
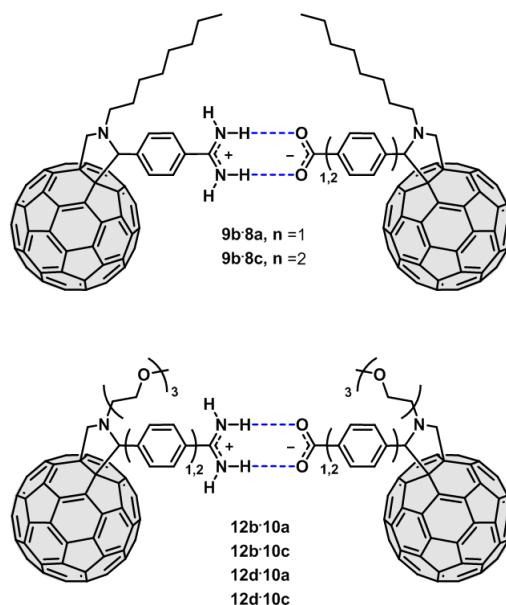
Figura S1: Complejos supramoleculares derivados de fulleropirrolidina de tipo dumbbells, **9b·8a,c** and **12b,d·10a,c**.

En los experimentos de ^{1}H NMR se encuentra la prueba efectiva de la formación de los complejos supramoleculares a través del apantallamiento, dependiente de la concentración, de los protones del

grupo amidinio implicados en el enlace de hidrógeno con el carboxilato.

El estudio morfológico con concentración creciente de estos agregados supramoleculares ha demostrado que, primero, se forman islas de moléculas, que posteriormente se fusionan llevando a la creación de monocapas con espesor de una molécula, cuya tendencia, a la más alta concentración, es la de formar agregados supramoleculares de mayor espesor.

Además, sus propiedades electrónicas como cables supramoleculares unidos por enlaces de hidrógeno se probaron mediante STMBJ, evidenciando que el valor de conductancia correspondiente era probablemente demasiado bajo respecto al límite de detección del aparato, observandose sólo los picos de las mitades aisladas y no el complejo supramolecular.

b) *Series de cables supramoleculares lineales caracterizados por el enlace amidinio-carboxilato*

Para obtener un conocimiento más profundo sobre la interacción amidinio-carboxilato como conexión supramolecular alternativa al enlace covalente en cables moleculares, se sintetizaron sistemas simples basados en un diseño lineal para facilitar la investigación y la comprensión de las propiedades de conductancia a través de su estructura supramolecular.
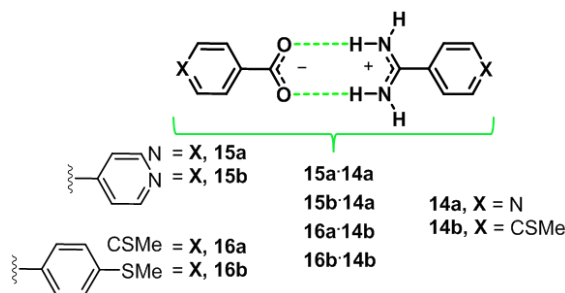
Figura S3: Series de cables supramoleculares lineales **15a,b·14a** and **16a,b·14b**.

También se llevó a cabo la síntesis de un compuesto de control (**17**) para comparar la conductancia del conjunto supramolecular **16a·14b** con el análogo covalente más similar.
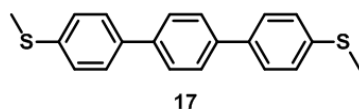
Figura S4: Compuesto de referencia **17**.

Los experimentos de valoración mediante ^{1}H NMR demostraron cualitativamente la formación de los complejos supramoleculares mostrando la aparición de una banda ancha, atribuible a la señal de los protones de amidinio implicados en la interacción no covalente, que modifica su anchura y posición en función de la concentración de los huéspedes. Los experimentos cuantitativos, por otro lado, permitieron determinar valores de K_a superiores a 10^4 M^{-1} para todos los complejos.

Los experimentos STM revelaron tres resultados principales. i) los derivados de piridina se han demostrado inadecuados para ser investigados, resultando imposible detectar los valores de conductancia de cualquiera de las dos mitades aisladas y de los complejos. ii) Por primera vez se ha demostrado que el grupo amidino puede ser tan eficaz como el carboxilo como grupo de anclaje, debido a que los valores de conductancia obtenidos para ambas mitades del complejo corto resultan muy similares entre ellos. iii) El valor de conductancia correspondiente al complejo anterior resulta inesperadamente bajo, más de dos órdenes de magnitud inferior al del terfenilo utilizado como compuesto de referencia (**17**). Por lo tanto, en principio, la naturaleza mixta de la interacción amidinio-carboxilato, basada en enlaces de hidrógeno y fuerzas electrostáticas (debido a su separación de carga) se puede considerar responsable de la interrupción del proceso de CT a lo largo del cable.

Interruptores Moleculares Basados en Éteres Corona:

a) *4,5'-diaminodibenzo[18]corona-6*

La síntesis y la caracterización completa del 4,5'-diaminodibenzo[18] corona-6 se llevó a cabo con éxito.
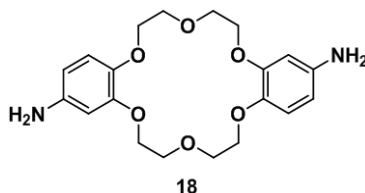
Figura S4: 4,5'-diaminodibenzo[18]corona-6.

Sin embargo, resultó imposible detectar la señal de conductancia correspondiente a la molécula vacía, probablemente debido a la falta de conjugación directa entre la estructura del éter corona y los anillos aromáticos. Por lo tanto, el estudio de las moléculas complejadas no pudo llevarse a cabo.

b) *Series de cables moleculares de éter corona sobre esqueletos de OPE y PPP*

Sobre la base del resultado anterior, se formuló la síntesis de los derivados de OPE y PPP, con la unidad de éter corona unida únicamente a la unidad central de benceno, para evitar que su posicionamiento interrumpa la conjugación π a lo largo de la estructura del cable. Mientras los derivados de PPP se sintetizaron y caracterizaron con éxito, los derivados de OPE, desafortunadamente, se obtuvieron como complejos irreversibles de TPPO.
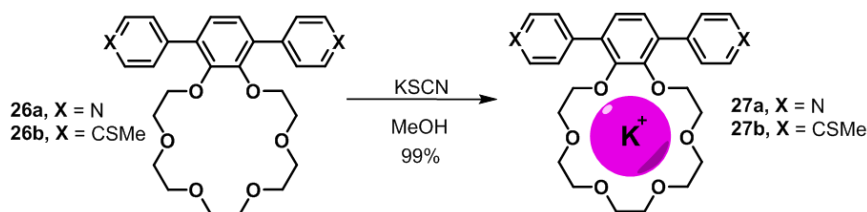
Figura S5: Síntesis de los cables moleculares **27a,b** derivados de PPP y caracterizados por éteres corona complejados con K$^+$.

El estudio STMBJ de transferencia de carga a través de los compuestos sin complejar **26a,b** mostró, sin sorpresa, valores de conductancia realmente similares a los sistemas basados en *p*-terfenilenos. Por otro lado, la determinación de las propiedades electrónicas de los cables complejados **27a**,**b** está actualmente en curso.

Conclusiones

Se llevó a cabo la síntesis de nuevos cables supramoleculares, basados, por un lado, en la interacción amidinio-carboxilato y, por otro, en la interacción ion-dipolo de un catión con la cavidad de un éter corona. La conexión no covalente entre los grupos amidinio-carboxilato se investigó más profundamente, también desde el punto de vista de sus propiedades de conductancia. Los bajos valores de conductancia

observados en comparación con el compuesto de referencia covalente podrían justificarse mediante una combinación de la unión a través de fuerzas supramoleculares con una fuerte separación de cargas. El estudio de las propiedades electrónicas de los derivados de éter de corona-PPP sintetizados está actualmente en curso.

Chapter 2.

Objetivos

Síntesis de Materiales Basados en Grafeno Sobre Superficie

Teniendo en cuenta las conocidas propiedades electrónicas del [60]fullereno y las características destacadas e interesantes demostradas por la lámina de grafeno, se desarrollaron nuevas uniones basadas en la combinación de esas características en estructuras nanohíbridas de láminas de grafeno modificado covalentemente con derivados de fullereno. Específicamente, el diseño de los nanomateriales objetivo se formuló con la finalidad de estudiar las propiedades termoeléctricas de sistemas de cables híbridos con diferentes conexiones entre el espaciador y la capa de grafeno.

Resultados y discusión

La síntesis de los compuestos de grafeno **GOS1,2,3**, y los híbridos de control **FLG1,2**, se logró después de algunos pasos fundamentales, y su caracterización química, física y teórica se llevó a cabo positivamente.
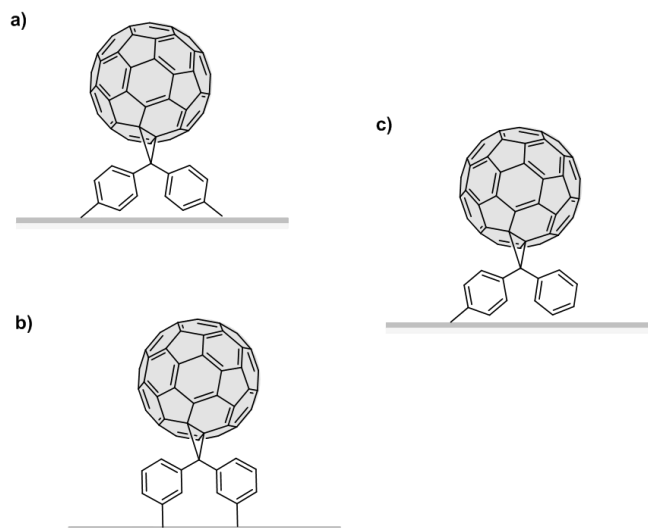
Figura S6: Materiales híbridos basados en grafeno sobre superficie: a) **GOS1**, b) **GOS2** y c) **GOS3.**

El éxito del proceso de funcionalización fue confirmado por:

- Estudios Raman en los FLGs y GOS, antes y después del tratamiento químico, mostrando el aumento en la banda D asociado con un mayor grado de defectos en los nanomateriales.

- Análisis termogravimétrico (TGA), llevado a cabo solo en los derivados de FLG, ha permitido estimar el grado de funcionalización de la superficie como 1 molécula orgánica por 224 átomos de carbono para **FLG1** y 1 molécula orgánica por 139 átomos de carbono para **FLG2**.

- FTIR, mediante el cual se pudieron observar los picos vibracionales característicos del C_{60} (alrededor de 1454 y 525 cm^{-1}) en todos los derivados de FLG funcionalizados covalentemente.

- Análisis XPS, que han evidenciado un componente C 1s principal junto con dos señales más, asignadas a O 1s y N 1s. Estas dos señales, respectivamente, se consideran debidas al oxígeno atmosférico y a los grupos amino sin reaccionar, todavía presentes en la molécula orgánica.

- El análisis TEM ha permitido reconocer algunas formas esféricas en los bordes de los derivados de grafeno, no observables en micrografías TEM de FLG prístinos, que se atribuyeron a las compuestos de C_{60} covalentemente unidos al grafeno, ya que su diámetro (~1 nm) resulta compatible con el diámetro descrito en la bibliografía para moléculas de C_{60}.

- El análisis AFM de los nuevos materiales basados en GOS también ha revelado la presencia de islas moleculares, cubriendo parcialmente la lámina de grafeno, con una altura de ~1,2 nm (de acuerdo con el tamaño de una unidad de fullereno).

- Mediante medidas de conductancia a través de c-AFM, las propiedades termoeléctricas de los materiales nanohíbridos sintetizados se revelaron como sorprendentemente altas respecto a las de otras moléculas orgánicas. Además, los derivados de [60]fullereno doblemente anclados a la monocapa de grafeno muestran dos valores principales de termopower (*S*), uno positivo alrededor de 74 µV/K y el otro negativo a -56 ± 21 µV/K y -27 ± 8 µV/K, respectivamente para **GOS1** y **GOS2**. Por lo tanto, el valor positivo, en perfecto acuerdo con el valor de termopower derivado para el híbrido **GOS3**, se consideró

atribuible a la presencia de derivados de fullereno que reaccionaron con sólo uno de los dos grupos amino.

Conclusiones

Se han preparado novedosos materiales moleculares hibridos de grafeno y [60]fullereno. Los altos valores de termopower obtenidos para **GOS1** y **GOS2** sugieren un gran potencial para estos materiales moleculares híbridos de grafeno en aplicaciones termoeléctricas. Además, el cambio de signo de los valores de termopower, en función del número de grupos de anclaje de la molécula orgánica a la lámina de grafeno, hace que sean candidatos valiosos para ser utilizados en el diseño de dispositivos más complejos.

Bibliography

Bibliography

1. a) M. Faraday, *Experimental relations of gold (and other metals) to light, Philos. Trans. R. Soc. London* **1857**, *147*, 145; b) G. Mie, *Beiträge zur Optik trüber Medien, speziell kolloidaler Metallösungen, Ann. Phys.* **1908**, *25*, 377.

2. R. Feynmann, *Plenty of Room at the Bottom*, American Physical Society annual meeting, CalTech, **1959**.

3. N. Taniguchi, *On the Basic Concept of Nano-Technology*, Proc. ICPE, Tokyo, Part II, Japan Society of Precision Engineering, **1974**; "nano-technology mainly consists of the processing of separation, consolidation, and deformation of materials by one atom or one molecule".

4. G. Binnig, H. Rohrer, C. Gerber, E. Weibel, *Tunneling through a controllable vacuum gap, Appl. Phys. Lett.* **1982**, *40*, 178.

5. G. Binnig, C. F. Quate, C. Gerber, *Atomic Force Microscope, Phys. Rev. Lett.* **1986**, *56*, 930.

6. Meridien Institute, Nanotechnology and the Poor, Opportunities and Risks, **2005**, http://www.merid.org.

7. In 2011, for example, a group calling itself the "ELF Switzerland Earth Liberation Front" was caught in Switzerland trying to bomb an IBM nanotechnology facility while it was under construction. The same year, a group in Mexico, known as "Individualidades Tendiendo a lo Salvaje" sent letter bombs to nanotechnology researchers injuring several people.

8. D. Xiang, X. Wang, C. Jia, T. Lee, X. Guo, *Molecular-Scale Electronics: From Concept to Function, Chem. Rev.* **2016**, *116*, 4318.

9. a) E. Lortscher, *Wiring molecules into circuits, Nat. Nanotechnol.* **2013**, *8*, 381; b) L. Wilson, *International Technology Roadmap for Semiconductors (ITRS)*; Semiconductor Industry Association, **2013**.

10. A. T. Haedler, K. Kreger, A. Issac, B. Wittmann, M. Kivala, N. Hammer, J. Kohler, H. W. Schmidt, R. Hildner, *Long-range energy transport in single supramolecular nanofibres at room temperature, Nature* **2015**, *523*, 196.

11. a) J. M. Tour, W. A. Reinerth, L. Jones, T. P. Burgin, C. W. Zhou, C. J. Muller, M. R.; Deshpande, M. A. Reed, *Recent Advances in. Molecular Scale Electronics, Ann. N. Y. Acad. Sci.* **1998**, *852*, 197; b) A. H. Flood, J. F. Stoddart, D. W. Steuerman, J. R. Heath, *Chemistry. Whence molecular electronics?, Science* **2004**, *306*, 2055; c) R. L. McCreery,

A. J. Bergren, *Progress with molecular electronic junctions: meeting experimental challenges in design and fabrication, Adv. Mater*. **2009**, *21*, 4303; d) K. Moth-Poulsen, T. Bjornholm, *Molecular electronics with single molecules in solid-state devices, Nat. Nanotechnol*. **2009**, *4*, 551; e) Q. Shen, X. F. Guo, M. L. Steigerwald, C. Nuckolls, *Integrating Reaction Chemistry into Molecular Electronic Devices, Chem. Asian J*. **2010**, *5*, 1040; f) M. G. Schultz, *Quantum transport through single-molecule junctions with orbital degeneracies, Phys. Rev. B* **2010**, *82*, 155408; g) J. C. Cuevas, E. Scheer, *Molecular Electronics: An Introduction to Theory and Experiment*; World Scientific: River Edge, NJ, **2010**; h) D. Natelson, Y. J. Li, J. B. Herzog, *Nanogap structures: combining enhanced Raman spectroscopy and electronic transport, Phys. Chem. Chem. Phys*. **2013**, *15*, 5262; i) L. Sun, Y. A. Diaz-Fernandez, T. A. Gschneidtner, F. Westerlund, S. Lara-Avila, K. Moth-Poulsen, *Single-molecule electronics: from chemical design to functional devices, Chem. Soc. Rev*. **2014**, *43*, 7378; l) L. Sánchez, R. Otero, J. M. Gallego, R. Miranda, N. Martín, *Ordering Fullerenes at the Nanometer Scale on Solid Surfaces, Chem. Rev.*, **2009**, *109*, 2081; m) D. M. Guldi, B. M. Illescas, C. M. Atienza, M. Wielopolski, N. Martín, *Fullerene for organic electronics, Chem. Soc. Rev*., **2009**, *38*, 1587.

12. E. G. Emberly, G. Kirczenow, *Theoretical study of electrical conduction through a molecule connected to metallic nanocontacts, Phys. Rev. B* **1998**, *58*, 10911.

13. A. Nitzan, M. A. Ratner, *Electron transport in molecular wire junctions, Science* **2003**, *300*, 1384.

14. W. B. Davis, W. A. Svec, M. A. Ratner, M. R. Wasielewski, *Molecular-wire behaviour in p-phenylenevinylene oligomers , Nature* **1998**, *396*, 60.

15. J. Jortner, *Temperature dependent activation energy for electron transfer between biological molecules, J. Chem. Phys.* **1976**, *64*, 4860.

16. M. P. Eng, B. Albinsson, *Non-Exponential Distance Dependence of Bridge-Mediated Electronic Coupling, Angew. Chem. Int. Ed.* **2006**, *45*, 5626.

17. H. A. Kramers, *L'interaction Entre les Atomes Magnétogènes dans un Cristal Paramagnétique, Physica* **1934**, *1*, 182.

18. a) P. W. Anderson, *Antiferromagnetism. Theory of Superexchange Interaction, Phys. Rev*. **1950**, *79*, 350; b) P. W. Anderson, *New Approach to the Theory of Superexchange Interactions, Phys. Rev*. **1959**, *115*, 2.

19. J. M. Tour, M. Kozaki, J. M. Seminario, *Molecular Scale Electronics: A Synthetic/Computational Approach to Digital Computing, J. Am. Chem. Soc.* **1998**, *120*, 8486.

20. R. M. Metzger, NATO ASI Ser. **1991**, B248, 659.

21. L. Sun, Y. A. Diaz-Fernandez, T. A. Gschneidtner, F. Westerlund, S. Lara-Avilab, K. Moth-Poulsen, *Single-molecule electronics: from chemical design to functional devices, Chem. Soc. Rev.* **2014**, *43*, 7378.

22. a) B. Xu and N. J. Tao, *Measurement of single-molecule resistance by repeated formation of molecular junctions, Science* **2003**, *301*, 1221; b) L. A. Zotti, T. Kirchner, J. C. Cuevas, F. Pauly, T. Huhn, E. Scheer, A. Erbe, *Revealing the role of anchoring groups in the electrical conduction through single-molecule junctions, Small* **2010**, *6*, 1529; c) C. Jia, X. Guo, *Molecule-electrode interfaces in molecular electronic devices, Chem. Soc. Rev.* **2013**, *42*, 5642; d) E. Leary, A. La Rosa, M. T. González, G. Rubio-Bollinger, N. Agraït, N. Martín, *Incorporating single molecules into electrical circuits. The role of the chemical anchoring group, Chem. Soc. Rev*. **2015**, *44*, 920.

23. a) A. Danilov, S. Kubatkin, S. Kafanov, P. Hedegard, N. Stuhr-Hansen, K. Moth-Poulsen, T. Bjornholm, *Electronic Transport in Single Molecule Junctions: Control of the Molecule-Electrode Coupling through Intramolecular Tunneling Barriers, Nano Lett.* **2008**, *8*, 1; b) Y. Cao, S. Dong, S. Liu, Z. Liu, X. Guo, *Toward Functional Molecular Devices Based on Graphene–Molecule Junctions , Angew. Chem. Int. Ed*. **2013**, *52*, 3906; c) X. Y. Zhou, Z. L. Peng, Y. Y. Sun, L. N. Wang, Z. J. Niu, X. S. Zhou, *Conductance measurement of pyridyl-based single molecule junctions with Cu and Au contacts, Nanotechnology* **2013**, *24*, 465204.

24. a) M. Kamenetska, S. Y. Quek, A. C. Whalley, M. L. Steigerwald, H. J. Choi, S. G. Louie, C. Nuckolls, M. S. Hybertsen, J. B. Neaton, L. Venkataraman, *Conductance and Geometry of Pyridine-Linked Single-Molecule Junctions, J. Am. Chem. Soc*. **2010**, *132*, 6817; b) S. V. Aradhya, L. Venkataraman, *Single-molecule junctions beyond electronic transport, Nat. Nanotechnol*. **2013**, *8*, 399.

25. L. Venkataraman, J. E. Klare, C. Nuckolls, M. S. Hybertsen, M. L. Steigerwald, *Dependence of single-molecule junction conductance on molecular conformation, Nature*, **2006**, *442*, 904.

26. M. A. Reed, C. Zhou, C. J. Muller, T. P. Burgin, J. M. Tour, *Conductance of a Molecular Junction, Science* **1997**, *278*, 252.

27. A. F. Morpurgo, C. M. Marcus and D. B. Robinson, *Controlled fabrication of metallic electrodes with atomic separation, Appl. Phys. Lett.* **1999**, *74*, 2084.

28. H. Park, A. K. L. Lim, A. P. Alivisatos, J. Park and P. L. McEuen, *Fabrication of metallic electrodes with nanometer separation by electromigration, Appl. Phys. Lett*. **1999**, *75*, 301.

29.   A. Bezryadin, C. Dekker and G. Schmid, *Electrostatic trapping of single conducting nanoparticles between nanoelectrodes, Appl. Phys. Lett.* **1997**, *71*, 1273.

30.   S. Kubatkin, A. Danilov, M. Hjort, J. Cornil, J. L. Bredas, N. Stuhr-Hansen, P. Hedegard, T. Bjornholm, *Single-electron transistor of a single organic molecule with access to several redox states, Nature* **2003**, *425*, 698.

31.   X. D. Cui, A. Primak, X. Zarate, J. Tomfohr, O. F. Sankey, A. L. Moore, T. A. Moore, D. Gust, G. Harris, S. M. Lindsay, *Reproducible measurement of single-molecule conductivity, Science* **2001**, *294*, 571.

32.   L. Qin, S. Park, L. Huang, C. A. Mirkin, *On-wire lithography, Science* **2005**, *309*, 113.

33.   T. Dadosh, Y. Gordin, R. Krahne, I. Khivrich, D. Mahalu, V. Frydman, J. Sperling, A. Yacoby, I. Bar-Joseph, *Measurement of the conductance of single conjugated molecules, Nature* **2005**, *436*, 677.

34.   National Science and Technology Council, Committee on Technology, Subcommittee on Nanoscale Science, Engineering and Technology, "National nanotechnology initiative: The initiative and its implementation plan", July **2000**. [Online]. Available: http://www.nano.gov/nni2.pdf

35.   L. Gross, *Recent advances in submolecular resolution with scanning probe microscopy, Nature Chem.* **2011**, *3*, 273.

36.   L. Gross, F. Mohn, N. Moll, G. Meyer, R. Ebel, W. M. Abdel-Mageed, M. Jaspars, *Organic structure determination using atomic-resolution scanning probe microscopy, Nature Chem.* **2010**, *2*, 821.

37.   J. I. Martínez, E. Abad, C. González, F. Flores, J. Ortega, *Improvement of Scanning Tunneling Microscopy Resolution with H-Sensitized Tips*, *Phys. Rev. Lett.* **2012**, *108*, 246102.

38.   a) F. Giacalone, J. L. Segura, N. Martín, D. M. Guldi, *Exceptionally Small Attenuation Factors in Molecular Wires, J. Am. Chem. Soc*. **2004**, *126*, 5340; b) G. de la Torre, F. Giacalone, J. L. Segura, N. Martín, D. M. Guldi, *Electronic Communication through π-Conjugated Wires in Covalently Linked Porphyrin/C60 Ensembles, Chem. Eur. J.* **2005**, *11*, 1267; c) K. Pettersson, J. Wiberg, T.Ljungdahl, J. Mårtensson, B. Albinsson, *Interplay between Barrier Width and Height in Electron Tunneling: Photoinduced Electron Transfer in Porphyrin-Based Donor−Bridge−Acceptor Systems, J. Phys. Chem. A* **2005**, *110*, 319; d) C. Atienza, N. Martín, M. Wielopolski, N. Haworth, T. Clark, D. M. Guldi, *Tuning electron transfer through p-phenyleneethynylene molecular wires, Chem. Commun.* **2006**, *0*, 3202; e) E. A. Weiss, M. J. Ahrens, L. E. Sinks, A. V. Gusev, M. A.

Ratner, M. R. Wasielewski, *Making a Molecular Wire: Charge and Spin Transport through para-Phenylene Oligomers, J. Am. Chem. Soc*. **2004**, *126*, 5577; f) C. Schubert, M. Wielopolski, L. H. Mewes, G. de Miguel Rojas, C. van der Pol, K. C. Moss, M. R. Bryce, J. E. Moser, T. Clark, D. M. Guldi, *Precise Control of Intramolecular Charge-Transport: The Interplay of Distance and Conformational Effects, Chem. Eur. J.* **2013**, *19*, 7575; g) C. Atienza, M. Wielopolski, D. M. Guldi, C. van der Pol, M. R. Bryce, S. Filippone, N. Martín, *Determination of the attenuation factor in fluorene-based molecular wires, Chem. Commun.* **2007**, *0*, 5164; h) A. B. Ricks, K. E. Brown, M. Wenninger, S. D. Karlen, Y. A. Berlin, D. T. Co, M. R. Wasielewski, *Exponential Distance Dependence of Photoinitiated Stepwise Electron Transfer in Donor–Bridge–Acceptor Molecules: Implications for Wirelike Behavior, J. Am. Chem. Soc.* **2012**, *134*, 4581.

39. G. J. Ashwell, P. Wierzchowiec, L. J. Phillips, C. J. Collins, J. Gigon, B. J. Robinson, C. M. Finch, I. R. Grace, C. Lambert, P. D. Buckle, K. Ford, B. J. Wood, I. R. Gentle, *Functional molecular wires, Phys. Chem. Chem. Phys*. **2008**, *10*, 1859.

40. S. H. Choi, C. Risko, M. C. R. Delgado, B. S. Kim, J. L. Brédas, C. D. Frisbie, *Transition from Tunneling to Hopping Transport in Long, Conjugated Oligo-imine Wires Connected to Metals, J. Am. Chem. Soc.* **2010**, *132*, 4358.

41. P. J. F. de Rege, S. A. Williams, M. J. Therien, *Direct evaluation of electronic coupling mediated by hydrogen bonds: implications for biological electron transfer, Science* **1995**, *269*, 1409.

42. F. Wessendorf, B. Grimm, D. M. Guldi, A. Hirsch, *Pairing Fullerenes and Porphyrins: Supramolecular Wires That Exhibit Charge Transfer Activity, J. Am. Chem. Soc*. **2010**, *132*, 10786.

43. S. Vela, S. Bauroth, C. Atienza, A. Molina-Ontoria, D. M. Guldi, N. Martín, *Determining the Attenuation Factor in Molecular Wires Featuring Covalent and Noncovalent Tectons, Angew. Chem. Int. Ed*. **2016**, *55*, 15076.

44. B. Capozzi, E. J. Dell, T. C. Berkelbach, D. R. Reichman, L. Venkataraman, L. M. Campos, *Length-Dependent Conductance of Oligothiophenes, J. Am. Chem. Soc*. **2014**, *136*, 10486.

45. a) Y. Li, M. Baghernejad, A. G. Qusiy, D.Z. Manrique, G. Zhang, J. Hamill, Y. Fu, P. Broekmann, W. J. Hong, T. Wandlowski, D. Zhang, C. Lambert, *Three-State Single-Molecule Naphthalenediimide Switch: Integration of a Pendant Redox Unit for Conductance Tuning, Angew. Chem. Int. Ed*. **2015**, *54*, 13586; b) H. M. Osorio, S. Catarelli, P. Cea, J. B. Gluyas, F. Hartl, S. J. Higgins, E. Leary, P. J. Low, S. Martin, R. J.

Nichols, J. Tory, J. Ulstrup, A. Vezzoli, D. C. Milan, Q. Zeng, *Electrochemical Single-Molecule Transistors with Optimized Gate Coupling, J. Am. Chem. Soc*. **2015**, *137*, 14319.

46.   a) C. R. Arroyo, S. Tarkuc, R. Frisenda, J. S. Seldenthuis, C. H. Woerde, R. Eelkema, F. C. Grozema, H. S. J. van der Zant, *Signatures of quantum interference effects on charge transport through a single benzene ring, Angew. Chem. Int. Ed*. **2013**, *52*, 3152; b) R. Frisenda, V. A. E. C. Janssen, F. C. Grozema, H. S. J. van der Zant, N. Renaud, *Mechanically controlled quantum interference in individual π-stacked dimmers, Nature Chemistry* **2016**, *8*, 1099.

47.   X. L. Li, J. He, J. Hihath, B. Q. Xu, S. M. Lindsay, N. J. Tao, *Conductance of Single Alkanedithiols: Conduction Mechanism and Effect of Molecule−Electrode Contacts, J. Am. Chem. Soc.* **2006**, *128*, 2135.

48.   H. Li, M. H. Garner, Z. Shangguan, Q. Zheng, T. A. Su, M. Neupane, P. Li, A. Velian, M. L. Steigerwald, S. Xiao, C. Nuckolls, G. C. Solomon, L. Venkataraman, *Conformations of cyclopentasilane stereoisomers control molecular junction conductance, Chem. Sci.* **2016**, *7*, 5657.

49.   a) P. T. Bui, T. Nishino, Y. Yamamoto, H. Shiigi, *Quantitative Exploration of Electron Transfer in a Single Noncovalent Supramolecular Assembly, J. Am. Chem. Soc.* **2013**, *135*, 14, 5238; b) L. Wang, Z. L. Gong , S. Y. Li, W. Hong, Y. W. Zhong, D. Wang, L. J. Wan, *Molecular Conductance through a Quadruple-Hydrogen-Bond-Bridged Supramolecular Junction, Angew. Chem. Int. Ed*. **2016**, *55*, 1; c) W. Zhang, S. Gan, A. Vezzoli, R. J. Davidson, D. C. Milan, K. V. Luzyanin, S. J. Higgins, R. J. Nichols, A. Beeby, P. J. Low, L. Buyi, L. Niu, *Single-Molecule Conductance of Viologen–Cucurbit[8]uril Host–Guest Complexes, ACS Nano* **2016**, *10*, 5, 5212.

50.   X. Li, D. Hu, Z. Tan, J. B. Zongyuan, X. Y. Yang, J. Shi, W. Hong, *Supramolecular Systems and Chemical Reactions in Single-Molecule Break Junctions, Top Curr. Chem. (Z)* **2017**, *375*, 42.

51.   S. Wu, M. T. González, R. Huber, S. Grunder, M. Mayor, C. Schoenenberger, M. Calame, *Molecular junctions based on aromatic coupling, Nat. Nanotechnol*. **2008**, *3*, 569.

52.   S. Martin, I. Grace, M. R. Bryce, C. Wang, R. Jitchati, A. S. Batsanov, S. J. Higgins, C. Lambert, R. J. Nichols, *Identifying Diversity in Nanoscale Electrical Break Junctions, J. Am. Chem. Soc.* **2010**, *132*, 9157.

53. M. T. González, E. Leary, R. l. García, P. Verma, M. A. N. Herranz, G. Rubio-Bollinger, N. Martín, N. S. Agraït, *Break-Junction Experiments on Acetyl-Protected Conjugated Dithiols under Different Environmental Conditions, J. Phys. Chem. C* **2011**, *115*, 17973.

54. S. Fujii, T. Tada, Y. Komoto, T. Osuga, T. Murase, M. Fujita, M. Kiguchi, *Rectifying Electron-Transport Properties through Stacks of Aromatic Molecules Inserted into a Self-Assembled Cage, J. Am. Chem. Soc.* **2015**, *137*, 5939.

55. L. Sánchez, M. Sierra, N. Martín, A. J. Myles, T. J. Dale, J. Rebek, Jr., W. Seitz, D. Guldi, *Exceptionally Strong Electronic Communication through Hydrogen Bonds in Porphyrin–C_{60} Pairs*, Angew. Chem. Int. Ed.* **2006**, *45*, 4637.

56. M. Kotiuga, P. Darancet, C. R. Arroyo, L. Venkataraman, J. B. Neaton, *Adsorption-Induced Solvent-Based Electrostatic Gating of Charge Transport through Molecular Junctions, Nano Lett.* **2015**, *15,* 4498.

57. T. Nishino, N. Hayashi, P. T. Bui, *Direct Measurement of Electron Transfer through a Hydrogen Bond between Single Molecules, J. Am. Chem. Soc.* **2013**, *135*, 4592.

58. L. Wang, Z. L. Gong, S. Y. Li, W. J. Hong, Y. W. Zhong, D. Wang, L. J. Wan, *Molecular Conductance through a Quadruple-Hydrogen-Bond-Bridged Supramolecular Junction, Angew. Chem. Int. Ed.* **2016**, *55*, 12393.

59. G. I. Livshits, A. Stern, D. Rotem, N. Borovok, G. Eidelshtein, A. Migliore, E. Penzo, S. J. Wind, R. Di Felice, S. S. Skourtis, J. C. Cuevas, L. Gurevich, A. B. Kotlyar, D. Porath, *Long-range charge transport in single G-quadruplex DNA molecules, Nat. Nanotech.* **2014**, *9*, 1040.

60. J. Hihath, B. Xu, P. Zhang, N. Tao, *Study of single-nucleotide polymorphisms by means of electrical conductance measurements, PNAS* **2005**, *102*, 47, 16979.

61. M. Kiguchi, S. Nakashima, T. Tada, S. Watanabe, S. Tsuda, Y. Tsuji, J. Terao, *Single-molecule conductance of π-conjugated rotaxane: new method for measuring stipulated electric conductance of π-conjugated molecular wire using STM break junction, Small* **2012**, *8*, 5, 726.

62. P. W. Anderson, P. A. Lee, M. Saitoh, *Remarks on giant conductivity in TTF-TCNQ, Solid State Commun.* **1973**, *13*, 595.

63. R. García, M. A. Herranz, E. Leary, M. T. González, G. Rubio Bollinger, M. Buerkle, L. A. Zotti, Y. Asai, F. Pauly, J. C. Cuevas, N. Agraït, N. Martín, *Single-molecule conductance of a chemically modified, π-extended tetrathiafulvalene and its charge-transfer complex with F4TCNQ, Beilstein J. Org. Chem.* **2015**, *11*, 1068.

64.   T. Nishino, T. Ito, Y. Umezawa, *A fullerene molecular tip can detect localized and rectified electron tunneling within a single fullerene–porphyrin pair, PNAS* **2005**, *102* ,5659.

65.   J. F. Stoddart, H. M. Colquhoun, *Big and little Meccano, Tetrahedron* **2008**, *64*, 8231.

66.   a) B. de Boer, M. M. Frank, Y. J. Chabal, W. Jiang, E. Garfunkel, Z. Bao, *Metallic Contact Formation for Molecular Electronics: Interactions between Vapor-Deposited Metals and Self-Assembled Monolayers of Conjugated Mono- and Dithiols, Langmuir* **2004**, *20*, 1539; b) J. M. Beebe, J. G. Kushmerick, *Nanoscale switch elements from self-assembled monolayers on silver,* Appl. Phys. Lett. **2007**, *90*, 083117.

67.   P. Liljeroth, J. Repp, G. Meyer, *Current-induced hydrogen tautomerization and conductance switching of naphthalocyanine molecules., Science* **2007**, *317*, 1203.

68.   Y. Wang, J. Kroger, R. Berndt, W. A. Hofer, *Pushing and Pulling a Sn Ion through an Adsorbed Phthalocyanine Molecule, J. Am. Chem. Soc*. **2009**, *131*, 3639.

69.   E. Lörtscher, J. W. Ciszek, J. Tour, H. Riel, *Reversible and Controllable Switching of a Single-Molecule Junction, Small* **2006**, *2*, 973.

70.   S. Castellanos, A. A. Vieira, B.M. Illescas, V. Sacchetti, C. Schubert, J. Moreno, D. M. Guldi, S. Hecht, N. Martín, *Gating Charge Recombination Rates through Dynamic Bridges in Tetrathiafulvalene–Fullerene Architectures, Angew. Chem. Int. Ed.* **2013**, *52*, 13985.

71.   T. Sendler, K. Luka-Guth, M. Wieser, W. J. Lokamani, M. Helm, S. Gemming, J. Kerbusch, E. Scheer, T. Huhn, A. Erbe, *Light-Induced Switching of Tunable Single-Molecule Junctions, Adv. Sci.* **2015**, *2*, 1500017.

72.   a) M. J. Marsella, T. M. Swager, *Designing conducting polymer-based sensors: selective ionochromic response in crown ether-containing polythiophenes, J. Am. Chem. Soc.* **1993**, *115*, 25, 12214; b) P. V. Bernhardt, E. J. Hayes, *Crown Ether Appended Cyclam Receptors for Cationic Guests, Inorg. Chem.* **2002**, *41*, 2892; c) J. Guo, J. Lee, C. I. Cu, N. C. Gallego, S. T. Pantelides, S. J. Pennycook, B. A. Moyer, M. F. Chisholm, *Crown ethers in graphene, Nat. Commun.* **2014**, *5*, 5389; d) J. Li, D. Yim, W.D. Jang, J. Yoon, *Recent progress in the design and applications of fluorescence probes containing crown ethers., Chem. Soc. Rev.* **2017**, *46*, 2437.

73.   C. Liu, D. Walter, D. Neuhauser, R. Baer, *Molecular Recognition and Conductance in Crown Ethers, J. Am. Chem. Soc.* **2003**, *125*, 13936.

74.   A. K. Ismael, A. A. Jobory, I. Grace, C. Lambert, *Discriminating single-molecule sensing by crown-ether-based molecular junctions, J. Chem. Phys.* **2017**, *146*, 064704.

75. J. Ponce, C. R. Arroyo, S. Tatay, R. Frisenda, P. Gaviña, D. Aravena, E.Ruiz, H. S. J. van der Zant, E. Coronado, *Effect of Metal Complexation on the Conductance of Single-Molecular Wires Measured at Room Temperature, J. Am. Chem. Soc*. **2014**, *136*, 8314.

76. J. L. Segura, N. Martín, *[60]Fullerene dimers, Chem. Soc. Rev.* **2000**, *29*, 13.

77. M. T. Rispens, L. Sánchez, J. Knol, J. C. Hummelen, *Supramolecular organization of fullerenes by quadruple hydrogen bonding, Chem. Commun*. **2001**, *0*, 161.

78. J. J. González, S. González, E. Priego, Ch. Luo, D. M. Guldi, J. de Mendoza, N. Martín, *A new approach to supramolecular C60-dimers based in quadruple hydrogen bonding, Chem. Commun.* **2001**, *0*, 163.

79. a) C. A. Martin, D. Ding, J. K. Sørensen, T. Bjørnholm, J. M. van Ruitenbeek, H.S. J. van der Zant, *Fullerene-Based Anchoring Groups for Molecular Electronics, J. Am. Chem. Soc.* **2008**, *130*, 13198; b) K. Gillemot, C. Evangeli, E. Leary, A. La Rosa, M. T. González, S. Filippone, I. Grace, G. Rubio-Bollinger, J. Ferrer, N. Martín, C. J. Lambert, N. Agraït, *A detailed experimental and theoretical study into the properties of C_{60} dumbbell junctions, Small* **2013**, *9*, 3812.

80. M. Maggini, G. Scorrano, M. Prato, *Addition of azomethine ylides to C_{60}: synthesis, characterization, and functionalization of fullerene pyrrolidines, J. Am. Chem. Soc.* **1993**, *115*, 9798.

81. T. Da Ros, M. Prato, F. Novello, M. Maggini, E. Banfi, Easy Access to Water-Soluble Fullerene Derivatives via 1,3-Dipolar Cycloadditions of Azomethine Ylides to C_{60}, J. Org. Chem. **1996**, *61*, 9070.

82. D. G. Hall, *Boronic Acids: Preparation and Applications in Organic Synthesis and Medicine*, Wiley-VCH Verlag GmbH & Co. KGaA., **2006**.

83. R. A. Garigipati, *An Efficient Conversion Of Nuriles To Amidinrs, Tetrahedron Lett.* **1990**, *31*, 1969.

84. J. I. Levin, E. Turos, S. M. Weinreb, *An Alternative Procedure for the Aluminum-Mediated Conversion of Esters to Amides, Synthetic Communications* **1982**, *12*, 989.

85. It was firstly recorded the 1H NMR spectra of amidinium half 10a by preparing a solution of the compound at 10-3M in CHCl3. Following, an equivalent quantity of the carboxylic unit 12d, corresponding to a 1:1 ratio, was added. The resulting solution of the complex 12d•10a, at the final concentration of 10-3M in CHCl3, was formed by light sonication of the mixture to favour the solubilisation of the proton acceptor moiety into the proton donor solution and finally analyzed.

86. The 1:1 solutions of 9b•8a and 9b•8c were prepared by mixing the volumes' solutions of the corresponding proton donor and proton acceptor compounds at the final concentration of 10-6M and 10-5M in CHCl3. Each solution of the preformed complexes was deposited by drop casting method on the surface of the HOPG sample. The solvent on the samples is dried by evaporation in a preheated oven at 60°C overnight and then analyzed at AFM.

87. The 1:1 solutions of **9b•8a** and **9b•8c** were prepared by mixing the volumes' solutions of the corresponding proton donor and proton acceptor compounds at the final concentration of 10-6M in CHCl3. The solution of the preformed complex was deposited by drop casting method on the surface of a gold sample. The sample is dried by evaporating the solvent in air and then analyzed at STM-BJ.

88. Y. Joseph, A. Peic, X. Chen, J. Michl, T. Vossmeyer, A. Yasuda, *Self-Assembled Gold Nanoparticle/Alkanedithiol Films: Preparation, Electron Microscopy, XPS-Analysis, Charge Transport, and Vapor-Sensing Properties, J. Phys. Chem. C* **2007**, *111*, 12855.

89. C. S. Wilcox, *Frontiers in Supramolecular Organic Chemistry and Photochemistry*, H. J. Schneider and H. Dürr, VCH, Weinheim, **1991**, pp. 123–144; b) P. Thordarson, *Determining association constants from titration experiments in supramolecular chemistry, Chem. Soc. Rev*. **2011**, *40*, 1305.

90. See in Annex Titration Section for more details.

91. S. Ahn, S. V. Aradhya, R. S. Klausen, B. Capozzi, X. Roy, M. L. Steigerwald, C. Nuckolls, L. Venkataraman, *Electronic transport and mechanical stability of carboxyl linked single-molecule junctions, Phys. Chem. Chem. Phys.* **2012**, *14*, 13841

92. F. Pauly, J. K. Viljas, U. Huniar, M. Häfner, S. Wohlthat, M. Bürkle, J. C. Cuevas, G. Schön, *Cluster-based density-functional approach to quantum transport through molecular and atomic contacts, New J. Phys*. **2008**, *10*, 125019.

93. S. Y. Quek, L. Venkataraman, H. J. Choi, S. G. Louie, M. S. Hybertsen, J. B. Neaton, *Amine−Gold Linked Single-Molecule Circuits: Experiment and Theory, Nano Lett.* **2007**, *7*, 3477.

94. D. L. Bao, R. Liu, J. C. Leng, X. Zuo, Y. Jiao, Z. L. Li, C. K. Wang, *Theoretical study on mechanical and electron-transport properties of conjugated molecular junctions with carboxylic or methyl sulfide linksPhys. Lett. A* **2014**, *378*, 1290.

95. C. J. Pedersen, *Cyclic polyethers and their complexes with metal salts, J. Am. Chem. Soc.* **1967**, *89*, 2495.

96. C. J. Pedersen, *The discovery of crown ethers, J. Inclusion Phenom.* **1988**, *6*, 337.

97. C. J. Pedersen, *Cyclic polyethers and their complexes with metal salts, J. Am. Chem. Soc.* **1967**, *89*, 7017.

98. N. K. Dailey, in R. M. Izatt and J.J. Christensen (Eds.), *Synthetic Multidentate Macrocyclic Compounds*, Academic Press, New York, **1978**, 207.

99. Y. L. Zhao, L. Liu, W. Zhang, C. H. Sue,Q. Li, O. Š. Miljanić, O. M. Yaghi, J. F. Stoddart, *Rigid-Strut-Containing Crown Ethers and [2]Catenanes for Incorporation into Metal–Organic Frameworks, Chem. Eur. J. 2009, 15, 13356.*

100. Y. Arakawa, S. Kang, H. Tsuji, J. Watanabe, G. Konishi, *The design of liquid crystalline bistolane-based materials with extremely high birefringence, RSC Adv*. **2016**, *6*, 92845.

101. S. Banerjee , P. Dey , S. Basu, *Antagonism in extraction of cesium with 18-crown-6 and phosphine oxides from aqueous perchlorate solution, Radiochemistry* **2010**, *52*, 2, 162.

102. W. L. F. Armarego, C. L. L. Chai, *Purification of Laboratory Chemicals*, Elsevier, **2003**.

103. E. Lörtscher, D Widmer, B. Gotsmann, *Next-generation nanotechnology laboratories with simultaneous reduction of all relevant disturbances, Nanoscale* **2013**, *5*, 10542.

104. T. Ishiyama, M. Murata, N. Miyaura, *Palladium(0)-Catalyzed Cross-Coupling Reaction of Alkoxydiboron with Haloarenes: A Direct Procedure for Arylboronic Esters, J. Org. Chem.* **1995**, *60*, 23, 7508.

105. T. Yamamoto, T. Morita, J. Takagi, T. Yamakawa, *NiCl$_2$(PMe$_3$)$_2$-Catalyzed Borylation of Aryl Chlorides, Org. Lett.* **2011**, *13*, 5766.

106. P. Li, C. Fua, S. Ma, *Gorlos-Phos for palladium-catalyzed borylation of aryl chlorides, Org. Biomol. Chem.* **2014**, *12*, 3604.

107. Y. L. Zhao, Y. Li, S. M. Li, Y. G. Zhou, F. Y. Sun, L. X. Gao, F. S. Han, *A Highly Practical and Reliable Nickel Catalyst for Suzuki–Miyaura Coupling of Aryl Halides, Adv. Synth. Catal*. **2011**, *353*, 1543.

108. J. I. Urgel, D. Ecija, W. Auwärter, D. Stassen, D. Bonifazi, J. V. Barth, *Orthogonal insertion of lanthanide and transition-metal atoms in metal-organic networks on surfaces., Angew. Chem. Int. Ed.* **2015**, *54*, 6163.

109. T. Fujimori, P. Wirsching, K. D. Janda, *Preparation of a Kröhnke Pyridine Combinatorial Library Suitable for Solution-Phase Biological Screening, J. Comb. Chem*. **2003**, *5*, 625.

110. M. Segura, L. Sánchez, J. de Mendoza, N. Martín, D. M. Guldi, *Hydrogen Bonding Interfaces in Fullerene•TTF Ensembles, J. Am. Chem. Soc.* **2003**, *125*, 49, 15093.

111. B. R. Pandya, Y. K. Agrawal, *Synthesis and characterisation of crown ether based azo dyes, Dyes and Pigments* **2002**, *52*, 161.

112. HyperPhysics, Georgia State University, *Abundance of Elements in Earth's Crust*.

113. H. W. Kroto, J. R. Heath, S. C. O'Brien, R. F. Curl, R. E. Smalley, *C_{60}: Buckminsterfullerene, Nature* **1985**, *318*, 162.

114. W. Kratschmer, L. D. Lamb, K. Fostiropoulos, D. R. Huffman, *Solid C_{60}: a new form of carbon, Nature* **1990**, *347*, 354.

115. a) C. S. Yannoni, P. P. Bernier, D. S. Bethune, G. Meijer, J. R. Salem, *NMR determination of the bond lengths in C_{60}, J. Am. Chem.Soc.* **1991**, *113*, 3190; b) M. S. Dresselhaus, G. Dresselhaus, P. C. Eklund, *Science of Fullerenes and Carbon Nanotubes*, Academic Press, San Diego, **1996**.

116. R. C. Haddon, *Electronic structure, conductivity and superconductivity of alkali metal doped (C_{60}), Acc. Chem. Res.* **1992**, *25*, 127.

117. T. G. Schmalz, W. A. Seitz, D. J. Klein, G. E. Hite, *C_{60} carbon cages, Chem. Phys. Lett.* **1986**, *130*, 203.

118. H. W. Kroto, *The stability of the fullerenes C_n, with n = 24, 28, 32, 36, 50, 60 and 70, Nature* **1987**, *329*, 529.

119. A. Hirsch, *Fullerenes and Related Structure, Top Curr. Chem. 199*, Springer, Berlin Heidelberg New York Springer, **1999**.

120. A. L. Balch, M. M. Olmstead, *Reactions of Transition Metal Complexes with Fullerenes (C_{60}, C_{70}, etc.) and Related Materials, Chem. Rev.* **1998**, *98*, 2123.

121. D. M. Guldi, *Fullerenes: three dimensional electron acceptor materials, Chem. Commun.,* **2000**, *5*, 321.

122. D. M. Guldi, M. Prato, *Excited-State Properties of C60 Fullerene Derivatives, Acc. Chem. Res.* **2000**, *33*, 695.

123. N. Martín, L. Sánchez, B. Illescas, I. Pérez, *C60-Based Electroactive Organofullerenes, Chem. Rev.* **1998**, *98*, 2527.

124. a) C. A. Reed, R. D. Bolskar, *Discrete Fulleride Anions and Fullerenium Cations, Chem. Rev.* **2000**, *100*, 1075; b) A. D. J. Haymet, *C_{120} and C_{60}: Archimedean solids constructed from sp^2 hybridized carbon atoms, Chem. Phys. Lett.* **1985**, *122*, 421; c) P. D. Hale, *Discrete-variational-X.alpha. electronic structure studies of the spherical C60 cluster: prediction of ionization potential and electronic transition energy, J. Am. Chem. Soc.* **1986** *108*, 6087.

125. a) F. Arias, Q. Xie, Y. Wu, Q. Lu, S. R. Wilson, L. Echegoyen, *Kinetic Effects in the Electrochemistry of Fullerene Derivatives at Very Negative Potentials, J. Am. Chem. Soc.* **1994**, *116*, 6388; b) P.M. Allemand, A. Koch, F. Wudl, Y. Rubin, F. Diederich, M. M. Alvarez, S. J. Anz, R. L. Whetten, *Two different fullerenes have the same cyclic voltammetry, J. Am. Chem. Soc.* **1991**, *113*, 1050.

126. R. E. Haufler, J. Conceicao, L. P. F. Chibante, Y. Chai, N. E. Byrne, S. Flanagan, M. M. Haley, S. C. O'Brien, C. Pan, *Efficient production of C60, J. Phys. Chem.* **1990**, *94*, 8634.

127. Q. Xie, E. Pérez-Cordero, L. Echegoyen, *Electrochemical detection of C606- and C706-: Enhanced stability of fullerides in solution, J. Am. Chem. Soc.* **1992**, *114*, 3978.

128. R. C. Haddon, L. E. Brus, K. Raghavachari, *Electronic structure and bonding in icosahedral C60, Chem. Phys. Lett.* **1986**, *125*, 459.

129. Q. Xie, F. Arias, L. Echegoyen, *Electrochemically-reversible, single-electron oxidation of C_{60} and C_{70}, J. Am. Chem. Soc.* **1993**, *115*, 9818.

130. H. Imahori, Y. Sakata, *Fullerenes as Novel Acceptors in Photosynthetic Electron Transfer, Eur. J. Org. Chem.* **1999**, *1999*, 2445.

131. M. S. Meier, R. G. Bergosh, M. E. Gallagher, H. P. Spielmann, Z. Wang, *Alkylation of Dihydrofullerenes, J. Org. Chem.* **2002**, *67*, 5946.

132. a) R. A. Marcus, *On the Theory of Oxidation-Reduction Reactions Involving Electron Transfer. I, J. Chem. Phys. I* 1956, 24, 966; b) 11m.

133. a) P. H. Wöbkenberg, D. D. C. Bradley, D. Kronholm, J. C. Hummelen, D. M. de Leeuw, M. Cölle, T. D. Anthopoulos, *High mobility n-channel organic field-effect transistors based on soluble C_{60} and C_{70} fullerene derivatives, Synthetic Metals* **2008**, *158*, 468; b) K. Shibata, Y. Kubozono, T. Kanbara, T. Hosokawa, A. Fujiwara, Y. Ito, H. Shinohara, *Fabrication and characteristics of C 84 fullerene field-effect transistors, Appl. Phys. Lett.* **2004**, *14*, 84, 2572.

134. L. Qiu, Y. Zhang, T. L. Krijger, X. Qiu, P. van't Hof, J. C. Hummelen, R. C. Chiechi, *Rectification of current responds to incorporation of fullerenes into mixed-monolayers of alkanethiolates in tunneling junctions, Chem. Sci.* **2017**, *8*, 2365.

135. a) P. Hudhomme, *An overview of molecular acceptors for organic solar cells, EPJ Photovolt,* **2013**, *4*, 40401; b) Y. He, Y. Li, *Fullerene derivative acceptors for high performance polymer solar cells, Phys. Chem. Chem. Phys.* **2011**, *13*, 1970; c) S. Vidal, M. Izquierdo, W. Kit Law, K. Jiang, S. Filippone, J. Perles, H. Yan, N. Martín, *Photochemical site-selective synthesis of [70] methanofullerenes, Chem. Commun.* **2016**, *52*, 12733.

136. J. D. Chen, C. Cui, Y. Q. Li, L. Zhou, Q. D. Ou, *Single-Junction Polymer Solar Cells Exceeding 10% Power Conversion Efficiency, Adv. Mater.* **2015**, *27*, 1035.

137. J. C. Withers, R. O. Loutfy, T. P. Lowe, *Fullerene Commercial Vision, Fullerene Sci. Technol.* **1997**, *5*, 1.

138. A. A. Peera, L. B. Alemany, W. E. Billups, *Hydrogen storage in hydrofullerides , Appl. Phys. A* **2004**, *78*, 995.

139. S. R. Chae, E. M. Hotze, M. R. Wiesner, *Environmental implications and applications of carbon nanomaterials in water treatment, Water Sci Technol*. **2013**, *67*, 11, 2582.

140. A. S. Basso, l. D. Frenke, F. J. Quintana, F.A. Costa-Pinto, S. Petrovic-Stojkovic, L. Puckett, A. Monsonego, A. Bar-Shir, Y. Engel, M. Gozin, H. L. Weiner, *Reversal of axonal loss and disability in a mouse model of progressive multiple sclerosis, J. Clin. Invest*. **2008**, *118*, 4, 1532.

141. L. L. Dugan, D. M. Turetsky, C. Du, D.Lobner, M. Wheeler, C. R. Almli, C. K. F. Shen, T. Y. Luh, D. W. Choi, T. S. Lin, *Carboxyfullerenes as neuroprotective agents, PNAS* **1997**, *94*, 17, 9434.

142. a) S. Bosi, R. T. Da, G. Spalluto, J. Balzarini, M. Prato, *Synthesis and anti-HIV properties of new water-soluble bis-functionalized[60]fullerene derivatives, Bioorg. Med. Chem. Lett.* **2003**, *13*, 24, 4437; b) S. Marchesan, R. T. Da, G. Spalluto, J. Balzarini, M. Prato, *Anti-HIV properties of cationic fullerene derivatives, Bioorg. Med. Chem. Lett*. **2005**, *15*, 15, 3615.

143. a) A. Muñoz, D. Sigwalt, B. M. Illescas, J. Luczkowiak, L. Rodríguez-Pérez, I. Nierengarten, M. Holler, J. Remy, K. Buffet, S. P. Vincent, J. Rojo, R. Delgado, J. Nierengarten, N. Martín, *Synthesis of giant globular multivalent glycofullerenes as potent inhibitors in a model of Ebola virus infection, Nat. Chem.* **2016**, *8*, 50; b) B. M. Illescas, J. Rojo, R. Delgado, N. Martín, *Multivalent Glycosylated Nanostructures To Inhibit Ebola Virus Infection, J. Am. Chem. Soc.* **2017**, *139*, 17, 6018.

144. C. S. Berger, J. W. Marks, R. D. Bolskar, M. G. Rosenblum, L. J. Wilson, *Cell Internalization Studies of Gadofullerene-(ZME-018) Immunoconjugates into A375m Melanoma Cells, Transl. Oncol.* **2011**, *4*, 6, 350.

145. B. Daroczi, G. Kari, M. F. McAleer, J. C. Wolf, U. Rodeck, A. P. Dicker, *In vivo Radioprotection by the Fullerene Nanoparticle DF-1 as Assessed in a Zebrafish Model, Clin. Cancer Res.* **2006**, *12*, 23, 7086.

146. Y. L. Lai, P. Murugan, K. C. Hwang, *Fullerene derivative attenuates ischemia-reperfusion-induced lung injury., Life Sci.* **2003**, *72*, 11, 1271.

147. K. A. Gonzalez, L. J. Wilson, W. Wu, G. H. Nancollas, *Synthesis and in vitro characterization of a tissue-selective fullerene: vectoring C(60)(OH)(16)AMBP to mineralized bone, Bioorg. Med. Chem.* **2002**, *10*, 6, 1991.

148. A. Dellinger, Z. Zhou, R. Lenk, D. Macfarland, C. L. Kepley, *A Steroid-Mimicking Nanomaterial That Mediates Inhibition Of Human Lung Mast Cell Responses, Exp. Dermatol.* **2009**, *18*, 2, 1079.

149. N. Tsao, T. Y. Luh, C. K. Chou, T. Y. Chang, J. J. Wu, C. C. Liu, H. Y. Lei, *In vitro action of carboxyfullerene, J. Antimicrob. Chemother.* **2002**, *49*, 4, 641.

150. D. D. L. Chung, *Review Graphite, J. Mater. Sci.* **2002**, *37*, 1475.

151. W. Andreoni, *The Physics of Fullerene-Based and Fullerene-Related Materials*, Springer, Berlin, **2000**.

152. a) R. Saito, G. Dresselhaus, M. S. Dresselhaus, *Physical Properties of Carbon Nanotubes*, Imperial College Press, London, **1998**; b) J. C. Charlier, X. Blase, S. Roche, *Electronic and transport properties of nanotubes, Rev. Mod. Phys.* **2007**, *79*, 677.

153. K. S. Novoselov, A. K. Geim, S. V. Morozov, D. Jiang, Y. Zhang, S. V. Dubonos, I. V. Gregorieva, A. A. Firsov, *Electric Field Effect in Atomically Thin Carbon Films, Science* **2004**, *306*, 666.

154. L. Pauling, *The nature of the chemical bond and the structure of molecules and crystals: an introduction to modern structural chemistry*, Cornell University Press., Ithaca, NY, **1939**.

155. K. S. Novoselov, A. K. Geim, S. V. Morozov, D. Jiang, M. I. Katsnelson, I. V. Grigorieva, S. V. Dubonos, A. A. Firsov, *Two-dimensional gas of massless Dirac fermions in graphene, Nature* **2005**, *438*, 197.

156. C. Lee, X. D. Wei, J. W. Kysar, J. Hone, *Measurement of the elastic properties and intrinsic strength of monolayer graphene, Science* **2008**, *321*, 385.

157. M. D. Stoller, S. J. Park, Y. W. Zhu, J. H. An, R. S. Ruoff, *Graphene-Based Ultracapacitors , Nano Lett.* **2008**, *8*, 3498.

158. A. Reina, X. Jia, J. Ho, D. Nezich, H. Son, V. Bulovic, M. S. Dresselhaus, J. Kong, *Large Area, Few-Layer Graphene Films on Arbitrary Substrates by Chemical Vapor Deposition, Nano Lett.* **2009**, *9*, 30.

159. R. R. Nair, P. Blake, A. N. Grigorenko, K. S. Novoselov, T. J. Booth, T. Stauber, N. M. R.Peres, A. K. Geim, *Fine Structure Constant Defines Visual Transparency of Graphene, Science* **2008**, *320*, 1308.

160. A. A. Balandin, S. Ghosh, W. Bao, I. Calizo, D. Teweldebrhan, F. Miao, C. N. Lau, *Superior Thermal Conductivity of Single-Layer Graphene, Nano Lett.* **2008**, *8*, 902.

161. A. K. Geim, *Graphene: Status and Prospects, Science* **2009**, *324*, 1530.

162. R. E. Peierls, *Quelques propriétés typiques des corps solides, Ann. Inst. Henri Poincare* **1935**, *5*, 177.

163. L. D. Landau, *Theory of phase transformations. I, Phys. Z. Sowjetunion* **1937**, 11, 26.

164. J. C. Meyer, A. K. Geim, M. I. Katsnelson, K. S. Novoselov, T. J. Booth, S. Roth, *The structure of suspended graphene sheets, Nature* **2007**, *446*, 60.

165. L. Yan, Y. B. Zheng, F. Zhao, S. Li, X. Gao, B. Xu, P. S. Weiss, Y. Zhao, *Chemistry and physics of a single atomic layer: strategies and challenges for functionalization of graphene and graphene-based materials, Chem. Soc. Rev.* **2012**, *41*, 97.

166. A. K. Geim, K. S. Novoselov, *The rise of graphene, Nat. Mater*. **2007**, *6*, 183.

167. E. Hobsbawm, *The Age of Revolution: Europe 1789-1848*, Weidenfeld&Nicolson Ltd., **1962**.

168. H. G. Elias, *Plastics, General Survey*, Ullmann's Encyclopedia of Industrial Chemistry, Wiley-VCH, Weinheim, **2005**.

169. Patent Analysis Report on Graphene, PatSeer Pro, **2017**.

170. A. Colli, S. A. Awan, A. Lombardo, T. J. Echtermeyer, T. S. Kulmala, A. C. Ferrari, *US 20130162333*, **2013**.

171. O. Rozhin, A. Ferrari, W. I. Milne, *US 20100003528*, **2010**.

172. Y. Woo, S. A. Seo, D. Kim, H. Chung, *US 20110089403*, **2011**.

173. T. Kobayashi, *EP 2393107*, **2013**.

174. L. Song, A. Zhamu, J. Guo, B. Z. Jang, *US 7623340*, **2009**.

175. S. M. Yoon, W. M. Choi, H. J. Shin, J. Y. Choi, *EP 2439779*, **2014**.

176. G. Owen, *GB 2471672*, **2011**.

177. a) B. Z. Jang, A. Zhamu, *US 20100000441*, **2008**; b) R. Murphy, O. Rozhin, A. C. Ferrari, J. Robertson, W. I. Milne, *US 20070275230*, **2007**; c) F. Torrisi, T. Hasan, F. Bonaccorso, A. C. Ferrari, *WO 2014064432* A1, **2014**.

178. H. Andersson, *US 20110311029*, **2011**.

179. O. Rozhin, A. Ferrari, W. I. Milne, *US 8323789 B2*, **2007**.

180. P. Avouris, M. B. Steiner, M. Engel, R. Krupke, A. C. Ferrari, A. Lombardo, *US 20130107344* A1, **2013**.

181. H. Lammer, *US 20100125013*, **2010**.

182. a) K. S. Kim, Y. Zhao, H. Jang, S. Y. Lee, J. M. Kim, K. S. Kim, J. H. Ahn, P. Kim, J. Y. Choi, B. H. Hong, *Large-scale pattern growth of graphene films for stretchable transparent electrodes, Nature* **2009**, *457*, 706. b) A. H. C. Neto, F. Guinea, N. M. R. Peres, K. S. Novoselov, A. K. Geim, *The electronic properties of graphene, Rev. Mod. Phys.* **2009**, *81*, 109.

183. K. V. Emtsev, A. Bostwick, K. Horn, J. Jobst, G. L. Kellogg, L. Lay, J. L. McChesney, T. Ohta, S. A. Reshanov, J. Röhrl, E. Rotenberg, A. K. Schmid; D. Waldmann, H. B. Weber, T. Seyller, *Towards wafer-size graphene layers by atmospheric pressure graphitization of silicon carbide, Nat. Mater.* **2009**, *8*, 203.

184. A. Balan, R. Kamar, M. Boukhicha, O. Beyssac, J. C. Bouillard, D. Taverna, W. Sacks, M. Marangolo, E. Lacaze, R. Gohler, W. Escoffier, J. M. Poumiroi, A. Shukla, *Anodic bonded graphene, J. Phys. D: Appl. Phys.* **2010**, *43*, 374013.

185. D. V. Kosynkin, A. L. Higginbotham, A. Sinitskii, J. R. Lomeda, A. Dimiev, K. Price, J. M. Tour, *Longitudinal unzipping of carbon nanotubes to form graphene nanoribbons, Nature* **2009**, *458*, 872.

186. X. Yang, X. Dou, A. Rouhanipour, L. Zhi, H. J. Räder, K. Müller, *Two-Dimensional Graphene Nanoribbons, J. Am. Chem. Soc.* **2008**, *130*, 4216.

187. Y. Zhu, S. Murali, M. D. Stoller, K. J. Ganesh, W. Cai, P. J. Ferreira, A. Pirkle, R. M. Wallace, K. A. Cychosz, M. Thommes, D. Su, E. A.Stach, R. S. Ruoff, *Carbon-Based Supercapacitors Produced by Activation of Graphene, Science* **2011**, *332*, 1537.

188. X. Li, X. Wang, L. Zhang, H. Dai, *Chemically derived, ultrasmooth graphene nanoribbon semiconductors, Science* **2008**, *319*, 1229.

189. Y. Hernandez, V. Nicolosi, M. Lotya, F. M. Blighe, Z. Y. Sun, S. De, I. T. McGovern, B. Holland, M. Byrne, Y. K. Gun'ko, J. J. Boland, P. Niraj, G. Duesberg, S. Krishnamurthy, R. Goodhue, J. Hutchison, V. A. C. Scardaci, J. Ferrari, N. Coleman, *High-yield production of graphene by liquid-phase exfoliation, Nat. Nanotechnol.* **2008**, *3*, 563.

190. J. Lu, J. Yang, J. Wang, A. Lim, S. Wang, K. P. Loh, *One-Pot Synthesis of Fluorescent Carbon Nanoribbons, Nanoparticles, and Graphene by the Exfoliation of Graphite in Ionic Liquids , ACS Nano* **2009**, *3*, 2376.

191. C. Valles, C. Drummond, H. Saadaoui, C. A. Furtado, M. He, O. Roubeau, L. Ortolani, M. Monthioux, A. Pénicaud, *Solutions of Negatively Charged Graphene Sheets and Ribbons, J. Am. Chem. Soc.* **2008**, *130*, 15802.

192. V. Léon, M. Quintana, M. A. Herrero, J. L. G. Fierro, A. de la Hoz, M. Prato, E. Vázquez, *Few-layer graphenes from ball-milling of graphite with melamine, Chem. Commun.* **2011**, *47*, 10936.

193. J. Park, W. H. Lee, S. Huh, S. H. Sim, S. B. Kim, K. Cho, B. H. Hong, K. S. J. Kim, *Work-Function Engineering of Graphene Electrodes by Self-Assembled Monolayers for High-Performance Organic Field-Effect Transistors, Phys. Chem. Lett.* **2011**, *2*, 841.

194. J. Park, S. B. Jo, Y. J. Yu, Y. Kim, J, W. Yang, W. H. Lee, H. H. Kim., B. H. Hong, P. Kim, K. Cho, K. S. Kim, *Single-Gate Bandgap Opening of Bilayer Graphene by Dual Molecular Doping, Adv. Mater.* **2012***, 24,* 407.

195. H. X. Wang, Q. Wang, K. G. Zhou, H. L. Zhang, *Graphene in Light: Design, Synthesis and Applications of Photo-active Graphene and Graphene-Like Materials, Small* **2013**, *9*, 1266.

196. M. L. Mueller, X. Yan, B. Dragnea, L. S. Li, *Slow Hot-Carrier Relaxation in Colloidal Graphene Quantum Dots, Nano Lett.* **2011**, *11*, 56.

197. T. Ohta, A. Bostwick, T. Seyller, K. Horn, E. Rotenberg, *Controlling the Electronic Structure of Bilayer Graphene, Science* **2006**, *313*, 951.

198. L. Jiao, L. Zhang, X. Wang, G. Diankov, H. Dai, *Narrow graphene nanoribbons from carbon nanotubes, Nature* **2009**, *458*, 877.

199. H. Liu, Y. Liu, D. Zhu, *Chemical doping of graphene, J. Mater. Chem.* **2011**, *21*, 3335.

200. a) Z. Sun, D. K. James, J. M. Tour, *Graphene Chemistry: Synthesis and Manipulation, J. Phys. Chem. Lett.* **2011**, *2*, 2425; c) M. Quintana, E. Vazquez, M. Prato, *Organic Functionalization of Graphene in Dispersions, Acc. Chem. Res.* **2013**, *46*, 1, 138; d) K. P. Loh, Q. Bao, P. K. Ang, J. Yang, J. Mater. Chem. **2010**, *20*, 2277; e) K. Dirian, M. A. Herranz, G. Katsukis, J. Malig, L. Rodríguez-Pérez, C. Romero-Nieto, V. Strauss, N. Martín, D. M. Guldi, *Low dimensional nanocarbons–chemistry and energy/electron transfer reactions, Chem. Sci.* **2013**, *4*, 4335; f) G. Bottari, M. Á. Herranz, L. Wibmer, M. Volland, L. Rodríguez-Pérez, D. M. Guldi, A. Hirsch, N. Martín, F. D'Souza, T. Torres, *Chemical functionalization and characterization of graphene-based materials, Chem. Soc. Rev.* **2017**, *46*, 4464.

201. S. Ryu, M. Y. Han, J. Maultzsch, T. F. Heinz, P. Kim, M. L. Steigerwald, L. E. Brus, *Reversible Basal Plane Hydrogenation of Graphene, Nano Lett.* **2008**, *8*, 4597.

202. a) K. Nakada, M. Fujita, G. Dresselhaus, M. S. Dresselhaus, Edge state in graphene ribbons: *Nanometer size effect and edge shape dependence, Phys. Rev. B: Condens. Matter Mater. Phys.* **1996**, *54*, 17954; b) D. E. Jiang, B. G. Sumpter, S. Dai, *Unique chemical reactivity of a graphene nanoribbon's zigzag edge, J. Chem. Phys.* **2007**, *126*, 134701; c) R. Sharma, N. Nair, M. S. Strano, *Structure−Reactivity Relationships for Graphene Nanoribbons, J. Phys. Chem. C* **2009**, *113*, 14771.

203. X. Gao, Y. Wang, X. Liu, T. L. Chan, S. Irle, Y. Zhao, S. B. Zhang, *Regioselectivity control of graphene functionalization by ripples, Phys. Chem. Chem. Phys*. **2011**, *13*, 19449.

204. a) D. R. Dreyer, S. Park, C. W. Bielawski, R. S. Ruoff, *The chemistry of graphene oxide, Chem. Soc. Rev*. **2010**, *39*, 228; b) D. Chen, H. Feng, J. Li, *Graphene Oxide: Preparation, Functionalization, and Electrochemical Applications, Chem. Rev.* **2012**, *112*, 6027; c) F. Li, X. Jiang, J. Zhao, S. Zhang, *Graphene oxide: A promising nanomaterial for energy and environmental applications, Nano Energy* **2015**, *16*, 488; d) W. L. Xu, C. Fang, F. Zhou, Z. Song, Q. Liu, R. Qiao, M. Yu, *Self-Assembly: A Facile Way of Forming Ultrathin, High-Performance Graphene Oxide Membranes for Water Purification, Nano Lett.* **2017**, *17*, 2928.

205. a) A. Lerf, H. He, M. Forster, J. Klinowski, *Structure of Graphite Oxide Revisited , J. Phys. Chem. B* **1998**, *102*, 4477; b) D. C. Marcano, D. V. Kosynkin, J. M. Berlin, A. Sinitskii, Z. Sun, A. Slesarev, L. B. Alemany, W. Lu, J. M. Tour, *Improved Synthesis of Graphene Oxide, ACS Nano* **2010**, *4*, 8, 4806; b) J. Chen, B. Yao, C. Li, G. Sh, *An improved Hummers method for eco-friendly synthesis of graphene oxide, Carbon* **2013**, *64*, 225.

206. a) V. Georgakilas, M. Otyepka, A. B. Bourlinos, V. Chandra, N. Kim, K. C. Kemp, P. Hobza, R. Zboril, K. S. Kim, *Functionalization of Graphene: Covalent and Non-Covalent Approaches, Derivatives and Applications, Chem. Rev.* **2012**, *112*, 6156; b) A. Ciesielski, P. Samorì, *Supramolecular Approaches to Graphene: From Self-Assembly to Molecule-Assisted Liquid-Phase Exfoliation, Adv. Mater*. **2016**, *28*, 6030.

207. a) K. S. Subrahmanyam, P. Kumar, U. Maitra, A. Govindaraj, K. P. S. S. Hembram, U. V. Waghmare, C. N. R. Rao, *Chemical storage of hydrogen in few-layer graphene, PNAS* **2011**, *108*, 2674; b) S. Sarkar, E. Bekyarova, S. Niyogi, R. C. Haddon, *Diels−Alder Chemistry of Graphite and Graphene: Graphene as Diene and Dienophile, J. Am. Chem. Soc*. **2011**, *133*, 3324; c) X. Zhong, J. Jin, S. Li, Z. Niu, W. Hu, R. Li, J. Ma, *Aryne cycloaddition: highly efficient chemical modification of graphene, Chem. Commun.* **2010**, *46*, 7340; d) E. K. Choi, I. Y. Jeon, S. Y. Bae, H. J. Lee, H. S. Shin, L. Daib, J. B. Baek, *High-yield exfoliation of three-dimensional graphite into two-dimensional graphene-like*

sheets, Chem. Commun. **2010**, *46*, 6320; e) L. H. Liu, M. M. Lerner, M. Yan, *Derivitization of Pristine Graphene with Well-Defined Chemical Functionalities, Nano Lett.* **2010**, *10*, 3754; f) E. Bekyarova, M. E. Itkis, P. Ramesh, C. Berger, M. Sprinkle, W. A. de Heer, R. C. Haddon, *Chemical Modification of Epitaxial Graphene: Spontaneous Grafting of Aryl Groups, J. Am. Chem. Soc.* **2009**, *131*, 1336; g) M. Quintana, A. Montellano, A. E. del Rio Castillo, G. Van Tendeloo, C. Bittencourt, M. Prato, *Selective organic functionalization of graphene bulk or graphene edges, Chem. Commun.* **2011**, *47*, 9330; h) L. Rodríguez-Pérez, M. Á. Herranz, N. Martín, *The chemistry of pristine graphene, Chem. Commun.* **2013**, *49*, 3721.

208. A. Savchenko, *Transforming Graphene, Science* **2009**, *323*, 589.

209. L. Zheng, Z. Li, S. Bourdo, F. Watanabe, C. C. Ryersonb, A. S. Biris, *Catalytic hydrogenation of graphene films, Chem. Commun*. **2011**, *47*, 1213.

210. R. A. Schafer, J. M. Englert, P. Wehrfritz, W. Bauer, F. Hauke, T. Seyller, A. Hirsch, *On the way to graphane-pronounced fluorescence of polyhydrogenated graphene, Angew. Chem. Int. Ed.* **2013**, *52*, 754.

211. a) R. R. Nair, W. Ren, R. Jalil, I. Riaz, V. G. Kravets, L. Britnell, P. Blake, F. Schedin, A. S. Mayorov, S. Yuan, M. I. Katsnelson, H. Ming Cheng, W. Strupinski, L. G. Bulusheva, A. V. Okotrub, I. V. Grigorieva, A. N. Grigorenko, K. S. Novoselov, A. K. Geim, *Fluorographene: A Two-Dimensional Counterpart of Teflon, Small* **2010**, *6*, 2877; b) H. L. Poh, P. Šimek, Z. Sofer, M. Pumera, *Halogenation of Graphene with Chlorine, Bromine, or Iodine by Exfoliation in a Halogen Atmosphere, Chem. Eur. J.* **2013**, *19*, 2655.

212. H. Liu, S. Ryu, Z. Chen, M. L. Steigerwald, C. Nuckolls, L. E. Brus, *Photochemical Reactivity of Graphene, J. Am. Chem. Soc*. **2009**, *131*, 17099.

213. J. L. Bahr, J. Yang, D. V. Kosynkin, M. J. Bronikowski, R. E. Smalley, J. M. Tour, *Functionalization of Carbon Nanotubes by Electrochemical Reduction of Aryl Diazonium Salts: A Bucky Paper Electrode, J. Am. Chem. Soc*. **2001**, *123*, 6536.

214. a) J. R. Lomeda, C. D. Doyle, D. V. Kosynskin, W. F. Hwang, J. M. Tour, *Diazonium Functionalization of Surfactant-Wrapped Chemically Converted Graphene Sheets, J. Am. Chem. Soc.* **2008**, *130*, 16201; b) Z. Jin, J. R. Lomeda, B. K. Price, W. Lu, Y. Zhu, J. M. Tour, *Mechanically Assisted Exfoliation and Functionalization of Thermally Converted Graphene Sheets, Chem. Mater.* **2009**, *21*, 3045.

215. M. E. Lipińska, S. L. H. Rebelo, M. F. R. Pereira, J. A. N. F. Gomes, C. Freire, J. L. Figueiredo, *New insights into the functionalization of multi-walled carbon nanotubes with aniline derivatives, Carbon* **2012**, *50*, 3280.

216. P. Huang, H. Zhu, L. Jing, Y. Zhao, X. Gao, Graphene Covalently Binding Aryl Groups: Conductivity Increases Rather than Decreases, ACS Nano **2011**, *5*, 7945.

217. J. M. Englert, C. Dotzer, G. Yang, M. Schmid, C. Papp, J. M. Gottfried, H. P. Steinruck, E. Spiecker, F. Hauke, A. Hirsch, *Covalent bulk functionalization of graphene, Nat. Chem.* **2011**, *3*, 279.

218. Z. Sun, S. Kohama, Z. Zhang, J. R. Lomeda, J. M. Tour, *Soluble graphene through edge-selective functionalization, Nano Res.* **2010**, *3*, 117.

219. a) F. Amblard, J. H. Cho, R. F. Schinazi, *Cu(I)-Catalyzed Huisgen Azide−Alkyne 1,3-Dipolar Cycloaddition Reaction in Nucleoside, Nucleotide, and Oligonucleotide Chemistry, Chem. Rev.* **2009**, *109*, 4207; b) H. C. Kolb, M. G. Finn, K. B. Sharpless, *Click Chemistry: Diverse Chemical Function from a Few Good Reactions., Angew. Chem. Int. Ed.* **2001**, *40*, 2004; c) Z. Jin, T. P. McNicholas, C. J. Shih, Q. H. Wang, G. L. C. Paulus, A. J. Hilmer, S. Shimizu, M. S. Strano, *Click Chemistry on Solution-Dispersed Graphene and Monolayer CVD Graphene, Chem. Mater.* **2011**, *23*, 3362.

220. a) H. X. Wang, K. G. Zhou, Y. L. Xie, J. Zeng, N. N. Chai, J. Li, H. L. Zhang, *Photoactive graphene sheets prepared by "click" chemistry, Chem. Commun.* **2011**, *47*, 5747; b) M. Castelaín, G. Martínez, P. Merino, J. A. Martín-Gago, J. L. Segura, G. Ellis, H. J. Salavagione, Chem. Eur. J. **2012**, *18*, 4965.

221. K. Fukui, *Theory of Orientation and Stereoselection*, Springer-Verlag, Berlin, Germany, **1970**.

222. S. Sarkar, E. Bekyarova, R. C. Haddon, *Chemistry at the Dirac Point: Diels–Alder Reactivity of Graphene, Acc. Chem. Res.* **2012**, *45*, 673.

223. D. García, L. Rodríguez-Pérez, M. A. Herranz, D. Peña, E. Guitián, S. Bailey, Q. Al-Galiby, M. Noori, C. J. Lambert, D. Pérez, N. Martín, *A C_{60}-aryne building block: synthesis of a hybrid all-carbon nanostructure, Chem. Commun.* **2016**, *52*, 6677.

224. a) F. Liu, J. Y. Choi, T. S. Seo, *DNA mediated water-dispersible graphene fabrication and gold nanoparticle-graphene hybrid, Chem. Commun.* **2010**, *46*, 2844; b) J. Liu, W. Yang, L. Tao, D. Li, C. Boyer, T. P. Davis, *Thermosensitive graphene nanocomposites formed using pyrene-terminal polymers made by RAFT polymerization, J. Polym. Sci., Part A: Polym. Chem.* **2010**, *48*, 425; c) D. W. Lee, T. Kim, M. Lee, *An amphiphilic pyrene sheet for selective functionalization of graphene, Chem. Commun.* **2011**, *47*, 8259.

225. a) J. F. Shen, Y. H. Hu, C. Li, C. Qin, M. X. Ye, *Synthesis of Amphiphilic Graphene Nanoplatelets, Small* **2009**, *5*, 82; b) E. Y. Choi, T. H. Han, J. Hong, J. E. Kim, S. H. Lee,

H. W. Kim, S. O. Kim, *Noncovalent functionalization of graphene with end-functional polymers, J. Mater. Chem*. **2010**, *20*, 1907.

226. a) M. A. Rafiee, J. Rafiee, Z. Wang, H. Song, Z. Z. Yu, N. Koratkar, *Enhanced Mechanical Properties of Nanocomposites at Low Graphene Content, ACS Nano* **2009**, *3*, 3884; b) E. R. Margine, M. L. Bocquet, X. Blase, *Thermal Stability of Graphene and Nanotube Covalent Functionalization, Nano Lett.* **2008**, *8*, 3315.

227. Q. Bao, H. Zhang, J. Yang, S. Wang, D. Y. Tang, R. Jose, S. Ramakrishna, C. T. Lim, K. P. Loh, *Graphene–Polymer Nanofiber Membrane for Ultrafast Photonics, Adv. Funct. Mater.* **2010**, *20*, 782.

228. Q. Yang, X. Pan, F. Huang, K. Li, *Fabrication of High-Concentration and Stable Aqueous Suspensions of Graphene Nanosheets by Noncovalent Functionalization with Lignin and Cellulose Derivatives, J. Phys. Chem.* C **2010**, *114*, 3811.

229. a) Y. Xu, H. Bai, G. Lu, C. Li, G. Shi, *Flexible Graphene Films via the Filtration of Water-Soluble Noncovalent Functionalized Graphene Sheets, J. Am. Chem. Soc.* **2008**, *130*, 5856; b) M. Quintana, K. Spyrou, M. Grzelczak, W. R. Browne, P. Rudolf, M. Prato, *Functionalization of Graphene via 1,3-Dipolar Cycloaddition, ACS Nano* **2010**, *4*, 3527; c) Q. Su, S. Pang, V. Alijani, C. Li, X. Feng, K. Mullen, *Composites of Graphene with Large Aromatic Molecules, Adv. Mater.* **2009**, *21*, 3191.

230. a) N. Petrone, I. Meric, J. Hone, K. L. Shepard, *Graphene Field-Effect Transistors with Gigahertz-Frequency Power Gain on Flexible Substrates, Nano Lett.* **2012**, *13*, 121; b) D. Kuzum, H. Takano, E. Shim, J. C. Reed, H. Juul, A. G. Richardson, J. de Vries, H. Bink, M. A. Dichter, T. H. Lucas, D. A. Coulter, E. Cubukcu, B. Litt, *Transparent and flexible low noise graphene electrodes for simultaneous electrophysiology and neuroimaging, Nat. Commun.* **2014** , *5* , 5259; c) J. Li, J. Liang, L. Li, F. Ren, W. Hu, J. Li, S. Qi, Q. Pei, *Healable Capacitive Touch Screen Sensors Based on Transparent Composite Electrodes Comprising Silver Nanowires and a Furan/Maleimide Diels–Alder Cycloaddition Polymer, ACS Nano* **2014**, *8*, 12874; d) B. Zhu, Z. Niu, H. Wang, W. R. Leow, H. Wang, Y. Li, L. Zheng, J. Wei, F. Huo, X. Chen, *Microstructured Graphene Arrays for Highly Sensitive Flexible Tactile Sensors, Small* **2014** , *10*, 3625.

231. a) T. Skaltsas, S. Pispas, N. Tagmatarchis, *Photoinduced Charge-Transfer Interactions on a Graphene/Block Copolymer Electrostatically Bound to Tetracationic Porphyrin in Aqueous Media, Chem. Eur. J.* **2013**, *19*, 9286; b) Y. Xu, Z. Liu, X. Zhang, Y. Wang, J. Tian, Y. Huang, Y. Ma, X. Zhang, Y. Chen, *A Graphene Hybrid Material Covalently Functionalized with Porphyrin: Synthesis and Optical Limiting Property, Adv. Mater.* **2009**, *21*, 1275; c) J. Malig, N. Jux, D. Kiessling, J. J. Cid, P. Vázquez, T. Torres, D. M.

266

Guldi, *Towards tunable graphene/phthalocyanine-PPV hybrid systems, Angew. Chem. Int. Ed.* **2011**, *50*, 3561; d) L. Brinkhaus, G. Katsukis, J. Malig, R. D. Costa, M. Garcia-Iglesias, P. Vázquez, T. Torres, D. M. Guldi, *Tuning the Stability of Graphene Layers by Phthalocyanine-Based oPPV Oligomers Towards Photo- and Redoxactive Materials, Small* **2013**, *9*, 2348; e) M. E. Ragoussi, J. Malig, G. Katsukis, B. Butz, E. Spiecker, G. de la Torre, T. Torres, D. M. Guldi, *Linking Photo- and Redoxactive Phthalocyanines Covalently to Graphene, Angew. Chem. Int. Ed.* **2012**, *51*, 6421.

232. T. Zhuang, X. F. Wang, T. Sano, Z. Hong, Y. Yang, J. Kido, *Fullerene derivatives as electron donor for organic photovoltaic cells, Appl. Phys. Lett.* **2013**, *103*, 203301.

233. X. Y. Zhang, Y. Huang, Y. Wang, Y. F. Ma, Z. F. Liu, Y. S. Chen, *Synthesis and characterization of a graphene–C60 hybrid material, Carbon* **2009**, *47*, 1, 334.

234. Z. B. Liu, Y. F. Xu, X. Y. Zhang, X. L. Zhang, Y. S. Chen, J. G. Tian, *Porphyrin and Fullerene Covalently Functionalized Graphene Hybrid Materials with Large Nonlinear Optical Properties, J. Phys. Chem. B* **2009**, *113*, 29, 9681.

235. X. Y. Zhang, Z. B. Liu, Y. Huang, X. J. Wan, J. G. Tian, Y. F. Ma, Y. S. Chen, *Synthesis, Characterization and Nonlinear Optical Property of Graphene-C-60 Hybrid, J. Nanosci. Nanotechnol.* **2009**, *9*, 10, 5752.

236. Y. Zhang, L. Ren, S. Wang, A. Marathe, J. Chaudhuri, G. Li, *Functionalization of graphene sheets through fullerene attachment, J. Mater. Chem.* **2011**, *21*, 5386.

237. D. Yu, K. Park, M.Durstock, L. Dai, *Fullerene-Grafted Graphene for Efficient Bulk Heterojunction Polymer Photovoltaic Devices, J. Phys. Chem. Lett.* **2011**, *2*, 1113.

238. L. Rincón-García, C. Evangeli, G. Rubio-Bollingerac, N. Agraït, *Thermopower measurements in molecular junctions, Chem. Soc. Rev.* **2016**, *45*, 4285.

239. C. Evangeli, K. Gillemot, E. Leary, M. T. González, G. Rubio-Bollinger, C. J. Lambert, N. Agraït, *Engineering the Thermopower of C60 Molecular Junctions, Nano Lett*. **2013**, *13*, 2141.

240. J. A. Malen, P. Doak, K. Baheti, T. D. Tilley, A. Majumdar, R. A. Segalman, *The Nature of Transport Variations in Molecular Heterojunction Electronics, Nano Lett*. **2009**, *9*, 3406.

241. P. Reddy, S. Y. Jang, R. A. Segalman, A. Majumdar, *Thermoelectricity in Molecular Junctions, Science* **2007**, *315*, 1568.

242. a) J. A. Malen, P. Doak, K. Baheti, T. D. Tilley, R. A. Segalman, A. Majumdar, *Identifying the Length Dependence of Orbital Alignment and Contact Coupling in*

Molecular Heterojunctions, Nano Lett. **2009**, *9*, 1164; b) W. B. Chang, C. K. Mai, M. Kotiuga, J. B. Neaton, G. C. Bazan, R. A. Segalman, *Controlling the Thermoelectric Properties of Thiophene-Derived Single-Molecule Junctions, Chem. Mater.* **2014**, *26*, 7229.

243. J. R. Widawsky, P. Darancet, J. B. Neaton, L. Venkataraman, *Simultaneous Determination of Conductance and Thermopower of Single Molecule Junctions, Nano Lett.* **2012**, *12*, 354.

244. K. Baheti, J.A.Malen, P. Doak, P. Reddy, S. Y. Jang, T. D. Tilley, A. Majumdar, R. A. Segalman, *Probing the Chemistry of Molecular Heterojunctions Using Thermoelectricity, Nano Lett.* **2008**, *8*, 715.

245. S. K. Yee, J. A. Malen, A. Majumdar, R. A. Segalman, *Thermoelectricity in Fullerene– Metal Heterojunctions, Nano Lett.* **2011**, *11*, 4089.

246. W. R. Bamford, T. S. Stevens, *The decomposition of toluene-p-sulphonylhydrazones by alkali, J. Chem. Soc.* **1952**, 4735.

247. R. Gómez, J. L. Segura, N. Martín, *Highly Efficient Light-Harvesting Organofullerenes, Org. Lett.* **2005**, *7*, 717.

248. R. A. J. Janssen, J. C. Hummelen, F. Wudl, *Photochemical Fulleroid to Methanofullerene Conversion via the Di-.pi.-methane (Zimmerman) Rearrangement, J. Am. Chem. Soc.* **1995**, *117*, 544.

249. a) A. Fateh, M. Aliofkhazraei, A. R. Rezvanian, *Review of corrosive environments for copper and its corrosion inhibitors.* Arabian Journal of Chemistry, **2017** (in press); b) *The Role Of Corrosive Sulfur In Transformers And Transformer Oil* L. R. Lewand Doble Engineering Company, USA, **2002**.

250. J. Guan, X. Chen, T. Wei, F. Liu, S. Wang, Qi. Yang, Y. Lua, S. Yang, *Directly bonded hybrid of graphene nanoplatelets and fullerene: facile solid-state mechanochemical synthesis and application as carbon-based electrocatalyst for oxygen reduction reaction, J. Mater. Chem. A* **2015**, *3*, 4139.

251. C. Enkvist, S. lunell, B. Sjögren, S. Svensson, P. A. Brühwiler, A. Nilsson, A. J. Maxwell, N. Martensson, *C_{1s} shakeup spectrum of C_{60}: Global charge-transfer satellites and their relation to the x-ray threshold singularities in macroscopic systems, Phys. Rev. B: Condens. Matter Mater. Phys.* **1993**, *48*, 14629.

252. X. Zhang, Z. Zhi, Y. Huang, X. Wan, J. Tian, Y. Ma, Y. Chen, *Synthesis, characterization and nonlinear optical property of graphene-C_{60} hybrid, J. Nanosci. Nanotech.* **2009**, *9*, 5752.

253. L. Dobusch, M. M. Furchi, A. Pospischil, T. Mueller, E. Bertagnolli, A. Lugstein, *Electric field modulation of thermovoltage in single-layer MoS$_2$, Appl. Phys. Lett.* **2014**, *105*, 25, 253103.

254. a) M. Buscema, M. Barkelid, V. Zwiller, H. S. J. van der Zant, G. A. Steele, A. Castellanos-Gomez, *Large and Tunable Photothermoelectric Effect in Single-Layer MoS$_2$, Nano Lett.* **2013**, *13*, 2, 358; b) J. Wu; H. Schmidt, K. K. Amara, X. Xu, G. Eda, B. Özyilmaz, *Large Thermoelectricity via Variable Range Hopping in Chemical Vapor Deposition Grown Single-Layer MoS$_2$, Nano Lett.* **2014**, *14*, 5, 2730.

255. J. M. Soler, E. Artacho, J. Gale, A. García, J. Junquera, P. Ordejón, D. Sánchez Portal, *The SIESTA method for ab initio order-N materials simulation, J. Phys. Condens. Matter.* **2002**, *14*, 2745.

256. a) M. Dion, H. Rydberg, E. Schröder, D. C. Langreth, B. I. Lundqvist, *Van der Waals Density Functional for General Geometries, Phys. Rev. Lett.* **2004**, *92*, 246401; b) D. C. Langreth, M. Dion, H. Rydberg, E. Schröder, P. Hyldgaard, B. I. Lundqvist, *Van der Waals density functional theory with applications, J. Quantum Chem.* **2005**, *101*, 599.

257. H. B. Jansen, P. Ross, *Non-empirical molecular orbital calculations on the protonation of carbon monoxide, Chem. Phys. Lett.* **1969**, *3*, 140.

258. J. Ferrer, C. J. Lambert, V. M. García-Suárez, D. Z. Manrique, D. Visontai, L. Oroszlany, R. Rodríguez-Ferradás, I. Grace, S. W. D. Bailey, K. Gillemot, *GOLLUM: a next-generation simulation tool for electron, thermal and spin transport, New J. Phys.* **2014**, *16*, 093029.